University of Alberta

Stratigraphic and Tectonic Evolution of the Jurassic Hazelton Trough–Bowser Basin, Northwest British Columbia, Canada

by

Jean-François Gagnon

A thesis submitted to the Faculty of Graduate Studies and Research
in partial fulfillment of the requirements for the degree of

Doctor of Philosophy

Department of Earth and Atmospheric Sciences

Fall 2010
Edmonton, Alberta

Examining Committee

Dr. John Waldron, Department of Earth and Atmospheric Sciences, University of Alberta

Dr. Murray Gingras, Department of Earth and Atmospheric Sciences, University of Alberta

Dr. Ben Rostron, Department of Earth and Atmospheric Sciences, University of Alberta

Dr. Claire Currie, Department of Physics, University of Alberta

Dr. Bill Arnott, Department of Earth Sciences, University of Ottawa

Abstract

The Hazelton trough–Bowser basin is a large sedimentary basin that developed on volcanic arc rocks of the Stikine terrane in northern British Columbia, Canada. Its fill mostly consists of the Lower to Middle Jurassic Hazelton Group and the Middle Jurassic to Lower Cretaceous Bowser Lake Group. Regional correlations indicate that the Hazelton Group can be divided in two distinct lithostratigraphic intervals separated in most places by an unconformity. The lower Hazelton Group (LHG) is dominated by arc-related volcanic rocks, whereas the upper Hazelton Group (UHG) contains mainly fine-grained clastic rocks and lesser bimodal rift-related volcanic rocks. Lowermost coarse-grained strata of the UHG, including the bioturbated and fossiliferous units of the Smithers Formation and the Spatisizi River Formation, record a transgressive trend consistent with thermal subsidence and relative sea-level rise. Transgression of the Stikine arc culminated with the establishment of deep-water conditions in the Late Toarcian-Early Aalenian, and deposition of the Quock Formation. Interbedded siliceous mudstone and rusty-weathered tuff of the Quock Formation are correlated throughout most of the basin, except in the Iskut River area on the northwestern margin of the basin, where contemporaneous strata of the Iskut River Formation are dominated by rift-related volcanic rocks and conglomerates. Inception of rifting in the Iskut River area constitutes an independent extensional event on Stikinia, and could be related to reorganization of tectonic plates during a protracted period of terrane accretion in the Middle Jurassic. Obduction of the Cache Creek terrane over Stikinia in early Middle Jurassic provided a new source of sediment, which led to accumulation of the Bowser Lake Group. The second pulse of subsidence observed at Todagin Mountain can be explained by sediment loading of the accommodation previously generated during extension of the Hazelton trough in Early Jurassic time.

Acknowledgments

I am heartily thankful to my supervisor, John Waldron, whose encouragement, guidance and support throughout this project enabled me to develop an unbiased and critical mind to carry scientific research at the highest level. His restless enthusiasm and incredible knowledge of geology had a positive impact on my learning experience as a graduate student. I would like to thank members of my thesis committee, Murray Gingras and Ben Rostron, for their valuable advice and professional expertise that significantly improved the quality of this research. I owe my deepest gratitude to Walter Loogman, JoAnne Nelson, Terry Poulton, Fabrice Cordey, Carol Evenchick, Tony Barresi, and Larry Heaman, for enlightened discussion and support in a number of ways. I must also acknowledge reviewers Bill Arnott, Dominic Armitage, Andrea Fildani, Dale Issler, Stephen Johnston, Claire Currie, and Darrel Long for their helpful comments and suggestions on portions of the this thesis submitted/accepted for publication into peer-reviewed journals.

It is a pleasure for me to thank the people who assisted me in the field, such as Cory Bloomberg, Heidi Tomes, David Dockman and Marc-André Bourgault. Their positive attitude made life in camp enjoyable and their presence always kept me safe. Access to remote areas in the rugged terrain of northern British Columbia would not have been possible without the amazing pilot skills of Jim Reed, Pat Rooney, and the regretted Dave Reid. I would like to show my gratitude to Diane Caird, Judy Schultz, Mark Labbé, David Pirie, Don Resultay, Guangcheng Chen, Heather Clough, Valery Companiytsev, Marsha Boyd, Mike Fisher and Igor Jakab for their invaluable technical support. The completion of this thesis would not have been possible without the financial support from many different sources, including scholarships and research grants from NSERC, Geoscience BC and the Faculty of Graduate Student at the University of Alberta.

I am indebted to many of my friends and colleagues at the Earth and Atmospheric Sciences department for their continuous support and companionship during my experience as a graduate student. I am especially grateful to Hilary Corlett, Shawna White, Alberto Reyes, Stefane Lalonde, Britta Jensen, Jamie Kraft, Tyler Hauck, Larry Amskold, Kenny Wallace, Guillaume Lesage and Neil Fernandes. Lastly, I offer my regards and blessings to my beloved girlfriend, Jennifer, my inspiring and caring sister, Isabelle, and to my wonderful parents, Louise et Gilles, who were always there to support me in the most difficult of times, and never stopped believing in me.

Table of contents

List of Tables

List of Figures

Chapter 1: Introduction

The Hazelton trough is an extensional Early Jurassic sedimentary basin that developed within the Stikine terrane of the Intermontane Belt in northern British Columbia, Canada, and which subsequently evolved into a larger synorogenic basin in the Middle Jurassic, the Bowser basin (figure 1.1). The Hazelton and Bowser Lake groups, which constitute the fill of the Hazelton trough and the Bowser basin respectively, are characterized by a combination of formal and informal units that contain many overlaps and inconsistencies in stratigraphic nomenclature (figure 1.2). The primary objective of this thesis is to provide a revised stratigraphic framework for the Hazelton trough-Bowser basin that can be applied at the regional scale. Since specific strata of the Hazelton trough-Bowser basin have been recognized for their petroleum and/or precious metal potential, a simplified stratigraphic framework makes these prospective units more predictable. In addition, a revised nomenclature defined by significant lithological changes and/or important stratigraphic boundaries can provide insights into different depositional environments, and basin-forming mechanisms. Understanding the stratigraphic and tectonic evolution of the Hazelton trough–Bowser basin also has broader implications for evolution of the northern Canadian Cordillera. Tectonic interactions between Stikinia and its neighbouring terranes, and the precise timing of their eventual accretion to the continental margin have been subjects of much debate for some time. The controversy is mostly based on conflicting paleontological, geochronologic, structural, paleomagnetic, stratigraphic, geochemical, and provenance studies. The new data presented in this thesis provide additional constraints on the Early to Middle Jurassic evolution of the northern Canadian Cordillera, and evaluates how the tectonic setting of the Hazelton trough-Bowser basin affected subsequent sedimentation patterns of its basin fill.

1.1 Previous work

Depositional units of the Hazelton Group and Bowser Lake Group have been the subject of many studies. These have included work by government survey programs, exploration geologists, and research by numerous graduate students from different universities. Early mapping work is documented by Tipper and Richards (1976); Gabrielse and Tipper (1984); Woodsworth et al. (1985); Grove (1986) and Gabrielse (1998). Subsequent biostratigraphic work was done by Thomson et al. (1986); Nadaraju (1993); Palfy et al. (2000); Evenchick et al. (2001). Reconnaissance mapping in the eastern and northern part of the Bowser basin by the Geological Survey of Canada produced several reports and geological maps such as Evenchick (1987,

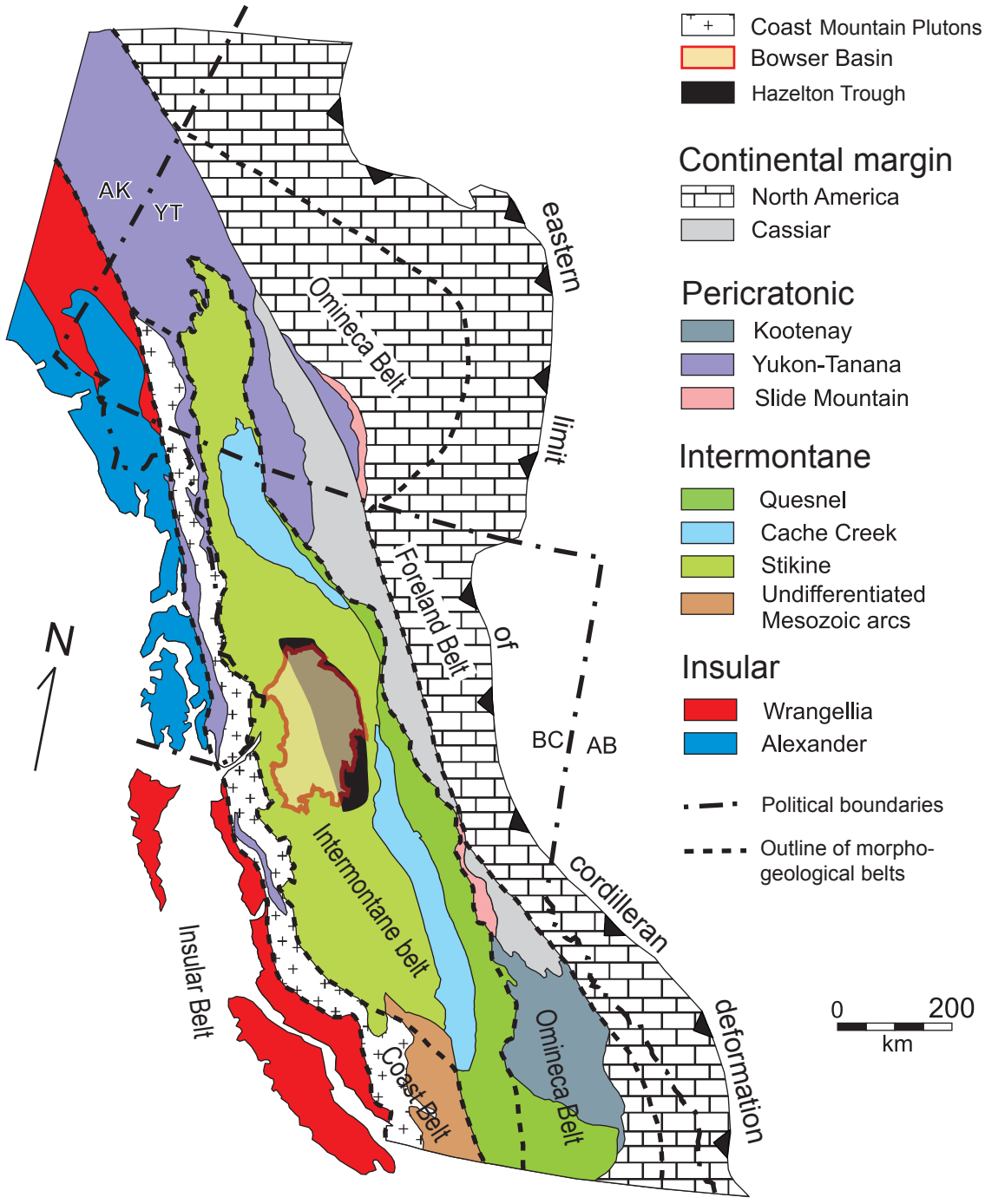

Figure 1.1: Simplified map of the Canadian Cordillera showing the location of the Hazelton trough–Bowser basin, and distribution of terranes and major morphogeological belts. Modified from Wheeler and McFeely (1991); Colpron et al. (2006) and Evenchick et al. (2009).

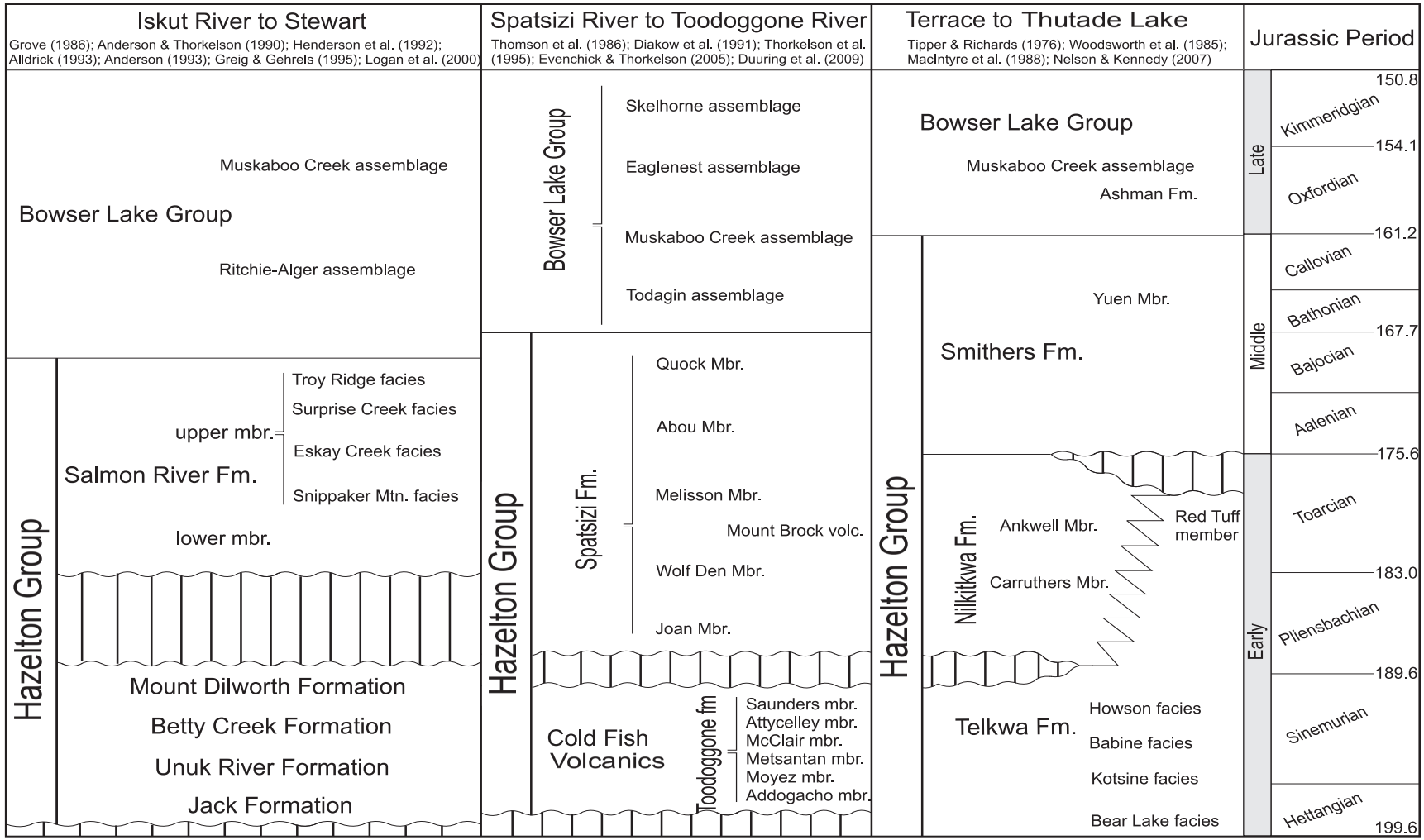

Figure 1.2: Summary of the current nomenclature for the Hazelton Group in north-cenral British Columbia. The inherent complexity in the terminology used to describe the units of the Hazelton Group stems from the existence of three independent stratigraphic frameworks each related to a limited geographic area.

1989, 1991); Evenchick and Porter (1993); Greig and Evenchick (1993). The discovery of mineral deposits at Eskay Creek, Silbak Premier and Toodoggone River led to research by Anderson and Thorkelson (1990); Alldrick (1991); Diakow et al. (1991); Anderson (1993); McDonald et al. (1996); Logan et al. (2000); Roth (2002); Alldrick et al. (2004, 2005a, 2005b); Barresi et al. (2005) and Alldrick et al. (2006). This was followed by a major energy-related investigation by the Geological Survey of Canada led by C.A. Evenchick, which yielded significant results including work by Osadetz et al. (2003); Ferri et al. (2004); Evenchick and Thorkelson (2005); Evenchick et al. (2005); O'Sullivan et al. (2005); Stasiuk et al. (2005); Osadetz et al. (2007); Evenchick et al. (2008a, 2008b, 2009). The superb quality of outcrop combined with the well-established biostratigraphic framework in the vicinity of Tsatia and Todagin mountains led to detailed sedimentological and stratigraphic studies by Green (1992); Ricketts and Evenchick (1999, 2007) and Gagnon et al. (2009). Other significant contributions to the advancement of the general knowledge of the Hazelton and Bowser Lake groups include the work of Marsden and Thorkelson (1992); Ricketts et al. (1992); Thorkelson (1992); Greig and Gehrels (1995); Thorkelson et al. (1995); Evenchick (2001); Evenchick et al. (2007) and Nelson et al. (2007). Earlier reports from the current project were published by Waldron et al. (2006); Gagnon et al. (2007); Loogman et al. (2007); Loogman (2008); Gagnon and Waldron (2008, 2009).

1.2 Methods

Most of the observations presented in this study are based on detailed examination of well-exposed stratigraphic sections located on the periphery of the Bowser basin. Field mapping was conducted in selected areas where the exposed contact between the Hazelton Group and the overlying Bowser Lake Group could be observed. Four summer seasons of field work were completed between 2005 and 2008, during which a total of 24 camps in 14 different geographic areas were visited. Camp locations (see figure 2.1) were chosen from available published geological maps, and based on extensive aerial photograph interpretation where well exposed outcrop could be observed. Most areas were accessed from helicopter-supported camps, from which daily traverses involving two to three people were undertaken. Each camp involved 4-7 days of reconnaissance geological mapping, followed by detailed measurements of stratigraphic sections where the rock exposure was suitable.

Lithological samples collected in the field were cut and prepared as thin sections for petrological investigations. X-ray diffraction analyses were performed on selected altered clay-rich samples in order to document the mineral crystallography and chemical

composition of the very fine-grained matrix. Additional laboratory work included crushing, mineral separation, and detrital zircon U-Pb geochronology using laser ablation inductively coupled mass spectrometry (LA-ICP-MS) technique at the Radiogenic Isotope Facility of the University of Alberta. Siliceous sediment samples collected from measured sections were sent to Dr. Fabrice Cordey of the Université de Lyon in France for HF extraction and identification of radiolarian microfossils. Diverse macrofossils, such as ammonoids and bivalves, were sent to Dr. Terry Poulton (Geological Survey of Canada, Calgary) for paleontological identification. These fossils are now part of the Geological Survey of Canada collection located in Calgary, Alberta.

1.3 Presentation and main objectives

This thesis comprises a series of five manuscripts that incorporate a broad range of geology-related disciplines to document the tectonic evolution and subsequent depositional environments of the Hazelton trough–Bowser basin. A paper-based format was chosen to facilitate eventual publication of portions of this thesis in peer-review journals. Some repetition between chapters is unavoidable, in order to provide the necessary context so that each chapter constitutes a separate entity. The subject of each chapter is described below.

Chapter 2 provides an overview of the main stratigraphic units described in this study. It includes a thorough review of previous work on the stratigraphy of the Lower to Middle Jurassic Hazleton Group, and highlights the inconsistencies and inherent complexity of the current nomenclature. This chapter attempts to evaluate potential correlations of mappable lithostratigraphic units at the regional scale by comparing multiple sections measured in the field and available from the literature. Main stratigraphic packages are defined by significant lithological changes or important stratigraphic boundaries, and a revised stratigraphic framework including new formation names is proposed. A version of this chapter will be published under the authorship of Gagnon, J.-F., Barresi, T., Waldron, J.W.F., Nelson, J.L., Poulton, T.P., Cordey, F. and Heaman, L.M. The first draft was written by Gagnon. Barresi provided data and descriptions for the section on volcanic-dominated areas in the northwestern part of the basin. Waldron and Nelson suggested edits and revisions to the first draft. Cordey extracted and identified radiolarian microfossils and Poulton identified macrofossils. Heaman assisted with the U-Pb geochronology. The version presented here was compiled and edited by Gagnon based on some material provided by the other authors.

Chapter 3 presents the first detailed sedimentological and ichnological study of the Smithers Formation of the upper Hazleton Group. It includes an extensive

description of trace fossils and sedimentary structures that characterize the Smithers Formation. Integration of lithofacies and ichnofacies analyses from detailed measured sections provides a new depositional model for the volcanic and sedimentary rocks of the Smithers Formation. A version of this chapter will be published under the authorship of Gagnon, J.-F., Gingras, M.K., Waldron, J.W.F. and Poulton, T.P. The first draft was written by Gagnon. Waldron and Gingras suggested edits and revisions to the first draft. Poulton identified macrofossils. The version presented here was compiled and edited by Gagnon based on some material provided by the other authors.

Chapter 4 documents the subsidence history of the Hazelton trough–Bowser basin in the northwestern part of the study area. Backstripping calculations were performed on a continuous stratigraphic section at Todagin Mountain, where a complete succession from the volcanic basement into the overlying sedimentary cover is exposed. In this chapter, the first quantitative subsidence analysis of the Hazelton trough–Bowser basin is presented in order to document the origin of the basin. By determining how and when most of the accommodation space was generated, different basin-forming mechanisms are evaluated, and a revised tectonic model for the basin is proposed. A version of this chapter has been published: Gagnon, J.-F., Evenchick, C.A., Waldron, J.W.F., Cordey, F. and Poulton, T.P. 2009; Jurassic subsidence history of the Hazelton trough–Bowser basin in the area of Todagin Mountain, north-central Bristish Columbia, Canada; Bulletin of Canadian Petroleum Geology, vol. 57, no. 4, pp. 430-448. The first draft was written by Gagnon. Waldron and Evenchick suggested edits and revisions to the first draft. Cordey extracted and identified radiolarian microfossils and Poulton identified macrofossils. The version presented here was compiled and edited by Gagnon based on some material provided by the other authors.

Chapter 5 evaluates various sedimentation styles and depositional processes that affected deep-water sedimentation at the base of the Bowser Lake Group. Comparison of two well-exposed successions of the Todagin assemblage documents the stratigraphic evolution of deep-water architectures in the evolving Bowser basin. A version of this chapter has been accepted for publication on June 3rd 2010 in Marine and Petroleum Geology under the authorship of Gagnon, J.-F. and Waldron, J.W.F. The first draft was written by Gagnon, and Waldron suggested edits and revisions.

Chapter 6 discusses the development of the Hazelton trough–Bowser basin based on the main findings of this study. A tectonic model evaluating potential interactions between Stikinia and adjacent terranes for evolution of the Canadian Cordillera is presented. A version of this chapter will be published under the authorship of Gagnon, J.-F., Waldron, J.W.F. and Heaman, L.M. The first draft was written by Gagnon.

Waldron suggested edits and revisions to the first draft. Heaman assisted with the U-Pb geochronology.

1.4 References

Alldrick, D.J. 1991. Geology and ore deposits of the Stewart Mining Camp. Ph.D. thesis, Department of Earth and Ocean Sciences, University of British Columbia, Vancouver, B.C.

Alldrick, D.J., Stewart, M.L., Nelson, J.L. and Simpson, K.A. 2004. Tracking the Eskay Rift Through Northern British Columbia - Geology and Mineral Occurrences of the Upper Iskut River Area (Telegraph Creek NTS 104G/1, 2, 7, 8, 9, 10). *In*: Geological Fieldwork 2003. British Columbia Ministry of Energy, Mines and Petroleum Resources, Paper 2004-1, pp. 1-19.

Alldrick, D.J., Nelson, J.L. and Barresi, T. 2005a. Geology of the More Creek - Palmiere Creek area, northwestern British Columbia. British Columbia Ministry of Energy, Mines and Petroleum Resources, Open File Map 2005-5.

Alldrick, D.J., Nelson, J.L. and Barresi, T. 2005b. Geology and mineral occurrences of the Upper Iskut River Area: tracking the Eskay rift trough northern British Columbia (Telegraph Creek NTS 104G/1, 2; Iskut River NTS 104B/9, 10, 15, 16). *In:* Geological Fieldwork 2004. British Columbia Ministry of Energy, Mines and Petroleum Resources, Paper 2005-1, pp. 1-30.

Alldrick, D.J., Nelson, J.L., Barresi, T., Stewart, M.L. and Simpson, K.A. 2006. Geology of the Upper Iskut River Area, British Columbia. British Columbia Ministry of Energy, Mines and Petroleum Resources, Open File Map 2006-2.

Anderson, R.G. 1993. A Mesozoic stratigraphic and plutonic framework for northwestern Stikinia (Iskut River area), northwestern British Columbia, Canada. *In:* Dunne, G., McDougall, K. (Eds.), Mesozoic Paleogeography of the Western United States--II. Society of Economic Paleontologists and Mineralogists, Pacific Section, vol. 77, pp. 477-494.

Anderson, R.G. and Thorkelson, D.J. 1990. Mesozoic stratigraphy and setting for some mineral deposits in Iskut River map area, northwestern British Columbia. *In:* Current Research, Part E. Geological Survey of Canada, Paper 90-1E, pp. 131-139.

Barresi, T., Nelson, J.L., Alldrick, D.J. and Dostal, J. 2005. Pillow Basalt Ridge Facies: Detailed mapping of Eskay Creek-Equivalent Stratigraphy in Northwestern British Columbia. *In:* Geological Fieldwork 2004. British Columbia Ministry of Energy, Mines and Petroleum Resources, Paper 2005-1, pp. 31-38.

Colpron, M., Nelson, J.L. and Murphy, D.C. 2006. A tectonostratigraphic framework for the pericratonic terranes of the northern Canadian Cordillera. *In:* Colpron, M., Nelson, J.L. (Eds.), Paleozoic Evolution and Metallogeny of Pericratonic Terranes at the Ancient Pacific Margin of North America. Geological Association of Canada, Special Paper 45, pp. 1-23.

Diakow, L.J., Panteleyev, A. and Schroeter, T.G. 1991. Jurassic Epithermal Deposits in the Toodoggone River Area, Northern British Columbia: Examples of Well-Preserved, Volcanic-Hosted, Precious Metal Mineralization. Economic Geology, vol. 86, pp. 529-554.

Evenchick, C.A. 1987. Stratigraphy and structure of the northeastern margin of the Bowser Basin, Spatsizi map area, north-central British Columbia. *In:* Current Research, Part A. Geological Survey of Canada, Paper 87-1A, pp. 719-726.

Evenchick, C.A. 1989. Stratigraphy and structure in east Spatsizi map area, north-central British Columbia.

In: Current Research, Part E. Geological Survey of Canada, Paper 89-1E, pp. 133-138.

Evenchick, C.A. 1991. Geometry, evolution, and tectonic framework of the Skeena Fold Belt, north-central British Columbia. Tectonics, vol. 10, pp. 527-546.

Evenchick, C.A. 2001. Northeast-trending folds in the western Skeena Fold Belt, northern Canadian Cordillera: a record of Early Cretaceous sinistral plate convergence. Journal of Structural Geology, vol. 23, pp. 1123-1140.

Evenchick, C.A. and Porter, J.S. 1993. Geology of west McConnell Creek map area, British Columbia. *In:* Current Research, Part A. Geological Survey of Canada, Paper 93-1A, pp. 47-55.

Evenchick, C.A., Poulton, T.P., Tipper, H.W. and Braidek, I. 2001. Fossils and facies of the northern two-thirds of the Bowser Basin, British Columbia. Geological Survey of Canada, Open File 3956, 103 p.

Evenchick, C.A. and Thorkelson, D.J. 2005. Geology of the Spatsizi River map area, north-central British Columbia. Geological Survey of Canada, Bulletin 577, 276 p.

Evenchick, C.A., Gabrielse, H. and Snyder, D. 2005. Crustal structure and lithology of the northern Canadian Cordillera: alternative interpretations of SNORCLE seismic reflection lines 2A and 2b. Canadian Journal of Earth Sciences, vol. 42, pp. 1149-1161.

Evenchick, C.A., McMechan, M.E., McNicoll, V.J. and Carr, S.D. 2007. A synthesis of the Jurassic-Cretaceous tectonic evolution of the central and southeastern Canadian Cordillera: exploring links across the orogen. *In:* Sears, J.W., Harms, T.A., Evenchick, C.A. (Eds.), Whence the mountains? The contribution of Raymond A. Price. Geological Society of America., Special Paper 433, pp. 117-145.

Evenchick, C.A., McMechan, M.E., Mustard, P.S., Ritcey, D., Smith, G.T., Ferri, F. and Waldron, J.W.F. 2008a. Geology, Hazelton, British Columbia. Geological Survey of Canada, Open File 5704.

Evenchick, C.A., Mustard, P.S., McMechan, M.E., Ritcey, D.H. and Smith, G.T. 2008b. Geology, Northeast Terrace and northwest Smithers, British Columbia. Geological Survey of Canada, Open File 5895.

Evenchick, C.A., Mustard, P.S., McMechan, M.E., Greig, C.J., Ferri, F., Ritcey, D., Smith, G., Hadlari, T. and Waldron, J.W.F. 2009. Geology, Compilation Geology of Bowser and Sustut Basins Draped on Shaded Relief Map, North-central British Columbia. Geological Survey of Canada , Open File 5794.

Ferri, F., Osadetz, K.G. and Evenchick, C.A. 2004. Petroleum source rock potential of Lower to Middle Jurassic clastics, Intermontane Basins, British Columbia. *In:* Summary of Activities 2004. British Columbia Ministry of Energy and Mines. pp. 87-97.

Gabrielse, H. 1998. Geology of the Cry Lake and Dease Lake map areas, north-central British Columbia. Geological Survey of Canada, Bulletin 504, 147 p.

Gabrielse, H. and Tipper, H.W. 1984. Bedrock Geology of the Spatsizi Map Area (104H). Geological Survey of Canada, Open File 1005.

Gagnon, J.-F., Loogman, W., Waldron, J.W.F., Cordey, F. and Evenchick, C.A. 2007. Stratigraphic Record of Initiation of Sedimentation in the Bowser Basin (NTS 104A, H), Northwestern British Columbia. *In:* Geological Fieldwork 2006. British Columbia Ministry of Energy, Mines and Petroleum Resources, Paper 2007-1, pp. 275-283.

Gagnon, J.-F. and Waldron, J.W.F. 2008. Ashman Ridge Section Revisited: New Insights for the Evolution of the Bowser Basin, Northwestern British Columbia (NTS 93L/13). *In:* Summary of Activities 2007. Geoscience BC, Report 2008-1, pp. 121-128.

Gagnon, J.-F. and Waldron, J.W.F. 2009. Sedimentation Patterns and Reservoir Distribution in a Siliciclastic, Tectoniacally Active Slope Environment, Bowser Basin, Northwestern British Columbia (NTS 104B/01). *In:* Summary of Activities 2008. Geoscience BC, Report 2009-1, pp.

193-200.

Gagnon, J.-F., Evenchick, C.A., Waldron, J.W.F., Cordey, F. and Poulton, T.P. 2009. Jurassic subsidence history of the Hazelton Trough-Bowser Basin in the area of Todagin Mountain, north-central British Columbia, Canada. Bulletin of Canadian Petroleum Geology, vol. 57, pp. 430-448.

Green, G.M. 1992. Detailed sedimentology of the Bowser Lake Group, northern Bowser Basin, north-central British Columbia. M.Sc. thesis, Department of Earth Sciences, Carleton Universiy, Ottawa, Ont.

Greig, C.J. and Evenchick, C.A. 1993. Geology of Oweegee Dome (geochemistry and paleontology), Delta Peak (104A/12) and Taft Creek (104A/11W) map areas, northwestern British Columbia. Geological Survey of Canada, Open File 2688.

Greig, C.J. and Gehrels, G.E. 1995. U-Pb zircon geochronology of Lower Jurassic and Paleozoic Stikinian strata and Tertiary intrusions, northwestern British Columbia. Canadian Journal of Earth Sciences, vol. 32, pp. 1155-1171.

Grove, E.W. 1986. Geology and mineral deposits of the the Unuk River - Salmon River - Anyox area. British Columbia Ministry of Energy, Mines and Petroleum Resources, Bulletin 63, 152 p.

Logan, J.M., Drobe, J.R. and McClelland, W.C. 2000. Geology of the Forest Kerr - Mess Creek area, Northwestern British Columbia (104B/10,15 & 104G/2 & 7W). British Columbia Ministry of Energy and Mines, Bulletin 104, 164 p.

Loogman, W., Gagnon, J.-F., Waldron, J.W.F. and Evenchick, C.A. 2007. Structural Overprinting in the Northwestern Skeena Fold Belt (NTS 104B, H), Northwestern British Columbia. *In:* Geological Fieldwork 2006. British Columbia Ministry of Energy, Mines and Petroleum Resources, Paper 2007-1, pp. 325-332.

Loogman, W. 2008. Structure and Kinematic Development of the northwest Skeena Fold Belt, northwestern British Columbia. M.Sc. thesis, Department of Earth and Atmospheric Sciences, University of Alberta, Edmonton, Ab.

Marsden, H. and Thorkelson, D.J. 1992. Geology of the Hazelton Volcanic Belt in British Columbia: Implications for the Early to Middle Jurassic Evolution of Stikinia. Tectonics, vol. 11, pp. 1266-1287.

McDonald, A.J., Lewis, P.D., Thomson, J.F.H., Nadaraju, G., Bartsch, R.D., Bridge, D.J., Rhys, D.A., Roth, T., Kaip, A., Godwin, C.I. and Sinclair, A.J. 1996. Metallogeny of an Early to Middle Jurassic Arc, Iskut River Area, Northwestern British Columbia. Economic Geology, vol. 91, pp. 1098-1114.

Nadaraju, G. 1993. Triassic-Jurassic Biochronology of the eastern Iskut River map area, northwestern British Columbia. M.Sc. thesis, Department of Earth and Ocean Sciences, University of British Columbia, Vancouver, B.C.

Nelson, J.L., Kennedy, R., Angen, J. and Newman, S. 2007. Geology of Terrace area. British Columbia Ministry of Energy, Mines and Petroleum Resources, Open File 2007-04.

Osadetz, K.G., Evenchick, C.A., Ferri, F., Stasiuk, L.D. and Wilson, N.S.F. 2003. Indications for effective Petroleum Systems in Bowser and Sustut Basins, North-Central British Columbia. *In:* Geological Fieldwork 2002. British Columbia Ministry of Mines, Energy and Petroleum Resources, Paper 2003-1, pp. 257-264.

Osadetz, K.G., Jiang, C., Evenchick, C.A., Ferri, F., Stasiuk, L.D., Wilson, N.S.F. and Hayes, M. 2007. Compositions and significance of crude oil stains in Bowser and Sustut basins (Intermontane Belt) British Columbia. Bulletin of Canadian Petroleum Geology, vol. 55, pp. 285-305.

O'Sullivan, P.B., Donelick, R.A., Osadetz, K.G., Evenchick, C.A., Ferri, F., Wilson, N.S.F. and Hayes, M. 2005. Apatite Fission-Track Data from seventy-one Bowser and Sustut Basin rock samples. Geological Survey of Canada, Open File 4840, 500 p.

Palfy, J., Mortensen, J.K., Smith, P.L., Friedman, R.M., McNicoll, V.J. and Villeneuve, M. 2000. New U-Pb zircon ages integrated with ammonite biochronology from the Jurassic of the Canadian Cordillera Canadian Journal of Earth Sciences, vol. 37, pp. 549-567.

Ricketts, B.D. and Evenchick, C.A. 1999. Shelfbreak gullies; products of sea-level lowstand and sediment failure: examples from Bowser Basin, northern British Columbia. Journal of Sedimentary Research, vol. 69, pp. 1232-1240.

Ricketts, B.D. and Evenchick, C.A. 2007. Evidence of different contractional styles along foredeep margins provided by Gilbert deltas: examples from Bowser Basin, British Columbia, Canada. Bulletin of Canadian Petroleum Geology, vol. 55, pp. 243-261.

Ricketts, B.D., Evenchick, C.A., Anderson, R.G. and Murphy, D.C. 1992. Bowser Basin, northern British Columbia: constraints on the timing of initial subsidence and Stikinia-North America terrane interactions. Geology, vol. 20, pp. 1119-1122.

Roth, T. 2002. Physical and chemical constraints on mineralization in the Eskay Creek Deposit, northwestern British Columbia; evidence from petrography, mineral chemistry, and sulfur isotopes. Ph.D. thesis, Department of Earth and Ocean Sciences, University of British Columbia, Vancouver, B.C.

Stasiuk, L.D., Evenchick, C.A., Osadetz, K.G., Ferri, F., Ritcey, D., Mustard, P.S. and McMechan, M.E. 2005. Regional thermal maturation and petroleum stage assessment using vitrinite reflectance, Bowser and Sustut basins, north-central British Columbia. Geological Survey of Canada, Open File 4945, 13 p.

Thomson, R.C., Smith, P.L. and Tipper, H.W. 1986. Lower to Middle Jurassic (Pliensbachian to Bajocian) stratigraphy of the northern Spatsizi area, north-central British Columbia. Canadian Journal of Earth Sciences, vol. 23, pp. 1963-1973.

Thorkelson, D.J. 1992. Volcanic and Tectonic Evolution of the Hazelton Group in the Spatsizi River (104H) map-area, North-Central British Columbia. Ph. D. thesis, Department of Earth Sciences, Carleton University, Ottawa, Ont.

Thorkelson, D.J., Mortensen, J.K., Marsden, H. and Taylor, D.C. 1995. Age and tectonic setting of Early Jurassic episodic volcanism along the northeastern margin of the Hazelton Trough, northern British Columbia. *In:* Miller, D.M., Busby, C.J. (Eds.), Jurassic magmatism and tectonics of the North American Cordillera. Geological Society of America, Special Paper 299, pp. 83-94.

Tipper, H.W., and Richards, T.A. 1976. Jurassic stratigraphy and history of north-central British Columbia. Geological Survey of Canada, Bulletin 270, 73 p.

Waldron, J.W.F., Gagnon, J.-F., Loogman, W. and Evenchick, C.A. 2006. Initiation and deformation of the Jurassic-Cretaceous Bowser Basin: implications for hydrocarbon exploration. *In:* Geological Fieldwork 2005. British Columbia Ministry of Energy, Mines and Petroleum Resources, Paper 2006-1, pp. 349-360.

Wheeler, J.O. and McFeely, P. 1991. Tectonic assemblage map of the Canadian Cordillera and adjacent parts of the United States of America Geological Survey of Canada, Map 1712A.

Woodsworth, G.J., Hill, M.L., and Van der Heyden, P. 1985. Preliminary geologic map of Terrace (NTS 103I East Half) map area, British Columbia. Geological Survey of Canada, Open File 1136.

Chapter 2: Revised stratigraphic framework of the Lower to Middle Jurassic Hazelton Group, northern Stikine Terrane, British Columbia[1]

2.1 Introduction

The Lower to Middle Jurassic Hazelton Group is the most widespread assemblage of volcanic rocks and associated sedimentary strata exposed in the Stikine terrane of northwestern British Columbia (figures 1.1 and 2.1). It is stratigraphically underlain by the Middle to Upper Triassic Stuhini Group and equivalent units of the Takla Group (e.g. Tipper and Richards 1976; Monger and Church 1977; Monger 1980; Grove 1986; Gunning 1986; MacIntyre et al. 1988; Alldrick et al. 1989), and the Lower Devonian to Upper Permian Stikine assemblage (e.g. Monger 1977; Stevens and Rycerski 1989; Brown et al. 1991; McClelland 1992; Logan et al. 2000; Diakow 2001). These two older stratigraphic packages contain volcanic arc rock characterized by juvenile Sr and Nd isotopic signatures, suggesting that the Stikine terrane has Paleozoic arc basement (Gabrielse et al. 1980; Armstrong 1988; Samson et al. 1989, 1991). The Hazelton Group constitutes the youngest and most voluminous volcanic phase of the long-lived Stikine volcanic arc. Economically, specific stratigraphic intervals of the Hazelton Group are associated with polymetallic massive sulphide deposits (Alldrick 1993; Barrett and Sherlock 1996; McDonald et al. 1996; Roth et al. 1999; Sherlock et al. 1999; Barresi and Dostal 2005; Wojdak and Febbro 2009) and potential petroleum source units (Evenchick et al. 2003, 2005; Ferri et al. 2004; Ferri and Boddy 2005; Osadetz et al. 2007).

The wide variety of rock types combined with the lack of continuous exposure around the periphery of the Bowser basin are the greatest impediments to a complete understanding of the depositional history of the Hazelton Group. In addition, these rocks have been described in great detail by numerous authors in different areas, leading to overlaps and inconsistencies in stratigraphic nomenclature. This paper attempts to evaluate potential correlations of mappable lithostratigraphic units at the regional scale by comparing multiple sections measured in the field and available in the literature. Existing stratigraphic nomenclature of the Hazelton Group is reviewed first in order to emphasize its inherent complexity and to highlight inconsistencies and contradictions (figure 2.2). New paleontological data and measured sections are then presented by

[1] *A version of this chapter will be published under the authorship of Gagnon, J.-F., Barresi, T., Waldron, J.W.F., Nelson, J.L., Poulton, T.P., Cordey, F. and Heaman, L.M.*

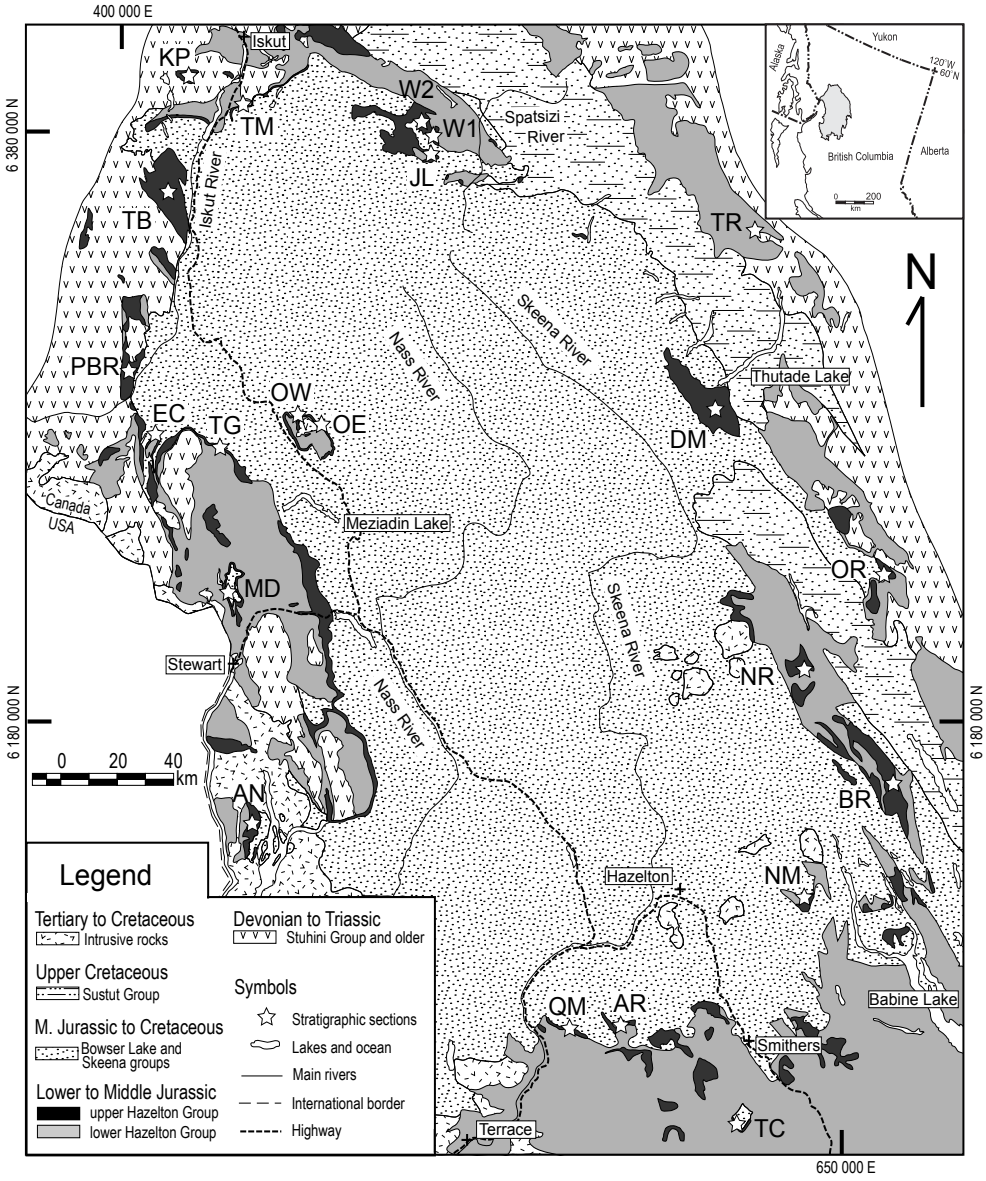

Figure 2.1: Simplified geology map showing the distribution of the Hazelton Group rocks on the periphery of the Bowser Basin. Location of stratigraphic sections include: AN-Anyox; AR-Ashman Ridge; BR-Bait Range; DM-Diagonal Mountain; EC-Eskay Creek; JL-Joan Lake; KP-Klastine Plateau; MD-Mount Dilworth; NM-Netalzul Mountain; NR-Nilkitkwa Range; OE-Oweegee East; OR-Omineca Range; OW-Oweegee West; PBR-Pillow Basalt Ridge; QM-Quinlan Mountain; TB-Table Mountain; TC-Tenas Creek; TG-Treaty Glacier; TM-Todagin Mountain; TR-Toodoggone River; W1-Mount Will 1; W2-Mount Will 2. Universal Transverse Mercator Projection in NAD 83 Datum. Modified from Alldrick et al. (2006) and Evenchick et al. (2009). Inset shows the location of the Bowser basin (grey) in British Columbia, Canada.

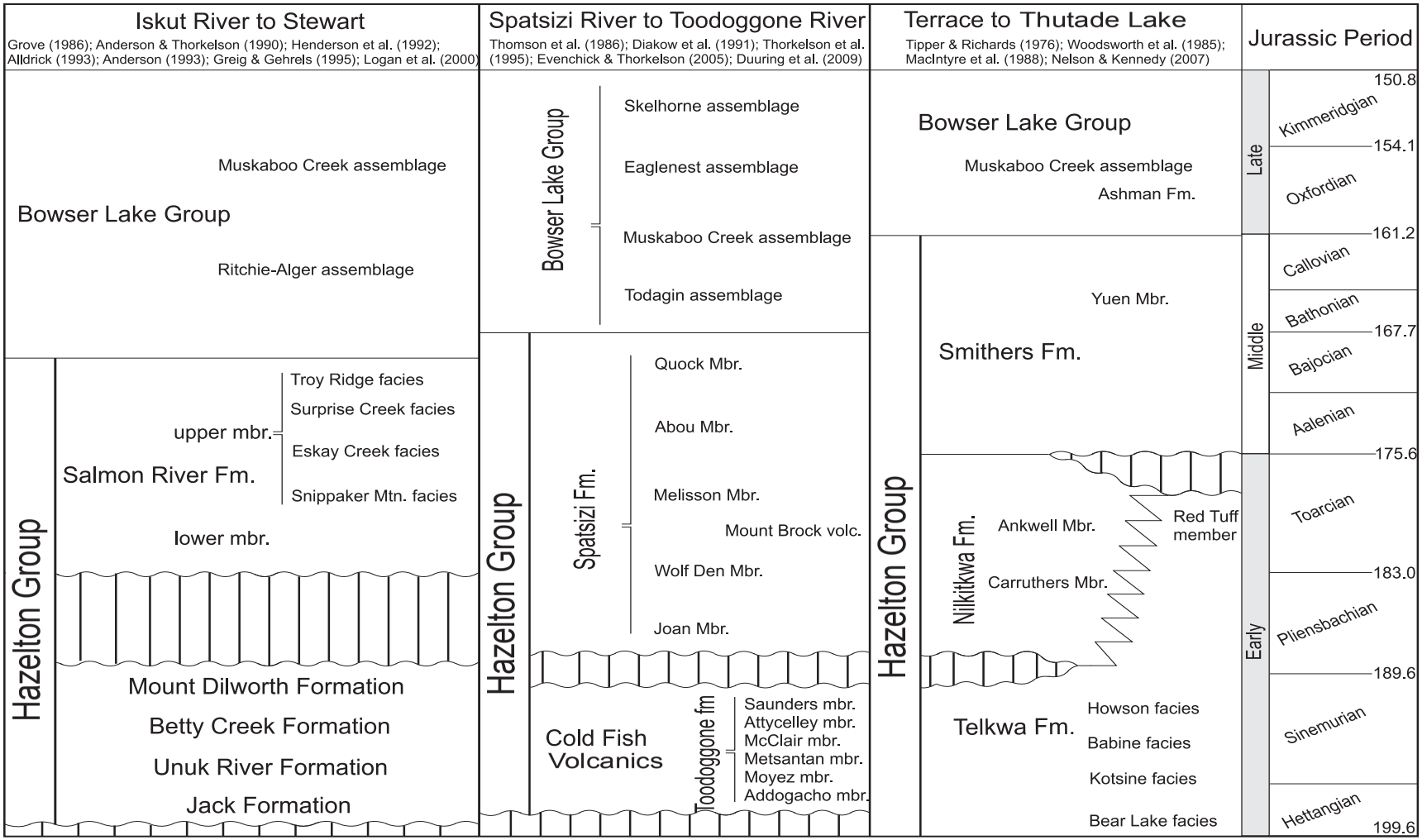

Figure 2.2: Summary of the current nomenclature for the Hazelton Group in north-cenral British Columbia. The inherent complexity in the terminology used to describe the units of the Hazelton Group stems from the existence of three independent stratigraphic frameworks each related to a limited geographic area.

geographical areas. Where appropriate, new formal stratigraphic names are proposed and ambiguous units are either revised or abandoned. By doing so, we hope to highlight the main stratigraphic packages within the Hazelton Group, defined by significant lithological changes or important stratigraphic boundaries; and based on these design a revised classification that can be applied at the regional scale.

2.2 Previous work on the stratigraphy of the Hazelton Group

The term Hazelton Group was first introduced by Leach (1910) to describe an assemblage of Jurassic volcanic and sedimentary rocks exposed in north-central British Columbia. It replaced in part the broader term "Porphyrite Group" previously proposed by Dawson (1877). Leach (1910) described the basal units of the Hazelton Group as andesitic flows, tuffs and agglomerates that pass northward in a gradual transition to sedimentary rocks near the town of Hazelton (figure 2.1). In the following decades, the Hazelton Group was subject to various minor modifications (e.g. Hanson 1925; Armstrong 1944; Duffell and Souther 1964). However, even with these refinements, the Hazelton Group remained an imprecise term in which diverse poorly constrained stratigraphic units were commonly included due to the lack of precise age control. Important clarifications of the Hazelton Group came from Tipper and Richards (1976), who completely redefined the Jurassic nomenclature of north-central British Columbia. They established the first regional stratigraphic framework of the Hazelton Group and divided it into various formations and members (figure 2.2).

In the Terrace to Thutade Lake area (figure 2.1), Tipper and Richards (1976) and Woodsworth et al. (1985) used the term Telkwa Formation to describe an extensive Sinemurian to Upper Pliensbachian andesitic volcanic succession. Basaltic to rhyolitic lava and pyroclastic rocks of similar age have subsequently been correlated with the Telkwa Formation in the Babine Lake area (MacIntyre et al. 1988, 1997) and further south (Diakow and Mihalynuk 1987). The Telkwa Formation is divided in four distinct facies (i.e. Howson, Babine, Kotsine and Bear Lake), which record lateral variations between subaerial and marine deposition (Tipper and Richards 1976). In Early Pliensbachian time, widespread calc-alkaline volcanism of the Telkwa Formation was replaced by restricted marine sedimentation of the Nilkitkwa Formation. Thick sections of shale and siltstone accumulated in the central portion of the northwest–trending Hazelton trough, punctuated by two episodes of mafic volcanism (recorded in the Carruthers and Ankwell members) (Tipper and Richards 1976). In the Toarcian, an extensive bright red pyroclastic unit was deposited on the periphery of the trough. This unit (Red Tuff member) was originally interpreted as a subaerial equivalent of the

contemporaneous Ankwell member by Tipper and Richards (1976). However, recent mapping by Nelson and Kennedy (2007) included the Red Tuff member at the top of the Telkwa Formation, as no discernable break occurs between it and the main volcanic phase of the Telkwa. A U-Pb date of ca. 178 Ma (Late Toarcian) was obtained from the top of this unit (T. Barresi and R. Friedman, unpublished data 2010) (figure 2.2).

The uppermost formation of the Hazelton Group, as previously defined in central British Columbia, consists of limy sandstone and tuffaceous siltstone of the Smithers Formation. Extensive collections of marine fossils suggest that the Smithers Formation ranges in age from Middle Toarcian to Early Callovian (e.g. Tipper and Richards 1976; Poulton and Tipper 1991; Johnston 2002). In the northeastern part of the Hazelton trough, Tipper and Richards (1976) also described a distinctive unit of interbedded argillite and ash-fall tuff near the top of the Smithers Formation, which they named the Yuen Member.

Northwest of Thutade Lake, in the Spatsizi River area (figure 2.1), the lowermost units of the Hazelton Group are known informally as the Griffith Creek volcanics (Thorkelson 1992; Thorkelson et al. 1995). They consist mostly of Hettangian to Lower Sinemurian intermediate lavas and clastic sedimentary rocks (Marsden and Thorkelson 1992). The succession disconformably overlies the Stuhini Group, as suggested by a basal heterolithic conglomerate containing Permian and Triassic limestone clasts (Thorkelson 1988). The overlying Cold Fish Volcanics are separated from the Griffith Creek volcanics and older rocks by an angular unconformity (Thorkelson et al. 1995; Evenchick and Thorkelson 2005). They consist of a bimodal felsic-mafic succession of basaltic flows, felsic sills and tuffaceous rocks predominantly deposited in a subaerial environment (Thorkelson 1992, Thorkelson et al., 1995). Although the Cold Fish Volcanics were previously regarded as Lower Pliensbachian (Thorkelson et al. 1995), recent improvement in the geological timescale (Gradstein et al. 2004) suggests that all the U-Pb zircon ages (ca. 192–196 Ma) obtained by Thorkelson et al. (1995) are in fact Sinemurian.

Contemporaneous volcanism to the Cold Fish Volcanics was also reported 50 km east of the Spatsizi River area in the Toodoggone River area (figure 2.1). There, a thick succession of subaerial volcanic rocks of intermediate composition is informally known as the Toodoggone formation, which consists of seven members (figure 2.2) (e.g. Carter 1972; Marsden 1990; Diakow et al. 1991). Toodoggone volcanism is constrained by K-Ar, Ar-Ar and U-Pb isotopic dating to two major cycles spanning approximately 11 m.y. (ca. 201–190 Ma) (Diakow 2001, 2006; Dickinson 2006; Duuring et al. 2009).

Above the Cold Fish Volcanics rests a 700 m thick Pliensbachian to Bajocian sedimentary succession named the Spatsizi Group by Thomson et al. (1986). Based on

biostratigraphic and lithostratigraphic observations, Thomson et al. (1986) concluded that the Spatsizi Group was sufficiently distinct from the underlying Cold Fish Volcanics to be treated as a separate entity from the Hazelton Group. However, other authors (Marsden and Thorkelson 1992; Evenchick and Thorkelson 2005) pointed out that such exclusion was problematic because it contradicts the widely accepted Tipper and Richards' (1976) definition of the Hazelton Group further south as a "widespread assemblage of volcanic rocks, sedimentary rocks and their tuffaceous equivalents deposited in Early to Middle Jurassic time". It also made regional correlations even more difficult, as other clastic-dominated sedimentary successions located at a similar stratigraphic level (e.g. Smithers, Nilkitkwa and Salmon River formations) have traditionally been assigned formation status within the Hazelton Group. These arguments led Evenchick and Thorkelson (2005) to propose a demotion of the Spatsizi Group to the Spatsizi Formation (and consequently its formations to members) in order to avoid inconsistencies in regional nomenclature. Treating the Spatsizi strata as a formation inside the Hazelton Group has the advantage of making correlation of regional stratigraphic markers clearer. Thus, the Spatsizi Formation is divided into five distinct members (Thomson et al. 1986; Evenchick and Thorkelson 2005), listed here in stratigraphic order from oldest to youngest (figure 2.2):

1. Fossiliferous coarse-grained limy sandstone and siltstone of the Joan Lake Member (Lower Pliensbachian);
2. Recessive mudstone of the Wolf Den Member (Upper Pliensbachian to Middle Toarcian);
3. Fine-grained sandstone and siltstone of the Melisson Member (Middle Toarcian);
4. Calcareous to siliceous organic shale of the Abou Member (Upper Toarcian to Aalenian);
5. Thinly bedded siliceous shale and air-fall tuff of the Quock Member (Lower Bajocian);

Correlative sedimentary rocks to the Spatisizi Formation have also been reported in the Toodoggone River area, where Toarcian calcareous volcanic sandstone disconformably overlies the uppermost trachydacite ash-flow tuff (Saunders member) of the Toodogoone volcanic section (Diakow et al. 1991; Marsden and Thorkelson 1992).

In the Iskut River area (figure 2.1), the Hazelton Group has traditionally been divided into five distinct formations (figure 2.2). The lowest unit exposed consists of a fining-upward sedimentary sequence characterized by an interval of heterolithic pebble to cobble conglomerate at the base, overlain by calcareous sandstone and siltstone which yielded Hettangian to Sinemurian marine fossils (Henderson et al. 1992; Nadaraju 2003). In the Sulphurets area, this unit has been assigned to the Jack Formation and rests

unconformably on the underlying Triassic rocks of the Stuhini Group (Henderson et al. 1992). Basal sedimentary rocks of the Jack Formation are stratigraphically overlain by andesitic volcanic breccia and lesser sedimentary rocks of the Unuk River Formation (Grove 1986; Anderson and Thorkelson 1990). Correlative intrusive rocks of the Premier porphyry yielded a U-Pb zircon age of 194.8 +/- 2 Ma (Alldrick et al. 1987), which corresponds to a Sinemurian age. The Unuk River Formation is disconformably to conformably overlain by andesitic maroon to green volcanic breccia, lahar, lava and tuff of the Betty Creek Formation (Grove 1986; Anderson and Thorkelson 1990). Above the Betty Creek Formation is the widespread Mount Dilworth Formation, a relatively thin unit composed of dacitic pyroclastic tuff dated at ca. 192–189 Ma (Alldrick et al. 1989; Anderson 1993). Lithostratigraphically equivalent felsic volcanic rocks in the Oweegee, Cambria and Kinskuch areas yielded significantly older U-Pb zircon ages (ca. 196–199 Ma), suggesting that widespread felsic volcanism was diachronous on the western edge of the Hazelton arc (Greig and Gehrels 1995). An apparent Pliensbachian to Toarcian hiatus separates those felsic volcanics from the overlying Salmon River Formation (Anderson 1993; Greig and Gehrels 1995). The Salmon River Formation includes a lower member of coarse-grained calcareous sandstone with abundant Toarcian marine fossils, and an upper member divided into four facies: siltstone, mudstone and sandstone of the Surprise Creek facies; thinly interbedded dark cherty shales and light-coloured ash-tuffs (informally known as “pyjama beds”, a term coined by Howard Tipper in the late 1980’s to describe their “pinstriped” appearance) of the Troy Ridge facies; felsic and mafic pillow lavas of the Eskay Creek facies, and a possibly correlative andesitic unit known as the Snippaker Mountain facies (e.g. Anderson and Thorkelson 1990; Evenchick et al. 1992; Anderson 1993). Aalenian to Early Bajocian ages from radiolarian microfossils were reported from the mineralized unit at the Eskay Creek mine (Nadaraju 1993) (figure 2.1) and multiple U-Pb zircon ages ca. 181–173 Ma (McDonald et al. 1996) suggest that the upper member could range as old as Late Toarcian.

A recently enlarged geochronological and biostratigraphic database for the Hazelton Group in the Iskut River area provided significant improvements on the age constraint of the stratigraphic units described above (e.g. Lewis et al. 1993; McDonald et al. 1996; Logan et al. 2000). The revised stratigraphic framework includes five lithostratigraphic units which consist of:

1. Basal coarse clastic unit containing fossiliferous sandstone and trough cross-stratified conglomerate, roughly equivalent to the Jack Formation. Fossil ages range from Hettangian to Sinemurian;
2. Andesitic volcanic flows and breccias, maroon to green volcaniclastic sandstone

and conglomerate and lapili to block tuff, similar to the Betty Creek and Unuk River formations. U-Pb zircon ages in the range of ca. 193–195 Ma;

3. Dacitic domes and flows with rhyolitic welded tuff that yielded U-Pb zircon ages from 186.5 +/- 1.0 to 194 +/- 3 Ma (probably including equivalents of the Mount Dilworth Formation).
4. Bioclastic calcareous siltstone and tuffaceous sandstone roughly equivalent to the lower member of the Salmon River Formation. Fossil collections range from Late Pliensbachian to Late Aalenian;
5. Bimodal volcanic rocks including pillow basalt flows, rhyolite flows, hyaloclastite, dacitic tuff and interstratified siliceous mudstone and tuffaceous siltstone ("pyjama beds"); these units are generally equivalent to the upper member of the Salmon River Formation with U-Pb zircon ages from ca. 181-173 Ma and Aalenian to Bajocian fossil collections.

In all the areas mentioned above, uppermost sedimentary clastic rocks of the Hazelton Group (e.g. Smithers, Spatsizi and part of Salmon River formations) are conformably overlain by an assemblage of mudstone, siltstone, sandstone and chert-pebble conglomerate of the Bowser Lake Group (BLG) (figure 2.2). At the southeastern margin of the basin, Tipper and Richards (1976) originally assigned Upper Bajocian to Middle Oxfordian clastic rocks to the Ashman Formation, and included this unit in the BLG. However, recent mapping by Evenchick et al. (2007, 2008a, 2008b) identified "pyjama beds" that were mapped as part of the Ashman Formation, and therefore included in the BLG by Tipper and Richards (1976) largely based on their paleontological content. Similar conclusions were also drawn by Gagnon and Waldron (2008) at the type section (Ashman Ridge) where Tipper and Richards (1976) included both "pyjama beds" and overlying clastic rocks characteristic of the Muskaboo Creek assemblage of the BLG (Evenchick and Thorkelson 2005) as part of the Ashman Formation. Consequently, the term Ashman Formation has been abandoned and beds previously assigned to the latter were either reassigned to one of the BLG lithofacies assemblages defined by Evenchick and Thorkelson (2005), or to the upper Hazelton Group based on the absence or presence of tuffs (Evenchick et al. 2007, 2008a, 2008b, *submitted*).

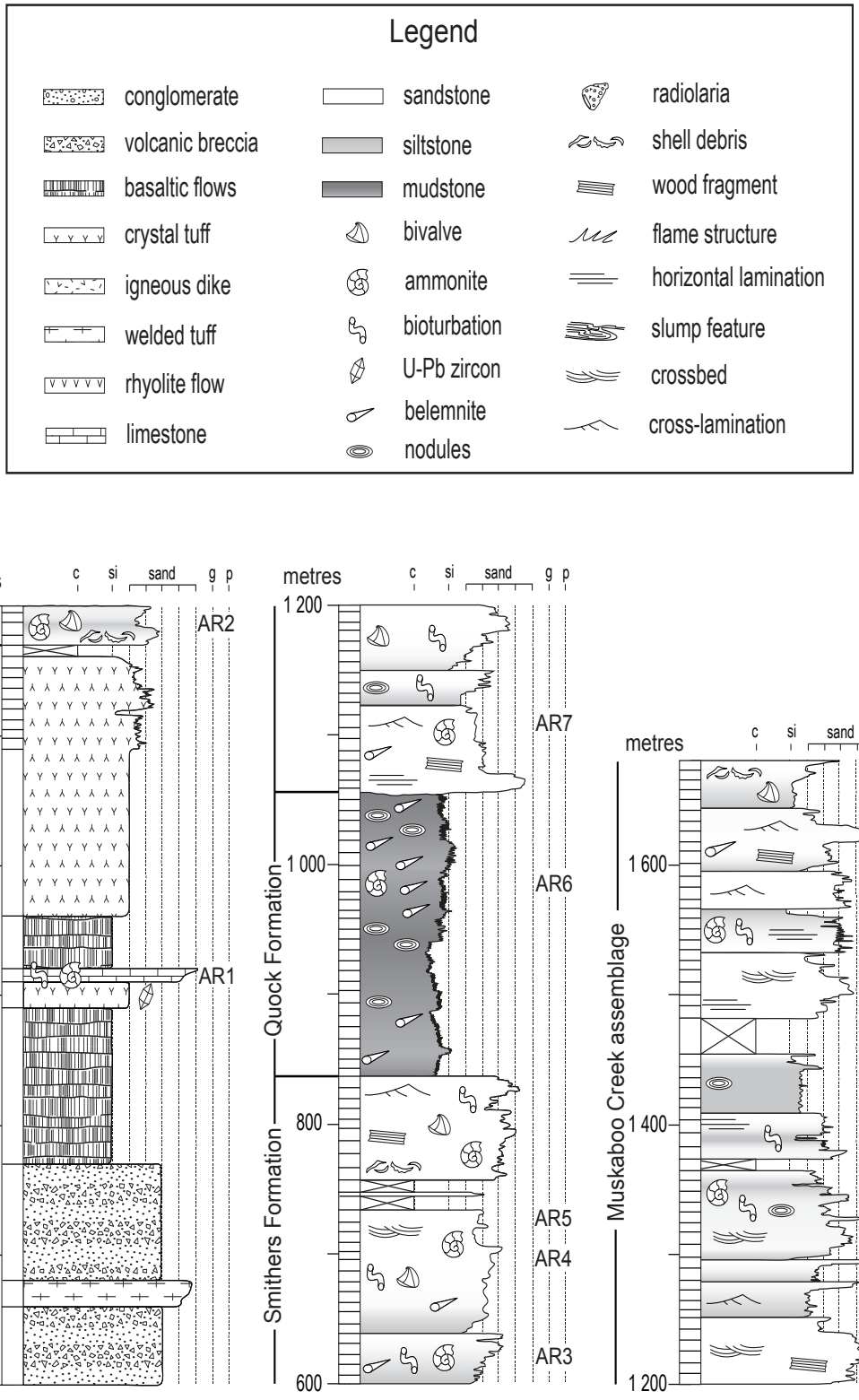

Figure 2.3: Detailed measured section at Ashman Ridge (AR) showing the different lithological units and grain size variation. Descriptions of fossil localities (AR1-AR10) are given in Appendix A.

2.3 New measured sections

2.3.1 Terrace to Thutade Lake area

2.3.1-1 Ashman Ridge

Ashman Ridge is located approximately 45 km west of Smithers (figure 2.1). The section was originally described as a part of a project involving regional stratigraphic mapping of north-central British Columbia by Tipper and Richards (1976), who defined the Ashman Formation of the BLG and proposed Ashman Ridge as the type section. Stratigraphically lower units of the Hazelton Group are also well exposed along the section and provide a complete record of the changing depositional environment. Figure 2.3 shows the different lithostratigraphic units identified in this study and the stratigraphic positions of fossil localities (Tipper and Richards 1976; Palfy and Schmidt 1994; Johnston 2002). Complete paleontological information for each fossil collection in the measured sections is given in Appendix A.

The lowest stratigraphic units exposed at Ashman Ridge consist of amygdaloidal andesitic to dacitic flows and associated pyroclastic rocks (figure 2.3). These rocks were assigned to the Howson subaerial facies of the Telkwa Formation by Tipper and Richards (1976). The volcanic flows identified in the section are typically 5 to 15 m thick, and autobrecciated near their top. Most flows are aphanitic, but the section contains lesser amounts of feldspar-phyric andesite. The presence of highly indurated ignimbrite containing flattened pumice suggests that these volcanic rocks were mostly deposited in a subaerial environment. Recently, Palfy et al. (2000) obtained a minimum U-Pb age of 192 Ma on discordant zircon fractions collected from an andesitic tuff located at 295 m on the section.

There is a good correlation between this isotopic age and overlying Upper Sinemurian ammonites reported from a bioclastic sandstone located at 325 m on the section (Tipper and Richards 1976; Palfy and Schmidt 1994). The asteroceratid-bearing layer immediately overlies a 10 m thick light grey limestone. The fossiliferous packstone contains well preserved silicified burrows, algal oncoids and ooids indicating deposition in a relatively warm subtidal environment (figures 2.4A, B). These marine sedimentary rocks are capped by a 40 m thick rusty-weathered vesicular basalt flow with epidote-bearing quartz veins.

The uppermost volcanogenic unit of the section consists of at least 200 m of maroon to bright red fine-grained crystal-lithic tuff. It comprises well-bedded and non-welded ash flow tuff, poorly sorted rubbly lapilli tuff and lahar. Rounded bombs up to

30 cm in diameter are common and indicate deposition in a predominantly subaerial environment. Tipper and Richards (1976) previously assigned this unit to the Red Tuff Member of the Nilkitkwa Formation. Because no clear lithological boundary can be established with the underlying andesitic volcanics, these oxidized pyroclastic rocks are here included as the uppermost unit in the Telkwa Formation. This is consistent with mapping relationships established by Woodsworth et al. (1985) and Nelson and Kennedy (2007) in the Terrace area.

Volcanic rocks of the Telkwa Formation are disconformably overlain by tuffaceous sandstone and siltstone of the Smithers Formation (figures 2.3 and 2.4C). A high concentration of volcanic-derived clasts in the tuffaceous sandstone suggests recycling of the underlying pyroclastic rocks. The Smithers Formation mostly comprises medium to fine-grained greenish-brown sandstone with abundant marine fauna including belemnites, gastropods, solitary scleratinian corals, ammonoids and a wide variety of ornate bivalves such as *Myophorella* sp. (figure 2.4D). At Ashman Ridge, the Smithers Formation ranges from Lower Bajocian to Bathonian. Bioturbation is pervasive and tends to be particularly well displayed in beds of green chlorite-rich sandstone. Common ichnogenera include *Teichichnus, Cylindrichnus, Rosselia, Planolites and Chondrites*. The abundant faunal assemblage, biogenic traces typical of the *Cruziana* ichnofacies and common occurrence of wave-generated sedimentary structures suggest deposition in a lower shoreface environment (see Chapter 3).

Fossiliferous calcareous sandstone of the Smithers Formation is conformably overlain by thinly-bedded blocky dark grey siliceous mudstone with recessive laminations, typically only millimetres to a few centimetres thick, of pale orange-weathered ash tuff ("pyjama beds"). These units were originally mapped as Ashman Formation of the BLG by Tipper and Richards (1976), but are assigned (below) to the revised Quock Formation; this is consistent with the recent inclusion of the "pyjama beds" as part of the undivided upper Hazelton Group by Evenchick et al. (*submitted*). "Pyjama beds" contrast with the underlying sandstones; they lack abundant bivalves, show only sparse bioturbation and are significantly finer grained. The contact is easily mappable on the ridge over a short interval. Well-preserved Early Callovian ammonites, including *Kepplerites* sp. aff. *K. mclearni* Imlay, were collected approximately 66.5 m below the top of the thinly-bedded unit (AR6 in figure 2.3). Belemnites and calcareous concretions are abundant in the upper half of this unit, which totals 220 m in thickness. The fine grain size, laterally continuous bedding, and lack of current-generated structures indicate that the "pyjama beds" accumulated mostly from suspension.

The siliceous fine-grained succession is overlain with a sharp boundary by

brown and white-weathering arkosic sandstone and finely laminated siltstone of the Bowser Lake Group. The contact is apparently conformable though it is offset 10 m in a dextral sense along a steep fault close to the point where it crosses the crest of the ridge. Hummocky-cross stratification, trough cross-bedding and climbing ripples are common sedimentary structures in the sandstone beds. Abundant ammonite fauna throughout the unit indicate a Middle Callovian to Early Oxfordian depositional age (Tipper and Richards 1976; Evenchick et al. *submitted*). Continuous exposure along the ridge enabled us to measure up to 615 m of Middle to Upper Jurassic sedimentary strata and no significant overall lithological change was observed.

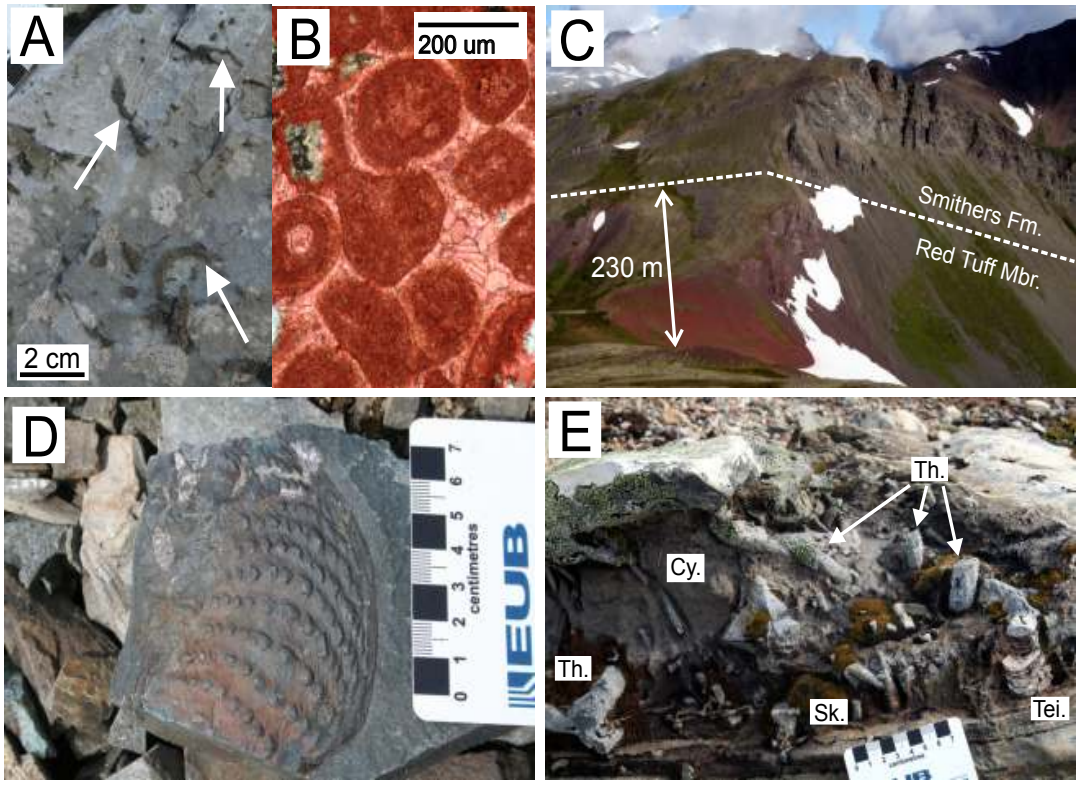

Figure 2.4: Photographs of distinctive lithological characteristics of units exposed at Ashman Ridge and Quinlan Mountain. A) Outcrop view of silicified burrows (arrows) in a fine-grained oolitic limestone of the Telkwa Formation (located at ~320 m in figure 2.3). B) Stained photo-micrograph of the limestone unit in cross-polarized light showing concentric layers of coated grains (oolites), and the recrystalized calcite cement (sparite). C) Stratigraphic contact at Ashman Ridge between the subaerial crystal lithic tuff (Red tuff member) of the Telkwa Formation and the thickly bedded fossiliferous siltstone and sandstone of the Smithers Formation. D) *Trigoniid* bivalve (*Myophorella* sp.) of the Smithers Formation (located at ~575 m in figure 2.3). These thick-shelled bivalves are interpreted to represent a shallow-marine depositional environment. E) Bioturbated fine-grained tuffaceous sandstone of the Smithers Formation at Quinlan Mountain (located at 135 m in figure 2.6A). The high diversity and abundance of traces are indicative of the Cruziana ichnofacies. Identified traces include: *Skolithos* (Sk); *Teichichnus* (Tei); *Cylindrichnus* (Cy) and *Thalassinoides* (Th). Scale bar in cm.

2.3.1-2 Quinlan Mountain

The Quinlan Mountain section is located 50 km northeast of Terrace (figure 2.1). It contains stratigraphic units laterally equivalent to those exposed at Ashman Ridge, with minor differences. A detailed geology map of the area is shown in figure 2.5. The lowermost stratigraphic unit exposed at Quinlan Mountain consists of a non-welded maroon to brick-red dacitic crystal-lithic ash tuff of the Telkwa Formation (figure 2.6A). The interpreted age of this unit is ca. 178 Ma based on a concordant U-Pb zircon population (T. Barresi and R. Friedman, unpublished data 2010). Euhedral white plagioclase crystals are the most common mineral present in the very fine-grained glass matrix. Abundant pyroclastic bombs 30 to 50 cm in diameter occasionally display distorted concentric layering, probably related to rapid compaction when the material was still in a partly molten state.

The subaerial volcanic rocks of the Telkwa Formation are disconformably overlain by 265 m of siliciclastic sedimentary rocks of the Smithers Formation (figure 2.6A). The basal layer consists of a 10 m thick, clast-supported monolithic conglomerate. The granule to pebble clasts are generally well sorted, moderately to well rounded and consist of white, silicified crystal-lithic dust tuffs. Their rhyolitic composition differs drastically from the underlying bright red andesitic to dacitic pyroclastics, which suggests that they were not locally derived. The conglomerate rapidly fines upward into interbedded limy sandstone and tuffaceous siltstone containing abundant marine fossils. Well-preserved ammonoids and bivalves collected immediately above the conglomerate unit yielded a Middle Aalenian age, and Early Bajocian fauna occur higher in the section. Bioturbation is also common in the finer-grained sedimentary strata and includes a high diversity assemblage of *Teichichnus*, *Planolites*, *Cylindrichnus*, *Ophiomorpha*, *Paleophycos*, *Skolithos*, *Rosselia, Thalassinoides* and *Chondrites* (figure 2.4E). The Smithers Formation gradually fines upward into grey siltstone and shale near the top, where shallow water fauna become less abundant.

The Smithers Formation is conformably overlain by 120 m of thinly bedded dark siliceous mudstones and pale orange ash tuffs (“pyjama beds”) currently mapped as units of undivided upper Hazelton Group (Evenchick et al. 2008a) and assigned (below) to the revised Quock Formation of the Hazelton Group (figure 2.6A). Even though radiolarian samples were recovered from various mudstone units within the “pyjama beds”, their state of preservation was too poor to allow precise identification. A fossil collection located near the base of the unit yielded Lower Callovian ammonites (QM7 in figure 2.6A). Isolated very fine-grained limestone beds suggest that the environmental conditions were above the carbonate compensation depth. Occasional monospecific

assemblages of *Chondrites* traces could be attributed to dysaerobic bottom water conditions (Bromley and Ekdale 1984).

The uppermost stratigraphic unit preserved at Quinlan Mountain consists of laminated bluish-grey, medium to very fine-grained sandstone and siltstone (figure 2.6A). These rocks were mapped as BLG by Evenchick et al. (2008a). The dark grey siltstone beds are fissile and show a strong fabric, which is significantly different from the blocky habit of the underlying siliceous "pyjama beds". Individual layers are normally graded and show incomplete Bouma sequences with abundant biogenic reworking in the uppermost T_E subdivision. The ichnological suite in the turdidite deposits includes traces such as *Asterosoma*, *Chondrites*, *Planolites*, *Zoophycos*, *Teichichnus*, *Phycosiphon* and *Cosmorathes*, which corresponds to a distal *Cruziana* ichnofacies of medial type diversity. Lower Oxfordian fossils were recovered approximately 300 m above the base of the Bowser Lake Group.

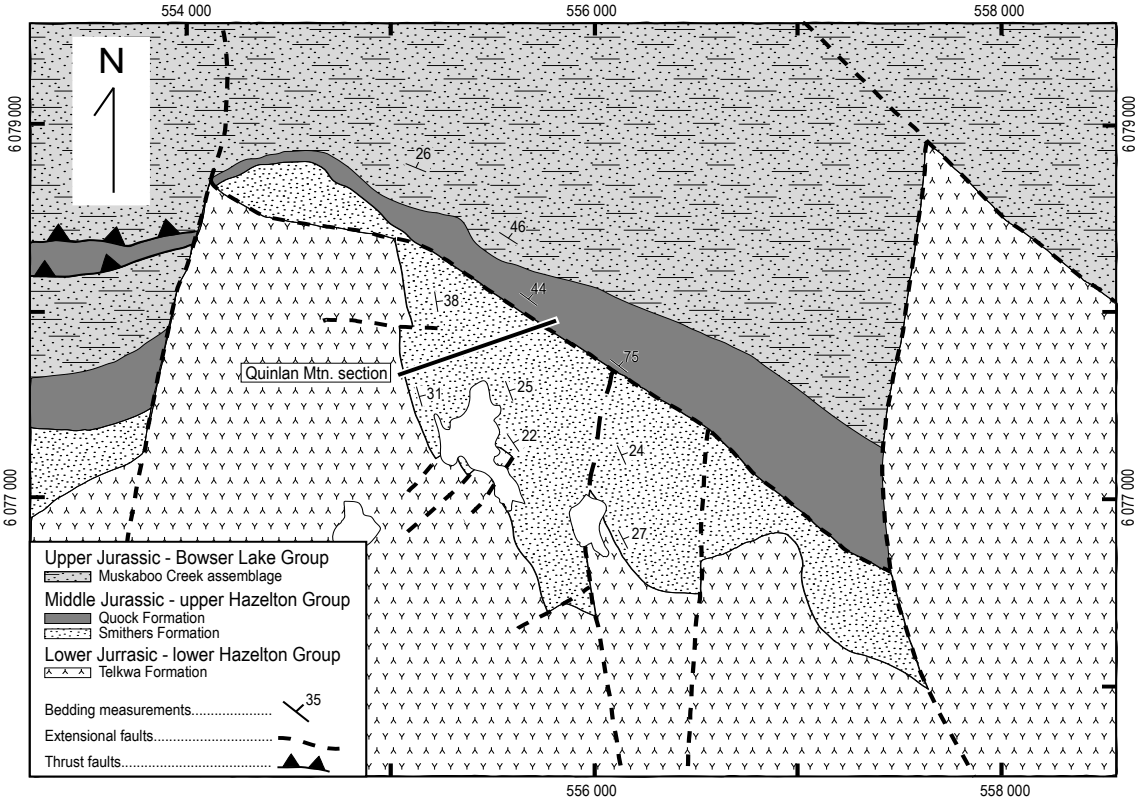

Figure 2.5: Simplified geology map of the Quinlan Mountain area showing the location of the unit stratotype of the Smithers Formation. Universal Transverse Mercator Projection in NAD 83 Datum. Modified from Nelson et al. (2007).

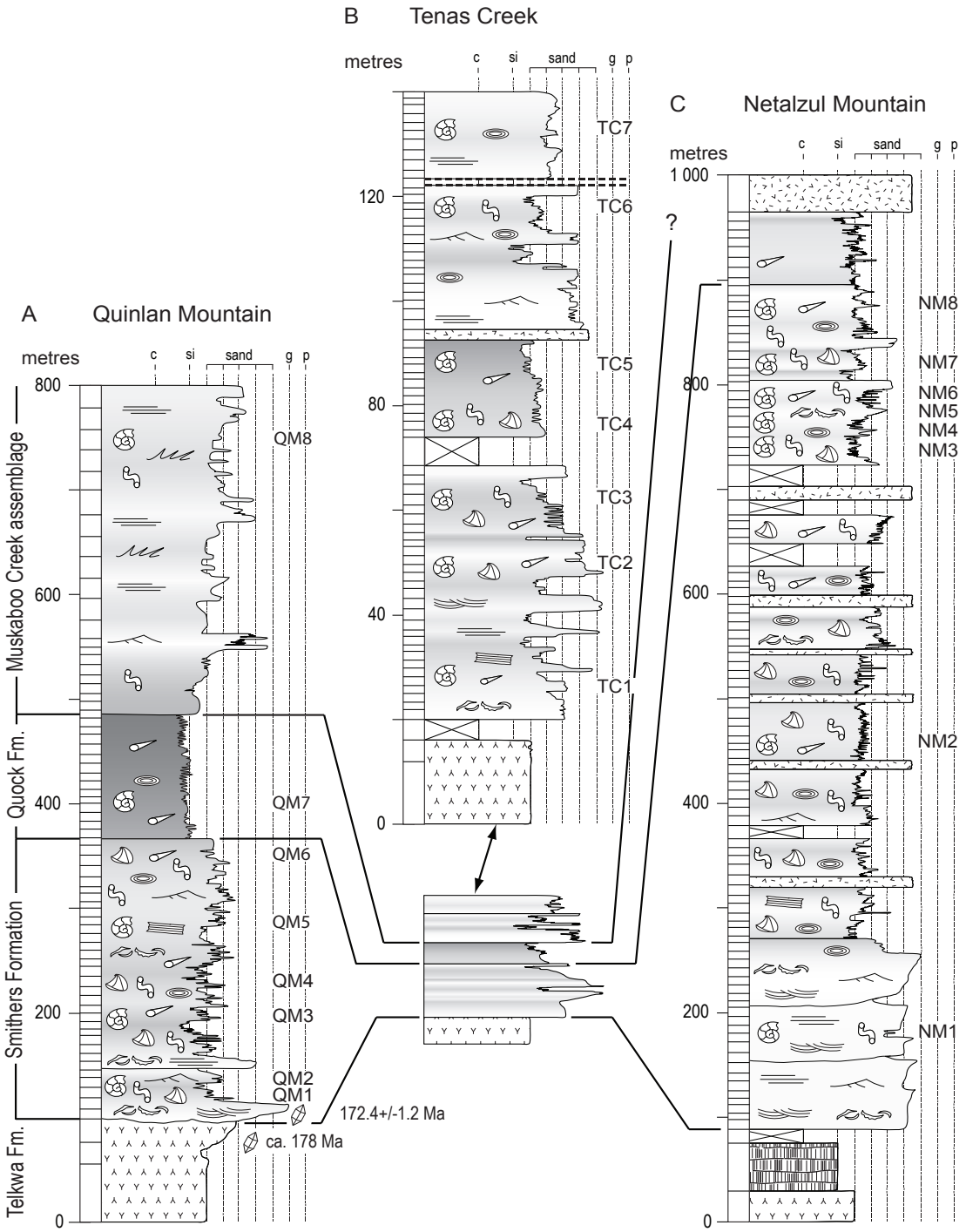

Figure 2.6: Detailed measured sections in the Terrace to Smithers area south of the Bowser basin. A) Quinlan Mountain (unit stratotype of the Smithers Formation). B) Tenas Creek. C) Netalzul Mountain. Each section is characterized by the same stratigraphic succession, which contains four lithostratigraphic units: crystal-lithic tuff and intermediate flows (Telkwa Formation); fossiliferous and bioturbated tuffaceous sandstone and siltstone (Smithers Formation); blocky, thinly bedded siliceous mudstone and tuff (here assigned to the Quock Formation); overlying siliciclastic rocks of the Muskaboo Creek assemblage (Bowser Lake Group). See figure 2.3 for legend details and figure 2.1 for geographic locations.

2.3.1-3 Tenas Creek

The Tenas Creek section is located 30 km south of the town of Smithers (figure 2.1). It was first measured by Tipper and Richards (1976) who provided detailed lithological and paleontological data. The section is exposed in a northerly-plunging syncline crosscut by numerous NE–SW extensional faults and dykes. Despite the structural complexities in the area, lithostratigraphic units were identified based on mappable contacts and correlated with regional stratigraphic units. Volcanogenic rocks of the Telkwa Formation are well exposed on the west-facing ridge above Tenas Creek. They consist of medium to thickly-bedded pyroclastic breccias, agglomerates and plagioclase-phyric dust tuffs. The abundance of bombs and accretionary lapilli throughout the Telkwa Formation suggests deposition in a subaerial environment proximal to a volcanic edifice.

The overlying sedimentary succession (figure 2.6B) is only 140 m thick but is stratigraphically similar to the sections described at Ashman Ridge and Quinlan Mountain. Bioturbated greenish-grey spotted sandstones of the Smithers Formation contain a diversified assemblage of marine fossils which yielded Upper Bajocian to Upper Bathonian ammonites (Tipper and Richards 1976; Johnston 2002, this paper). The Smithers Formation is conformably overlain by a 25 m interval of hard, blocky siliceous mudstone interbedded with millimetre-thick beige-weathering ash tuffs. The sporadic occurrence of heavily bioturbated light green medium siltstone beds in the basal 10 m of the "pyjama beds" unit suggests that the lower contact is gradational with the underlying Smithers Formation. The section is interrupted by an intermediate dyke at 92 m, above which coarse-grained tuffaceous sandstones of the BLG are exposed in medium to thick beds. Ammonite collections below and above a fault located at 123 m yielded Lower to Middle Callovian ammonites (Tipper and Richards 1976; Johnston 2002). Thickness of the BLG at Tenas Creek cannot be estimated due to an apparent tectonic offset, but is certainly greater than 300 m.

2.3.1-4 Netalzul Mountain

The section exposed south of Netalzul Mountain is the easternmost new stratigraphic section described in this study. It is located 55 km northeast of the town of Smithers and exposed along a faulted contact with the Oxfordian intermediate volcanic rocks of the Netalzul Formation (Evenchick et al. 2008b; Bourgault 2009). Lower Jurassic volcanic rocks of the Telkwa Formation are the stratigraphically lowermost units exposed in the hanging wall of the fault. They consist of at least 450 m of interbedded brick-red feldspar-phyric fragmental ash tuffs and vesicular intermediate volcanic flows;

only the uppermost 75 m are included in the section (figure 2.6C). The contact with the overlying Smithers Formation was not observed in the field due to extensive Quaternary cover, but map relationships suggest that it may be disrupted by a fault.

The basal portion of the Smithers Formation consists of medium- to thick-bedded, well-sorted, coarse-grained arkosic sandstone. In outcrop, the sandstone beds are characterized by trough cross-stratification, planar horizontal laminations and coarsening-upward cycles. Thick coquina beds containing disarticulated shell fragments supported in a very coarse-grained sandy matrix are common. Bioturbation is sparse, mostly localized in finer-grained intervals, and contains a low diversity assemblage of *Skolithos* and *Diplocraterion*. Tipper and Richards (1976) reported an Aalenian age for an ammonite located approximately at 85 m from the base of the Smithers Formation (NM1 in figure 2.6C). Up-section, the percentage of siltstone and mudstone increases progressively and centimetre-scale calcareous concretions are abundant. Trace fossils including ichnogenera such as *Teichichnus*, *Thalassinoides* and *Chondrites* are indicative of lower energy depositional conditions characterized by deposit-feeding organisms. A broad variety of bivalves, ammonites and belemnites present throughout the finer-grained interval of the Smithers Formation suggest an Aalenian to Early Bajocian age (Tipper and Richards 1976; Appendix A). At about 895 m in the section, regularly spaced very thin beds of orange weathered ash tuff become interbedded with belemnite-bearing siltstone beds. This boundary was arbitrarily picked to define the basal contact of the overlying unit, assigned to the revised Quock Formation (below), which consists mostly of thinly bedded, blocky greyish siltstone with sparse pale weathered ash tuff laminae ("pyjama beds"). The section is interrupted at 965 m by a porphyritic quartz monzodiorite of the early Eocene Babine plutonic suite (MacIntyre et al. 1988, 1997, 2001), which prevents determination of the true thickness of the Quock Formation. Even though the upper contact was not directly observed, regional mapping relationships and fossil collections by Evenchick et al. (2008b) suggest that chert-rich pebble conglomerates, sandstones and siltstones of the Upper Jurassic BLG constitute the highest stratigraphic unit at Netalzul Mountain.

2.3.2 Spatsizi River to Toodoggone River area

2.3.2-1 Joan Lake

The Spatsizi Formation type section previously measured by Thomson et al. (1986) was revisited during this study (figure 2.1). Additional fossil localities and new sedimentological observations are reported here. The unconformable contact between the

Cold Fish Volcanics and overlying sedimentary rocks, assigned by Thomson et al. (1986) and Evenchick and Thorkelson (2005) to the Spatsizi Formation, represents the most significant lithological transition in the area. A rusty-weathering pyroclastic ash-flow unit is disconformably overlain by a 2 m thick monomictic, clast-supported conglomerate of the Joan Member (figure 2.7A). The whitish grey volcanic pebbles are well-rounded, poorly sorted, and include occasional cobble and boulder clasts (figure 2.8A). The conglomerate rapidly fines upward into medium to thick beds of very fine to fine-grained sandstone. The presence of diagnostic fossils such as bivalve *Weyla bodenbenderi* and ammonite *Dubariceras freboldi* confirms the Early Pliensbachian age proposed by previous authors (Thomson et al. 1986; Thomson and Smith 1992; Evenchick and Thorkelson 2005) (JL1 in figure 2.7A). These fossils are typically concentrated in distinctive brown-weathering calcareous sandstone beds (figure 2.8B). Moderately inclined to vertical biogenic traces, such as *Skolithos* and *Cylindrichnus*, are abundant in the fine-grained sandstone intervals.

Above 100 m in the measured section, fossil-rich fine-grained sandstone of the Joan Member is overlain by 427 m of dark grey calcareous siltstone and mudstone of the Wolf Den Member (figure 2.7A). The sudden decrease in grain size at the contact suggests that the latter represents a flooding surface, consistent with the interpretation of water-depth increase proposed by Thomson et al. (1986). Large blocks containing a high diversity assemblage of trace fossils (*Teichichnus*, *Cylindrichnus*, *Palaeophycus*, *Rosselia*, *Asterosoma,* and *Chondrites*) occur 22 m above the contact. Unlike the trace fossil assemblage found in surrounding recessive mudstone, which contains only rare *Chondrites*, the calcareous blocks consist of well-bedded very fine-grained sandstone. This suggests that the blocks might have been transported from a more proximal environment through gravity flow processes perhaps associated with penecontemporaneous faults. Various collections of ammonites throughout the Wolf Den Member indicate a Late Pliensbachian to Middle Toarcian depositional age (Thomson et al. 1986; Thomson and Smith 1992; Jakobs 1997). Pale beige ash tuffs and rare wood fragments are found near the top of the unit.

The monotonous shale succession of the Wolf Den Member grades upward into well-sorted, thin to medium, fine-grained sandstone beds previously assigned to the Melisson Member by Thomson et al. (1986) (figures 2.7A and 2.8C). The basal 20 m of this unit are characterized by greyish beige calcareous sandstones interbedded with very thin mudstone intervals. Up-section, the sandstone beds become amalgamated and current-generated structures such as asymmetric ripples and cross-laminations are common. The uppermost layer of the Melisson Member consists of a very thick

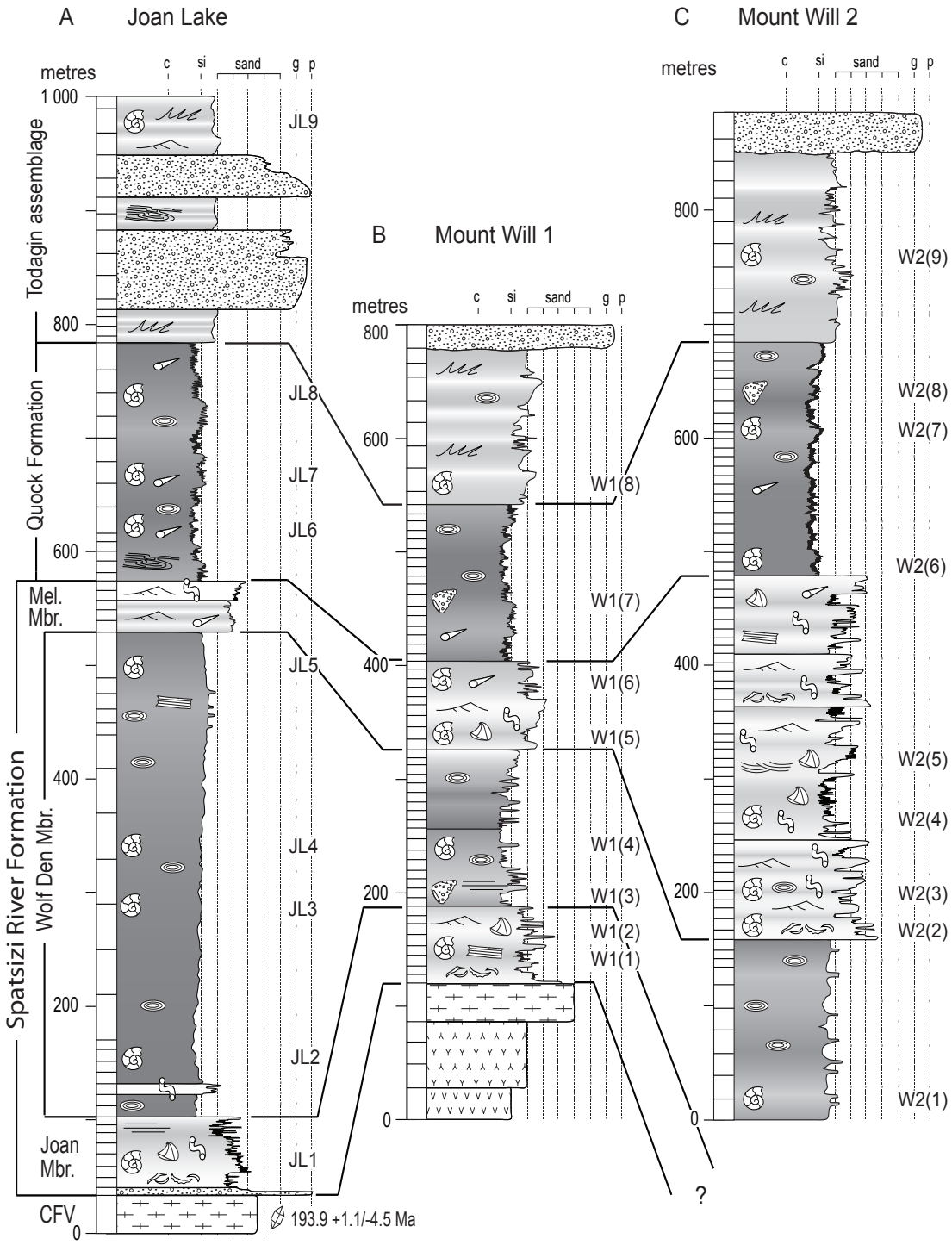

Figure 2.7: Detailed measured sections in the Spatsizi River area north of the Bowser basin. A) Joan Lake (unit stratotype of the Spatsizi River Formation and the Quock Formation). B) Mount Will 1. C) Mount Will 2. The revised Spatsizi River Formation includes three formally defined members: fossiliferous coarse-grained sandstone of the Joan Member, dark mudstone of the Wolf Den Member, and the bioturbated sandstone and siltstone of the Melisson Member. See figure 2.3 for legend details and figure 2.1 for geographic locations.

tuffaceous sandstone bed with abundant trace fossils. They include *Teichichnus*, *Cylindrichnus*, *Palaeophycus*, *Rhizocorallium*, *Ophiomorpha*, *Granularia* and pervasive *Chondrites*. All these observations are consistent with the shoaling interpretation of Thomson et al. (1986) and further suggest that the depositional environment remained fully marine throughout the entire interval. No fossils were recovered from the Melisson Member at the Joan Lake section, but numerous fossil localities in the underlying and overlying units suggest a Middle to Late Toarcian age (Thomson et al. 1986).

The boundary with the overlying unit is placed at the top of the uppermost bioturbated medium-grained tuffaceous sandstone of the Melisson Member (located at 575 m on figure 2.7A). The overlying unit, designated as Quock Formation by Thomson et al. (1986) but reduced to Quock Member by Evenchick and Thorkelson (2005), is re-elevated to the rank of formation in this study. It consists of alternating thinly bedded dark siliceous mudstones and light beige rusty tuffaceous siltstones ("pyjama beds") with rare limestone intervals (figure 2.8D). According to Thomson et al. (1986), rocks

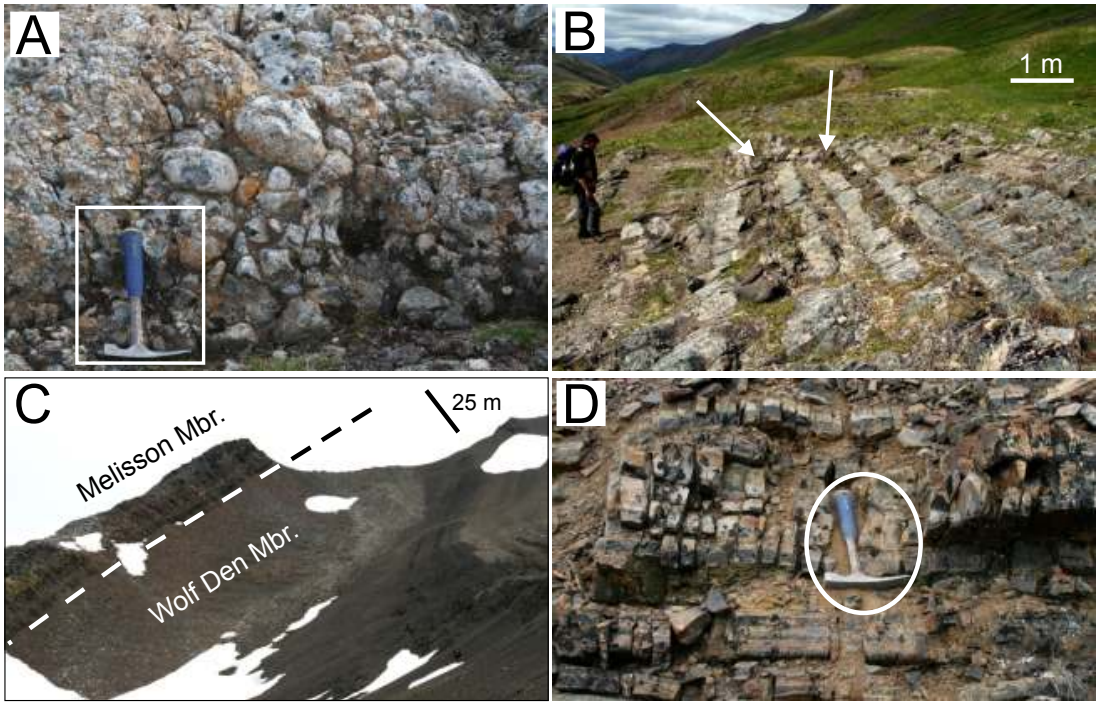

Figure 2.8: Photographs of distinctive lithostratigraphic units exposed at the Joan Lake section. A) Basal clast-supported conglomerate of the Joan Member (Spatsizi River Formation). The clasts range in size from pebbles to boulders, and mostly consist of recycled volcanic material from the underlying Cold Fish Volcanics. Hammer for scale is 30 cm in length. B) Thickly bedded tuffaceous sandstone of the Joan Member with distinctive brown weathering calcareous beds (arrows) containing abundant marine fossils. C) Stratigraphic contact between the recessive dark mudstone of the Wolf Den Member and the overlying more competent bioturbated sandstone of the Melisson Member. D) Thinly bedded dark siliceous mudstone and beige weathering ash tuff ("pyjama beds") of the revised Quock Formation. Hammer for scale is 30 cm in length.

of the Quock Formation were deposited in a deep-water environment of relatively slow sedimentation interrupted with sporadic ash falls. The Quock Formation in this section is approximately 200 m thick, and various ammonites indicate an Early Bajocian age (Thomson et al. 1986). It is overlain with a gradational boundary by chert-rich conglomerate and turbiditic siltstone of the Todagin assemblage of the BLG (Evenchick et al. *submitted*). According to Evenchick and Thorkelson (2005), the BLG is at least 1500 m thick in the vicinity of Joan Lake and ranges in age from Bathonian to Callovian.

2.3.2-2 Mount Will

In order to document the lateral variation of the units identified at Joan Lake, two additional sections were measured 5 and 10 km north of the type section respectively. In both sections, a similar stratigraphic succession was observed but the thicknesses of units differed (figures 2.7B, C). In section 1, the upper 120 m of Cold Fish Volcanics consist of oxidized rhyolite, poorly sorted epiclastic and indurated lapilli tuff and a unit of densely welded ignimbrite characterized by large open vugs, fiamme, lava particles and angular volcanic fragments. The indurated felsic ash flow is in turn overlain by medium-grained calcareous sandstone correlated with the Joan Member. Well-preserved radiolarian microfossils were recovered in a dark siliceous mudstone immediately above the Joan–Wolf Den boundary (230 m). Distinctive fauna including *Helvetocapsa minoensis* (Matsuoka) and *Parvicingula spinifera* (Takemura) indicate a Toarcian age (figure 2.9). This is consistent with Lower Toarcian ammonites *Hildaites murleyi* (Moxon) and *Harpoceras sp.* cf. *H. subplanatum* (Oppel) located 30 m above the contact. Finely laminated very fine-grained sandstone and mudstone of the Wolf Den Member are overlain by coarser grained, bioturbated beds of the Melisson Member. The contact is gradational over 20 m and displays a coarsening- and thickening-upward trend. Middle Toarcian ammonites of the Planulata regional Zone (*Peronoceras sp.* aff. *P. verticosum* (Buckman) and *Denckmannia sp*. cf. *D. tumefacta* (Buckman)) were collected both at the base and near the top of this unit. The ichnological assemblage of the Melisson Member is dominated by suspension feeder traces such as *Skolithos*, *Diplocraterion* and *Cylindrichnus*. Similarly to the Joan Lake section, the contact between the Melisson Member and the revised Quock Formation (below) is placed immediately above the uppermost mappable bioturbated medium-grained sandstone (405 m in figure 2.7B). Despite having the same stratigraphic succession with respect to the type section at Joan Lake, section 1 at Mount Will is only 424 m thick. This is mostly due to the relatively thin Wolf Den Member, which constitutes only one third of the thickness of the equivalent unit at Joan Lake. This suggests that the basin floor at Mount Will never

reached deep-water conditions and that the accommodation space was filled relatively rapidly in the Middle Toarcian.

Map relationships from NTS 104H/10 indicate that the Spatsizi Formation becomes progressively thicker northward along the east-facing side of the Eaglenest Range (Evenchick and Thorkelson 2004). This is in part attributed to the northeast-verging Mount Will thrust fault, which cuts progressively younger units as it is traced northwest across the area and eventually duplicates a significant portion of the Spatsizi Formation (Evenchick and Thorkelson 2004; Loogman 2008). Section 2 was measured entirely in the hangingwall portion of the Mount Will Thrust and includes a complete succession from the uppermost 160 m of the Wolf Den Member to the base of the BLG (figure 2.7C). Even after applying corrections to accommodate apparent thickening related to folding in the hangingwall, it seems that the Melisson Member in section 2 is significantly thicker than in the previous section measured 5 km to the south. Hummocky cross-stratification, sparse bioturbation and ammonites of the Middle Toarcian planulata regional zone occur throughout the 322 m of section assigned to the Melisson Member (figure 2.7C). The remainder of the section includes ash-tuff and siliceous radiolarian-bearing mudstone of the revised Quock Formation (below) overlain by fissile silty shale and chert-pebble conglomerate of the Todagin assemblage.

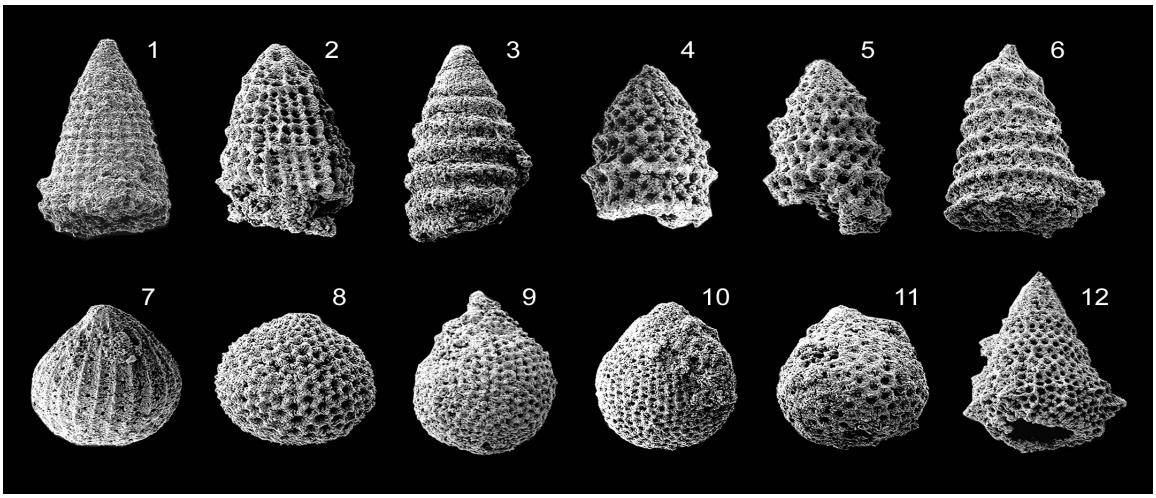

Figure 2.9: Jurassic radiolarians from the Quock Formation of the Hazelton Group (Scanning Electron Microscope). For each morphotype: taxon, sample number, collection number, and maximum width. Numbers 1-5 and 7-10 correspond to fossil MW1(3) of figure 2.7B. Numbers 6, 11, and 12 correspond to fossil OE(1) of figure 2.10B. 1) *Parahsuum* sp., LC064B, #7, 80 μm; 2) *Canustus* sp., LC064B, #3, 120 μm; 3) *Canoptum* sp., LC064B, #2, 90 μm; 4) and 5) *Praeparvicingula spinifera* (Takemura), LC064B, #6, #10, 80 μm; 6) *Praeparvicingula* sp. C (Pessagno & Whalen), LB045A, #15, 120 μm; 7) *Helvetocapsa minoensis* (Matsuoka), LC064B, #11, 75 μm; 8) *Zhamoidellum* sp., LC064B, #14, 115 μm; 9) *?Minocapsa* sp., LC064B, #4, 110 μm; 10) *?Minocapsa* sp., LC064B, #15, 120 μm; 11) *?Zhamoidellum* sp., LB045A, #1, 100 μm; 12) *?Reglia* sp., LB045A, #18, 120 μm.

Based on detailed paleontology and lithostrastigraphic descriptions, it appears that the subdivions established by Thomson et al. (1986) can be correlated throughout the Spatsizi River area except for the Abou Member which has only been reported locally west of Joan Lake anticline. The Abou Member probably accumulated in restricted sub-basinal environments where anaerobic conditions were maintained to ensure deposition and preservation of calcareous to siliceous dark organic shales.

2.3.3 Iskut River area

2.3.3-1 Oweegee Dome

The Oweegee Range is located approximately 25 km north of the Meziadin Lake (figure 2.1). It consists of a structural culmination where basement rocks of the Devonian through Permian Stikine assemblage and Upper Triassic Stuhini Group are unconformably overlain by Lower to Middle Jurassic Hazelton Group rocks (Greig and Evenchick 1993). The lower undifferentiated portion of the volcanic-dominated Hazelton Group is disconformably overlain by clastic rocks assigned to the Salmon River Formation and Bowser Lake Group, which delineate the outline of the dome-shaped structure (Greig 1991, 1992). Two stratigraphic sections on the northern side of Oweegee Dome were measured and are described below.

Lowermost rocks of the Hazelton Group observed in the north-western extremity of Oweegee Dome comprise well-stratified maroon and green volcaniclastic sandstones interbedded with lahars, volcanic breccias and minor andesitic volcanic flows (Waldron et al. 2006)(figure 2.10A). This unit is tentatively correlated with the Betty Creek Formation of Anderson and Thorkelson (1990). Pebble count analyses in a conglomeratic bed of the Betty Creek Formation indicate that the framework contains a significant proportion of clasts (~35%) resembling underlying Triassic and Permian units, supporting the interpretation of Greig (1991, 1992) that rocks of the Stikine assemblage and Stuhini Group were uplifted prior to deposition of the Hazelton Group. The >100 m thick volcaniclastic rocks of the Betty Creek Formation are overlain by a white, rusty weathering quartz-phyric rhyolite. The interpreted age of the felsic unit is 199 +/-2 Ma based on three concordant U-Pb zircon populations obtained by Greig and Gehrels (1995). At Oweegee Dome, this rhyolite constitutes the last major volcanic eruption of the Hazelton Group prior to establishment of a long-lived subsiding sedimentary basin.

The felsic volcanic unit is disconformably overlain by 5 m of polymictic cobble conglomerate which fines upward gradually into calcareous arkosic sandstone beds (figure 2.10A). Planar cross-bedding and asymmetric current ripples are common

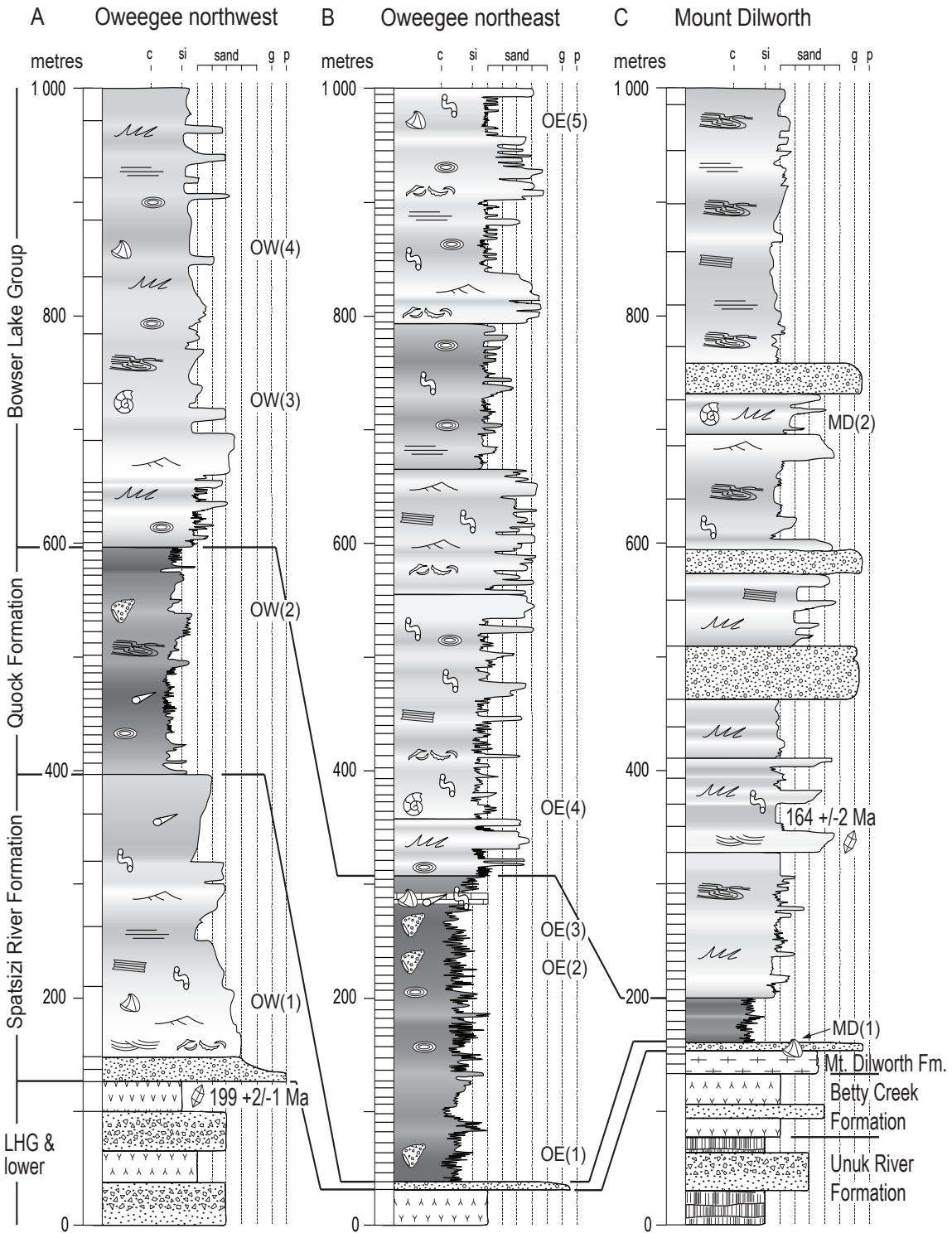

Figure 2.10: Detailed measured sections in the Iskut River area located on the border of the Eskay rift. A) Oweegee Dome northwest. B) Oweegee Dome northeast. C) Mount Dilworth. The unamed lower Toarcian member is here assigned to the revised Spatsizi River Formation. See figure 2.3 for legend details and figure 2.1 for geographic locations.

sedimentary structures near the base of the sandstone interval. Three kilometres to the south, stratigraphically equivalent tuffaceous bioclastic strata contain abundant Toarcian marine fossils (Greig and Gehrels 1995). This clastic unit is correlated with the unnamed lower member of the Salmon River Formation defined by Anderson and Thorkelson (1990). The uppermost Hazelton Group rocks in the north-western side of Oweegee Dome consist of siliceous mudstone and ash tuff ("pyjama beds") with Lower Bajocian to Upper Bathonian radiolarian fauna (Cordey et al. 1991). These strata are conformably overlain by fine-grained turbidites of the Ritchie-Alger assemblage of the BLG which contain Upper Kimmeridgian ammonites approximately 120 m above the contact (Evenchick et al. *submitted*).

On the eastern edge of Oweegee Dome, a thin layer of poorly sorted conglomerate, tentatively correlated with the Toarcian clastic rocks elsewhere in the vicinity, is separated from the underlying Stuhini Group by an angular unconformity (figure 2.10B). The absence of well-layered volcaniclastic rocks and felsic lava flows, in contrast with the succession only 5 km to the west, is consistent with the interpretation of Greig (1992) which suggested that the unconformity at the top of the Stuhini Group must have had significant relief during deposition of the Hazelton Group strata. The basal clast-supported conglomerate previously assigned to the lower member of Salmon River Formation is overlain by 270 m of thinly interbedded siliceous radiolarian mudstone and ash tuff. In this area of the basin, these rocks have been classified as the Troy Ridge facies of the Salmon River Formation (Anderson and Thorkelson 1990; Anderson 1993), the Spatsizi Formation (Ferri and Boddy 2005), and more recently to undifferentiated upper Hazelton Group clastic rocks (Evenchick et al. *submitted*); in this paper, the "pyjama beds" are assigned to the revised Quock Formation (below). The "pyjama beds" include numerous calcareous concretions, occasional wavy parallel laminations and convolute slump structures. Three radiolarian localities from the "pyjama beds" unit yielded Lower Bajocian to Callovian fauna (figure 2.9). A 2 m thick unit of dark grey limestone with complex boundstone textures was observed near the top of the "pyjama beds" (Waldron et al. 2006). The limestone includes shell fragments and is locally bioturbated (figure 2.11). Even though freshly broken pieces smell of bitumen, Rock-Eval data suggest that almost all the initial hydrogen content was removed by oxidation and/or high thermal maturity. Similar results, obtained by Ferri and Boddy (2005) for laterally equivalent strata, led them to propose that these units were once a rich source rock assuming that most of the organic matter was consumed during thermal maturation.

The transition into the overlying turbidites of the BLG appears gradational and concordant. Probable Middle Jurassic to Middle Oxfordian fossils have been reported low

in the Ritchie-Alger assemblage, and several Upper Oxfordian to Lower Kimmeridgian bivalve collections occur significantly higher in the coarser-grained Muskaboo Creek assemblage (Evenchick et al. 2001). The unusually thin succession of turbidites combined with the occurrence of shallow marine strata within 300 m of the base of the Bowser Lake Group led Evenchick et al. (*submitted*) to suggest that the area was a topographic high during the Middle to Late Jurassic.

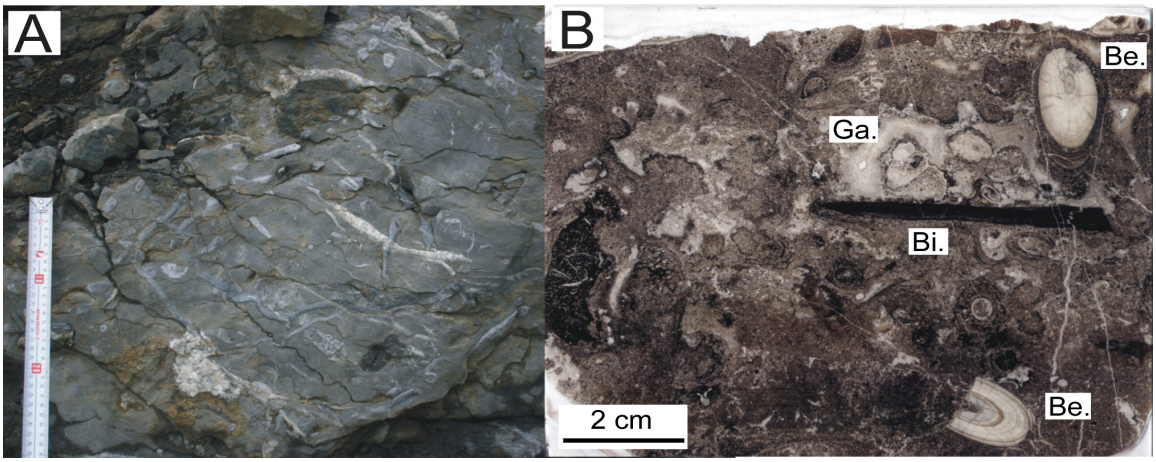

Figure 2.11: Dark grey fossiliferous limestone locate near the top of the Hazelton Group (~285 m in figure 2.10B). A) Field photograph showing complex boundstone texture. Measuring tape for scale is in cm. B) Large format thin section showing diversified fossils found in the limestone unit including belemnites (Be), gastropods (Ga), and broken shell fragments of bivalves (Bi).

2.3.3-2 Mount Dilworth

The Mount Dilworth section is located 25 km north of Stewart near the international border with the United States of America (figure 2.1). In this area, stratigraphy of the Lower Jurassic volcanic rocks of the Hazelton Group is well understood due to extensive drilling data from the Silbak Premier gold-silver mine (Alldrick et al. 1987; McDonald 1990; Alldrick 1991). Massive pyroxene-porphyric andesite flows, volcanic breccia and lapilli tuff of the Unuk River Formation are overlain by interbedded andesitic to dacitic tuff and volcaniclastics of the Betty Creek Formation (Alldrick 1987) (figure 2.10C). These rocks are in turn overlain by welded to non-welded ash flows of the Mount Dilworth Formation. The younger sedimentary succession is well exposed in the core of a SE-plunging overturned syncline (see Chapter 5). The basal sedimentary unit consists of a discontinuous reddish-brown-weathering siltstone with minor conglomerate lenses. This unit crops out intermittently on the periphery of the syncline and is separated from the underlying felsic volcanic rocks above an erosional surface. Abundant recrystallized belemnites and thick-shelled bivalves recovered from

the rusty calcareous siltstone beds yielded a Middle Toarcian to Callovian age, consistent with other Toarcian fossil localities reported from a lithologically similar unit in the vicinity (Alldrick 1987; Anderson 1993; Lewis et al. 1993). Up-section, the silica content of the siltstone increases and very thin tuff horizons become abundant ("pyjama beds"). Radiolaria recovered from this unit showed a high degree of recrystallization, preventing any definitive identification. These "pyjama beds", assigned to the revised Quock Formation (below), are conformably overlain by conglomerate, turbiditic sandstone and siltstone of the BLG (Evenchick and McNicoll 2002; Chapter 5). An ammonite located approximately 500 m above the base of the BLG yielded an Early Oxfordian age for the uppermost stratigraphic unit preserved.

2.3.3-3 Table Mountain

Table Mountain (informal topographic name) is a NW-elongate feature located between the upper Iskut River, the Little Iskut River, and the northern tributary of Ball Creek approximately 40 km SW of the town of Iskut (figure 2.1). The stratigraphic section described here is compiled from reports and maps of Alldrick et al. (2004a, 2004b, 2006) and Simpson and Nelson (2004), and has been traversed and mapped by authors T. Barresi and J. Nelson. The lowest stratigraphic unit exposed along the western slope of Table Mountain mainly consists of maroon and green plagioclase-phyric andesite flows and dacite breccias (figure 2.12A). Sparse intervals of black mudstone, greyish blue ash tuff and minor diorite intrusions with pegmatic pods were also observed. This unit is at least 720 m thick but only the uppermost 100 m are included for in figure 2.12A. Despite the absence of age control, rock types identified in this unit suggest that it likely represents lower Hazelton Group rocks, and possibly Stuhini Group rocks lower in the section.

The andesitic lower Hazelton Group rocks are unconformably overlain by volcanic and sedimentary rocks mapped as part of the informal "Willow Ridge Complex" of the upper Hazelton Group by Alldrick et al. (2006); in this paper, these rocks are assigned to the proposed Iskut River Formation (below). Regional map relationships suggest that the unconformity at the base of the Iskut River Formation dips steeply to the east and is onlapped by a variety of lithologies along strike, including polymictic fanglomerate, basalt and rhyolite (figure 2.13). At its best exposed locality (UTM 413550 E 6356000 N – NAD 83 Datum; figure 2.13), the unconformity is overlain by an extensive rhyolite regolith approximately 70 m thick. The rock is variably hematite or limonite altered, giving the groundmass a distinctive red or orange colour. In a few fresh outcrops, the rhyolite consists of 1 to 7 mm pale white spherulites within a semi-

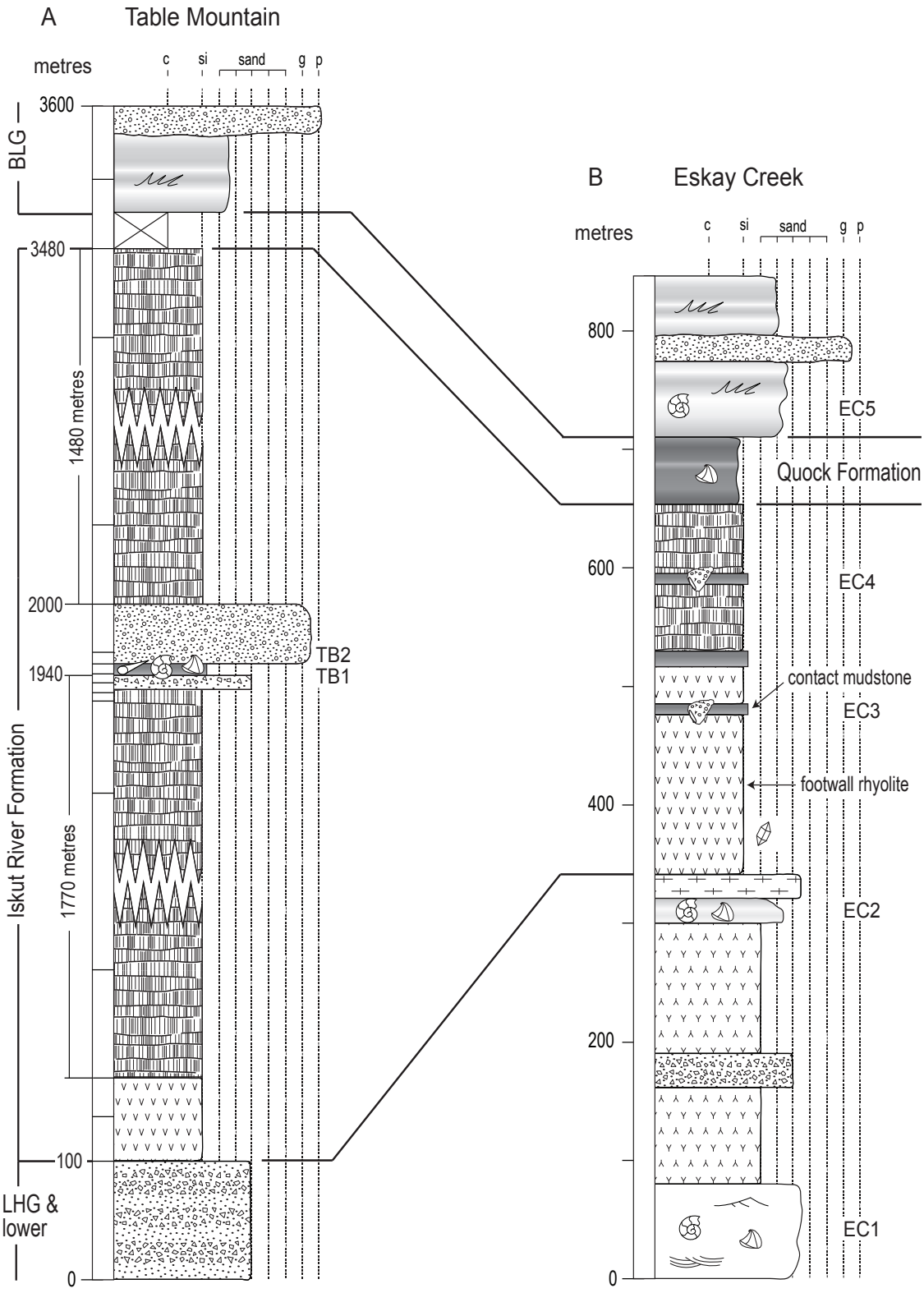

Figure 2.12: Detailed measured sections in the Iskut River area located inside the Eskay rift. A) Table Mountain (unit stratotype of the proposed Iskut River Formation). B) Eskay Creek. See figure 2.3 for legend details and figure 2.1 for geographic locations.

translucent pale blue-green siliceous matrix.

The rhyolite is overlain by 1770 m of dark green to olive green basalt (lower basalt unit of Alldrick et al. 2004b). The basalt is typically aphanitic or feldspar porphyritic, and forms eruptive units made up of pillowed flows or pillow breccias

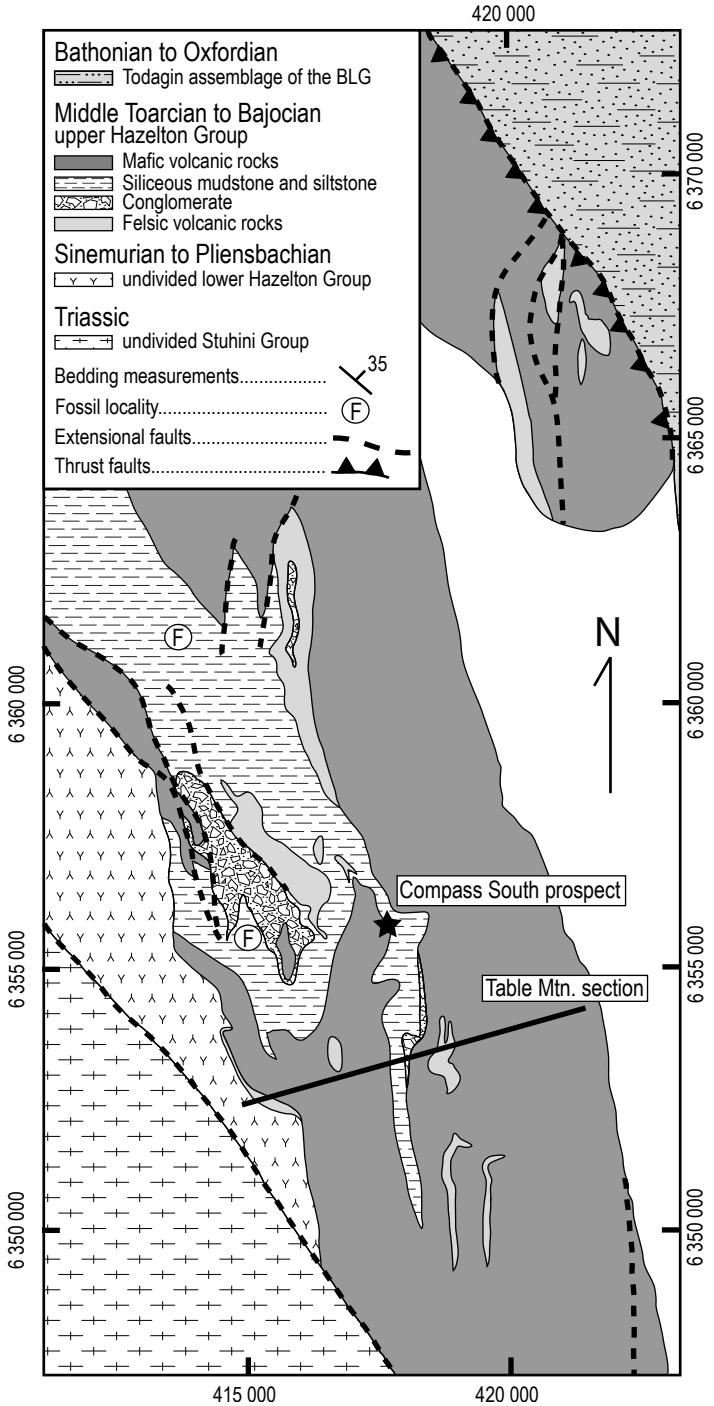

Figure 2.13: Simplified geology map of the Table Mountain area showing the location of the unit stratotype of the proposed Iskut River Formation. Universal Transverse Mercator Projection in NAD 83 Datum. Modified from Alldrick et al. (2006).

typically 5 to 20 m thick (figure 2.14A). Simpson and Nelson (2004) identified three basalt facies in this unit: aphyric, massive and coherent pillow basalt; monomictic, blocky basalt breccia; and fluidal-clast breccia. An abundance of 3 to 5 mm crowded variolites is a common and identifying feature of the lower basalt unit of the Iskut Formation at Table Mountain. This devitrification texture is best observed as overlapping pale yellow spots on weathered surfaces (figure 2.14B). The uppermost 5 m of the lower basalt unit is highly altered and contains up to 40 percent sulphides where hyaloclastite groundmass of the basalt breccia has been partly to completely replaced by very fine-grained pyrite (figure 2.14C). The replacement-style mineralization ends at the contact with the overlying mudstone where mineralizing fluids were apparently capped (located at 1940 m on figure 2.12A; this contact constitutes the base of the middle sedimentary unit of Alldrick et al. 2004b). However, laminated beds of pyrite (up 5 cm thick) immediately above the contact suggest that exhalative vents were still active during sedimentation.

The 10 m thick unit of thinly-bedded black mudstone and grey siltstone is overlain by 50 m of poorly sorted, matrix to clast supported polymictic conglomerate. The matrix of the conglomerate consists of coarse to very coarse sandstone and contains sub-angular to sub-rounded clasts of basalt, mudstone, rhyolite, massive fine-grained pyrite, and limestone. This unit also directly onlaps the basal unconformity in some places. Where it does, polymictic conglomerate grades into coarse fanglomerate composed of clasts identical to the underlying plagioclase-phyric andesites and dacites of the lower Hazelton Group. Five ammonoids and one radiolarian collections from laterally equivalent fine-grained sedimentary rocks indicate that the middle sedimentary unit ranges from Upper Toarcian to Middle Bajocian (Souther 1972; Evenchick et al. 2001). Up-section, the sedimentary rocks are overlain by at least 1480 m of basalt (upper basalt unit of Alldrick et al. 2004b), which is exposed on the eastern side of Table Mountain and on Willow Ridge (figure 2.13). This upper basalt unit possesses similar lithological characteristics to the lower basalt unit. The upper contact of the Iskut River Formation is not exposed in the section, but is interpreted to be conformable with the turbiditic sedimentary rocks of the Bowser Lake Group based on relationships at Eskay Creek (below) and on regional mapping.

2.3.3-4 Eskay Creek

The Eskay Creek Mine is located 80 km northwest of the town of Stewart (figure 2.1). Geology in the vicinity of Eskay Creek is well known from detailed bedrock mapping and extensive diamond drilling (e.g. Ettlinger 1992; Bartsch 1993; Nadaraju 2003; Roth 1993, 2002; Sherlock et al. 1994; McDonald et al. 1996). The following

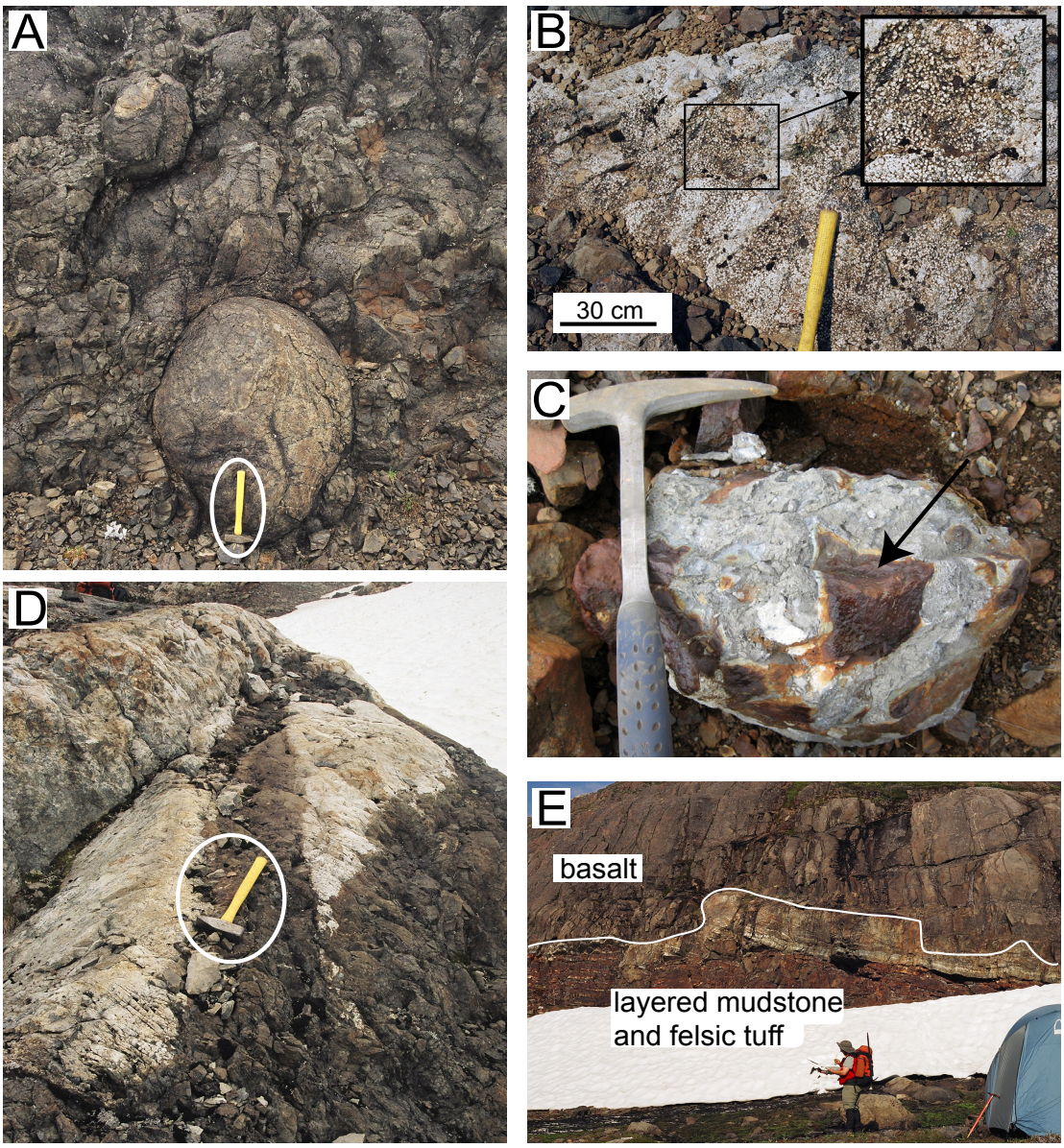

Figure 2.14: Field photographs of the Iskut River Formation showing distinctive lithological characteristics from units exposed at Pillow Basalt Ridge (PBR) and Table Mountain (TB). A) Pillow basalts exposed on PBR. Large (>1 m) diameter pillows, such as the one exposed near the base of the photograph, are interpreted to indicate close proximity to eruptive centres. Hammer for scale is 36 cm in length. B) Basalt exposed at TB displaying variolitic texture. White weathering variolites are characteristic devitrification features found on the glassy rims of basalt. C) Mineralized basalt breccia; dark rusty angular basalt fragments (arrow) are supported in a fine-grained sulphide matrix consisting mainly of pyrite. Compass South prospect on TB (see figure 2.13 for geographic location). D) Bimodal volcanic rocks on PBR. Light coloured rhyolite are intruded by a sub-volcanic mafic dike swarm that fed eruptions responsible for the overlying basalts. Hammer for scale is 36 cm in length. E) Outcrop on PBR showing rusty weathering mudstone interbedded with felsic tuff overlain by a basalt flow. The bedded rocks grade from mainly pyritic siliceous mudstone at the bottom to predominantly felsic tuff layers at the top. Incorporation of mudstone/tuff "rafts" into the overlying basalt during eruption resulted in an irregular contact.

reference stratigraphic section is compiled from the aforementioned sources and documents the general lithostratigraphic succession observed at the mine site.

Mineralized units and associated sedimentary and volcanic rocks of the Hazelton Group at Eskay Creek are exposed along the western limb and on the hinge of a NE-plunging anticline (Eskay Anticline).These rocks have traditionally been included as part of the Salmon River Formation by Anderson and Thorkelson (1990) and Anderson (1993); in this paper, they are assigned to the Iskut River Formation (below). Unlike at Table Mountain (figure 2.12A), the lower contact of the Iskut River Formation at Eskay Creek is concordant but disconformable (located at 340 m in figure 2.12B). Upper Pliensbachian units comprising andesitic breccia, volcaniclastics and dacitic volcanics (lower Hazelton Group) are overlain by a thick unit of rhyolite above an erosional surface. This felsic volcanic flow, locally termed the "footwall rhyolite", varies in texture from massive to autobrecciated, and was interpreted by Bartsch (1993) to represent a series of flow-dome complexes. The footwall rhyolite was dated at 175 +/- 2 Ma by U-Pb zircons, and a stratigraphically similar rhyolite on the eastern limb of the Eskay Anticline yielded an age of 174 +2/-1 Ma (Childe 1996). Overlying and interfingering in part with the rhyolite is a very fine-grained dark grey unit known as the "contact mudstone". The contact is irregular along strike and characterized by a black matrix rhyolite breccia, in which quench-fragmented rhyolite has interstices filled by black mudstone. This peperitic texture is interpreted to represent the contemporaneous deposition of mudstone and eruption/emplacement of the felsic domes. Clasts within the mudstone include fragmental sulphides and sulfosalts, and altered rhyolite and barite (Roth 2002). Graded sulphide beds with soft-sediment deformation structures and scoured contacts have been interpreted as evidence of syngenetic processes. Radiolarian microfossils from the mudstone yielded Aalenian to possibly Early Bajocian fauna (Nadaraju 1993). Massive basalt sills and pillowed basalt flows and breccia, with narrow (< 1 m thick) intervals of bedded argillite, chert and felsic tuff, overlie the contact mudstone. Conformably overlying the basalt is a thicker succession of tuffaceous mudstone, here attributed to the proposed Quock Formation (below). The age of the Quock Formation at Eskay is constrained by a collection of Early Bajocian bivalves (Roth 2002). Conformably overlying the Quock Formation strata are mudstone-siltstone turbidites and thickly bedded sandstone and conglomerate layers that contain Late Bathonian to Early Callovian ammonoids (Evenchick et al. 2001; Roth 2002).

2.3.4 Detrital zircon geochronology

Two samples of very coarse-grained sandstone from Quinlan Mountain and Mount Dilworth were collected for U-Pb detrital zircon dating. The objectives were to constrain the hiatus at the unconformity between the lower and upper Hazelton groups, and to provide new insights on the provenance for the Smithers Formation and the basal part of the BLG. Zircon grains were extracted, mounted on epoxy disks, and analysed by laser ablation multi-collector-inductively coupled plasma-mass spectrometry (MC-ICP-MS) using the methods of Simonetti et al. (2005). Results are shown in figure 2.15 as probability density plots for grains with <50% discordancy. Uncertainties based on $^{206}Pb/^{238}U$ ages are reported at the 95% confidence level (2σ). Full tables of results can be found in Appendix B.

2.3.4-1 Results from Quinlan Mountain

Sample LC022A was collected 2 m above the disconformable contact between the Telkwa and the Smithers formations in a cross-stratified sandstone bed (figure 2.6A). The density distribution of grains is strongly clustered between 185-165 Ma and has a calculated mode of 172.4 +/-1.2 Ma (figure 2.15A). This age is consistent with the depositional age predetermined from an extensive Aalenian fossil locality situated at an equivalent stratigraphic level (QM1 in figure 2.6A). Two older subsidiary peaks at ca. 193 Ma and ca. 202 Ma are also observed. These grains probably correspond to recycled volcanic detritus derived from the lower Telkwa Formation and the Takla Group respectively. The 172.4 +/- 1.2 Ma age is similar to various U-Pb dates obtained on felsic lapilli tuffs of the upper Hazelton Group in the Bella Coola region by Mahoney (2009). Because of their striking lithological difference from the underlying bright red andesitic to dacitic tuffs of the Telkwa Formation, the basal sedimentary rocks of the Smithers Formation at Quinlan Mountain likely represent the introduction of penecontemporaneous felsic detritus from the Bella Coola region to the south. The ca. 178 Ma age reported from a tuff high in the Telkwa Formation (T. Barresi and R. Friedman, unpublished data 2010) indicates a hiatus of about 6 m.y. before deposition of the lowermost sandstone of the Smithers Formation at Quinlan Mountain.

2.3.4-2 Results from Mount Dilworth

Sample LT035A was collected at 130 m above the base of a sandstone succession previously mapped as Salmon River Formation but correlated here with the Todagin assemblage of the BLG. Full details of the analytical methods and data are given in Appendix B. The density distribution of grains shows a strong peak at 196.4 +/-2 Ma

and a younger secondary peak at 164 +/-2 Ma (figure 2.15B). Scattered grains also display Early Triassic to Late Devonian ages with minor peaks at 245, 295 and 350 Ma respectively. The highest population of zircons at 196.4 +/-2 Ma suggests that the majority of grains were derived from local sources of the Betty Creek and Unuk River formations (McDonald et al. 1996; Logan et al. 2000). The youngest grain population at 164 +/-2 Ma (Late Bathonian to Early Callovian age) is interpreted to represent a probable depositional age. This is consistent with a Lower Oxfordian ammonite (MD1 in figure 2.10C; see Appendix A) located 380 m above sample LT035A. The density distribution of grains in LT035A is somewhat different from other Late Bathonian to latest Jurassic detrital zircon ages reported by McNicoll and Evenchick (2004) and Evenchick et al. (*submitted*) from samples elsewhere in the Bowser basin, in which the greatest population of grains is consistently as young as the paleontologically-determined depositional age. Siliciclastic sedimentary rocks of the Todagin assemblage at Mount Dilworth are also petrographically different from other Bowser Lake Group sandstone. The abundance of volcanic fragments in these rocks constitutes a strong contrast with the chert-dominated provenance typical elsewhere in the Bowser basin, where sediment was derived predominantly from the Cache Creek terrane to the northeast (Eisbacher 1985; Gabrielse 1991; Green 1992; Evenchick and Thorkelson 2005).

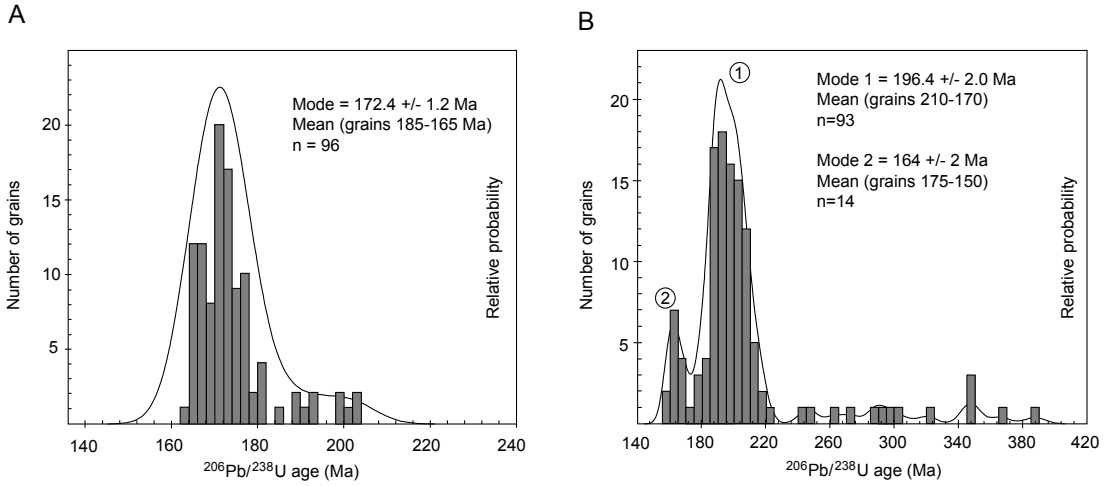

Figure 2.15: U-Pb detrital zircon relative probability plots for sandstone of the Smithers Formation (A) and the Bowser Lake Group (B). Plots were generated using ISOPLOT (Ludwig 2003). See Appendix B for full table of results and details on error calculations.

2.4 Proposed stratigraphic framework

Recent stratigraphic investigations and compilation maps have shown that the Hazelton Group rocks located outside the Eskay rift can be broadly divided into a lower suite dominated by arc volcanics and an upper sedimentary-dominated suite with variable amounts of interbedded rift-related volcanic rocks (Evenchick et al. 2009). Several authors (Ferri et al. 2004; Evenchick and Thorkelson 2005; Waldron et al. 2006; Gagnon et al. 2007; Evenchick et al. *sumitted*) informally used the term "upper Hazelton Group clastic rocks" when referring to sedimentary units of the Spatsizi, Salmon River, Smithers or Nilkitkwa formations. Based on mapping relationships in the Oweegee Range, Todagin Mountain and Joan Lake areas, Gagnon et al. (2007) suggested that the base of the upper Hazelton Group is marked by a widespread unconformity. From data presented here, it is clear that this boundary is diachronous; the change from predominantly arc volcanics to predominantly rift-related sediments and volcanics is significantly younger in the southern part of the basin. Underneath this erosional surface, undivided intermediate lavas and associated volcaniclastic rocks and lahars were assigned to the lower Hazelton Group (Waldron et al. 2006; Gagnon et al. 2007). With these guidelines in mind, a new stratigraphic framework is proposed based on an informal division of the group into the lower Hazelton Group (LHG) and upper Hazelton Group (UHG), and a formal revision of the formations and members in the upper Hazelton Group (figure 2.16).

2.4.1 Lower Hazelton Group

The LHG comprises a wide range of lithologies dominated by maroon and green volcaniclastic rocks, calc-alkaline andesitic to dacitic flows and associated volcanic breccias and tuffs. They include the Telkwa, Jack, Unuk River, Betty Creek, Mount Dilworth and Toodoggone formations as well as the Griffith Creek and Cold Fish volcanics (figure 2.16). These units rest unconformably above the Triassic volcanic rocks of the Stuhini Group (and equivalents), and in some localities, Paleozoic rocks of the Stikine assemblage. Their upper boundary is defined by an erosional surface that separates them from the overlying UHG clastic rocks in most places. Even though a precise correlation of the LHG units at the regional scale is difficult to assess due to their limited lateral extent and abrupt facies changes, volcanic successions from different localities can be compared with each other based on absolute age dating and relative stratigraphic position. The cluster of U-Pb ages at ca. 190-200 Ma obtained from volcanic rocks of the Stuhini, Telkwa and Toodoggone formations, and from the Cold Fish Volcanics, indicate that LHG volcanism was contemporaneous across the Stikine terrane (Greig and Gehrels 1995; Thorkelson et al. 1995; Gareau et al. 1997; Duuring

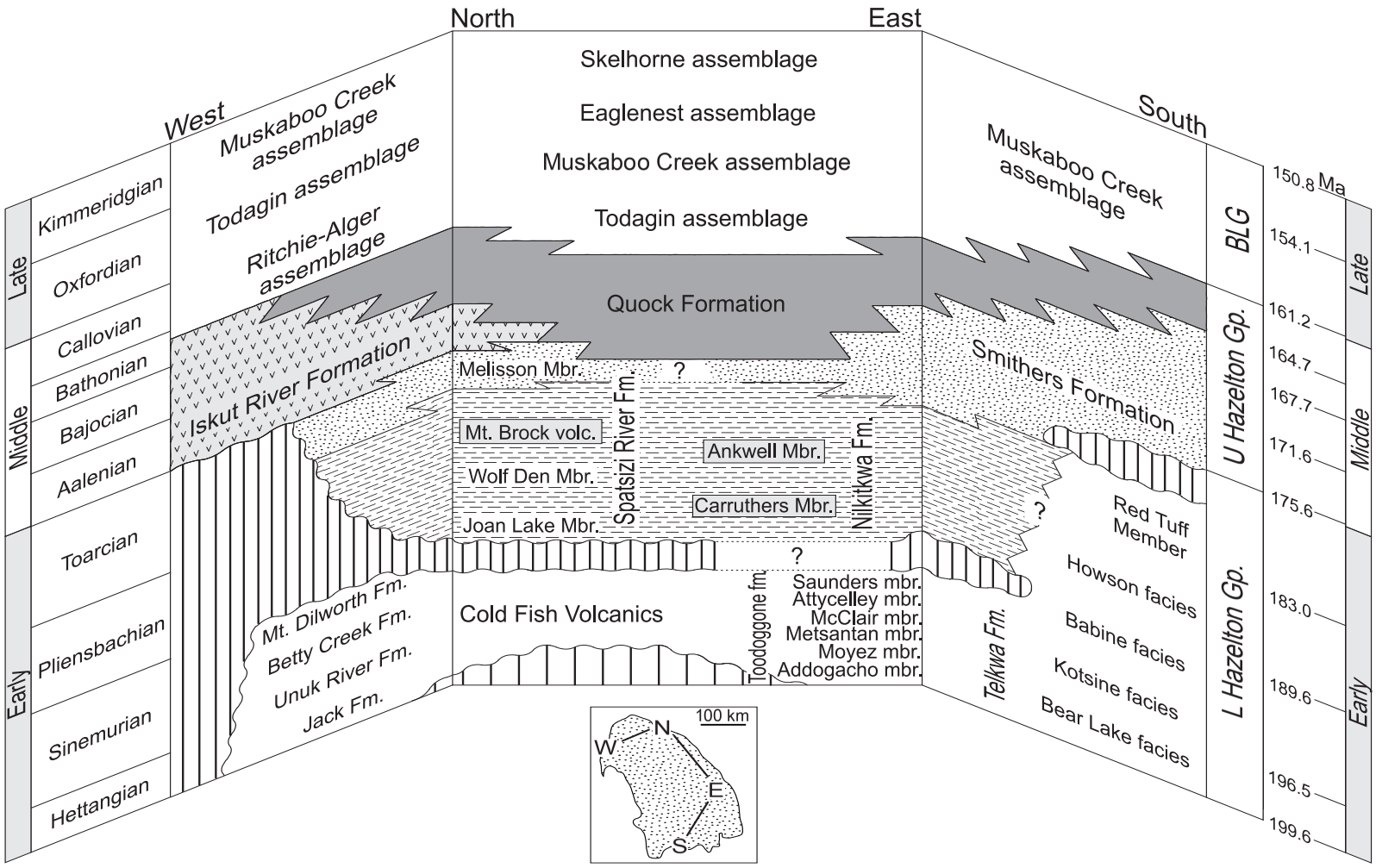

Figure 2.16: Proposed stratigraphic nomenclature for the Hazelton Group exposed in north-central British Columbia. Most significant changes include: recognition of a diachronous unconformity at the base of the upper Hazelton Group; revision of the Spatsizi River and Quock formations; introduction of a new stratigraphic unit (Iskut River Formation) for the rift-related facies in the Iskut River area.

et al. 2009). Volcanic rocks of the LHG are mainly calc-alkaline to tholeiitic and have a strong arc signature (Tipper and Richards 1976; Anderson and Thorkelson 1990; Diakow et al. 1991; Thorkelson et al. 1995; Logan et al. 2000). One exception is the Cold Fish Volcanics, which have a silica-bimodal geochemical signature that has been interpreted to be related to extensional volcanism in a contemporaneous back-arc setting (Thorkelson et al. 1995). Most of these units were deposited in subaerial, oxidizing environments, and likely built stratovolcanoes on an evolving arc system (Alldrick et al. 1989). Discontinuous siltstone beds bearing ammonite fossils of Hettangian to Upper Sinemurian age are locally interbedded with andesitic lavas and suggest periodic incursion of the sea onto the emergent arc in the Early Jurassic.

2.4.2 Upper Hazelton Group

2.4.2-1 Smithers Formation and equivalents

Because of their greater lateral continuity and their relatively constant thickness, sedimentary units of the UHG are more likely to be traceable regionally than the volcanic units associated with the LHG. A recognizable lower unit of the UHG includes strata of the Smithers and Nilkitkwa formations, along with specific units previously assigned to the Spatsizi (Joan, Wolf Den and Melisson members) and Salmon River (lower calcareous member) formations (figure 2.16). The erosional surface at the base of the clastic-dominated succession is used as the boundary between the lower and upper Hazelton groups. Where exposed, the unconformity is overlain by 1–5 m thick clast-supported conglomerate that fines upward into cross-bedded, coarse to medium-grained sandstone, as seen at the Quinlan Mountain, Joan Lake, Mount Will and Oweegee Dome sections (figures 2.6A; 2.7A, B; 2.10A, B). These units are here assigned to three laterally equivalent formations: the Smithers Formation (dominantly sandstone), the Nilkitkwa Formation (interbedded fine-grained sedimentary rocks and volcanics), and the revised Spatsizi River Formation (dominantly fine-grained sedimentary rocks).

For the most part, basal units of all three fromations consist of interbedded tuffaceous siltstone and sandstone layers containing abundant marine fossils and trace fossils. These basal units are diachronous, with ages ranging from Early Pliensbachian–Late Toarcian in the north to Early Aalenian–Late Bathonian in the south (figure 2.17). In the east, near the Nilkitkwa Range, there is a lateral facies change from coarser clastics to interbedded finer-grained sedimentary rocks and mafic volcanics. This is attributed to sedimentation in a deeper water setting with on-going extensional volcanism, consistent with Tipper and Richards's (1976) definition of the "Nilkitkwa depression" as the

main axis to the Hazelton trough. In almost all the observed and compiled stratigraphic sections, units of the Smithers Formation and equivalents are overlain by thinly bedded siliceous mudstone and tuffaceous siltstone of the Quock Formation (below).

Smithers Formation: No type locality has ever been described for the Smithers Formation because sections measured by Tipper and Richards (1976) were deemed incomplete. We propose the Quinlan Mountain section as the new unit stratotype (figures 2.5 and 2.6A). Based on our observations, this section meets all the necessary criteria established by the North American Stratigraphic Code (NASC 2005) to serve as a type section:

1. Lithological characteristics: bioturbated tuffaceous and calcareous siltstone and sandstone with abundant marine fossils;
2. Thickness: 240 metres;
3. Lower contact: unconformable above the oxidized tuffs of the Telkwa Formation. Boundary defined at the base of a basal conglomerate fining upward into cross-bedded medium to coarse-grained sandstone (UTM 555130 E 6077435 N – NAD83 datum);
4. Upper contact: conformable, defined by a fining-upward trend and gradational transition into units of the revised Quock Formation (below). The boundary is placed at the first occurrence of thinly interbedded siliceous siltstones and fine pale tuffaceous laminae ("pyjama beds") (UTM 554870 E 6078650 N – NAD83 datum);
5. Age: extensive fossil collections suggest an age from Middle Aalenian to Upper Bathonian (Appendix A);

Nilkitkwa Formation: In the eastern portion of the basin, the Nilkitkwa type section previously described by Tipper and Richards (1976) is considered valid and should be retained. Even though units of the Nilkitkwa Formation are demonstrably laterally continuous with some strata of the Smithers and Spatsizi River (below) formations, they possess enough lithological differences to merit a separate formal lithostratigraphic designation. The unit stratotype proposed by Tipper and Richards (1976) contains interbedded basaltic flows, argillite and sandstone which are unique to this part of the basin (see also section NR on figure 2.17).

Spatsizi River Formation: Stratigraphic correlations established in figure 2.17 clearly show that "pyjama beds" are distinct from the Smithers and Nilkitkwa formations and occupy a higher stratigraphic position in all measured sections. However, when correlations are extended to the northern part of the basin, this poses a problem because "pyjama beds" of the Quock Member have traditionally been included in the

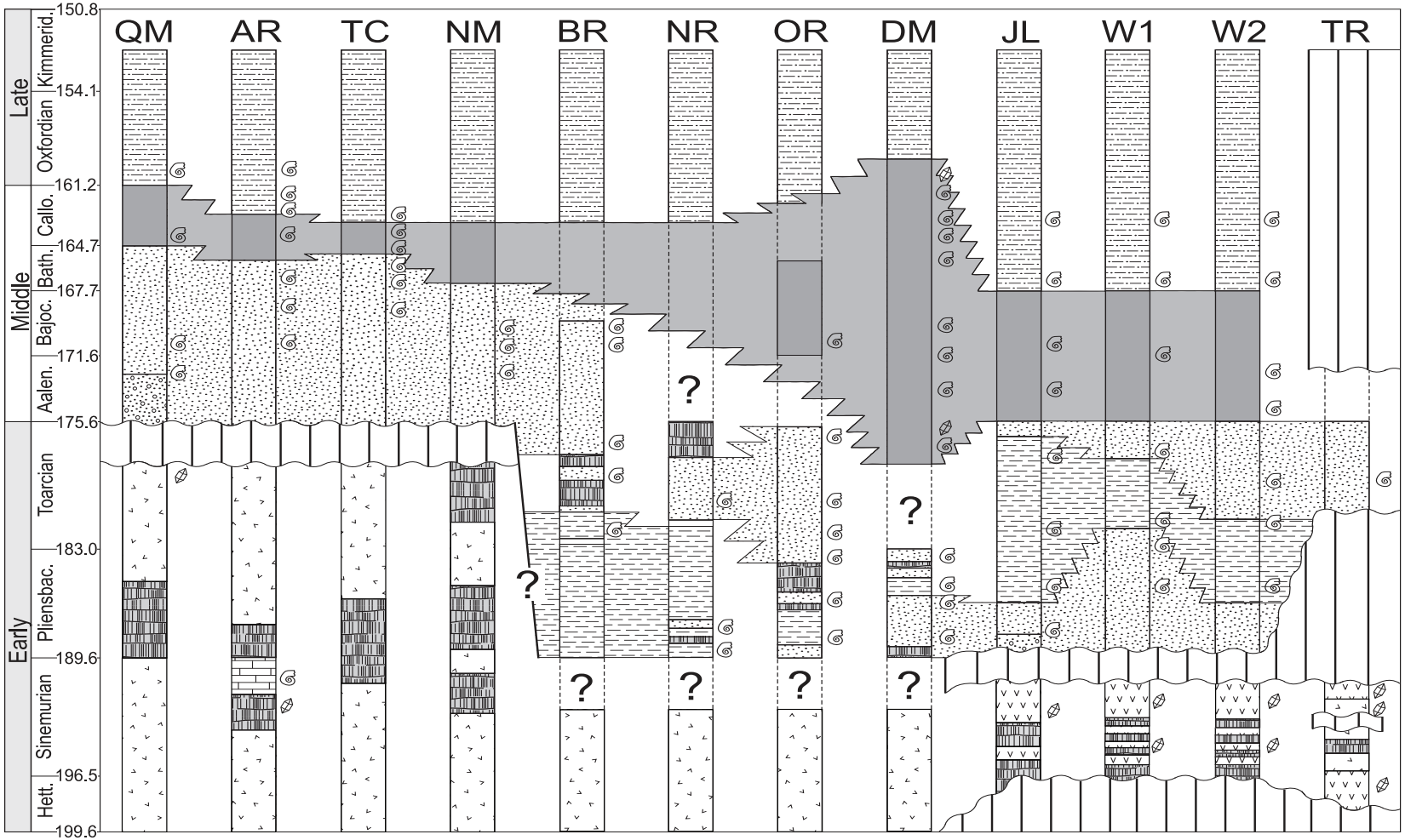

Figure 2.17: Time chart showing regional lithostratigraphic subdivisions of the Hazelton Group. Line of cross-section oriented SW-NE, at a high angle with respect to the Hazelton trough. The contact between LHG-UHG is represented by a diachronous unconformity on the margins of the trough, but might be conformable in its central portion. The Quock Formation constitutes the uppermost unit of the Hazelton Group, and is the only unit recognized throughout the basin.

Spatsizi Formation (Thomson et al. 1986; Evenchick and Thorkelson 2005). Since the lowest three members of the Spatsizi Formation (Joan, Wolf Den and Melisson) are lithostratigraphically equivalent to the Nilkitkwa and Smithers formations (figure 2.17), we propose a revision of the Spatsizi Formation to include only those three members (according to article 19 of the NASC (2005), revision of a formally defined unit is justifiable if a change of the boundaries of a unit makes it more natural for common usage). Even though the proposed revision constitutes a minor change, it alters the original type section of the Spatsizi Formation (Thomson et al. 1986) by changing its upper boundary (according to article 22c of the NASC (2005), a type section can never be changed once it is formally defined). Therefore, we propose a new name (Spatsizi River Formation) to include the Joan, Wolf Den and Melisson members into one formation. The type section at Joan Lake identified by Thomson et al. (1986) remains valid, but the upper boundary of the Spatsizi River Formation is now placed at the top of the Melisson Member (UTM 507560 E 6372125 N – NAD83 datum). The overlying Quock Member is elevated in rank to the Quock Formation and is described in the next section.

The Salmon River Formation in the Iskut River area poses even bigger challenges, as it presently includes a lower Toarcian member of bioclastic calcareous sandstone and siltstone, and an Aalenian–Bajocian member mainly comprising "pyjama beds" (Troy Ridge facies) and bimodal volcanic flows (Eskay Creek facies). Furthermore, refinements and redefinitions of the Salmon River Formation in the last two decades (Anderson and Thorkelson 1990; Anderson 1993; McDonald et al. 1996) considerably changed the scope of the formation from the original description of Schofield and Hanson (1921), such that the type area for the Salmon River Formation defined by Grove (1986) is no longer valid. In addition, the formal type section exposed near Mount Dilworth actually includes sedimentary rocks of the Bowser Lake Group (Evenchick and McNicoll 2002; Chapter 5) and lacks the characteristic pillow basalt lithology which is an essential component of the Salmon River Formation at Eskay Creek (McDonald et al. 1996; Logan et al. 2000; Alldrick et al. 2004b, 2005b; Barresi et al. 2005). In order to avoid any further confusion, we recommend the abandonment of the Salmon River Formation following article 20 of the NASC (2005) for the following reasons:

1. Invalid type area and no existing unit stratotype;
2. The term has been commonly misused in diverse ways and remains controversial;
3. Not recognizable or mappable outside the Iskut River area;
4. The name Salmon River Formation is of current usage by many local geologists and any re-assignation or modification will only add to the existing confusion;

As an alternative, we propose the following changes:

1. Correlation of the Toarcian bioclastic calcareous lower member with laterally equivalent units of the revised Spatsizi River Formation;
2. Correlation of the Troy Ridge facies with laterally equivalent units of the revised Quock Formation;
3. Introduction of a new formal geological unit: the Iskut River Formation;

A complete description of the revised Quock Formation and the proposed Iskut River Formation are presented in the following sections.

2.4.2-2 Quock Formation

Currently, the thinly bedded dark siliceous mudstone and pale-weathering tuffaceous siltstone ("pyjama beds") of the Troy Ridge facies are the only units of the Salmon River Formation recognized outside the Iskut River area (Anderson and Thorkelson 1990; Greig 1991, 1992; Marsden and Thorkelson 1992; Anderson 1993; Evenchick and Porter 1993; Jakobs 1993; Ferri et al. 2004; Evenchick and Thorkelson 2005; Ferri and Boddy 2005; Waldron et al. 2006; Gagnon et al. 2007; Gagnon and Waldron 2008). Elsewhere, they have previously been referred to as either the Yuen Member of the Smithers Formation (Tipper and Richards 1976) or the Quock Member of the Spatsizi Formation (Thomson et al. 1986; Evenchick and Thorkelson 2005). Lithostratigraphic correlations presented in this study indicate that "pyjama beds" are thinly interlayered grey to black siliceous siltstone and light coloured dust tuff found at an equivalent lithostratigraphic position across the basin (figure 2.17). The "pyjama beds" consistently occur between underlying bioturbated and fossiliferous tuffaceous sandstone and siltstone of the Smithers Formation (or equivalents), and overlying siliciclastic sedimentary rocks of the Bowser Lake Group. The widespread use of the informal term "pyjama beds" shows the need for a regionally recognized lithostratigraphic definition for this unit. We propose to elevate the rank of the Quock Member to the status of formation and to keep the original section described by Thomson et al. (1986) as the unit stratotype. The Quock Formation exposed at its type section north of Joan Lake (figure 2.7A) is defined as follows:

1. Lithological properties: thinly bedded, dark siliceous blocky mudstone and rusty-weathering tuff bands ("pyjama beds") (figure 2.8D). Thin section observations show abundant recrystalized radiolarian tests in the mudstone intervals as well as ferruginous clay, likely derived from kaolinisation of orthoclase minerals. The tuff bands are characterized by angular volcanic fragments and feldspar grains, including sanidine, in addition to white micas and chlorite. Calcareous concretionary lenses and thin limestone beds are occasionally found

throughout this unit. Discontinuous exposures of calcareous to siliceous dark shale outcropping in the lower portion of the section are included in the Quock Formation as the Abou Member;

2. Thickness: 200 m;
3. Lower boundary: conformable and gradational contact above the uppermost bioturbated sandstone of the revised Spatsizi River Formation (Melisson Member) (UTM 507560 E 6372125 N – NAD83 datum);
4. Upper boundary: conformable and gradational with the thinly-bedded fissile siltstone and shale of the BLG (Todagin assemblage) (UTM 505685 E 6373530 N – NAD83 datum);
5. Age: Bajocian, possibly Upper Aalenian (Appendix A);

On the cross-section shown in figure 2.17, it is convenient to use the first occurrence of "pyjama beds" as a definition for the base of the Quock Formation. However, the situation in the Iskut River area is slightly different because "pyjama beds" interfinger laterally with thick sections of bimodal volcanic rocks (figure 2.18). There, the uppermost package of "pyjama beds" is tentatively correlated with the Quock Formation whereas interbedded "pyjama beds" and thick piles of volcanics are included in the proposed Iskut River Formation (below).

2.4.2-3 Iskut River Formation

With assignment of the calcareous bioclastic lower member to the Spatsizi River Formation, and the "pyjama beds" of the Troy Ridge facies to the Quock Formation, the remaining Middle Jurassic facies of the now superseded Salmon River Formation require formal classification. Unlike laterally equivalent strata, these units are predominantly mafic volcanics and lesser felsic volcanics and sedimentary rocks. They consist mostly of: mafic flows with pillow basalt and pillow basalt breccia; rhyolite, in the form of flows, domes, cryptodomes, dykes, sills, rhyolitic-tuff and agglomerate; and cobble to pebble conglomerate, typically found at the base of the formation and along basin margins.

The lower contact of the Iskut River Formation is observed at many locations close to graben-bounding faults as an apparent angular unconformity where fanglomerates are juxtaposed with various units of the LHG, Stuhini Group or Stikine assemblage. In a few locations, the lower part of the formation can be traced farther from the graben margin such that the fanglomerates grade laterally into distal very fine-grained sedimentary rocks with intercalated tuff and chert, as well as bimodal volcanics including rhyolite and voluminous tholeiitic basalt (Alldrick et al. 2005b; Barresi et al. 2005). For example, at the Eskay Creek section (figures 2.12B and 2.18 section EC), rhyolite of the

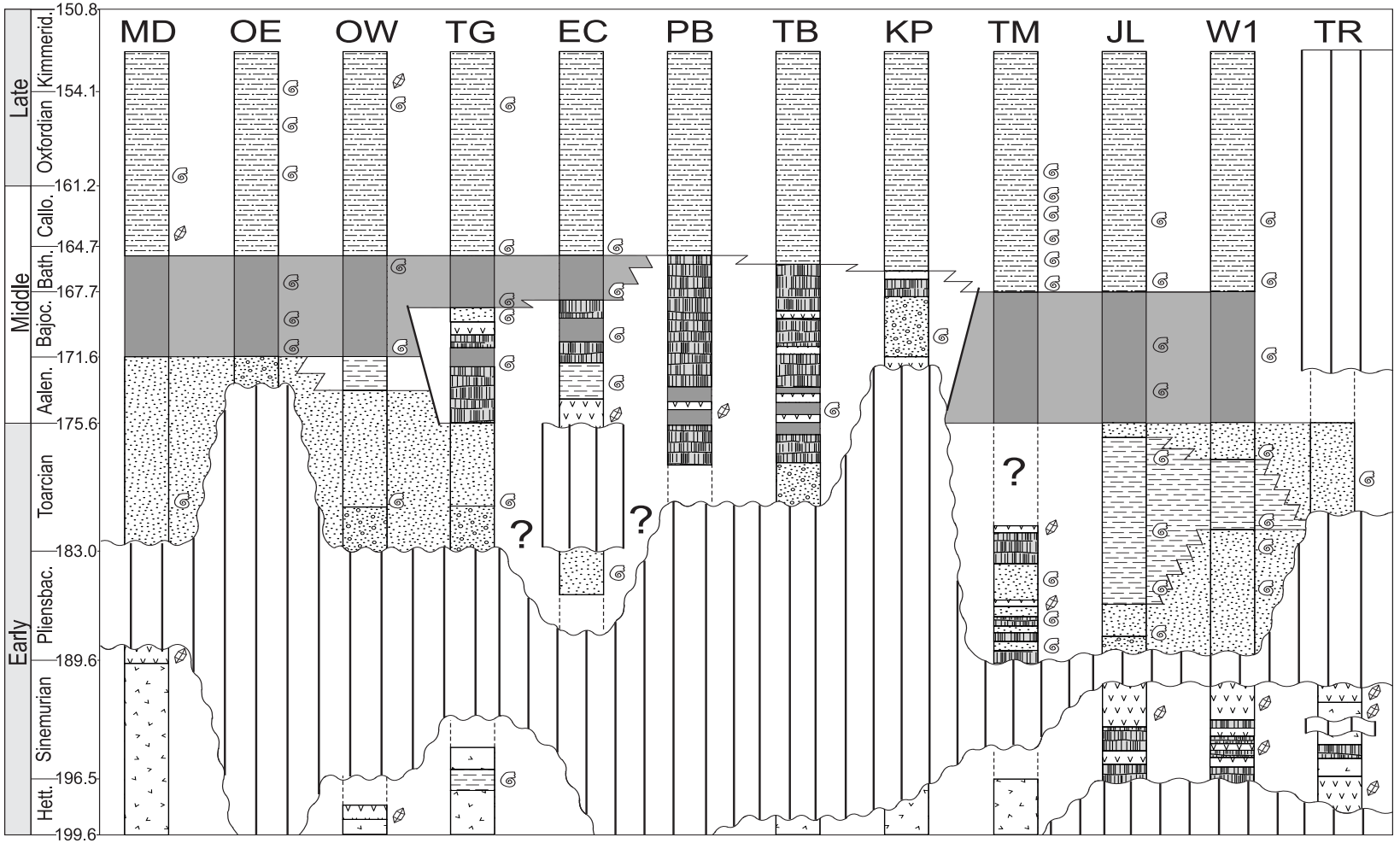

Figure 2.18: Time chart showing lithostratigraphic subdivisions of the Hazelton Group in the vicinity of the Iskut River area. Line of cross-section is oriented S-N, at a high angle with respect to the Eskay rift. The hiatus at the LHG-UHG contact is diachronous, with Middle Jurassic units of the UHG unconformably overlying Paleozoic rocks of the Stikine assemblage in some places. In this area of the basin, deposition of the pyjama beds of the Quock Formation was contemporaneous with accumulation of thick bimodal volcanic rocks of the Iskut River Formation.

Iskut River Formation disconformably overlies Upper Pliensbachian volcaniclastic rocks and felsic welded lapilli tuff of the LHG. The upper contact of the Iskut River Formation is typically conformable with the Quock Formation, or siliciclastic strata of the Bowser Lake Group. Since the section exposed at Table Mountain is the thickest and includes the greatest variety of lithological units, we proposed it as the unit stratotype for the Iskut River Formation (figures 2.12A and 2.13). Based on our observations, this section meets the necessary criteria to serve as a type section:

1. Lithological characteristics: thick volcanic piles of pillow basalt and pillow basalt breccia interbedded with intervals of rhyolite, conglomerate, and minor mudstone and dust tuff ("pyjama beds") (figure 2.14);
2. Thickness: at least 3480 metres;
3. Lower contact: angular unconformity along the ancient graben margin at which various stratigraphic levels of the Iskut River Formation onlap against the LHG; at the best exposed part of the contact (UTM 413550 E 6356000 N – NAD83 Datum), rhyolite of the Iskut River Formation rests above feldspar porphyritic andesite breccia of the lower Hazelton Group. Because the lower contact at Table Mountain is along a contemporaneous faulted graben margin, the disconformable boundary at Eskay Creek (UTM 416800 E 6279000 N – NAD83 Datum) is designated as a reference section to define the "within basin" lower contact (figure 2.12B). At this location, rhyolite of the Iskut River Formation is in contact with Upper Pliensbachian volcaniclastic rocks and felsic welded lapilli tuff of the LHG.
4. Upper contact: not observed in outcrop but closely constrained with the overlying siliciclastic rocks of the Bowser Lake Group (UTM 420000 E 6370000 N – NAD83 datum). Conformable with "pyjama beds" of the Quock Formation in the reference section at Eskay Creek (figure 2.12B);
5. Age: Upper Toarcian to Middle Bajocian fossils have been obtained from thin shale units here included in the Iskut River Formation (Souther 1972; Evenchick et al. 2001) (Appendix A). However, undated lower and higher part of the Formation could range as old as Early Toarcian and as young as Late Bajocian.

2.5 Discussion – Stratigraphic and tectonic evolution

Evolution of the Stikine terrane in Early Jurassic time was characterized by voluminous arc-related volcanism. The impressive width of the Hazelton volcanic field combined with the lack of chemical variability in major and trace element profiles led Marsden and Thorkelson (1992) to propose that volcanism was generated by concurrent

subduction of two opposing oceanic plates beneath Stikinia – one, the Cache Creek oceanic plate (east facing subduction in present coordinates), the other, west-facing subduction in present coordinates. In their model, the Hazelton Group evolved as a pair of coeval volcanic arcs separated by a NW-trending interarc basin termed the Hazelton trough (Tipper and Richards 1976; Marsden and Thorkelson 1992). Development of the Hazelton trough directly influenced the distribution of volcanic and sedimentary facies within the Hazelton Group. An understanding of these depositional units is therefore necessary in order to evaluate the stratigraphic evolution of the northern Stikine terrane in Early to Middle Jurassic.

The subsidence profile obtained by Gagnon et al. (2009; Chapter 4) in the northwest portion of the Hazelton trough indicates that extensional faulting and thermal contraction of the crust were responsible for high subsidence rates observed during the Pliensbachian. This was followed by exponentially decreasing subsidence throughout the Middle and Late Jurassic, as suggested by the concave-up profile of the backstripped tectonic subsidence curve. These results are consistent with the crustal subsidence model of Thorkelson et al. (1995) who proposed that accumulation of a thick volcanic pile in the Spatsizi River area represented at least 2 km of synvolcanic subsidence. Following a protracted period of volcanism during Late Sinemurian, as suggested by the abundant bimodal volcanic lava of the Cold Fish Volcanics (Marsden and Thorkelson 1992; Thorkelson, 1992; Thorkelson et al. 1995) and the thick succession of the Telkwa Formation (Tipper and Richards 1976), thermal contraction of the crust resulted in widespread subsidence of the Hazelton trough. Aside from a few basaltic eruptions restricted to the Nilkitkwa depression (i.e. Mount Brock volcanics, Ankwell and Carruthers members), the Hazelton trough then experienced a progressive decline of volcanic activity after Sinemurian time (figure 2.19A). Thermally subsiding volcanic remnants on the periphery of the graben became progressively submerged by the transgressive sea which led to deposition of shallow-water sedimentary rocks of the Smithers Formation and equivalents. Where exposed, the base of this unit is marked by a coarse-grained transgressive lag that fines upward into interbedded sandstone and siltstone. This contact constitutes the most important lithostratigraphic boundary within the Hazelton Group and marks the transition from the volcanic-dominated LHG to the overlying sedimentary-dominated UHG.

Stratigraphic cross-sections shown in figures 2.17 and 2.18 highlight the variability and diachronous nature of the LHG–UHG boundary. Although development of a graben structure ensured continuous marine deposition within the Nilkitkwa depression, rift margins of the Hazelton trough probably experienced occasional uplift and erosion

(Tipper and Richards 1976). This is a common feature in extensional settings, such as back-arcs and continental rifts, where graben flanks become subaerially exposed in response to block tilting, and can lead to development of unconformities (c.f. Baker et al. 1972; Kusznir and Egan 1990; Ebinger et al. 1991; Lin et al. 2003). The LHG–UHG contact appears conformable in the central part of the Hazelton trough (figure 2.17) where Lower Pliensbachian sedimentary rocks of the Nilkitkwa Formation directly overlie marine volcanic rocks of the Telkwa Formation (Tipper and Richards 1976). Elsewhere, outside the main trough axis, the base of the UHG is equivalent in age or younger, and is marked by an unconformity (figures 2.17 and 2.18). In the Spatsizi River area, Lower Pliensbachian shallow-marine sedimentary rocks of the Joan Member disconformably overlie the subaerial Cold Fish Volcanics whereas a Toarcian hiatus has been reported in the Toodoggone, Iskut, Smithers and Terrace areas (Diakow et al. 1991; Anderson 1993; Greig and Gehrels 1995; Waldron et al. 2006; Gagnon et al. 2007; Nelson et al. 2007). The diachronous nature of the LHG–UHG transition probably reflects the differential subsidence rates that affected the Hazelton arc during Early to Middle Jurassic. In depocenters characterized by intense volcanism and extensional faulting, onlap of the unconformity by shallow-marine sedimentary rocks occurred immediately after cessation of back-arc activity. This is attributed to greater post-rift subsidence rates in areas where the initial amount of lithospheric stretching was more significant (c.f. McKenzie 1978; Steckler and Watts 1978). On the other hand, sedimentation around slower subsiding areas began later, when marine transgression reached its maximum extent around the Toarcian–Aalenian boundary (figure 2.19B). This event was contemporaneous with the onset of sedimentation of the Quock Formation, whose base is interpreted to represent a maximum flooding surface.

Extensive paleontological data reported from the Quock Formation at Diagonal Mountain indicate that "pyjama beds" accumulated over a protracted period (Late Toarcian to Early Oxfordian) (Evenchick and Porter 1993; Jakobs 1993; Evenchick et al. 2001, *submitted*). The fine grain size and thinly bedded nature of the Quock Formation, combined with its high organic content (TOC values up to 6%, Ferri and Boddy 2005), suggest that it was deposited mainly from suspension in a deep-water, anoxic environment. Regionally, condensed sections of "pyjama beds" form a basin-wide stratigraphic marker and are commonly found near the top of the Hazelton Group (figure 2.17).

The situation is different in the Iskut River area where extension-controlled volcanism prevailed in an elongate, narrow rift basin during a short period, from Late Toarcian to Middle Bajocian time (figure 2.18). Fault-controlled subsidence led to

compartmentalization of at least 12 north-trending sub-basins within the 300 km long by 50 km wide volcanic belt of the Eskay rift (Alldrick et al. 2005b; T. Barresi, Dalhousie University, pers. comm. 2010) (figure 2.19C). The irregular topography of the rift basement characterized by depocenters and uplifted horst blocks considerably hampers stratigraphic correlations within the Iskut River Formation. Volcanic and sedimentary units have highly inconsistent stratigraphic order and thickness because of the limited connectivity between each sub-basin. In addition, the local nature of volcanic stratigraphy probably had a significant impact on the extreme thickness change of units observed

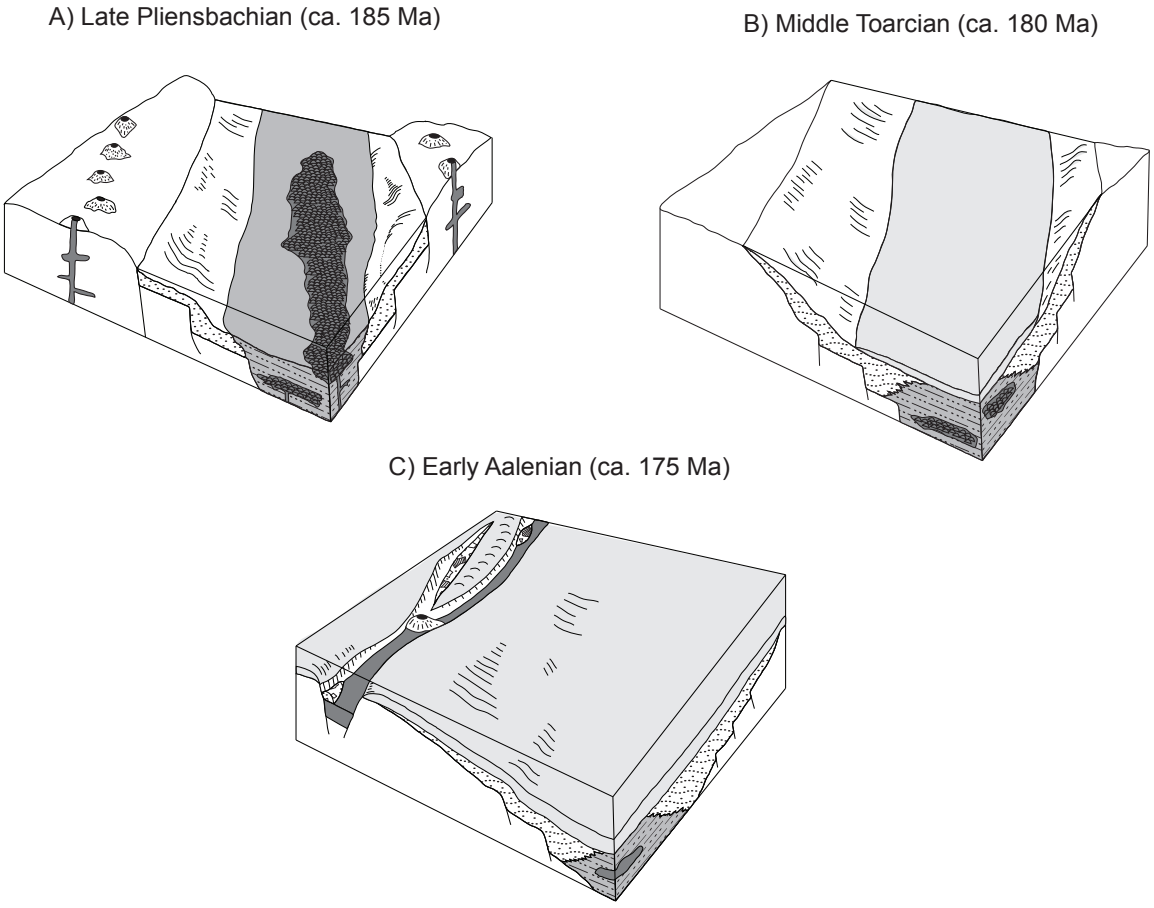

Figure 2.19: Conceptual block diagrams showing the interpreted depositional environment of the upper Hazelton Group in the Early to Middle Jurassic. A) In the Pliensbachian (ca. 185 Ma), mafic volcanism and deep-water sedimentation dominated the central portion of the Hazelton trough while coarser clastic rocks accumulated on the margins. B) In the Toarcian (ca. 180 Ma), progressive decrease in volcanic activity led to thermal subsidence of the Stikine terrane and relative sea-level rise. Pyjama beds of Quock Formation began to accumulate in the central portion of the Hazelton trough. C) In the Aalenian (ca. 175 Ma), pyjama beds of the Quock Formation were deposited throughout the basin and back-arc extension in the Iskut River area led to accumulation of the rift-related facies of the Iskut River Formation.

from different sub-basins. Nearly uninterrupted successions of pillow basalt up to 2 km thick exposed at Pillow Basalt Ridge (PBR) and Table Mountain (TB) suggest relatively rapid extrusion and basin filling, whereas other sub-basins (e.g. Eskay Creek - EC and Treaty Glacier - TG) have a higher proportion of fine-grained sedimentary rocks and lack thick basaltic flows (figure 2.18). Such intense volcanic activity above restricted feeder zones locally out-competed the accumulation of "pyjama bed" successions. However, rare occurrences of thin "pyjama bed" intervals between basaltic flows attest to short episodes of volcanic quiescence, when conditions favourable to pelagic sedimentation were re-established. According to Alldrick et al. (2004b), such quiescent depositional environments were more prone to accumulation and preservation of exhalative sulphides. In summary, the Iskut River Formation differs from the rest of the UHG in several ways:

1. Deposition was restricted to a set of narrow, north-trending sub-basins that extended from Anyox in the south to Kinaskan Lake in the north (figure 2.1);
2. Stratigraphic record dominated by bimodal volcanics and polymictic fanglomerates;
3. Extreme thickness changes related to fault-controlled subsidence and localised volcanic feeders;
4. Narrow age bracket (Upper Toarcian to Middle Bajocian) compared with the rest of the UHG (Lower Pliensbachian to Lower Oxfordian).

2.6 Conclusions

Regional correlations of lithostratigraphic units based on new detailed measured sections indicate that the Lower to Middle Hazelton Group can be divided in two distinct intervals separated by an unconformity in most places. The lower Hazelton Group is dominated by arc-related volcanic rocks whereas the upper Hazelton Group contains mainly fine-grained clastic rocks and bimodal rift-related volcanic rocks. A sharp decline of volcanic activity following a back-arc rifting event in the Sinemurian led to widespread thermal subsidence of the magmatic arc and initiation of sedimentation in the Hazelton trough. Thick mudstone-dominated successions (Nilkitkwa Formation and most of the Spatsizi River Formation) accumulated in the central portion of the Hazelton trough, whereas topographically higher areas along the margins were the loci of shallow marine coarse-grained sedimentation (Smithers Formation and parts of the Spatsizi River Formation). Continuation of subaerial arc volcanism as late as Toarcian is recorded in the Terrace to Smithers area with accumulation of the Red Tuff member. Progressive onlap of the unconformity by lowermost strata of the UHG was diachronous at the basin scale, reflecting differential subsidence rates across the Stikine terrane. Ongoing

rise in relative sea-level, in part attributed to eustasy, eventually led to accumulation of siliceous mudstone and tuff of the Quock Formation above a flooding surface, when the sea reached its maximum extent at the Toarcian–Aalenian boundary. Regionally, "pyjama beds" of the Quock Formation constitute an excellent stratigraphic marker and are characterized by moderate to high TOC values, which under the proper thermal maturity levels, would have been favourable for generation of hydrocarbons. In the northwest portion of the basin, the Quock Formation is laterally equivalent to bimodal volcanic rocks and associated volcanic massive sulphide deposits of the Iskut River Formation. In contrast to other units of the UHG, deposition of the rift-related rocks of the Iskut Formation was not diachronous. It mostly occurred during a limited period of time between the Aalenian and Bajocian, and was independent of extension and volcanism experienced earlier by the Hazelton trough. Therefore, northern Stikine was affected by at least two independent rifting events during deposition of the Hazelton Group: a widespread Late Sinemurian to Early Pliensbachian extension phase in the northwest-trending Hazelton trough, and a more restricted Aalenian to Bajocian extensional event in the north-trending Eskay rift.

2.7 References

Alldrick, D.J. 1987. Geology and Mineral Deposits of the Salmon River Valley, Stewart Area. British Columbia Ministry of Energy, Mines and Petroleum Resources, Open File Map 1987-22.

Alldrick, D.J. 1991. Geology and ore deposits of the Stewart Mining Camp. Ph.D. thesis, Department of Earth and Ocean Sciences, University of British Columbia, Vancouver, B.C.

Alldrick, D.J. 1993. Geology and metallogeny of the Stewart mining camp, northwestern British Columbia. British Columbia Ministry of Energy, Mines and Petroleum Resources, Report 85., 105 p.

Alldrick, D.J., Brown, D.A., Harakal, J.E., Mortensen, J.K. and Armstrong, R.L. 1987. Geochronology of the Stewart Mining Camp (104/B1), B.C. *In:* Geological Fieldwork 1986. British Columbia Ministry of Energy, Mines and Petroleum Resources, Paper 1987-1, pp. 81-92.

Alldrick, D.J., Britton, J.M., Webster, I.C.L. and Russell, C.W.P. 1989. Geology and mineral deposits of the Unuk area. British Columbia Ministry of Energy, Mines and Petroleum Resources, Open File 1989-10.

Alldrick, D.J., Stewart, M.L., Nelson, J.L. and Simpson, K.A. 2004a. Geology of the More Creek - Kinaskan Lake area, northwestern British Columbia. British Columbia Ministry of Energy, Mines and Petroleum Resources, Open File Map 2004-2.

Alldrick, D.J., Stewart, M.L., Nelson, J.L. and Simpson, K.A. 2004b. Tracking the Eskay Rift through northern British Columbia - geology and Mineral occurrences of the Upper Iskut River area. *In:* Geological Fieldwork 2003. British Columbia Ministry of Energy, Mines and Petroleum Resources, Paper 2004-1, pp.1-18.

Alldrick, D.J., Nelson, J.L. and Barresi, T. 2005a. Geology of the More Creek - Palmiere Creek area, northwestern British Columbia. British Columbia Ministry of Energy, Mines and Petroleum Resources, Open File Map 2005-5.

Alldrick, D.J., Nelson, J.L. and Barresi, T. 2005b. Geology and mineral occurrences of the Upper Iskut River Area: tracking the Eskay rift trough northern British Columbia (Telegraph Creek NTS 104G/1, 2; Iskut River NTS 104B/9, 10, 15, 16). *In:* Geological Fieldwork 2004. British Columbia Ministry of Energy, Mines and Petroleum Resources, Paper 2005-1, pp. 1-30.

Alldrick, D.J., Nelson, J.L., Barresi, T., Stewart, M.L. and Simpson, K.A. 2006. Geology of the Upper Iskut River Area, British Columbia. British Columbia Ministry of Energy, Mines and Petroleum Resources, Open File Map 2006-2.

Anderson, R.G. 1993. A Mesozoic stratigraphic and plutonic framework for northwestern Stikinia (Iskut River area), northwestern British Columbia, Canada. *In:* Dunne, G., McDougall, K. (Eds.), Mesozoic Paleogeography of the Western United States--II. Society of Economic Paleontologists and Mineralogists, Pacific Section, vol. 71, pp. 477-494.

Anderson, R.G. and Thorkelson, D.J. 1990. Mesozoic stratigraphy and setting for some mineral deposits in Iskut River map area, northwestern British Columbia. *In:* Current Research, Part E. Geological Survey of Canada, Paper 90-1E, pp. 131-139.

Armstrong, J.E. 1944. Smithers, British Columbia. Geological Survey of Canada, Paper 44-23.

Armstrong, R.L. 1988. Mesozoic and early Cenozoic magmatic evolution of the Canadian Cordillera. Geological Society of America Bulletin, Special Paper 218, pp. 55-91.

Baker, B.H., Mohr, P.A. and Williams, L.A.G. 1972. Geology of the Eastern Rift System of Africa. Geological Society of America Bulletin, Special Paper 136, pp. 1-67.

Barresi, T. and Dostal, J. 2005. Geochemistry and Petrography of Upper Hazelton Group volcanics: VHMS-Favourable Stratigraphy in the Iskut River and Telegraph Creek Map Areas, Northwestern British Columbia. *In:* Geological Fieldwork 2004. British Columbia Ministry of Energy, Mines and Petroleum Resources, Paper 2005-1, pp. 39-47.

Barresi, T., Nelson, J.L., Alldrick, D.J., and Dostal, J. 2005. Pillow Basalt Ridge Facies: Detailed mapping of Eskay Creek-Equivalent Stratigraphy in Northwestern British Columbia. *In:* Geological Fieldwork 2004. British Columbia Ministry of Energy, Mines and Petroleum Resources, Paper 2005-1, pp. 31-38.

Barrett, T.J. and Sherlock, R.L. 1996. Geology, Lithogeochemistry and Volcanic Setting of the Eskay Creek Au-Ag-Cu-Zn Deposit, Northwestern British Columbia. Exploration Mining Geology, vol. 5, pp. 339-368.

Bartsch, R.D. 1993. A rhyolite flow dome in the upper Hazelton Group, Eskay Creek area (104B/9, 10), British Columbia. *In:* Geological Fieldwork 1992. Ministry of Energy, Mines and Petroleum Resources, Report Paper 1993-1, pp. 331-334.

Bourgault, M.-A. 2009. Characterization of the Netalzul Volcanics: petrogenetic study and tectonic implication. B.Sc. thesis, Department of Earth and Planetary Sciences, McGill University, Montréal, Qc.

Bromley, R.G. and Ekdale, A.A. 1984. *Chondrites*: A Trace Fossil Indicator of Anoxia in Sediments. Science, vol. 224, pp. 872-874.

Brown, D.A., Gunning, M.H., Orchard, M.J. and Bamber, W.E. 1991. Stratigraphic evolution of the Paleozoic Stikine assemblage in the Stikine and Iskut rivers area, northwestern British Columbia. Canadian Journal of Earth Sciences, vol. 28, pp. 958-972.

Carter, N.C. 1972. Toodoggone River Area. *In:* Geology, Exploration and Mining. British Columbia Ministry of Energy, Mines and Petroleum Resources, pp. 63-70.

Childe, F.C. 1996. U-Pb Geochronology and Nb and Pb Isotopic Characteristics of the Au-Ag-Rich Eskay Creek Volcanogenic Massive Sulphide Deposit, British Columbia. Economic Geology, vol. 91, pp. 1209-1224.

Cordey, F., Greig, C.J. and Orchard, M.J. 1991. Permian, Triassic, and Middle Jurassic microfaunal associations, Stikine terrane, Oweegee and Kinskuch areas, northwestern British Columbia. *In:* Current Research. Geological Survey of Canada, Paper 92-1E, pp. 107-116.

Dawson, G.M. 1877. Report on explorations in British Columbia. Geological Survey of Canada, pp. 1875-1876.

Diakow, L. 2001. Geology of the southern Toodoggone River and northern McConnell Creek map areas, north-central British Columbia. British Columbia Ministry of Energy, Mines and Petroleum Resources, Open File Map 2001-1.

Diakow, L. 2006. Geology between the Finlay River and Chukachida Lake, central Toodoggone River map area, north-central British Columbia (parts of NTS 94E/2, 6, 7, 10 and 11). British Columbia Ministry of Energy, Mines and Petroleum Resources, Open File Map 2006-1.

Diakow, L., and Mihalynuk, M.G. 1987. Geology of Whitesail Reach and Troitsa Lake map areas (93E/10W, 11E). *In* Geological Fieldwork 1986. British Columbia Ministry of Energy, Mines and Petroleum Resources, Paper 1987-1, pp. 171-180.

Diakow, L.J., Panteleyev, A. and Schroeter, T.G. 1991. Jurassic Epithermal Deposits in the Toodoggone River Area, Northern British Columbia: Examples of Well-Preserved, Volcanic-Hosted, Precious Metal Mineralization. Economic Geology, vol. 86, pp. 529-554.

Dickinson, J.M. 2006. Jura-triassic magmatism and porphyry Au-Cu mineralization at the Pine deposit, Toodoggone district, north-central British Columbia. M.Sc. thesis, Department of Earth and Ocean Sciences, University of British Columbia, Vancouver, B.C.

Duffell, S., and Souther, J.G. 1964. Geology of Terrace Map-Area, British Columbia. Geological Survey of Canada, Memoir 329, 117 p.

Duuring, P., Rowins, S.M., McKinley, B.S.M., Dickinson, J.M., Diakow, L.J., Kim, Y.-S. and Creaser, R.A. 2009. Examining potential genetic links between Jurassic porphyry Cu-Au+/-Mo and epithermal Au+/-Ag mineralization in the Toodoggone district of North-Central British Columbia, Canada. Mineralium Deposita, vol. 44, pp. 463-496.

Ebinger, C.J., Karner, G.D. and Weissel, J.K. 1991. Mechanical strength of extended continental lithosphere. Constraints from the Western Rift System. Tectonics, vol. 10, pp. 1239-1256.

Eisbacher, G.H. 1985. Pericollisional strike-slip faults and synorogenic basins, Canadian Cordillera. *In:* Biddle, K.T., Christie-Blick, N. (Eds.), Strike-slip deformation, basin formation, and sedimentation. Society of Economic Paleontologists and Mineralogists, Special Publication 37, pp. 265-282.

Ettlinger, A.D. 1992. Hydrothermal alteration and brecciation underlying the Eskay Creek polymetallic massive sulphide deposit (104B/9W), British Columbia. *In* Geological Fieldwork 1991. British Columbia Ministry of Energy, Mines and Petroleum Resources, Report Paper 1992-1, pp. 535-542.

Evenchick, C.A. and Porter, J.S. 1993. Geology of west McConnell Creek map area, British Columbia. *In:* Current Research. Geological Survey of Canada, Paper 93-1A, pp. 47-55.

Evenchick, C.A. and McNicoll, V.J. 2002. Stratigraphy, structure, and geochronology of the Anyox Pendant, northwest British Columbia, and implications for mineral exploration. Canadian Journal of Earth Sciences, vol. 39, pp. 1313-1332.

Evenchick, C.A. and Thorkelson, D.J. 2004. Geology, Cold Fish Lake, British Columbia. Geological Survey of Canada, Map 2030A.

Evenchick, C.A. and Thorkelson, D.J. 2005. Geology of the Spatsizi River map area, north-central British Columbia. Geological Survey of Canada, Bulletin 577, 276p.

Evenchick, C.A., Mustard, P.S., Porter, J.R. and Greig, C.J. 1992. Regional Jurassic and Cretaceous facies assemblages, and structural geology in Bowser Lake map area (104A), B.C. Geological Survey of Canada, Open File 2582.

Evenchick, C.A., Poulton, T.P., Tipper, H.W. and Braidek, I. 2001. Fossils and facies of the northern two-thirds of the Bowser Basin, British Columbia. Geological Survey of Canada, Open File 3956.

Evenchick, C.A., Ferri, F., Mustard, P.S., McMechan, M.E., Osadetz, K.G., Stasiuk, L.D., Wilson, N.S.F., Enkin, R.J., Hadlari, T. and McNicoll, V.J. 2003. Recent results and activities of the Integrated Petroleum Resource Potential and Geoscience Studies of the Bowser and Sustut Basins project, British Columbia. *In:* Current Research. Geological Survey of Canada, Paper 2003-A13.

Evenchick, C.A., Ferri, F., Mustard, P.S., McMechan, M.E., Ritcey, D., McNicoll, V.J., Osadetz, K.G., O'Sullivan, P.B., Stasiuk, L.D., Wilson, N.S.F., Poulton, T.P., Lowe, C., Enkin, R.J., Waldron, J.W.F., Snyder, D.B., Turner, R.J.W., Nowlan, G. and Boddy, M. 2005. Highlights of recent research in the Bowser and Sustut Basins Project, British Columbia. *In:* Current research. Geological Survey of Canada, Paper 2005-A1.

Evenchick, C.A., Mustard, P.S., McMechan, M.E., Ferri, F., Porter, S., Hadlari, T. and Jakobs, G.K. 2007. Geology, McConnell Creek, British Columbia. Geological Survey of Canada, Open File 5571.

Evenchick, C.A., Mustard, P.S., McMechan, M.E., Ritcey, D.H. and Smith, G.T. 2008a. Geology, northeast Terrace and northwest Smithers, British Columbia. Geological Survey of Canada, Open File 5895.

Evenchick, C.A., McMechan, M.E., Mustard, P.S., Ritcey, D., Smith, G.T., Ferri, F. and Waldron, J.W.F. 2008b. Geology, Hazelton, British Columbia. Geological Survey of Canada, Open File 5704.

Evenchick, C.A., Mustard, P.S., McMechan, M.E., Greig, C.J., Ferri, F., Ritcey, D., Smith, G., Hadlari, T. and Waldron, J.W.F. 2009. Geology, Compilation Geology of Bowser and Sustut Basins Draped on Shaded Relief Map, North-central British Columbia. Geological Survey of Canada, Open File 5794.

Evenchick, C.A., Poulton, T.P. and McNicoll, V.J. *Submitted for publication*. Nature and significance of the diachronous contact between the Hazelton and the Bowser Lake groups (Jurassic), north-central British Columbia. Bulletin of Canadian Petroleum Geology.

Ferri, F. and Boddy, M. 2005. Geochemistry of Early to Middle Jurassic Organic-rich Shales, Intermontane Basins, British Columbia. *In:* Summary of Activities 2005. British Columbia Ministry of Energy, Mines and Petroleum Resources, pp. 132-151.

Ferri, F., Osadetz, K.G. and Evenchick, C.A. 2004. Petroleum source rock potential of Lower to Middle Jurassic clastics, Intermontane Basins, British Columbia. *In:* Summary of Activities 2004. British Columbia Ministry of Energy, Mines and Petroleum Resources, pp. 87-97.

Gabrielse, H., Wanless, R.K., Amrstrong, R.L. and Erdman, L.R. 1980. Isotopic dating of Early Jurassic volcanism and plutonism in north-central British Columbia. *In:* Current Research. Geological Survey of Canada, Paper 80-1A, pp. 27-32.

Gabrielse, H. 1991. Late Paleozoic and Mesozoic terrane interactions in north-central British Columbia. Canadian Journal of Earth Sciences, vol. 28, pp. 947-957.

Gagnon, J.-F. and Waldron, J.W.F. 2008. Ashman Ridge Section Revisited: New Insights for the Evolution

of the Bowser Basin, Northwestern British Columbia (NTS 93L/13). *In:* Summary of Activities 2007. Geoscience BC, Report 2008-1, pp. 121-128.

Gagnon, J.-F., Loogman, W., Waldron, J.W.F., Cordey, F. and Evenchick, C.A. 2007. Stratigraphic Record of Initiation of Sedimentation in the Bowser Basin (NTS 104A, H), Northwestern British Columbia. *In:* Geological Fieldwork 2006. British Columbia Ministry of Energy, Mines and Petroleum Resources, Paper 2007-1, pp. 275-283.

Gagnon, J.-F., Evenchick, C.A., Waldron, J.W.F., Cordey, F. and Poulton, T.P. 2009. Jurassic subsidence history of the Hazelton Trough-Bowser Basin in the area of Todagin Mountain, north-central British Columbia, Canada. Bulletin of Canadian Petroleum Geology, vol. 57, pp. 430-448.

Gareau, S.A., Friedman, R.M., Woodsworth, G.J. and Childe, F.C. 1997. U-Pb ages from the northeastern quadrant of the Terrace map area, west-central British Columbia. *In:* Current research. Geological Survey of Canada, Paper 1997-A/B, pp. 31-40.

Gradstein, F.M., Ogg, J.G., Smith, A.G., Agterberg, F.P., Bleeker, W., Cooper, R.A., Davydov, V., Gibbard, P., Hinnov, L.A., House, M.R., Lourens, L., Luterbacher, H.P., McArthur, J., Melchin, M.J., Robb, L.J., Shergold, J., Villeneuve, M., Wardlaw, B.R., Ali, J., Brinkhuis, H., Hilgen, F.J., Hooker, J., Howarth, R.J., Knoll, A.H., Laskar, J., Monechi, S., Plumb, K.A., Powell, J., Raffi, I., Röhl, U., Sadler, P., Sanfilippo, A., Schmitz, B., Shackleton, N.J., Shields, G.A., Strauss, H., Van Dam, J., van Kolfschoten, T., Veizer, J., and Wilson, D. 2004. Geological Time Scale 2004. Cambridge University Press.

Green, G.M. 1992. Detailed sedimentology of the Bowser Lake Group, northern Bowser Basin, north-central British Columbia. M.Sc. thesis, Department of Earth Sciences, Carleton University, Ottawa, Ont.

Greig, C.J. 1991. Stratigraphic and structural relations along the west-central margin of the Bowser Basin, Oweegee and Kinskuch areas, northwestern British Columbia. *In:* Current Research, Part A, Geological Survey of Canada, Paper 91-1A, pp. 197-205.

Greig, C.J. 1992. Fieldwork in the Oweegee and Snowslide ranges and Kinskuch Lake area, northwestern British Columbia. *In* Current Research, Part A, Geological Survey of Canada, Paper 92-1A, pp. 145-155.

Greig, C.J. and Evenchick, C.A. 1993. Geology of Oweegee Dome (geochemistry and paleontology), Delta Peak (104A/12) and Taft Creek (104A/11W) map areas, northwestern British Columbia. Geological Survey of Canada, Open File 2688.

Greig, C.J. and Gehrels, G.E. 1995. U-Pb zircon geochronology of Lower Jurassic and Paleozoic Stikinian strata and Tertiary intrusions, northwestern British Columbia. Canadian Journal of Earth Sciences, vol. 32, pp. 1155-1171.

Grove, E.W. 1986. Geology and mineral deposits of the the Unuk River - Salmon River - Anyox area. British Columbia Ministry of Energy, Mines and Petroleum Resources, Bulletin 63, 152p.

Gunning, M.H. 1986. Late Triassic to Middle Jurassic (Norian to Oxfordian) volcanic and sedimentary stratigraphy and structure in the southeastern part of the Iskut map sheet, north-central British Columbia. B.Sc. thesis, Department of Earth and Ocean Sciences, The University of British Columbia, Vancouver, B.C.

Hanson, G. 1925. Driftwood Creek map-area, Babine Mountains, British Columbia. *In:* Summary Report 1924, Geological Survey of Canada, Part A, pp. 19-37.

Henderson, J.R., Kirkham, R.V., Henderson, M.N., Payne, J.G., Wright, T.O. and Wright, R.L. 1992.

Stratigraphy and Structure of the Sulphurets Area, British Columbia. *In:* Current Research, Part A, Geological Survey of Canada, Paper 92-1A, pp. 323-332.

Jakobs, G.K. 1993. Jurassic stratigraphy of the Diagonal Mountain area, McConnell Creek map area, north-central British Columbia. *In:* Current Research, Part A, Geological Survey of Canada, Paper 93-1A, pp. 43-46.

Jakobs, G.K. 1997. Toarcian (Early Jurassic) ammonoids from Western North America. Geological Survey of Canada, Bulletin 428, 137 p.

Johnston, K.K. 2002. Taxonomy and biostratigraphy of Middle Jurassic ammonites, western and central British Columbia. M.Sc. thesis, Department of Geosciences, University of Calgary, Calgary, Ab.

Kusznir, N.J. and Egan, S.S. 1990. Simple-shear and pure-shear models of extensional sedimentary basin formation: Application to the Jeanne d'Arc Basin, Grand Banks of Newfoundland. *In:* Tankard, A.J., Balkwill, H.R. (Eds.), Extensional Tectonics of the North Atlantic Margins. AAPG Memoir 46, pp. 305-322.

Leach, W.W. 1910. The Skeena River District. *In:* Summary report 1910. Geological Survey of Canada, Sessional Paper 26, pp. 61-68.

Lewis, P.D., Thompson, J.F.H., Nadaraju, G., Anderson, R.G. and Johannson, G.G. 1993. Lower and Middle Jurassic stratigraphy in the Treaty glacier area and geological setting of the Treaty glacier alteration system, northwestern British Columbia. *In:* Current Research, Part A. Geological Survey of Canada, Paper 93-1A, pp. 75-86.

Lin, A.T., Watts, A.B. and Hesselbo, S.P. 2003. Cenozoic stratigraphy and subsidence history of the South China Sea Margin in the Taiwan region. Basin Research, vol. 15, pp. 453-478.

Logan, J.M., Drobe, J.R. and McClelland, W.C. 2000. Geology of the Forest Kerr - Mess Creek area, Northwestern British Columbia (104B/10,15 & 104G/2 & 7W). British Columbia Ministry of Energy, Mines and Petroleum Resources, Bulletin 104, 164 p.

Loogman, W. 2008. Structure and Kinematic Development of the northwest Skeena Fold Belt, northwestern British Columbia. M.Sc. thesis, Department of Earth and Atmospheric Sciences, University of Alberta, Edmonton, Ab.

Ludwig, K.R. 2003. User's manual for Isoplot 3.00. Berkeley Geochronology Center Special Publication 4, 71p.

MacIntyre, D.G., Desjardins, P. and Tercier, P. 1989. Jurassic stratigraphic relationships in the Babine and Telkwa Ranges (93L/10, 11, 14, 15). *In:* Geological Fieldwork 2008. British Columbia Ministry of Energy, Mines and Petroleum Resources, Paper 1989-1, pp. 195-208.

MacIntyre, D.G., Webster, I.C.L. and Villeneuve, M. 1997. Babine Porphyry Belt Project: Bedrock Geology of the Old Fort Mountain Area (93M/1), British Columbia. *In:* Geological Fieldwork 1996. British Columbia Ministry of Energy, Mines and Petroleum Resources, Paper 1997-1, pp. 47-68.

MacIntyre, D.G., Villeneuve, M. and Schiarrizza, P. 2001. Timing and tectonic setting of Stikine Terrane magmatism, Babine-Takla lakes area, central British Columbia. Canadian Journal of Earth Sciences, vol. 38, pp. 579-601.

Mahoney, J.B., Gordee, S.M., Haggart, J.W., Friedman, R.M., Diakow, L.J. and Woodsworth, G.J. 2009. Magmatic evolution of the eastern Coast Plutonic Complex, Bella Colla region, west-central British Columbia. Geological Society of America Bulletin, vol. 121, pp. 1362-1380.

Marsden, H. 1990. Stratigraphic, Structural and tectonic setting of the Shasta Au-Ag deposit, north-central British Columbia. M.Sc. thesis, Department of Earth Sciences, Carleton University, Ottawa, Ont.

Marsden, H. and Thorkelson, D.J. 1992. Geology of the Hazelton Volcanic Belt in British Columbia: Implications for the Early to Middle Jurassic Evolution of Stikinia. Tectonics, vol. 11, pp. 1266-1287.

McClelland, W.C. 1992. Permian and older rocks of the southwestern Iskut River map area, northwestern British Colombia. Geological Society of America Bulletin, Special Paper 343, pp. 159-182.

McDonald, D.W.A. 1990. The Silbak Premier silver-gold deposit; a structurally-controlled, base metal-rich Cordilleran epithermal deposit, Stewart, B.C. Ph.D. thesis, Department of Earth Sciences, University of Western Ontario, Ottawa, Ont.

McDonald, A.J., Lewis, P.D., Thomson, J.F.H., Nadaraju, G., Bartsch, R.D., Bridge, D.J., Rhys, D.A., Roth, T., Kaip, A., Godwin, C.I. and Sinclair, A.J. 1996. Metallogeny of an Early to Middle Jurassic Arc, Iskut River Area, Northwestern British Columbia. Economic Geology, vol. 91, pp. 1098-1114.

McKenzie, D. 1978. Some remarks on the development of sedimentary basins. Earth and Planetary Science Letters, vol. 40, pp. 25-32.

McNicoll, V.J. and Evenchick, C.A. 2004. New constraints provided by provenance studies on the depositional histories of the Bowser and Sustut Basins, and their implications for tectonic evolution of the northern Canadian Cordillera. *In:* Abstracts with Programs - Geological Society of America annual meeting, Denver, Col., vol. 36, p. 271.

Monger, J.W.H. 1977. Upper Paleozoic rocks of the western Canadian Cordillera and their bearing on Cordilleran evolution. Canadian Journal of Earth Sciences, vol. 14, pp. 1832-1859.

Monger, J.W.H. 1980. Upper Triassic stratigraphy, Dease Lake and Tulsequah map areas, Northwestern British Columbia. *In:* Current research. Geological Survey of Canada, Paper 80-1B, pp. 1-9.

Monger, J.W.H. and Church, B. 1977. Revised stratigraphy of the Takla Group, north-central British Columbia. Canadian Journal of Earth Sciences, vol. 14, pp. 318-326.

Nadaraju, G. 1993. Triassic-Jurassic Biochronology of the eastern Iskut River map area, northwestern British Columbia. M.Sc. thesis, Department of Earth and Ocean Sciences, University of British Columbia, Vancouver, B.C.

Nelson, J.L. and Kennedy, L.A. 2007. Terrace regional mapping project Year 2: New geological insights and exploration targets (NTS 103I/16S, 10W), west-central British Columbia. *In:* Geological Fieldwork 2006. British Columbia Ministry of Energy, Mines and Petroleum Resources, Paper 2007-1, pp. 149-162.

Nelson, J.L., Kennedy, R., Angen, J. and Newman, S. 2007. Geology of Terrace area. British Columbia Ministry of Energy, Mines and Petroleum Resources, Open File 2007-04.

North American Commission on Stratigraphic Nomenclature. 2005. North American Stratigraphic Code. AAPG Bulletin, vol. 89, pp. 1547-1591.

Osadetz, K.G., Jiang, C., Evenchick, C.A., Ferri, F., Stasiuk, L.D., Wilson, N.S.F. and Hayes, M. 2007. Compositions and significance of crude oil stains in Bowser and Sustut basins (Intermontane Belt) British Columbia. Bulletin of Canadian Petroleum Geology, vol. 55, pp. 285-305.

Palfy, J., and Schmidt, K.L. 1994. Biostratigraphic and facies studies of the Telkwa Formation (Lower Jurassic), Smithers map area, British Columbia. *In:* Current Research, Part E. Geological Survey of Canada, Paper 1994-E, pp. 29-38.

Palfy, J., Mortensen, J.K., Smith, P.L., Friedman, R.M., McNicoll, V.J. and Villeneuve, M. 2000. New U-Pb zircon ages integrated with ammonite biochronology from the Jurassic of the Canadian Cordillera. Canadian Journal of Earth Sciences, vol. 37, pp. 549-567.

Poulton, T.P., and Tipper, H.W. 1991. Aalenian ammonites and strata of western Canada. Geological Survey of Canada, Bulletin 411, 71p.

Roth, T. 1993. Surface geology of the 21A zone, Eslay Creek, British Columbia (104B/9W), British Columbia. *In:* Geological Fieldwork 1992. British Columbia Ministry of Energy, Mines and Petroleum Resources, Report Paper 1993-1, pp. 325-330.

Roth, T. 2002. Physical and chemical constraints on mineralization in the Eskay Creek Deposit, northwestern British Columbia; evidence from petrography, mineral chemistry, and sulfur isotopes. Ph.D. thesis, Department of Earth and Ocean Sciences, University of British Columbia, Vancouver, B.C.

Roth, T., Thompson, J.F.H. and Barrett, T.J. 1999. The precious metal - rich Eskay Creek deposit, northwestern British Columbia. *In:* Barrie, C.T., Hannington, M.D. (Eds.), Volcanic-Associated Massive Sulfide Deposits: Processes and Examples in Modern and Ancient Settings. Reviews in Economic Geology, vol. 8, pp. 357-373.

Samson, S.D., McClelland, W.C., Patchett, P.J., Gehrels, G.E., and Anderson, R.G. 1989. Evidence from neodymium isotopes for matle contributions to Phanerozoic crustal genesis in the Canadaian Cordillera. Nature, vol. 337, pp. 705-709.

Samson, S.D., Patchett, P.J., McClelland, W.C., and Gehrels, G.E. 1991. Nd isotopic characterization of metamorphic rocks in the Coast Mountains, Alaska and canadian Cordillera: ancient crust bounded by juvenile terranes. Tectonics, vol. 10, pp. 770-780.

Schofield, S.J. and Hanson, G. 1921. Salmon River District, British Columbia. *In:* Summary Report 1920. Geological Survey of Canada, Part A, pp. 6-12.

Sherlock, R.L., Barrett, T.J., Roth, T., Childe, F.C., Thomson, J.F.H., Kuran, D., Marsden, H. and Allen, R. 1994. Geological investigations of the 21B deposit, Eskay Creek, northwestern British Columbia (104B/9W). *In:* Geological Fieldwork 1993. British Columbia Ministry of Energy, Mines and Petroleum Resources, Report Paper 1994-1, pp. 357-364.

Sherlock, R.L., Roth, T., Spooner, E.T.C. and Bray, C.J. 1999. Origin of the Eskay Creek Pecious Metal-Rich Volcanogenic Massive Sulphide Deposit: Fluid Inclusion and Stable Isotope Evidence. Economic Geology, vol. 94, pp. 803-824.

Simonetti, A., Heaman, L.M., Hartlaub, R.P., Creaser, R.A., MacHattie, T.G. and Bohm, C. 2005. U-Pb zircon dating by laser ablation-MC-ICP-MS using a new multiple ion counting Faraday collector array. Journal of analytical atomic spectrometry, vol. 20, pp. 677-686.

Simpson, K.A. and Nelson, J.L. 2004. Preliminary interpretations of mid-Jurassic volcanic and sedimentary facies in the East Telegraph Creek map area. *In:* Current Research, Geological Survey of Canada, Paper 2004-A1, pp. 1-8.

Souther, J.G. 1972. Telegraph Creek map-area, British Columbia (104G). Geological Survey of Canada, Paper 71-44.

Steckler, M.S., and Watts, A.B. 1978. Subsidence of the Atlantic-type continental margin off New York. Earth and Planetary Science Letters, vol. 41, pp. 1-13.

Stevens, C.H. and Rycerski, B. 1989. Early Permian colonial rugose corals from the Stikine River area, British Columbia, Canada. Journal of Paleontology, vol. 63, pp. 158-181.

Thomson, R.C. and Smith, P.L. 1992. Pliensbachian (Lower Jurassic) Biostratigraphy and Ammonite Fauna of the Spatsizi Area, North-Central British Columbia. Geological Survey of Canada, Bulletin 437, 87 p.

Thomson, R.C., Smith, P.L. and Tipper, H.W. 1986. Lower to Middle Jurassic (Pliensbachian to Bajocian) stratigraphy of the northern Spatsizi area, north-central British Columbia. Canadian Journal of Earth Sciences, vol. 23, pp. 1963-1973.

Thorkelson, D.J. 1988. Jurassic and Triassic volcanic and sedimentary rocks in the Spatsizi map-area, north-central British Columbia. *In:* Current Research, Part E. Geological Survey of Canada, Paper 88-1E, pp. 43-48.

Thorkelson, D.J. 1992. Volcanic and Tectonic Evolution of the Hazelton Group in the Spatsizi River (104H) map-area, North-Central British Columbia. Ph.D. thesis, Department of Earth Sciences, Carleton University, Ottawa, Ont.

Thorkelson, D.J., Mortensen, J.K., Marsden, H. and Taylor, D.C. 1995. Age and tectonic setting of Early Jurassic episodic volcanism along the northeastern margin of the Hazelton Trough, northern British Columbia. *In* Miller, D.M., Busby, C.J. (Eds.), Jurassic magmatism and tectonics of the North American Cordillera. Geological Society of America, Special Paper 299, pp. 83-94.

Tipper, H.W. and Richards, T.A. 1976. Jurassic stratigraphy and history of north-central British Columbia. Geological Survey of Canada, Bulletin 270, 73 p.

Waldron, J.W.F., Gagnon, J.-F., Loogman, W. and Evenchick, C.A. 2006. Initiation and deformation of the Jurassic-Cretaceous Bowser Basin: implications for hydrocarbon exploration. *In:* Geological Fieldwork 2005. British Columbia Ministry of Energy, Mines and Petroleum Resources, Paper 2006-1, pp. 349-360.

Wojdak, P. and Febbro, G. 2009. Northwest Region. *In:* Exploration and mining in British Columbia. British Columbia Ministry of Energy, Mines and Petroleum Resources, pp. 1-33.

Woodsworth, G.J., Hill, M.L. and Van der Heyden, P. 1985. Preliminary geologic map of Terrace (NTS 103I East Half) map area, British Columbia. Geological Survey of Canada, Open File 1136.

Chapter 3: Ichnology and sedimentology of a volcanic arc succession: Jurassic Smithers Formation, north-central British Columbia, Canada[2]

3.1 Introduction

The upper Lower to Middle Jurassic Smithers Formation of the Hazelton Group, exposed south of the Bowser basin in north-central British Columbia, Canada, is a volcano-sedimentary succession deposited in a volcanic arc setting. It is also considered to be one of the most fossiliferous geologic units of all Mesozoic formations within the Canadian Cordillera (Tipper and Richards 1976; Poulton and Tipper 1991) (figure 3.1). Strata of the Smithers Formation contain an abundant and diversified fossil record including ammonites, bivalves, gastropods, belemnites and scleratinian corals. Recently, a well-preserved single carapace of an erymoid lobster was recovered from a fossiliferous unit of the Smithers Formation by Feldmann and Haggart (2007), which led to the introduction of a new species, *Eryma walkerea*. Even though the biostratigraphy of the Smithers Formation is well known from various related studies (e.g. Hanson 1926; Frebold and Tipper 1973; Tipper and Richards 1976; Poulton and Tipper 1991; Johnston 2002; Gagnon and Waldron 2008; Chapter 2), no detailed ichnological and/or sedimentological investigations have ever been reported for these strata. As a result, the sedimentary environments in which the shallow marine rocks of the Smithers Formation were deposited remain poorly understood.

Biogenic sedimentary structures are autochthonous indicators of environmental conditions and provide valuable information for paleoecological studies (Ekdale 1985; Pemberton et al. 2001). In fact, ichnology can sometimes constitute one of the most useful criteria in recognizing sub-environments of shallow marine siliciclastic systems (Pemberton et al. 1992). The most relevant ichnological classification scheme commonly used in paleoenvironmental reconstructions is known as the ichnofacies paradigm (MacEachern et al. 2005a). Ichnofacies are recurrent archetypal associations of trace fossils that reflect specific combinations of organism behaviour (ethology) in given environmental conditions (Seilacher 1967). The ichnofacies paradigm constitutes a benchmark in paleoenvironmental analyses, in which archetypal ichnofacies are used as a norm for comparison between different case studies (MacEachern et al. 2005b). When combined with the appropriate lithofacies, ichnofacies analyses provide a useful tool to

[2] *A version of this chapter will be submitted for publication under the authorship of Gagnon, J.-F., Gingras, M.K., Waldron, J.W.F. and Poulton, T.P.*

assist in the identification of a specific sedimentary environment (Gingras et al. 1998; Hubbard et al. 2004; Buatois et al. 2008; Carmona et al. 2009). However, there have been very few detailed ichnological analyses in environments influenced by volcanic ash fall (c.f. Grimm et al. 1989; Wetzel 2002, 2008), and the dominant ecological parameters in such settings remain poorly constrained.

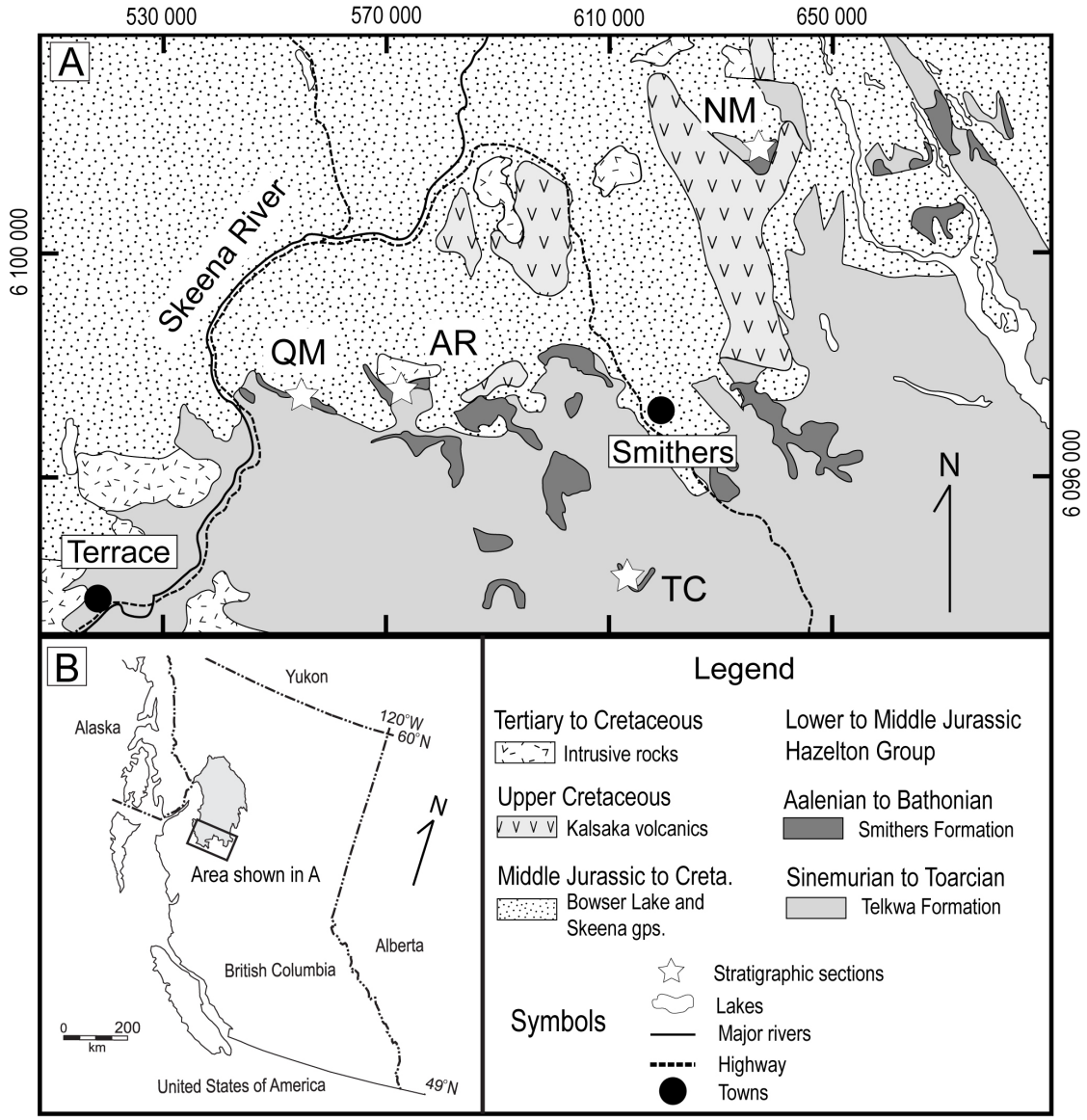

Figure 3.1: A) Simplified geology map showing the distribution of the sedimentary rocks of the Smithers Formation, and location of the four stratigraphic sections: QM-Quinlan Mountain, AR-Ashman Ridge, TC-Tenas Creek, NM-Netalzul Mountain. B) Geographic location of the Bowser basin in north-central British Columbia, Canada. Universal Transverse Mercator Projection in NAD 83 Datum. Modified after Evenchick et al. (2008a, 2008b).

In this paper, we present the first rigorous sedimentological and ichnological study of the Smithers Formation using field observations from four well-exposed stratigraphic sections in north-central British Columbia (figure 3.1). By fully integrating lithofacies and ichnofacies analyses, we aim to better constrain the paleoenvironmental conditions in which the tuffaceous strata of Smithers Formation were deposited. In addition, the well-preserved bioturbated rocks of the Smithers Formation could provide new insights on the animal response to distal volcanic activity in an island arc setting.

3.2 Geological setting

Siliciclastic strata of the Smithers Formation are well exposed on the southern margin of the Bowser basin in north-central British Columbia (figure 3.1). These sedimentary rocks were deposited in the shallow marine portion of the Hazelton trough, a northwest trending intra-arc extensional basin located on the Stikine terrane (Tipper and Richards 1976; Marsden and Thorkelson 1992; Chapter 2). The Smithers Formation mostly consists of interbedded tuffaceous siltstone and sandstone with thin intervals of conglomerate, shale, tuff and limestone. Extensive paleontological data suggest that most of the Smithers Formation is Aalenian to Bajocian in age, but ranges from Middle Toarcian to Lower Callovian in some places (e.g. Hanson 1926; Tipper and Richards 1976; Poulton and Tipper 1991; Johnston 2002; Gagnon and Waldron 2008; Evenchick et al. *submitted*).

The Smithers Formation constitutes one of the five units formally recognized within the upper Hazelton Group (figure 3.2). It is laterally equivalent to the Nilkitkwa Formation to the east, and to the Spatsizi River Formation to the north (Tipper and Richards 1976; Thomson et al. 1986; Chapter 2). In the vicinity of Terrace and Smithers, sedimentary rocks of the Smithers Formation unconformably overlie the calc-alkaline volcanic and volcaniclastic rocks of the Telkwa Formation (Tipper and Richards 1976; Nelson et al. 2007; Evenchick et al. 2008a, 2008b) (figure 3.2). Regionally, the Smithers Formation constitutes an important stratigraphic marker because it delineates the transition from the volcanic-dominated lower Hazelton Group to the sedimentary-dominated upper Hazelton Group. According to Tipper and Richards (1976), onlap of the shallow marine strata of the Smithers Formation over the subaerial volcanics of the Telkwa Formation corresponds to a widespread transgression over the Stikine terrane, probably triggered in part by thermal subsidence of the waning volcanic arc. Sustained relative sea-level rise eventually led to accumulation of thinly interstratified siliceous mudstone and dust tuff ("pyjama beds") of the Quock Formation, which conformably overlie the Smithers Formation above a flooding surface (Chapter 2). The

Quock Formation is conformably overlain by a variety of laterally equivalent lithofacies assemblages of the Bowser Lake Group over a gradational contact (Evenchick et al. 2008a, 2008b, *submitted*).

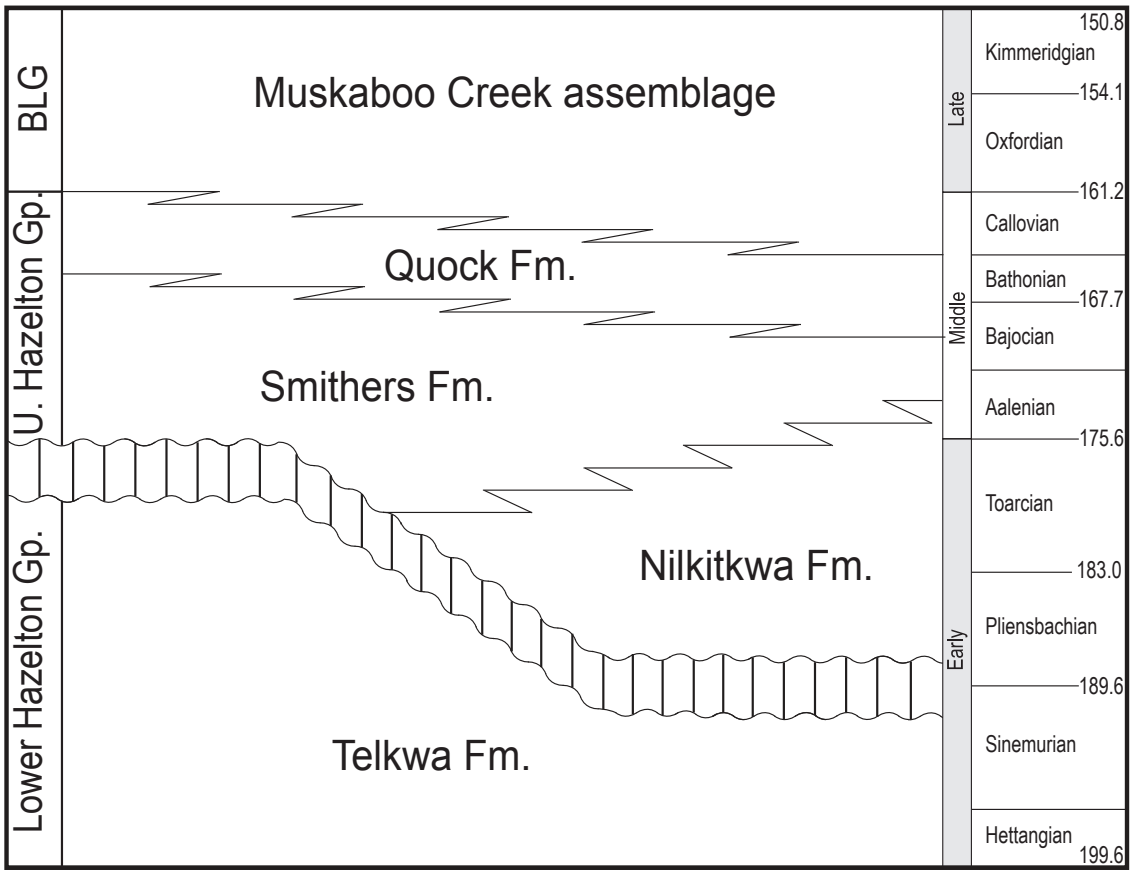

Figure 3.2: Generalized stratigraphic framework of the Hazelton Group showing the principal lithostratigraphic units recognized in the Smithers-Terrace area. Shallow-marine units of the Smithers Formation are in part laterally equivalent to the mudstone-dominated Nilkitkwa Formation, and are conformably overlain by the thinly bedded siliceous mudstone and ash tuff of the Quock Formation. Modified after figure 2.16.

3.3 Facies analysis and depositional environments

The geological data presented in this study primarily come from stratigraphic and structural field mapping. In addition to the extremely well exposed Quinlan Mountain section, which has recently been defined as the unit stratotype for the Smithers Formation (Chapter 2), three other stratigraphic sections originally described by Tipper and Richards (1976) were revisited during this study (i.e. Ashman Ridge, Tenas Creek and Netalzul Mountain; figure 3.1). Measurements and sedimentological observations for each section were recorded with 30 cm scale vertical resolution. Based on the integration of lithological, ichnological and paleontological data, individual sedimentary units of the

Smithers Formation were divided into six facies. The distribution and thickness of each facies in respective measured sections are presented in figure 3.3. Recurring packages of genetically related facies were then grouped into three facies associations, each representing distinct depositional environments.

3.3.1. Shoreface facies association

3.3.1-1 Facies 1: Clast-supported conglomerate

Medium to thick beds of poorly sorted conglomerate characterize most of facies 1, which was only observed at the base of the Quinlan Mountain section. Grain size varies from granule to pebble conglomerate, with less than 10% very coarse sandstone in the matrix. Bioclastic debris comprising disarticulated marine bivalve shells is commonly scattered throughout the unit. The remaining clasts are moderately to well rounded, and have a modal composition dominated by white, silicified, crystal lithic dust tuff. Individual beds are lenticular in shape and display lateral pinch-outs over a few metres. Cross-bedding and truncated beds are common (figure 3.4A). No evidence of bioturbation was observed in this facies.

Interpretation: The occurrence of facies 1 immediately above the subaerial maroon rhyodacite tuff of the Telkwa Formation marks a profound change in depositional conditions. It corresponds to the initial transgressive lag associated with inundation of the Hazelton volcanic arc by the Middle Jurassic sea (Tipper and Richards 1976). The well-rounded morphology of the clasts suggests significant transport and reworking prior to deposition. The presence of trough cross-bedding and lower scoured contacts is indicative of high energy conditions that were probably unsuitable for most shallow-marine organisms (figure 3.4A). Other environmental parameters, such as fluctuating salinity and elevated sedimentation rates, could have also precluded the establishment of an infaunal community. Based on these observations, facies 1 is interpreted to have accumulated in the upper shoreface of a coastal environment during the early stage of transgression.

3.3.1-2 Facies 2: Cross-bedded to massive sandstone

Facies 2 is present in all four measured sections, but the thickest and best preserved exposure was observed near the base of the Netalzul Mountain section. It consists of well-sorted, medium to coarse-grained light grey sandstone. The beds are mostly medium to thickly bedded, and arranged in coarsening- and thickening-upward successions (figure 3.3C). Oscillation ripple laminae, low-angle cross-stratification, and occasional trough cross-stratification indicate that sediments were repeatedly reworked

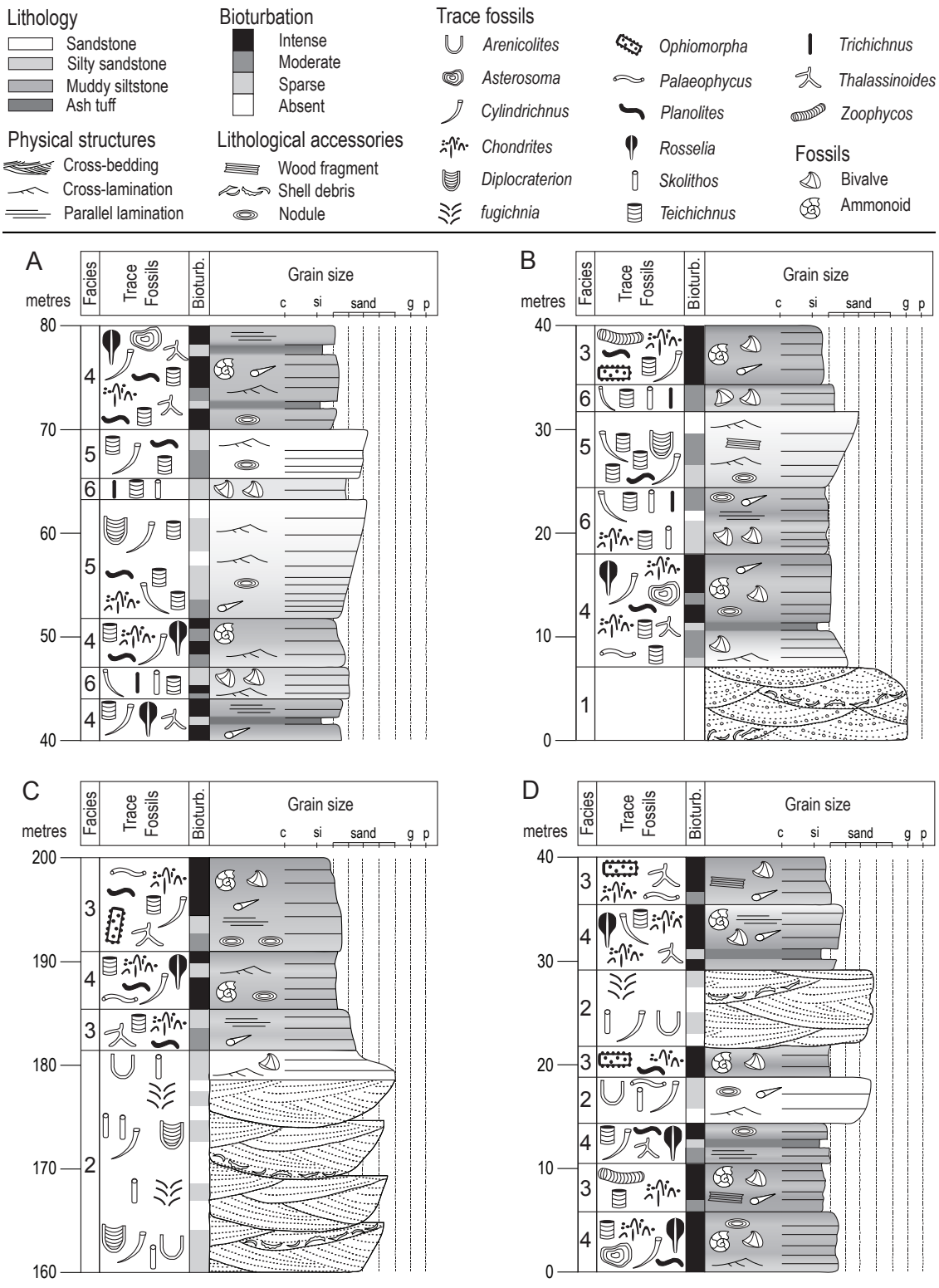

Figure 3.3: Detailed measured stratigraphic sections of the Smithers Formation showing the different facies decribed in this study. A) Ashman Ridge (AR). B) Quinlan Mountain (QM). C) Netalzul Mountain (NM). D) Tenas Creek (TC). Measured intervals are given in metres above the base of the Smithers Formation. See figure 3.1 for location of the sections.

by wave and current action. Multiple scour-based sandstone beds with shell fragments and hummocky cross-stratification (HCS) are also present. Scarce ammonites, belemnites and marine bivalves are haphazardly distributed throughout the interval. The ichnological suite associated with facies 2 is dominated by the ichnogenus *Skolithos,* which consists of vertical unbranching burrows (figure 3.4B). *Skolithos* is cylindrical in cross-section, 5-10 cm long, and usually shows thinly lined walls. Other common traces in sandstone beds include *Diplocraterion*, *Arenicolites* and *Cylindrichnus* (figures 3.4B, C). Rare escape biogenic structures (*fugichnia*) were also observed in HCS (figure 3.4D).

Interpretation: The moderate-diversity ichnological suite of predominantly vertical, cylindrical, and U-shaped burrows identified in facies 2 is characteristic of the S*kolithos* ichnofacies. This ichnofacies, found in well-sorted, loose or shifting sandy substrates, is usually indicative of high levels of wave or current energy (MacEachern et al. 2005a). Low angle cross-stratification and HCS present in medium- to coarse-

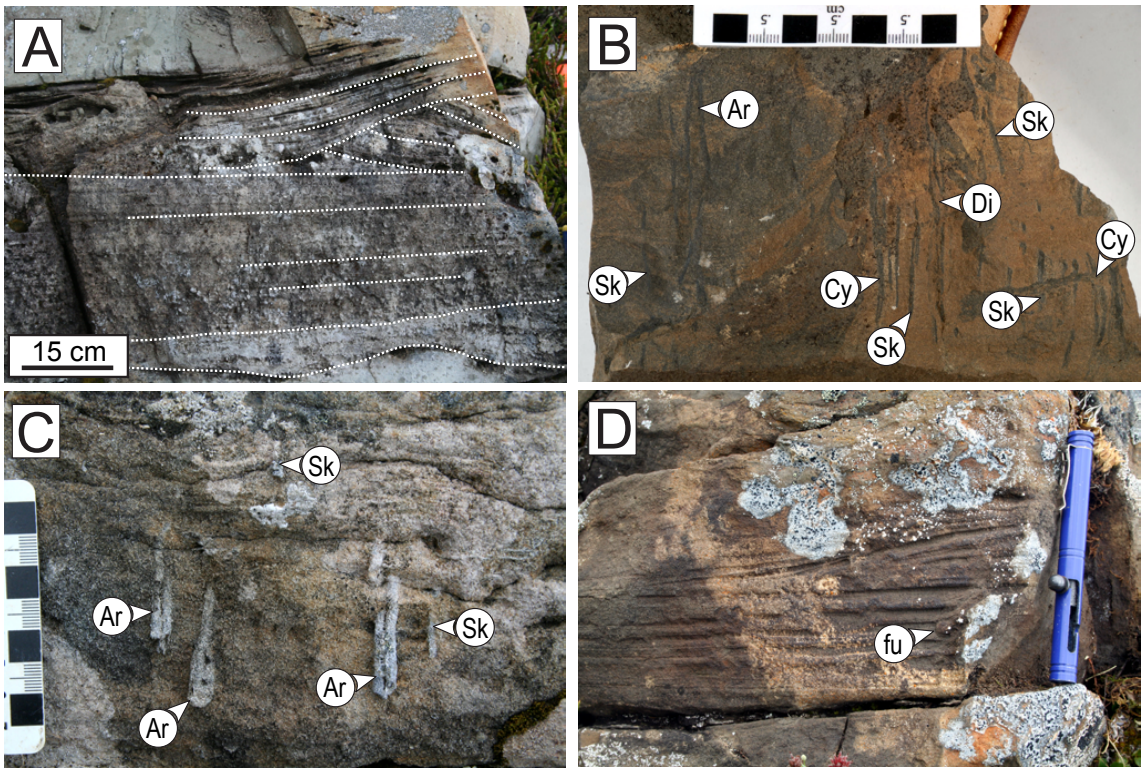

Figure 3.4: Shoreface facies association (facies 1 and 2). A) Trough-cross stratification in very coarse-grained sandstone of facies 1 at Quinlan Mountain. B) and C) Bioturbated medium-grained sandstone of the *Skolithos* ichnofacies (facies 2) located at the base of the Netalzul Mountain section. Trace fossils include: *Skolithos* (Sk), *Diplocraterion* (Di), *Cylindrichnus* (Cy), and *Arenicolites* (Ar). D) Hummocky cross stratification in medium-grained sandstone of facies 2 at Netalzul Mountain. The presence of escape traces (fugichnia - fu) in these deposits attest to rapid accumulation of sand during a storm event. Bear banger launcher for scale is 15 cm long.

grained sandstone are interpreted to represent the combined action of currents and waves in a high energy setting (Arnott and Southard, 1990). The moderate density of dwelling structures made by suspension-feeding vermiform organisms suggests a low level of water turbidity with sufficient food material held in suspension. Recurring tempestites with *fugichnia* attest to high-frequency storms during which the infauna had to rapidly adjust to a sudden increase in sedimentation rate (figure 3.4D). The occurrence of marine fossils, combined with the absence of apparent reduction in size of marine forms, suggest that salinity was relatively stable. When integrated with the available physical structures, the *Skolithos* ichnofacies observed in the Smithers Formation is interpreted to represent deposition in an unrestricted, storm-dominated shoreface setting.

3.3.2 Offshore facies association

3.3.2-1 Facies 3: Laminated muddy siltstone and very fine-grained sandstone

Facies 3 was observed near the top of the Smithers Formation at Netalzul Mountain and Quinlan Mountain. It is characterized by medium to thickly bedded, greenish-brown laminated silty sandstone, which contains a diversified marine fossil assemblage including bivalves, belemnites and ammonites. Low-angle cross-stratification occurs sporadically throughout the interval which indicates occasional reworking of the sediments by bottom currents. Elsewhere, physical sedimentary structures become indistinguishable, which suggests that they have been obliterated by intense biogenic reworking. The ichnological suite of facies 3 is comprised of *Thalassinoides*, *Ophiomorpha, Teichichnus*, *Cylindrichnus*, and *Chondrites* (figure 3.5A). Other less common traces include *Asterosoma*, *Granularia, Planolites, Palaeophycus, Zoophycos,* and *Phycoshiphon*. On bedding surfaces, *Ophiomorpha* is represented by irregular burrow systems in which tube margins are distinctly lined with agglutinated fecal pellets, whereas *Granularia* consists of fecal pellets packed in tubes (figure 3.5B). In finer-grained intervals, *Thalassinoides* become more common and consist of relatively large (1 to 2 cm diameter) galleries arranged in Y- and T-branching systems (figures 3.5 C). The cylindrical tubes display smooth unlined walls and are commonly enlarged at junctions. Pervasive *Chondrites*, which consists of a complex root-like burrow system of downward-branching tunnels, appear to crosscut most of the larger structures associated with a shallower tier (figure 3.5D). In some cases, *Chondrites* is restricted to the fill of other burrows such as *Thalassinoides* and *Palaeophycus*.

Interpretation: The high diversity of trace fossils observed in facies 3 indicates relatively stable physiochemical conditions in a fully marine environment. Structures

associated with deposit-feeding and grazing ethologies suggest abundant deposited food resources and low sedimentation rates (MacEachern et al. 2005a). Facies 3 also displays significant proportions of passive carnivore structures (*Palaeophycus*) and simple feeding structure of trophic generalists (*Planolites*). Rare occurrence of the specialized feeding structure *Zoophycos* in isolated intervals is indicative of a more complex feeding strategy, usually reserved for deeper depositional environment where food resources are less abundant. According to Ekdale (1985), alternating fodinichnia could correspond to periodic changes in organic influx to the basin.

Crosscutting relationships between shallow and deep tier structures provide information about the succession of burrows and have been interpreted in other studies

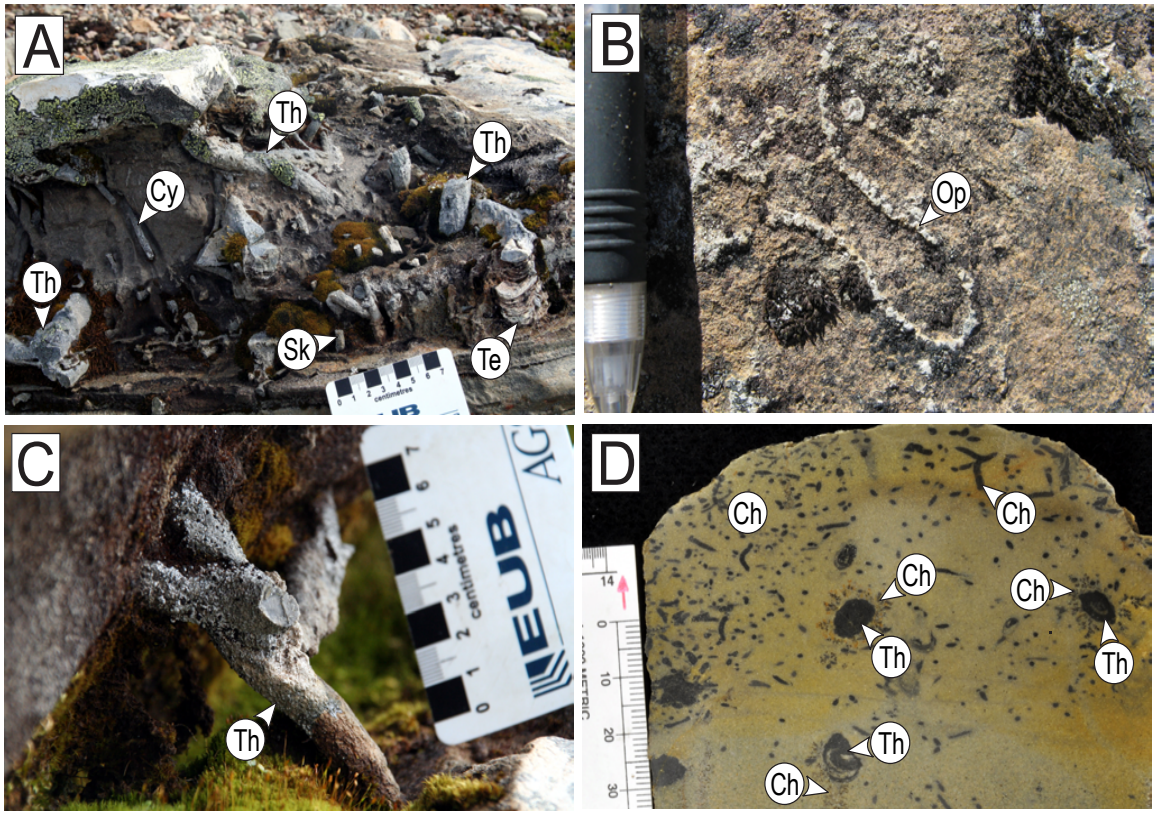

Figure 3.5: Trace fossil assemblage of facies 3 (proximal offshore). A) Ichnological assemblage of the *Cruziana* ichnofacies observed at Quinlan Mountain. The high diversity and high density of traces suggest abundant food resources and overall slow sedimentation rates. B) *Ophiomorpha* traces with tube margins distinctly lined with agglutinated fecal pellets. C) Cylindrical tubes with unlined walls characteristic of the trace *Thalassinoides*. Galleries are arranged in Y- and T-branching systems and commonly display enlargement at junctions. D) Mixed assemblage of *Thalassinoides* and *Chondrites* observed near the top of the Netalzul Mountain section. *Chondrites* is commonly observed as the deeper tier structure around abandoned larger burrows filled by mud. Trace fossils include: *Thalassinoides* (Th), *Ophiomorpha* (Op), *Cylindrichnus* (Cy), *Skolithos* (Sk), *Teichichnus* (Te), and *Chondrites* (Ch).

to represent environmental changes to which infaunal organism respond (c.f. Wetzel and Uchman 2001). In facies 3, the high diversity and large size of structures associated with the shallow tier suggest that the sediment-water interface was not significantly affected by oxygen depletion. However, overprinting of shallow tiers by animals producing *Chondrites* could reflect opportunistic feeding strategies. By maintaining open connection to the seafloor, small polychaete worms were able to burrow down 20 cm to feed on organics concentrated in abandoned *Thalassinoides* and *Palaeophycus* burrows (figure 3.5D). A similar situation was described by Bromley and Ekdale (1984), in Upper Cretaceous chalk units, where they suggested that *Chondrites* must have been emplaced later and at greater depth than any other associated traces. This evolution towards a *Chondrites*-dominated suite with increased burial could be regarded as indicating conditions of reduced bottom-water oxygenation, as suggested in other studies by Rhoads and Morse (1971); Bromley and Ekdale (1984); Savrda and Bottjer (1989) and Wignall (1991). The ichnological suite of facies 3 contains abundant and diversified deposit-feeding and grazing structures, corresponding to a distal *Cruziana* ichnofacies representative of the proximal offshore.

3.3.2-2 Facies 4: Densely bioturbated muddy siltstone and very fine-grained tuffaceous sandstone

Facies 4 is the most widespread facies of the Smithers Formation. It represents more than two thirds of the stratigraphic sections exposed at Ashman Ridge and Quinlan Mountain. It is composed of interbedded greenish-grey muddy siltstone, very fine-grained sandstone, and pale beige ash tuff. This facies is thinly bedded and sandy siltstone beds are normally graded. Common sedimentary structures consist of low-angle cross-lamination and asymmetric ripples. Marine bivalves found in facies 4 are diverse and abundant. They include *Plagiostoma* sp., *Myophorella* spp., *Pleuromya* sp., *Pinna* sp., *Grammatodon* sp., *Ostrea* sp., *Ctenostreon* sp., *Gervillella* sp., *Lima* sp. and *Entolium* sp. (figures 3.6A-F). Since most of these benthic organisms can only thrive within the photic zone, water depth is interpreted to have been less then a few tens of metres. Common ammonoids include *Sonninia* sp., *Stephanoceras* sp. and *Chondroceras* sp. (figures 3.6G, H). The belemnite *Cylindrotheuthis* sp. is also present throughout the succession (figure 3.6I).

In addition to its abundant marine fossil content, facies 4 hosts the most abundant and diverse trace fossil suite of the Smithers Formation. Dominant trace fossils include *Rosselia rotatus*, *Rosselia socialis, Cylindrichnus*, *Teichichnus*, *Palaeophycus*, *Asterosoma, Chondrites*, and *Planolites* (figures 3.7A-E). These structures constitute a

mixed association of horizontal to vertical burrows, corresponding to a combination of feeding burrows and permanent to semi-permanent dwellings of vermiform organisms such as polychaete worms. Rare *Thalassinoides* occur immediately below 5-10 cm thick tuff beds (figures 3.7G, H). Another less common trace fossil is *Piscichnus*, a concentric

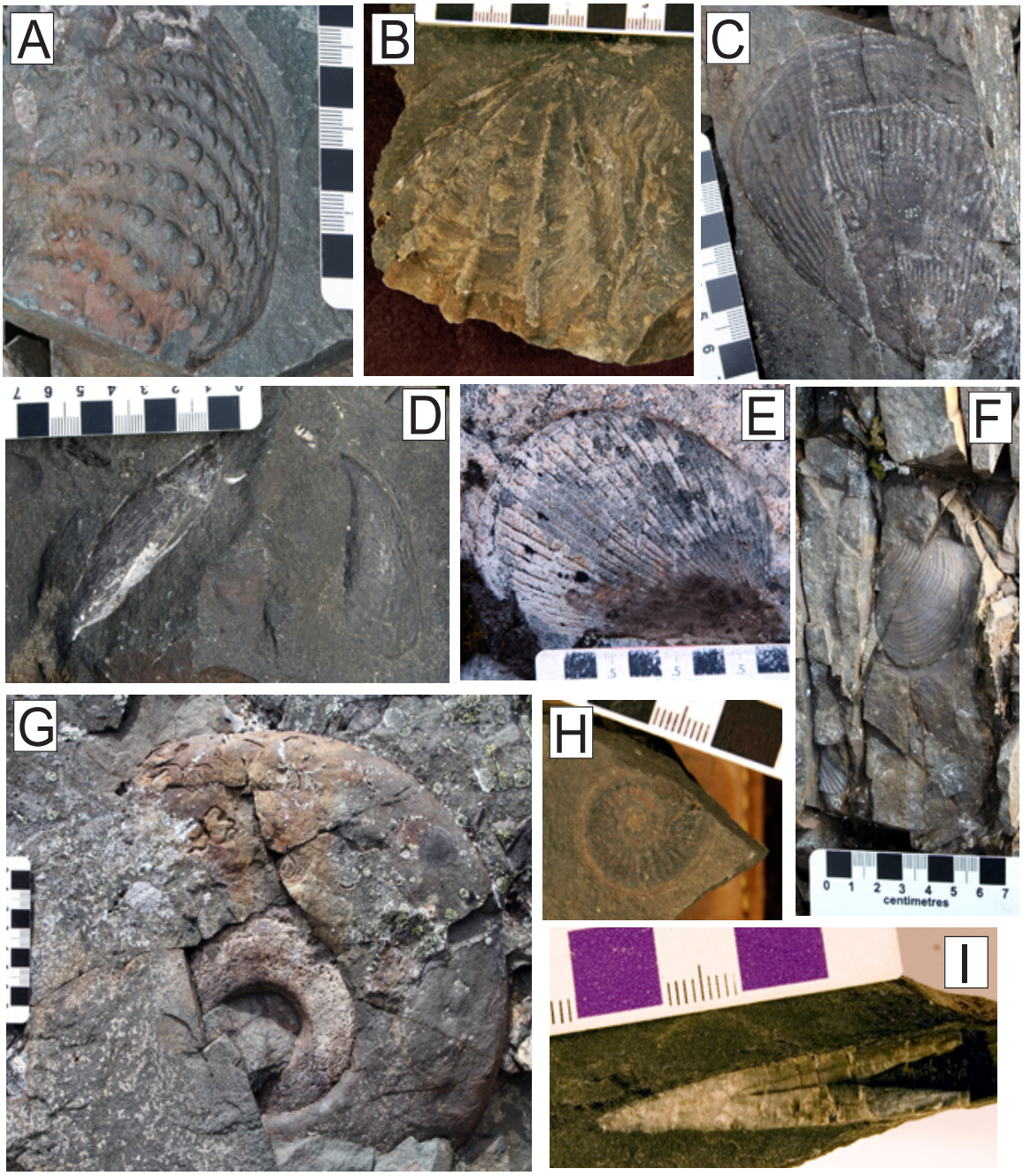

Figure 3.6: Abundant and diversified marine fossils found in the offshore facies association (facies 3 and 4) at Ashman Ridge and Quinlan Mountain. A) *Myophorella* sp. B) *Ctenostreon gikshanensis* McLearn. C) *Lima tizglensis* McLearn. D) *Pinna* sp. E) *Plagiostoma hazeltonense* McLearn. F) *Pleuromya* sp. G) *Stephanoceras* sp. aff. *S. skidegatensis* (Whiteaves). H) *Sonninia* sp. I) *Cylindrotheuthis* sp.

bowl-shaped trace interpreted to result from biogenically induced hydraulic excavation of sedimentary substrates by marine vertebrate animals such as sturgeons and rays (figure 3.7F) (Gregory 1991).

Interpretation: The general abundance and high diversity of horizontal, inclined and vertical trace fossils observed in facies 4 is characteristic of the *Cruziana* ichnofacies. This ichnofacies is commonly associated with soft, cohesive muddy substrates in a relatively low energy environment (MacEachern et al. 2005a). Predominance of mobile and sessile deposit-feeding structures suggests that food supply was available

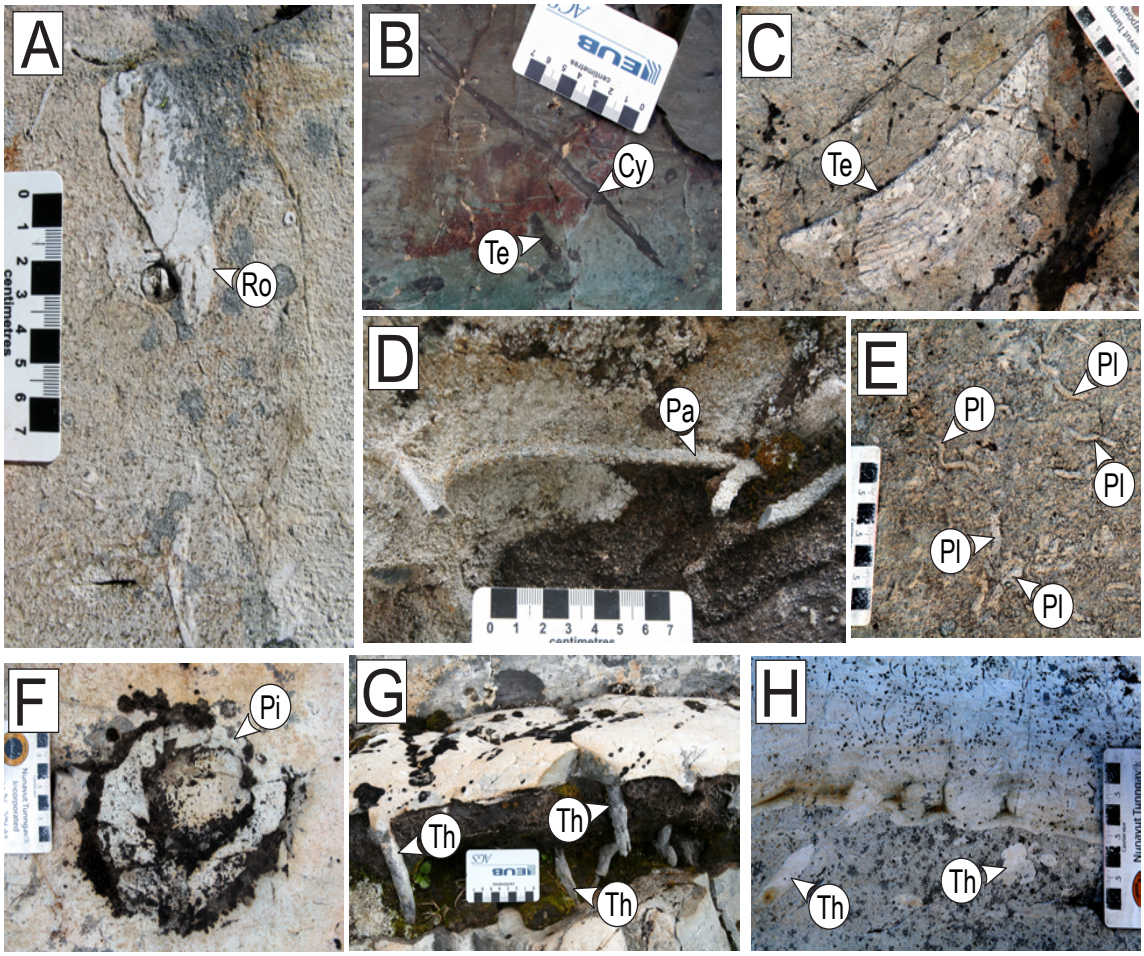

Figure 3.7: Trace fossil assemblage of facies 4 (inner shelf). Rare occurence of *Thalassinoides* (Th) in an otherwise densely bioturbated ichnological suite suggests an impoverished *Cruziana* ichnofacies. A) Cross-section view of *Rosselia socialis* (Ro) interpreted as a dwelling structure of filter-feeding vermiform organisms. B) Cross-section view of 25 cm-long *Cylindrichnus* (Cy). C) Cross-section view of *Teichichnus* (Te). D) Downward-branching galleries interpreted as the predatory trace *Palaeophycus* (Pa). E) Abundant *Planolites* (Pl) exposed on a bedding surface. F) Large concentric trace on bedding surface interpreted as *Piscichnus* (Pi). G) and H) Rare occurence of *Thalassinoides* (Th) concentrated below tuff beds. The incorporation of volcanic ash in underlying *Thalassinoides* burrows indicates that crustaceans were active shortly after deposition of the ash layer.

in both suspended and deposited components. However, one peculiarity with the ichnological suite of facies 4 is that traces commonly associated with crustaceans, such as *Ophiomorpha*, *Granularia, Gyrolithes*, *Thalassinoides,* and *Rhizocorallium,* are scarce. This is rather unusual for the archetypal *Cruziana* ichnofacies and suggests that some sort of environmental stress probably inhibited crustacean activities. In a recent survey on the global diversity of thalassinideans, Dworschak (2000) reported that the vast majority of modern burrowing decapod shrimps are found in a restricted water depth range between 0-20 m. Since units of facies 4 probably accumulated in relatively shallow water environment with abundant food resources, the reasons for under-representation of crustacean traces in this intensely bioturbated and diversified ichnological assemblage are unclear. Hence, the trace fossil suite of facies 4 is better described as a proximal impoverished *Cruziana* ichnofacies. Based on the great numbers of mollusc fossils and the diversity and density of biogenic structures, the fine-grained sedimentary rocks of facies 4 are interpreted to represent deposition in fully marine, low-energy conditions usually found on the inner shelf.

3.3.3 Deltaic facies association

3.3.3-1 Facies 5: Thickening- and coarsening-upward cross-laminated sandstone

Facies 5 consists of interbedded greenish sandy siltstone and tuffaceous pale beige fine-grained sandstone arranged in coarsening- and thickening-upward packages of medium to thick beds (figures 3.3A, B and 3.8A). The geographic distribution of this facies is limited to the middle part of the stratigraphic sections exposed at Ashman Ridge and Quinlan Mountain. Common symmetrical ripples throughout the interval indicate that sediments were continuously reworked by waves (figure 3.8B). Marine fossils such as belemnites and bivalves are common. These strata display a moderate degree of bioturbation in which *Teichichnus* and *Cylindrichnus* are the most common structures. In cross-section, *Teichichnus* consists of unlined retrusive spreite filled by dark grey to black mud (figure 3.8C). Well-preserved *Cylindrichnus* are represented by non-branching, vertical to gently-inclined sub-cylindrical burrows with concentric layered walls. The shafts range from 5-10 cm in length but reach up to 30 cm in some cases (figure 3.8D). Other less common traces include *Diplocraterion*, *Rosselia*, and *Planolites*.

Interpretation: The density of trace fossils observed in facies 5, though moderate, is much less than in facies 3 and 4. This suggests that one or more paleoenvironmental factors acted as a stress on the benthic community. The preponderance of structures produced by deposit feeders, combined with the variety of dwellings facilitating

readjustment, are indicative of relatively high sedimentation rates in an environment where turbidity was high enough to inhibit most filter-feeding strategies. Association of *Teichichnus*, *Diplocraterion* and *Cylindrichnus* has been reported from aggradational depositional environments, such as deltas, where the organisms consistently migrate upward to keep pace with sedimentation (MacEachern et al. 2005c; Buatois et al. 2008). Although deltaic environments are commonly associated with brackish water conditions, which could explain the reduction in number and diversity of ichnogenera observed in facies 5, the abundant marine fossil content suggests that salinity fluctuations were

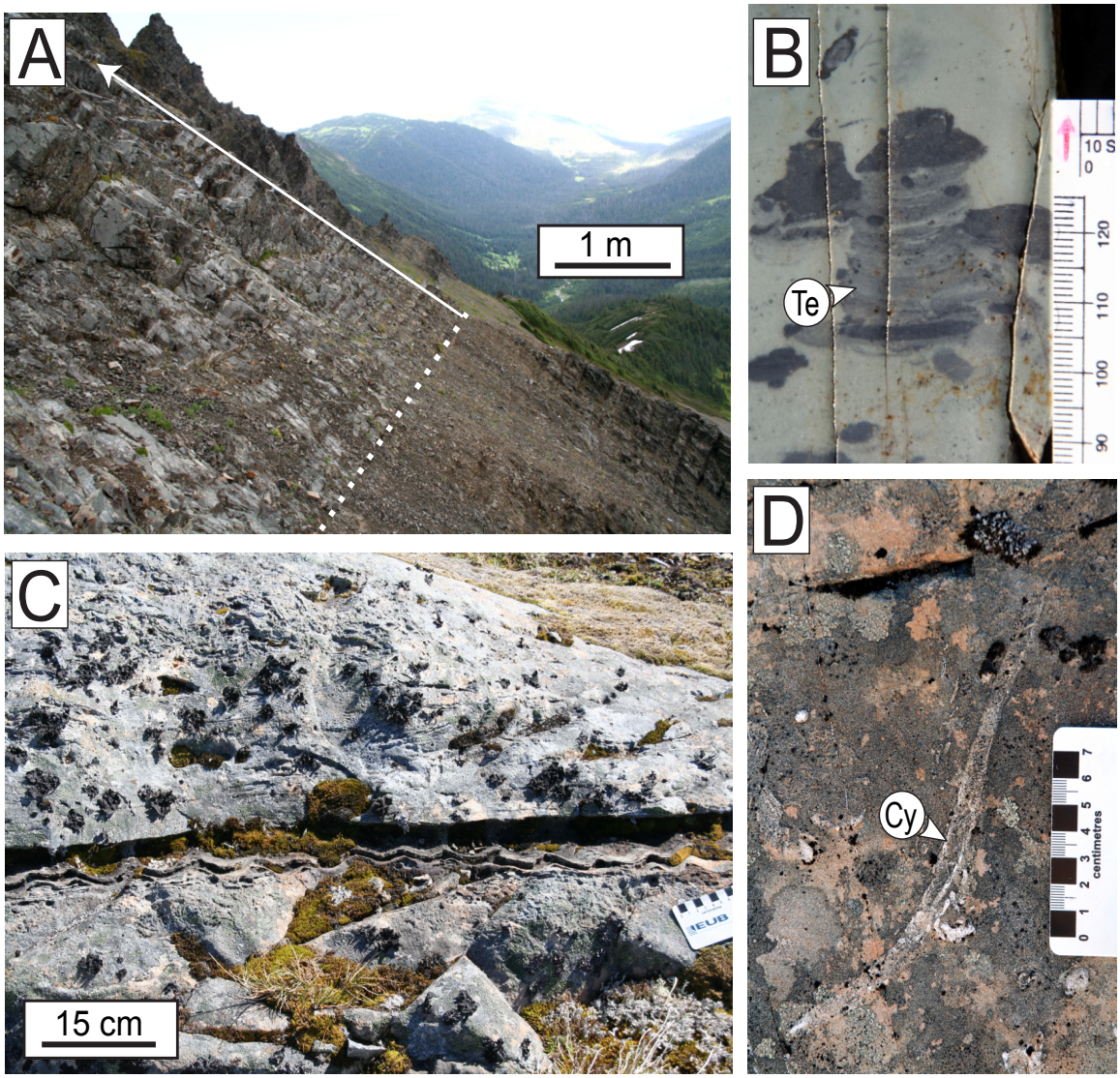

Figure 3.8: Characteristics of the wave-dominated delta (facies 5). A) Coarsening and thickening upward succession exposed at 45 m above the base of the Smithers Formation at Ashman Ridge. B) Cross-section view of *Teichichnus* (Te) displaying retrusive spreiten. This suggests heightened sedimentation rate locally. C) Layers of regularly spaced symmetrical ripples suggest continuous agitation of the substrate by fair-weather waves. D) Cross-section view of *Cylindrichnus* (Cy).

minimal. Also, no evidence of syneresis cracks was observed. Ichnological analyses from various delta types have shown that marine benthic communities found in wave-dominated deltas are less likely to be affected by reduced salinity levels compared to their fluvial-dominated equivalents (Gingras et al. 1998; Coates 2001; MacEachern and Loseth 2003; Bann and Fielding 2004; MacEachern et al. 2005c). In these sedimentary environments, wave energy generally buffers fluvial effect by dispersing suspended sediment and mixing waters of contrasting salinity. In addition, longshore drift has been shown to dissipate fluvial effects away from the fluvial input point, such that deltaic stresses may be very localized (Bhattacharya and Giosan 2003). Based on these observations, the stratal stacking pattern of facies 5 is interpreted to represent delta progradation in a wave-dominated setting with minimal fluvial influence.

3.3.3-2 Facies 6: Fossiliferous sandy siltstone with calcareous nodules

Thin to medium sandy siltstone beds and tuffs of facies 6 were observed in close association with interbedded units of facies 5 (figures 3.3A, B). Physical sedimentary structures include regularly spaced symmetrical ripples and wavy mud laminations. Systematic measurements of sub-parallel ripple crests and belemnite long-axes found on well-exposed bedding surfaces suggest a slight preferred orientation of oscillation currents towards NW-SE. Wood fragments, shell debris, bioherms of colonial scleratinian corals, and serpulid worm tubes are also present (figures 3.9A, B). A distinctive feature of facies 6 observed at Quinlan Mountain is the presence of large articulated bivalves aligned along specific horizons (figure 3.9C). They include 20 to 25 cm long *Plagiostoma* sp. and *Lima* sp. commonly associated with elliptical calcareous nodules up to 40 cm long. Small scale threadlike burrows similar to the trace fossil *Trichichnus linearis* were observed inside a few bivalve shells which likely provided refuge for sipunculid worms (figure 3.9D). Other traces included *Skolithos*, *Teichichnus*, *Cylindrichnus* and *Planolites*.

Interpretation: The ichnological suite of facies 6 is somewhat similar to that observed in facies 5 with the addition of *Skolithos* and *Trichichnus*. The occurrence of structures produced by filter feeders suggests a return to less turbid conditions. This is consistent with the presence of well-developed isolated patch-reefs and bioherms, which would not have prospered under a high turbidity level. Concentration of large articulated bivalves along individual layers probably indicates long periods of stability at the sediment-water interface, which allowed these organisms to remain stationary during filter-feeding (figure 3.9C). Equal abundance of deposit- and filter-feeding structures in facies 6 indicates a mixed *Skolithos*-*Cruziana* association. Decrease of turbidity and sedimentation rates in comparison to facies 5 reflects periods of lower

sediment discharge. Although most wave-dominated deltas are usually associated with extensive beach deposits which can form barrier-lagoon complexes (Bhattacharya and Giosan 2003), the diverse marine fauna observed in strata of facies 6 suggest that open connections to the sea were maintained. Therefore, facies 6 is interpreted as having formed in an interdistributary-bay complex adjacent to the distributary-mouth bars where wave influence was diminished to the point that longshore drift no longer isolated low-energy areas from the sea by building barriers.

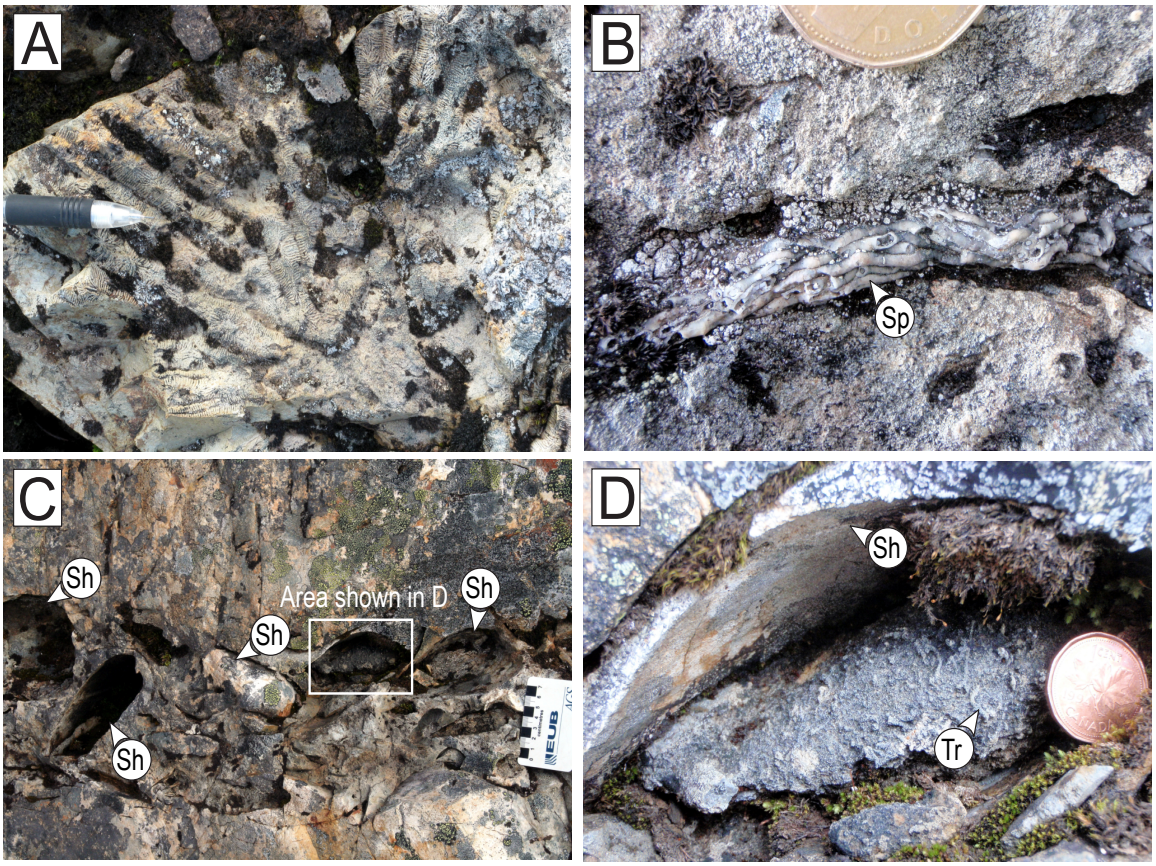

Figure 3.9: Characteristics of the interdistributary bay (facies 6). A) Bioherm of colonial scleratinian corals. B) Well-preserved serpulid worm tubes (Sp). These organisms are indicative of fully marine conditions in a low turbidity environment. C) Distinct layers containing large articulated bivalves (Sh). This suggests relatively slow sedimentation rate. D) *Trichichnus* (Tr) observed inside bivalve shells.

3.4 Petrography of the Smithers Formation

3.4.1 Thin-section observations

Microscopic investigations from thin sections indicate that sandstones of the Smithers Formation are mostly composed of volcanic lithic fragments and detrital feldspar grains. A rough estimate of the modal composition of these rock based on the abundance of the various grain types suggests that sandstones of the Smithers Formation correspond to volcanic litharenites (c.f. Folk et al. 1970). Detrital grains are mostly sub-angular to sub-rounded, and are poorly to moderately sorted. Some volcanic fragments are composed of euhedral lathwork (twinned) and microlitic feldspar phenocrysts arranged in an altered cryptocrystalline groundmass (figures 3.10D, F, H). Because of their unstable chemical nature, feldspar and plagioclase grains tend to show partial to complete replacement by calcite and authigenic clay minerals. Occasional siliceous speckled chert grains and felsic volcanic clasts were also identified. These grains usually display a higher degree of sphericity and roundness compared to the other lithic fragments. Fossil-rich intervals in volcanic litharenites of facies 2 contain abundant disarticulated bivalve fragments, which are supported in a dark brown very fine-grained calcareous matrix (figures 3.10A, B). The intergranular lime mud matrix probably corresponds to micrite formed as a result of microbial activity in the photic zone. This would further suggest that strata of facies 2 accumulated in an interval of less turbidity that allowed carbonate-producing organisms to get established. In a few places, the carbonates experienced dissolution during later diagenesis to generate secondary porosity in the order of 10–15% (figure 3.10C).

Thin section observations of finer grained lithologies from units of the offshore facies association are petrographically similar to sandstone of the shoreface and delta facies association. The framework is a very fine-grained volcanic litharenite dominated by lithic fragments, feldspar grains and detrital clays. Detrital feldspar and volcanic fragments are variably altered, including albitization of plagioclases and replacement by zeolites (figures 3.10G, H). Some detrital plagioclase grains display pronounced replacement by secondary calcite along the cleavage planes. Diagenetic chemical alteration of the labile volcanic fragments seems to be associated with precipitation of authigenic clays, which form a very fine-grained argillaceous cement. A portion of the apparently authigenic clays may also be related to recrystallization of detrital clays (Singer and Muller, 1983) These reactions generally occur early in the diagenetic sequence of volcanogenic sandstones (c.f. Surdam and Boles, 1979; Tang et al. 1997).

3.4.2 X-Ray diffraction analyses

Since the majority of samples observed in this study display strong post-depositional alteration due to the abundance of labile volcanic fragments, volcanic glass, and detrital feldspar grains, X-Ray diffraction analyses were conducted to document the crystallographic structure and chemical composition of the argillaceous matrix. The most common minerals encountered are quartz, muscovite, calcite, albite and clinochlore (figure 3.11). Preferential replacement of plagioclase and feldspar grains by calcite and dolomite is consistent with distinctive peaks at 34° and 36° (2θ) respectively.

Although previous authors have suggested that glauconite was responsible for the green color of the rocks (Tipper and Richards 1976), X-Ray diffraction analyses performed on greenish siltstones taken from all four stratigraphic sections indicate that clinochlore (chlorite group) is the most abundant Mg-bearing phyllosilicate (figure 3.11). Since minerals of the chlorite group are commonly found as an alteration product of mafic rocks, recycled basalt fragments from the underlying Telkwa Formation and contemporaneous volcanic ash are interpreted as the most likely source of iron and magnesium. Other less abundant clay minerals include kaolinite, nacrite and rectorite (figures 3.11A, B). These clay minerals probably precipitated from alteration of alumino-silicates such as albite and microcline, or from diagenesis of muscovite. Illite may also be present in the samples, but is indistinguishable from muscovite in X-Ray diffraction analyses since both minerals have a similar 2:1 basic structure in which potassium is the principal interlayer cation (Grodon and Eberl, 1984).

Zeolites also occur as pore-filling cement and as part of the cryptocrystalline groundmass in some samples. Different varieties of zeolite minerals include wairakite, analcime, and clinoptilolite (figures 3.11D, E). Formation of zeolites is most likely derived from devitrification of the extremely labile volcanic glass present in the volcaniclastic rocks (Hawkins 1981). According to Galloway (1979), zeolite authigenesis is common in back-arc and fore-arc basins where volcanic rocks react with alkaline interstitial water. The abundance of authigenic clay minerals and zeolites in the Smithers Formation significantly reduces the porosity and permeability of the rock, which can cause deterioration of reservoir potential.

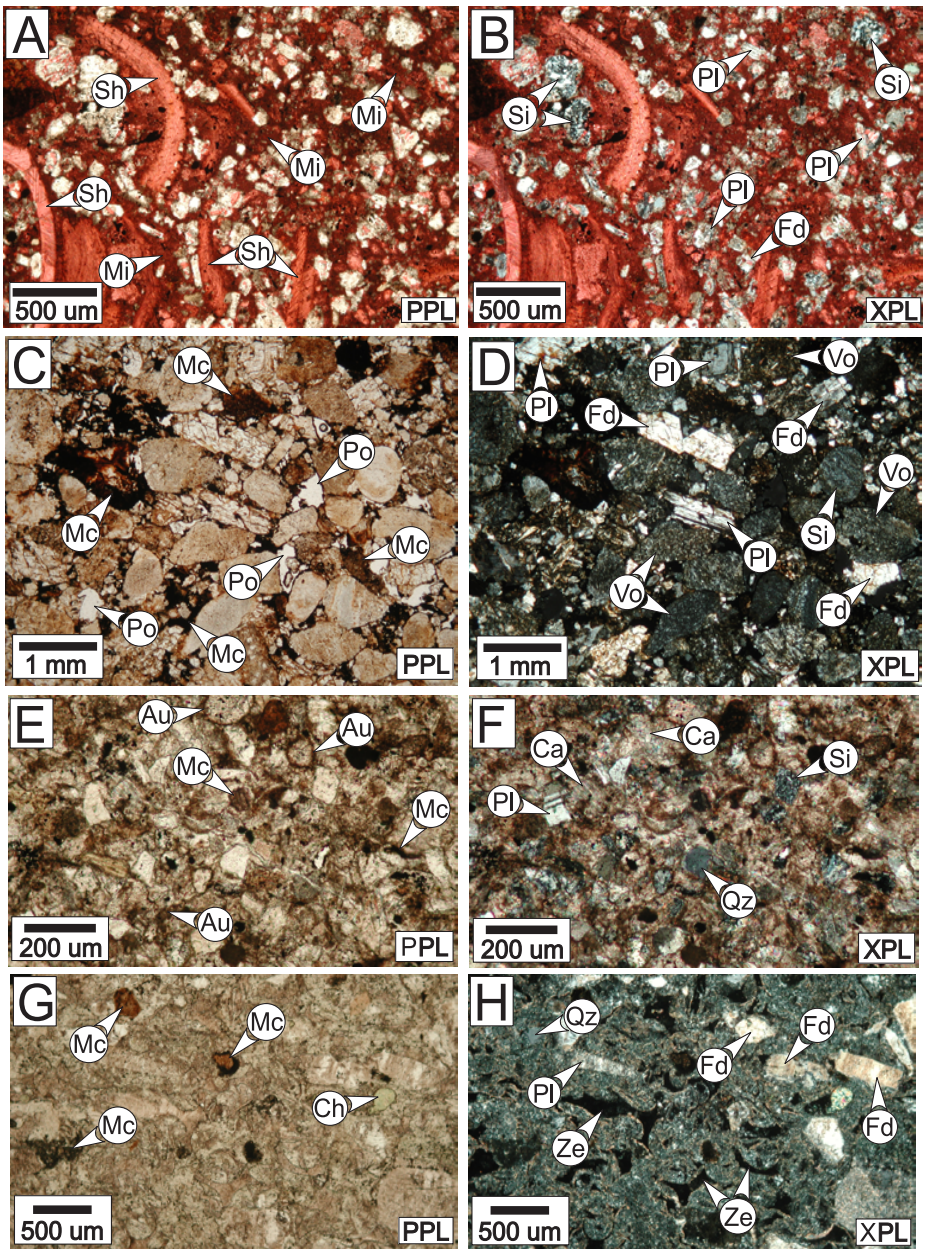

Figure 3.10: Thin-section photomicrographs of lithological units of the Smithers Formation. A) and B) Fossil-rich intervals of facies 2 containing abundant disarticulated bivalve fragments (Sh). Detrital plagioclase grains (Pl) and speckled chert grains (Si) are also present in the framework. C) and D) Coarse-grained volcanic litharenite typical of the lower Smithers Formation. Detrital grains include: volcanic fragments (Vo), plagioclases (Pl), feldspars (Fd), and intraformational mud clasts (Mc). Dissolution of micrite during later diagenesis produced secondary porosity in the order of 10-15% (Po). E) and F) Strongly altered fine-grained volcanic litharenite of facies 3 and 4. Bulk of the volcanic fragments and plagioclase grains are replaced by authigenic clays (Au) and calcite (Ca). Rare monocrystalline quartz grains (Qz) were also observed. G) and H) Greenish volcanic siltstone showing pronounced replacement of original grains by authigenic clays (Au). With increasing burial, the remaining porosity was filled by a variety of zeolite minerals (Ze). This phenomenon is commonly associated with devitrification of volcanic glass in volcanic-arc derived sedimentary rocks. PPL: plane poralized light; XPL: cross poralized light.

A

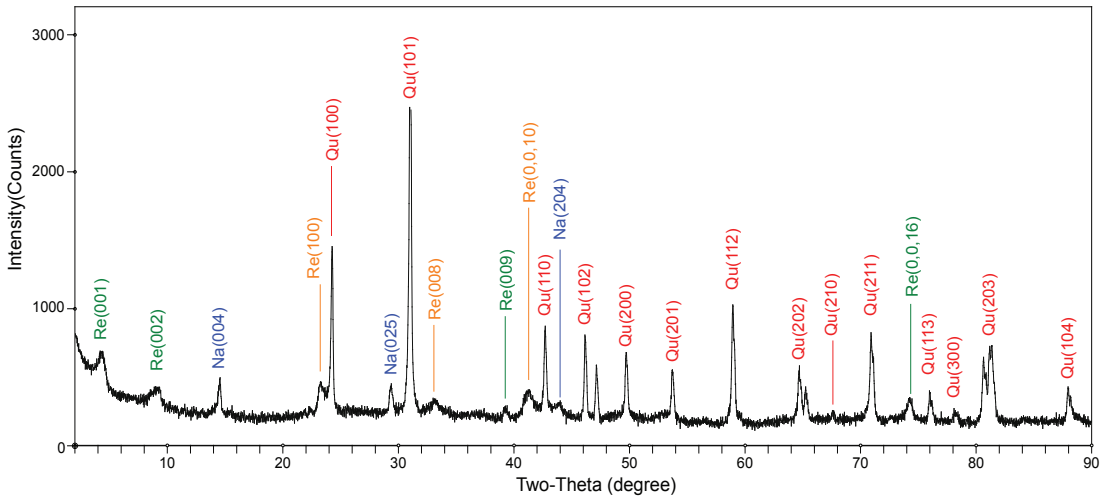
Intensity(Counts)
Two-Theta (degree)
Re(001)
Re(002)
Na(004)
Re(100)
Qu(100)
Na(025)
Qu(101)
Re(008)
Re(009)
Re(0,0,10)
Qu(110)
Na(204)
Qu(102)
Qu(200)
Qu(201)
Qu(112)
Qu(202)
Qu(210)
Qu(211)
Re(0,0,16)
Qu(113)
Qu(300)
Qu(203)
Qu(104)

B

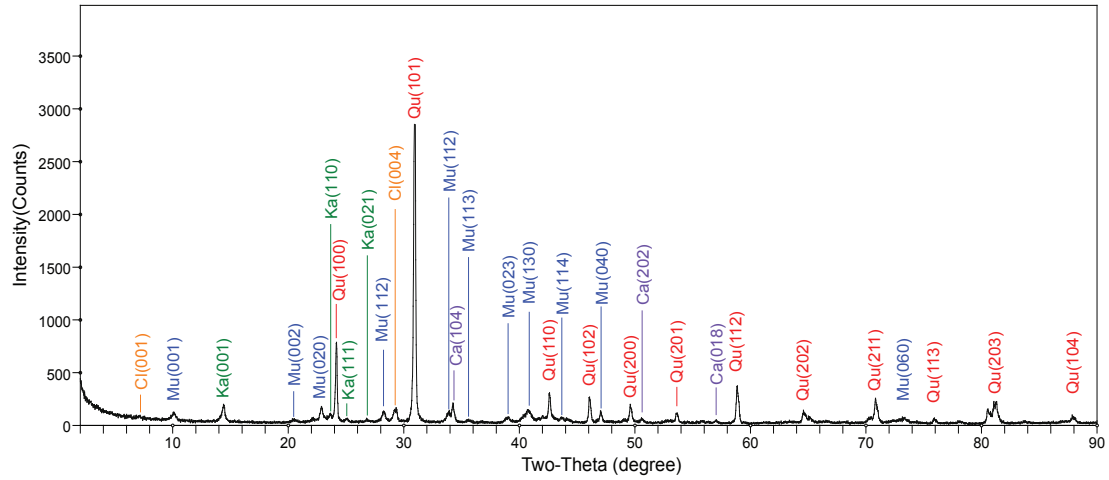
Intensity(Counts)
Two-Theta (degree)
Cl(001)
Mu(001)
Ka(001)
Mu(002)
Mu(020)
Ka(111)
Qu(100)
Ka(110)
Mu(112)
Ka(021)
Cl(004)
Qu(101)
Ca(104)
Mu(112)
Mu(113)
Mu(023)
Mu(130)
Qu(110)
Mu(114)
Qu(102)
Mu(040)
Qu(200)
Ca(202)
Qu(201)
Ca(018)
Qu(112)
Qu(202)
Qu(211)
Mu(060)
Qu(113)
Qu(203)
Qu(104)

C

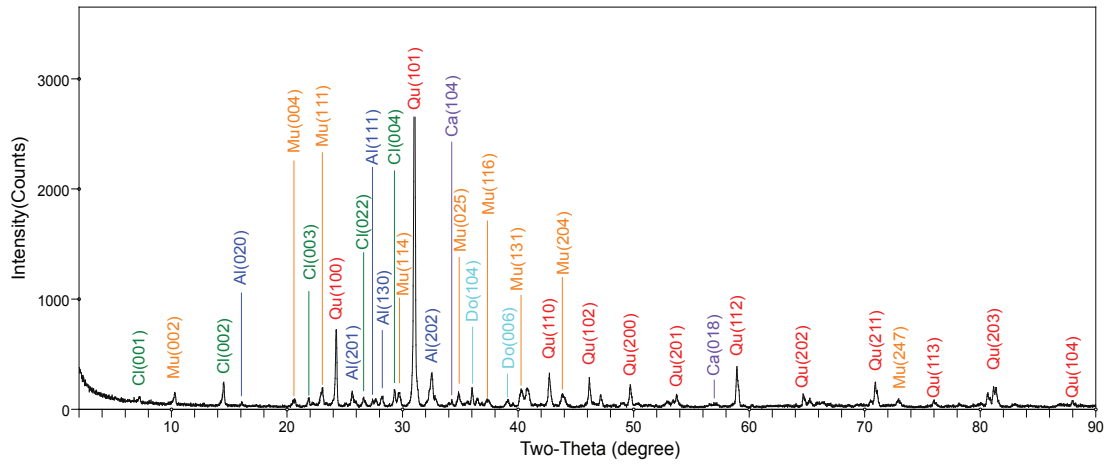
Intensity(Counts)
Two-Theta (degree)
Cl(001)
Mu(002)
Cl(002)
Al(020)
Mu(004)
Cl(003)
Mu(111)
Qu(100)
Al(201)
Cl(022)
Al(111)
Al(130)
Cl(004)
Mu(114)
Qu(101)
Al(202)
Ca(104)
Mu(025)
Do(104)
Mu(116)
Do(006)
Mu(131)
Qu(110)
Mu(204)
Qu(102)
Qu(200)
Qu(201)
Ca(018)
Qu(112)
Qu(202)
Qu(211)
Mu(247)
Qu(113)
Qu(203)
Qu(104)

D

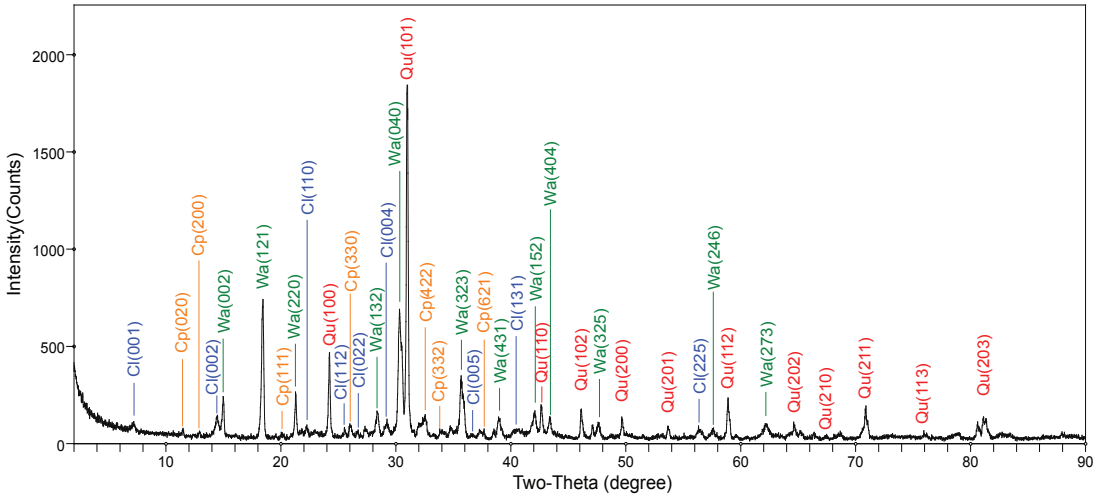
Intensity(Counts)
Two-Theta (degree)
Cl(001)
Cp(020)
Cp(200)
Cl(002)
Wa(002)
Wa(121)
Cp(111)
Wa(220)
Cl(110)
Qu(100)
Cl(112)
Cp(330)
Cl(022)
Wa(132)
Cl(004)
Wa(040)
Qu(101)
Cp(422)
Cp(332)
Wa(323)
Cl(005)
Cp(621)
Wa(431)
Cl(131)
Wa(152)
Wa(404)
Qu(110)
Qu(102)
Wa(325)
Qu(200)
Qu(201)
Cl(225)
Wa(246)
Qu(112)
Wa(273)
Qu(202)
Qu(210)
Qu(211)
Qu(113)
Qu(203)

E

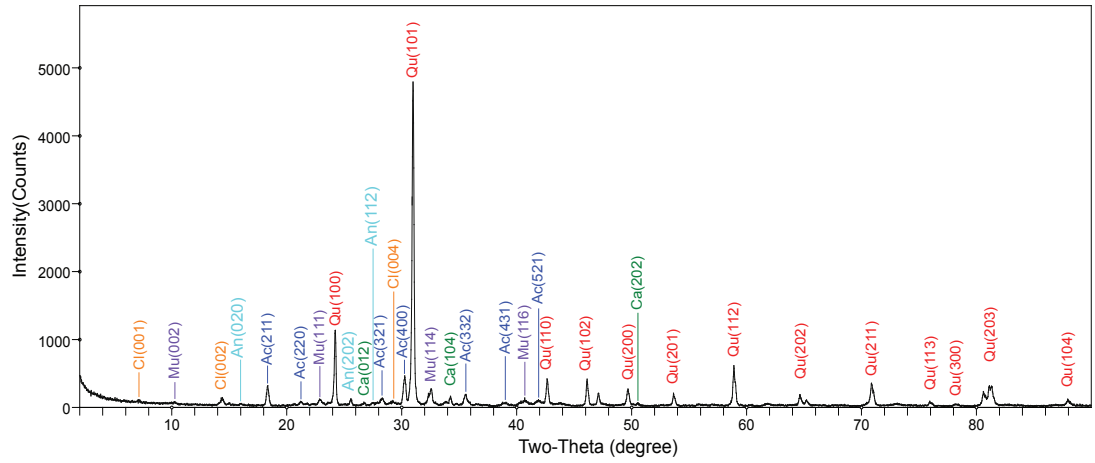
Intensity(Counts)
Two-Theta (degree)
Cl(001)
Mu(002)
Cl(002)
An(020)
Ac(211)
Ac(220)
Mu(111)
Qu(100)
An(202)
Ca(012)
Ac(321)
An(112)
Cl(004)
Ac(400)
Qu(101)
Mu(114)
Ca(104)
Ac(332)
Ac(431)
Mu(116)
Ac(521)
Qu(110)
Qu(102)
Qu(200)
Ca(202)
Qu(201)
Qu(112)
Qu(202)
Qu(211)
Qu(113)
Qu(300)
Qu(203)
Qu(104)

F

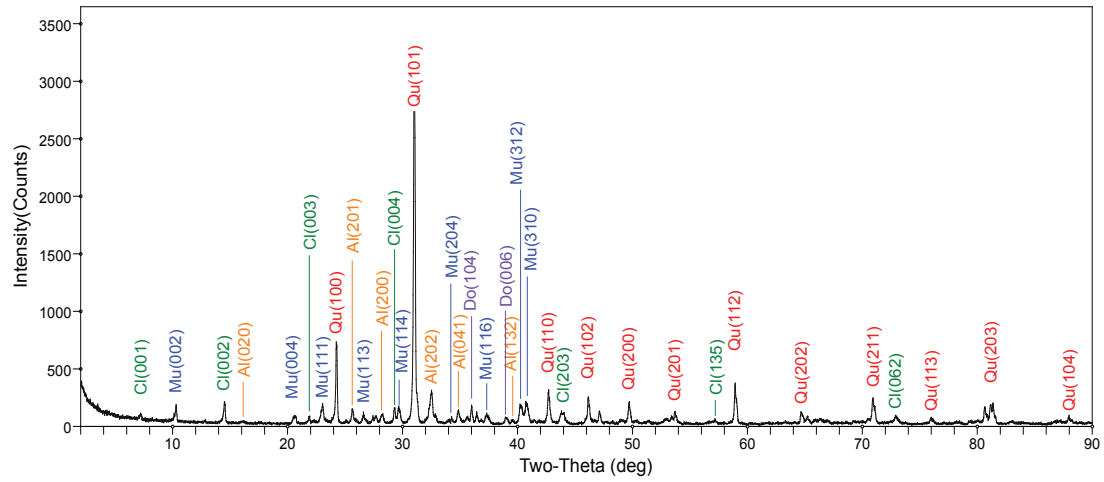
Intensity(Counts)
Two-Theta (deg)
Cl(001)
Mu(002)
Cl(002)
Al(020)
Mu(004)
Cl(003)
Mu(111)
Qu(100)
Al(201)
Mu(113)
Al(200)
Cl(004)
Mu(114)
Qu(101)
Al(202)
Mu(204)
Al(041)
Do(104)
Mu(116)
Al(132)
Do(006)
Mu(312)
Mu(310)
Qu(110)
Cl(203)
Qu(102)
Qu(200)
Qu(201)
Cl(135)
Qu(112)
Qu(202)
Qu(211)
Cl(062)
Qu(113)
Qu(203)
Qu(104)

Figure 3.11 (previous 2 pages): Diagrams of X-Ray Diffraction (XRD) showing the main peaks of mineral assemblages present in the very fine-grained argillaceous matrix. Identification of the mineral forms was based on their crystallographic structure. Major mineral phases include: quartz (Qu), muscovite (Mu), calcite (Ca), albite (Al), and clinochlore (Cl). Common clays include: kaolinite (Ka), nacrite (Na), and rectorite (Re). These clay minerals probably resulted from the alteration of alumino-silicates such as albite and microcline, or from diagenesis of muscovite. Common varieties of zeolite minerals include wairakite (Wa), analcime (Ac), and clinoptilolite (Cp). These minerals occur as pore-filling cement, and as part of the cryptocrystalline groundmass mainly composed of devitrified volcanic glass.

3.5 Discussion: Paleoenvironmental implications

The vertical succession of facies identified in this study clearly indicates a retrogradational depositional trend regionally (figure 3.3). Conglomerate and very coarse-grained sandstone are found exclusively at the base of the Smithers Formation, where they disconformably overlie subaerial volcanic rocks of the Telkwa Formation. These coarse-grained shoreface deposits generally fine upward into fossiliferous and highly bioturbated siltstone and mudstone, in which physical and biogenic structures suggest deposition in a more distal setting. This is consistent with a widespread marine transgression over the waning Hazelton volcanic arc in the late Early to Middle Jurassic (Tipper and Richards 1976). The best display of this transition was observed at the Netalzul Mountain section (figure 3.3C), where cross-bedded and massive sandstone (facies 2) is overlain by finely laminated siltstone and mudstone (facies 3). The contact is gradational over an interval of 20 m, and marks a change from a *Skolithos* archetypal ichnofacies to a *Cruziana* archetypal ichnofacies.

On the other hand, two other facies characterized by impoverished ichnological suites were identified at Quinlan Mountain and Ashman Ridge. Coarsening- and thickening-upward stacking patterns of facies 5 (figures 3.3A, B and 3.8A), in which trace fossil are predominantly associated with deposit feeding strategies, are consistent with deposition in a wave-dominated deltaic environment (c.f. Gingras et al. 1998; MacEachern et al. 2005c). Where exposed, the transition from the deltaic facies assemblage into the offshore facies assemblage is marked by a significant increase in trace fossil abundance. However, paucity of *Thalassinoides*, *Gyrolithes*, *Ophiomorpha* and *Rhizocorallium*, in the otherwise diversified and densely bioturbated suite of facies 4, indicates that one or more parameters inhibited crustacean activities on the inner shelf. Since organism behaviours and the resulting biogenic structures are principally controlled by physio-chemical parameters, departures from the archetypal ichnofacies are attributed to stresses operating in specific environmental conditions. According to MacEachern et al. (2005b), the most common stresses delineated ichnologically are reduced

salinity, oxygen depletion near the sediment-water interface, temperature, increased sedimentation rates, heightened water turbidity, and lack of food resources. However, given the tectonic setting in which volcanic litharenite of the Smithers Formation was deposited, less common factors such as occasional deposition of significant ash layers could also be envisaged. In the following sections, the potential roles played by these different environmental parameters are considered in order to explain the departures from archetypal ichnofacies observed in some sedimentary units of the Smithers Formation.

3.5.1 Salinity and oxygen fluctuations

Although most marginal marine settings are usually characterized by salinity gradients that lead to impoverished ichnological suites (e.g. Pemberton et al. 1982; Wightman et al. 1987; Pemberton and Wightman 1992; MacEachern and Pemberton 1994; Gingras et al. 1999), no clear evidence of brackish water conditions was observed in units of the Smithers Formation in this study. Anomalous ichnological suites of facies 4 and 5 show no pronounced size reduction of structures, and the bioturbation index is consistently moderate to high. The abundance of large and diversified marine fossils throughout the succession reflects fully marine conditions, in which pelagic and benthic organisms thrived (figure 3.6). Therefore, if units of facies 5 are indeed representative of a deltaic environment, as inferred from the isolated well-defined regressive trend in a regional transgressive setting, then fluvial-induced stresses must have been negligible. As observed in other case studies (Bhattacharya and Giosan 2003; MacEachern and Loseth 2003; MacEachern et al. 2005c), sustained wave energy and unidirectional longshore drift can significantly buffer the effects of fresh water discharge at the river mouth, especially for small ephemeral tributaries (figure 3.12). In such cases, trace fossil distribution displaying a more marine, less stressed suite is expected updrift of the river mouth.

In a similar way, dysaerobic conditions do not seem to have played an important role in depositional environment of the Smithers Formation. Low dissolved oxygen concentrations are usually associated with a noticeable reduction in the size of burrows, and affect the diversity of ichnogenera markedly (Savrda and Bottjer 1989; Wignall 1991). Although a deeper tier of low-diversity *Chondrites* was observed in the mud-rich distal *Cruziana* assemblage of facies 3, the high diversity and large size of structures associated with the shallow tier suggest that the sediment-water interface was not significantly affected by oxygen depletion.

3.5.2 Increased water turbidity and sedimentation rates

The preponderance of structures produced by deposit feeders in interbedded

sandstone and siltstone of facies 5 is interpreted to represent conditions of elevated turbidity in the water column. This bias towards deposit-feeding ethologies is typically derived from the fact that high suspended loads tend to clog the filter-feeding apparatus of organisms, while lowering the overall concentration of available organic material (Gingras et al. 1998; MacEachern et al. 2005b; 2005c). Consequently, this leads to a reduction of *Skolithos* ichnofacies structures while *Cruziana* ichnofacies elements remain abundant. These characteristics are considered typical of deltaic conditions (e.g. Moslow and Pemberton 1988; Gingras et al. 1998; MacEachern et al. 2005c). Close association of facies 5 and 6 suggests that sedimentation was episodic and overall sedimentation rate was relatively low. Concentration of large articulated bivalves along distinct layers of facies 6 indicates extended periods of non-deposition (figure 3.9C).

Although heightened turbidity levels might explain the impoverished ichnological assemblage in deltaic units of facies 5 reasonably well, the same argument does not apply for departures observed in facies 4. Filter-feeding traces such as *Rosselia rotatus* and *Rosselia socialis* are common (figure 3.7A), and the beds are heavily bioturbated throughout the succession. This suggests slow sedimentation rate in an overall low turbidity environment, in which suspended and deposited food resources were present in sufficient quantity to support a large and diverse infaunal community.

3.5.3 Deposition of ash layers (event beds)

The high proportion of tuff beds in the Smithers Formation indicates that sedimentation was contemporaneous with distal volcanism (figure 3.12). These tuff beds are especially well preserved in offshore units deposited on the inner shelf, where fair-weather wave activity was not significant. Frequent accumulation of 5-10 cm thick ash layers on the sea-floor repeatedly provided a new substrate, which could have affected the infaunal community. Wetzel (2002, 2008) recently documented the impacts of syn-sedimentary volcanism on benthic organisms in modern deep-marine turbidites of the South China Sea. According to Wetzel (2008), colonization of an ash layer shortly after the widespread 1991 Pinatubo volcanic eruption provides evidence for the restoration of the endobenthos. More specifically, Wetzel (2008) noted that *Thalassinoides* were commonly observed as the deepest tier of the post-recovery trace assemblage, whereas traces made by polychaetes tend to be missing when the ash layer exceeds 5 cm in thickness.

In units of the Smithers Formation, the few *Thalassinoides* identified in facies 4 are separated from the more representative, highly diverse ichnological assemblage dominated by polychaete traces, and appear to be concentrated below isolated tuff beds

(figures 3.3 and 3.7G). The burrows commonly contain ash, indicating that they were produced after deposition of the ash layer and filled by the burrowing organisms (figure 3.7H). This suggests that the burrowing shrimps were able to colonize the new substrate rapidly and exploit this open niche to their advantage. A similar scenario was documented by Grimm and Follmi (1994) in hemipelagic sedimentary rocks of the San Gregario Formation in Baja California, in which *Thalassinoides* traces are exclusively associated with gravity-flow event deposits. In their doomed pioneer model, Follmi and Grimm

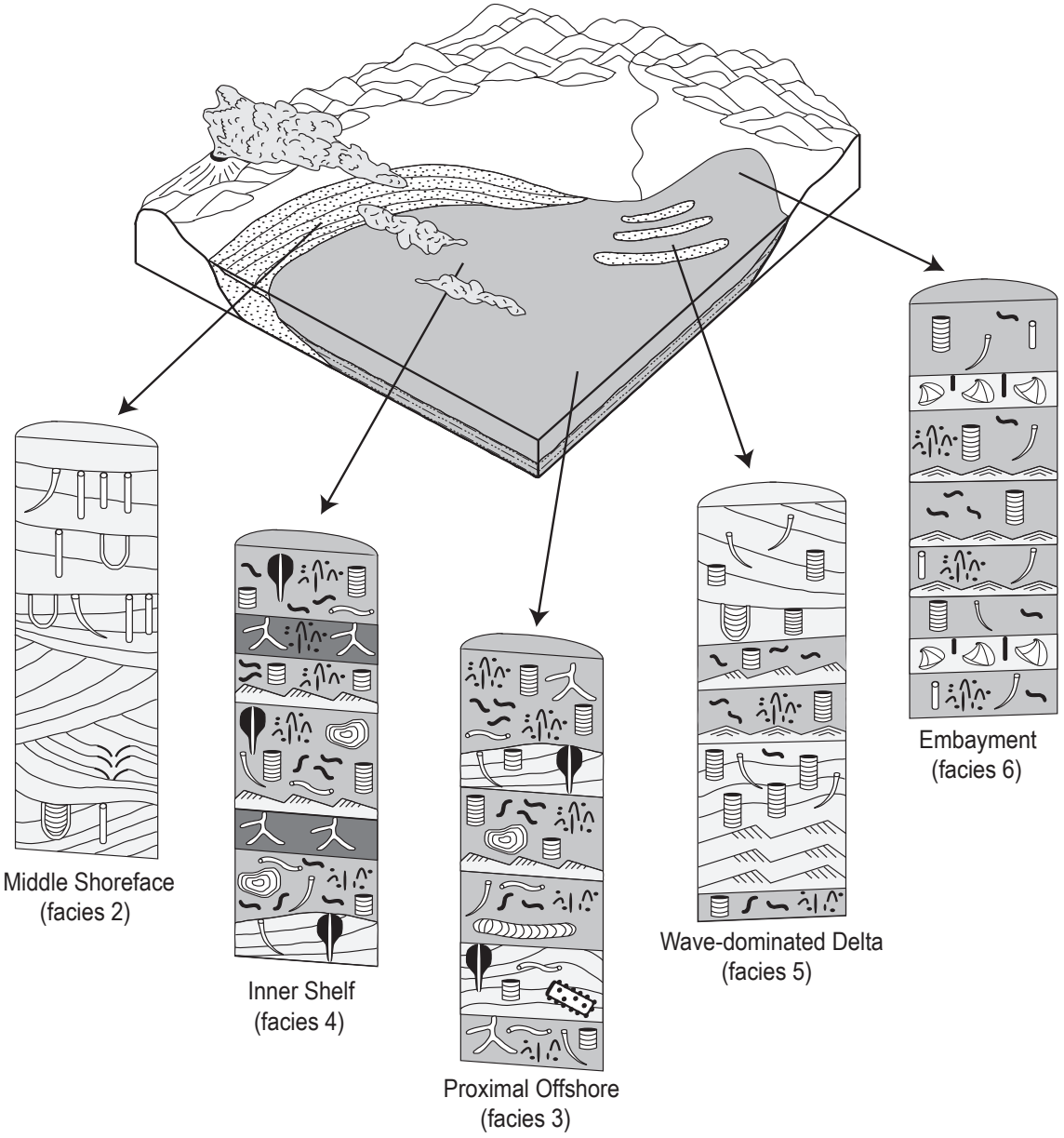

Figure 3.12: Conceptual diagram showing the interpreted depositional model of the Smithers Formation and the distribution of facies. See figure 3.3 for legend details.

(1990) proposed that crustaceans were introduced into a new environment during some type of turbulent event, but persistence of dysaerobic conditions limited their survival. However, in contrast to the doomed pioneer model (Follmi and Grimm 1990), it is unlikely that crustaceans of facies 4 were introduced during deposition of an ash layer. The data suggests that trace makers of *Thalassinoides* were preferentially able to survive the deposition of 5–10 cm thick ash layers; present in small numbers, or in an adjacent environment prior to ash deposition, they were able to exploit the environment of facies 4 when the majority of polychaetes were eliminated during the volcanic event. Eventually, the resident community largely composed of polychaetes re-established itself, but it remains unclear why arthropods became less abundant at this point.

3.6 Conclusions

Integration of lithological, petrological and ichnological data collected from four detailed measured sections in north-central British Columbia allow for a better understanding of the sedimentary environment in which volcanic litharenite of the Smithers Formation was deposited (figure 3.12). At Netalzul Mountain, a gradual change from a sandstone-rich *Skolithos* ichnofacies towards an intensively bioturbated, finer-grained *Cruziana* ichnofacies indicates a retrogradational trend in an unrestricted storm-dominated shoreface environment. This is consistent with the widespread transgression proposed by Tipper and Richards (1976) in late Early to early Middle Jurassic. An isolated regressive event marked by a thickening- and coarsening-upward succession was identified at Ashman Ridge and Quinlan Mountain (figures 3.3A, B and 3.8A). The high proportion of mobile deposit feeder traces and readjustment structures in sandy substrate suggest a turbid environment with moderate sedimentation rates commonly observed in deltaic environments (Gingras et al. 1998; MacEachern et al. 2005c). Although there is a noticeable absence of filter-feeding structures in these units, the impoverished deltaic ichnological suite shows no sign of brackish water influence, which suggest that fluvial effects were minimal. Therefore, the regressive cycle observed at Quinlan Mountain and Ashman Ridge probably corresponds to accumulation in a restricted, updrift portion of a wave-dominated delta (figure 3.12). These units are overlain by a thick package of intensively bioturbated sandstone, siltstone, and tuff, in which sedimentary structures and trace fossils are consistent with accumulation on the inner shelf. However, rare occurrence of traces attributed to decapod crustaceans, in this otherwise diversified ichnological assemblage, suggest some sort of environmental stress. Since none of the most common control parameters (i.e. salinity, oxygen, temperature, turbidity, and sedimentation rate) seems to have affected the infaunal community, the poor

representation of crustacean traces in facies 4 must have some other explanation. The rare *Thalassinoides*, mostly concentrated near or below distinctive tuff beds, represent opportunistic organisms that benefited from introduction of event beds and rapidly colonized the 5–10 cm thick tuff layers. The Smithers Formation thus clearly documents the modification of archetypal ichnofacies by volcanic activity. Return to more normal, but still ash-influenced conditions, led to re-establishment of the diverse and abundant polychaete community and demise of the the opportunistic crustaceans. Nevertheless, the response of shallow marine burrowing organisms to rapid deposition of ash beds remains poorly understood, and would greatly benefit from additional case studies of modern analogues, in which individual ecological parameters could be calibrated.

3.7 References

Arnott, R.W. and Southard, J.B. 1990. Exploratory flow-duct experiments on combined flow bed configuration, and some implications for interpreting storm-event stratification. Journal of Sedimentary Petrology, vol. 60, pp. 211-219.

Bann, K.L. and Fielding, C.R. 2004. An integrated ichnological and sedimentological comparison of non-deltaic shoreface and subaqueous delta deposits in Permian reservoir units of Australia. *In:* McIlroy, D. (Ed.), The Application of Ichnology to Palaeoenvironmental and Stratigraphic Analysis. The Geological Society of London, vol. 228, pp. 273-307.

Bhattacharya, J.P. and Giosan, L. 2003. Wave-influenced deltas: geomorphological implications for facies reconstruction. Sedimentology, vol. 50, pp. 187-210.

Bromley, R.G. and Ekdale, A.A. 1984. Chondrites: A Trace Fossil Indicator of Anoxia in Sediments. Science, vol. 224, pp. 872-874.

Buatois, L.A., Santiago, N., Parra, K. and Steel, R.J. 2008. Animal-substrate interactions in an Early Miocene wave-dominated tropical delta: delineating environmental stresses and depositional dynamics (Tacata Field, Eastern Venezuela). Journal of Sedimentary Research, vol. 78, pp. 458-479.

Carmona, N.B., Buatois, L.A., Ponce, J.J. and Mangano, M.G. 2009. Ichnology and sedimentology of a tide-influenced delta, Lower Miocene Chenque Formation, Patagonia, Argentina: Trace fossil distribution and response to environmnetal stresses. Palaeogeography, Palaeoclimatology, Palaeoecology, vol. 273, pp. 75-86.

Coates, L. 2001. Ichnological and sedimentological signature of wave- and river-dominated deltas, Dunvegan Formation and Basal Belly River Formation, west-central Alberta. M.Sc. thesis, Department of earth Sciences, Simon Fraser University, Burnaby, B.C.

Dworschak, P.C. 2000. Global diversity in the thalassinidea (decapoda). Journal of crustacean biology, vol. 20, pp. 238-245.

Ekdale, A.A. 1985. Paleoecology of the marine endobenthos. Palaeogeography, Palaeoclimatology, Palaeoecology, vol. 50, pp. 63-81.

Evenchick, C.A., Mustard, P.S., McMechan, M.E., Ritcey, D.H. and Smith, G.T. 2008a. Geology, Northeast Terrace and northwest Smithers, British Columbia. Geological Survey of Canada. Open File 5895.

Evenchick, C.A., McMechan, M.E., Mustard, P.S., Ritcey, D., Smith, G.T., Ferri, F. and Waldron, J.W.F.

2008b. Geology, Hazelton, British Columbia. Geological Survey of Canada. Open File 5704.

Evenchick, C.A., Poulton, T.P. and McNicoll, V.J. *Submitted for publication*. Nature and significance of the diachronous contact between the Hazelton and the Bowser Lake groups (Jurassic), north-central British Columbia. Bulletin of Canadian Petroleum Geology.

Feldmann, R.M. and Haggart, J.W. 2007. A new species of lobster (Astacidea, Erymidae) from the Smithers Formation (Middle Jurassic) of British Columbia, Canada. Canadian Journal of Earth Sciences, vol. 44, pp. 1791-1796.

Folk, R.L., Andrews, P.B. and Lewis, D.W. 1970. Detrital sedimentary rock classification and nomenclature for use in New Zealand. New Zealand Journal of Geology and Geophysics, vol. 13, pp. 937-968.

Follmi, K.B. and Grimm, K.B. 1990. Doomed pioneers: Gravity-flow deposition and bioturbation in marine oxygen-deficient environments. Geology, vol. 18, pp. 1069-1072.

Frebold, H. and Tipper, H.W. 1973. Upper Bajocian - Lower Bathonian Ammonite Fauna and Stratigraphy of Smithers Area, British Columbia. Canadian Journal of Earth Sciences, vol. 10, pp. 1109-1131.

Galloway, W.E. 1979. Diagenetic controls of reservoir quality in arc-related sandstones: implications for petroleum exploration. *In*: Scholle, P.A. and Schluger, P.R. (Eds.), Aspects of diagenesis. SEPM Special Publication, vol. 26, pp. 251-262.

Gagnon, J.-F. and Waldron, J.W.F. 2008. Ashman Ridge Section Revisited: New Insights for the Evolution of the Bowser Basin, Northwestern British Columbia (NTS 93L/13). *In:* Summary of Activities 2007. Geoscience BC, Report 2008-1, pp. 121-128.

Gingras, M.K., MacEachern, J.A. and Pemberton, S.G. 1998. A comparative analysis of the ichnology of wave and river-dominated allomembers of the Upper Cretaceous Dunvegan Formation. Bulletin of Canadian Petroleum Geology, vol. 46, pp. 51-73.

Gingras, M.K., Pemberton, S.G., Saunders, T. and Clifton, H.E. 1999. The Ichnology of Modern and Pleistocene Brackish-Water Deposits at Willipa Bay, Washington: Variability in Estuarine Settings. PALAIOS, vol. 14, pp. 352-374.

Gregory, M.R. 1991. New trace fossils from the Miocene of Northland, New Zealand: *Rorschachichnus amoeba* and *Piscichnus waitemata*. Ichnos, vol. **1**, pp. 195-205.

Grimm, K.A., Follmi, K.B., Ledesma. M. and Schwennicke, T. 1989. Role of explosive volcanism, event deposition and bioturbation in the genesis of stratification sequences in phosphatic and associated sediments, Oligocene San Gregorio Formation, Baja California Sur, Mexico. *In:* Geological Society Of America Abstract, vol. 21, p. A80.

Grimm, K.A. and Follmi, K.B. 1994. Doomed Pioneers: Allochtonous Crustacean Tracemakers in Anaerobic Basinal Strata, Oligo-Miocene San Gregorio Formation, Baja California Sur, Mexico. PALAIOS, vol. 9, pp. 313-334.

Grodon, J. and Eberl, D.D. 1984. Illite. *In:* Bailey, S.W. (Ed.), Micas. Mineralogical Society of America, vol. 13, pp. 495-544.

Hanson, G. 1926. Reconnaissance in Zymoetz River Area, Coast District, B.C. *In:* Summary Report 1925, Geological Survey of Canada, Part A, pp. 100-119.

Hawkins, D.B. 1981. Kinetics of glass dissolution and zeolite formation under hydrothermal conditions. Clays and Minerals, vol. 29, pp. 331-340.

Hubbard, S.M., Gingras, M.K. and Pemberton, S.G. 2004. Palaeoenvironmental implications of the trace fossils in estuarine deposits of the Cretaceous Bluesky Formation, Cadotte region, Alberta, Canada. *In:* Webby, B.D., Mangano, M.G. and Buatois, L.A. (Eds.), Fossils and Strata. First

international paleontological congress, Sydney, Australia, vol. 51, pp. 68-87.

Johnston, K.K. 2002. Taxonomy and biostratigraphy of Middle Jurassic ammonites, western and central British Columbia. M.Sc. thesis, Department of Geology and Geophysics, University of Calgary, Calgary, Ab.

MacEachern, J.A. and Pemberton, S.G. 1994. Ichnological aspects of incised valley fill systems from the Viking Formation of the Western Canada Sedimentary Basin, Alberta, Canada. *In:* Boyd, R., Dalrymple, R.W. and Zaitlin, B. (Eds.), Incised Valley Systems: Origin and Sedimentary Sequences. SEPM Special Publication, vol. 51, pp. 129-157.

MacEachern, J.A. and Loseth, T.M. 2003. Sedimentology and Ichnology of a transgressively back-stepped wave-dominated deltaic reservoir: Middle Jurassic Tarbert and Heather Formations, North Sea, Norway. *In:* American Association of Petroleum Geologists Annual Convention, Salt Lake City, Utah, p. A110.

MacEachern, J.A., Bann, K.L., Pemberton, S.G. and Gingras, M.K. 2005a. The ichnofacies paradigm: high-resolution paleoenvironmental interpretation of the rock record. *In:* MacEachern, J.A., Bann, K.L, Gingras, M.K. and Pemberton, S.G. (Eds.), Applied Ichnology. SEPM short course notes, vol. 52, pp. 27-64.

MacEachern, J.A., Pemberton, S.G., Bann, K.L., and Gingras, M.K. 2005b. Departures from the Archetypal Ichnofacies: Effective Recognition of Physico-Chemical Stresses in the Rock Record. *In:* MacEachern, J.A., Bann, K.L, Gingras, M.K. and Pemberton, S.G. (Eds.), Applied Ichnology. SEPM short course notes, vol. 52, pp. 65-93.

MacEachern, J.A., Bann, K.L., Bhattacharya, J.P. and Howell Jr, C. 2005c. Ichnology of Deltas: Organism responses to the dynamic interplay of rivers, waves, storms and tides. *In* Giosan, L. and Bhattacharya, J.P. (Eds.), River Deltas; concepts, models, and examples. SEPM Special Publication, vol. 83, pp. 49-85.

Marsden, H. and Thorkelson, D.J. 1992. Geology of the Hazelton Volcanic Belt in British Columbia: Implications for the Early to Middle Jurassic Evolution of Stikinia. Tectonics, vol. 11, pp. 1266-1287.

Moslow, T.F. and Pemberton, S.G. 1988. An integrated approach to the sedimentological analysis of some Lower Cretaceous shoreface and delta front sandstone sequences. *In:* James, D.J. and Leckie, D.A. (Eds.), Sequences, Stratigraphy, Sedimentology: Surface and Subsurface. Canadian Society of Petroleum Geologists, Memoir 15, pp. 373-386.

Nelson, J.L., Kennedy, R., Angen, J. and Newman, S. 2007. Geology of Terrace area. British Columbia Ministry of Energy, Mines and Petroleum Resources. Open File 2007-04.

Pemberton, S.G. and Wightman, D.M. 1992. Ichnological characteristics of brackish water deposits. *In:* Pemberton, S.G. (Ed.), Applications of Ichnology to Petroleum Exploration, a core workshop. SEPM, Core Workshop 17, pp. 141-167.

Pemberton, S.G., Flach, P.D. and Mossop, G.D. 1982. Trace Fossils from the Athabasca Oil Sands, Alberta, Canada. Science, vol. 217, pp. 825-827.

Pemberton, S.G., MacEachern, J.A. and Frey, R.W. 1992. Trace fossil facies model: environmental and allostratigraphic significance. *In:* Walker, R.G. and James, N.P. (Eds.), Facies Models: Response to Sea Level Change. Geological Association of Canada, Geotext 1, pp. 47-72.

Pemberton, S.G., Spila, M., Pulham, A.J., Saunders, T., MacEachern, J.A., Robbins, D. and Sinclair, I.K. 2001. Ichnology & sedimentology of shallow to marginal marine systems: Ben Nevis & Avalon

reservoirs, Jeanne d'Arc Basin. Geological Association of Canada. Short Course Notes, vol.15, 343 p.

Poulton, T.P. and Tipper, H.W. 1991. Aalenian ammonites and strata of western Canada. Geological Survey of Canada. Bulletin 411, 71 p.

Rhoads, D.C. and Morse, J.W. 1971. Evolutionary and ecologic significance of oxygen-deficient marine basins. Lethaia, vol. 4, pp. 413-428.

Savrda, C.E. and Bottjer, D.J. 1989. Trace-fossil model for reconstructing oxygenation histories of ancient marine bottom waters: application to Upper Cretaceous Niobrara Formation, Colorado. Palaeogeography, Palaeoclimatology, Palaeoecology, vol. 74, pp. 49-74.

Singer, A. and Muller, G. 1983. Diagenesis in argillaceous sediments. *In:* Larsen, G. and Chilinga, G.V. (Eds.), Diagenesis in Sediments and Sedimentary Rocks. Elsevier, Amsterdam, pp. 115-122.

Seilacher, A. 1967. Bathymetry of trace fossils. Marine Geology, vol. **5**, pp. 413-428.

Surdam, R.C. and Boles, J.R. 1979. Diagenesis of volcanogenic sandstones. *In:* Scholle, P.A. and Schluger P.R. (Eds), Aspects of diagenesis. SEPM Special Publication, vol. 26, pp. 227-247.

Tang, Z., Parnell, J. and Longstaffe, F.J. 1997. Diagenesis and Reservoir Potential of Permian-Triassic Fluvial/Lacustrine Sandstones in the Southern Juggar Basin, Northwestern China. AAPG Bulletin, vol. 88, pp. 1843-1865.

Thomson, R.C., Smith, P.L. and Tipper, H.W. 1986. Lower to Middle Jurassic (Pliensbachian to Bajocian) stratigraphy of the northern Spatsizi area, north-central British Columbia. Canadian Journal of Earth Sciences, vol. 23, pp. 1963-1973.

Tipper, H.W. and Richards, T.A. 1976. Jurassic stratigraphy and history of north-central British Columbia. Geological Survey of Canada, Bulletin 270, 73 p.

Wetzel, A. 2002. Modern *Nereites* in the South China Sea - Ecological Association with Redox Conditions in the Sediment. PALAIOS, vol. 17, pp. 507-515.

Wetzel, A. 2008. Recent bioturbation in the deep South China Sea: a uniformitarian approach. PALAIOS, vol. 23, pp. 601-615.

Wetzel, A. and Uchman, A. 2001. Sequential colonization of muddy turbidites in the Eocene Beloveza Formation, Carpathians, Poland. Palaeogeography, Palaeoclimatology, Palaeoecology, vol. 168, pp. 171-186.

Wightman, D.M., Pemberton, S.G. and Singh, C. 1987. Depositional modelling of the Upper Mannville (Lower Creataceous), central Alberta: implications for the recognition of brackish water deposits. *In:*Tillman, R.W. and Weber, K.J. (Eds.), Reservoir Sedimentology. SEPM Special Publication, vol. 40, pp. 189-220.

Wignall, P.B. 1991. Dysaerobic trace fossils and ichnofabrics in the Upper Jurassic Kimmeridge Clay of southern England. PALAIOS, vol. 6, pp. 264-270.

Chapter 4: Jurassic subsidence history of the Hazelton Trough–Bowser Basin in the area of Todagin Mountain, north-central British Columbia, Canada[3]

4.1 Introduction

The Bowser basin is a large sedimentary basin that developed during late Middle and Late Jurassic time on the Stikine terrane in the Intermontane Belt of the Canadian Cordillera in British Columbia (figure 4.1). Its tectonic evolution records the deposition of a thick (>6 km) sedimentary succession over the Lower to Middle Jurassic Hazelton trough (Evenchick and Thorkelson 2005). Recent work by the Geological Survey of Canada has shown the existence of an effective petroleum system in the basin, which already has significant proven coal resources (Bustin and Moffat 1989; Ryan and Dawson 1993; Evenchick et al. 2002, 2003; Osadetz et al. 2003; Ferri et al. 2004; Osadetz et al. 2007).

Models for the origin of the basin are based on regional stratigraphic relationships and interpretations of tectonic setting. One model proposed by Eisbacher (1985) and elaborated by Ricketts et al. (1992) suggests that overthrusting of the Cache Creek terrane (figure 4.1) in the Aalenian was responsible for flexural subsidence of Stikinia which created the accommodation space necessary to generate the Bowser basin. Other postulated basin-forming mechanisms include crustal stretching during a rifting episode on Stikinia (Anderson 1993; Thorkelson et al. 1995), a forearc setting (Dickinson 1976), and a strike-slip setting (Greig et al. 1991). Basin subsidence is also interpreted to have been a result of a combination of thermal contraction, sediment load, and flexure associated with obduction of Cache Creek terrane (Evenchick et al. 2007).

In this paper, we present the results of the first quantitative analysis of subsidence for the upper Hazelton and Bowser Lake groups, from examination of Lower Pliensbachian to Middle Oxfordian successions exposed at the northwestern limit of the Bowser basin (figure 4.2). By determining how and when most of the accommodation space was generated, we hope to determine the origin of this part of the basin and shed light on the timing and nature of terrane accretion in the Middle Jurassic. Understanding the tectonic setting of the Bowser basin has important implications for the evolution of the Canadian Cordillera and for the petroleum prospectivity of the basin.

[3] *A version of this chapter has been published. Gagnon, J.-F., Evenchick, C.A., Waldron, J.W.F, Cordey, F. and Poulton, T.P. 2009. Bulletin of Canadian Petroleum Geology, vol. 57, no. 4, pp. 430-448.*

4.2 *Geological setting and stratigraphy*

The allochthonous Stikine terrane, on which the northern Bowser basin was developed, consists mainly of Lower Devonian to Middle Jurassic magmatic arc rocks and associated sedimentary units (Anderson and Thorkelson 1990; Brown et al. 1991; Anderson 1993; Gunning et al. 2006). Most earlier studies suggest that the Stikinia substratum is isotopically primitive, mantle-derived and Paleozoic in age or younger

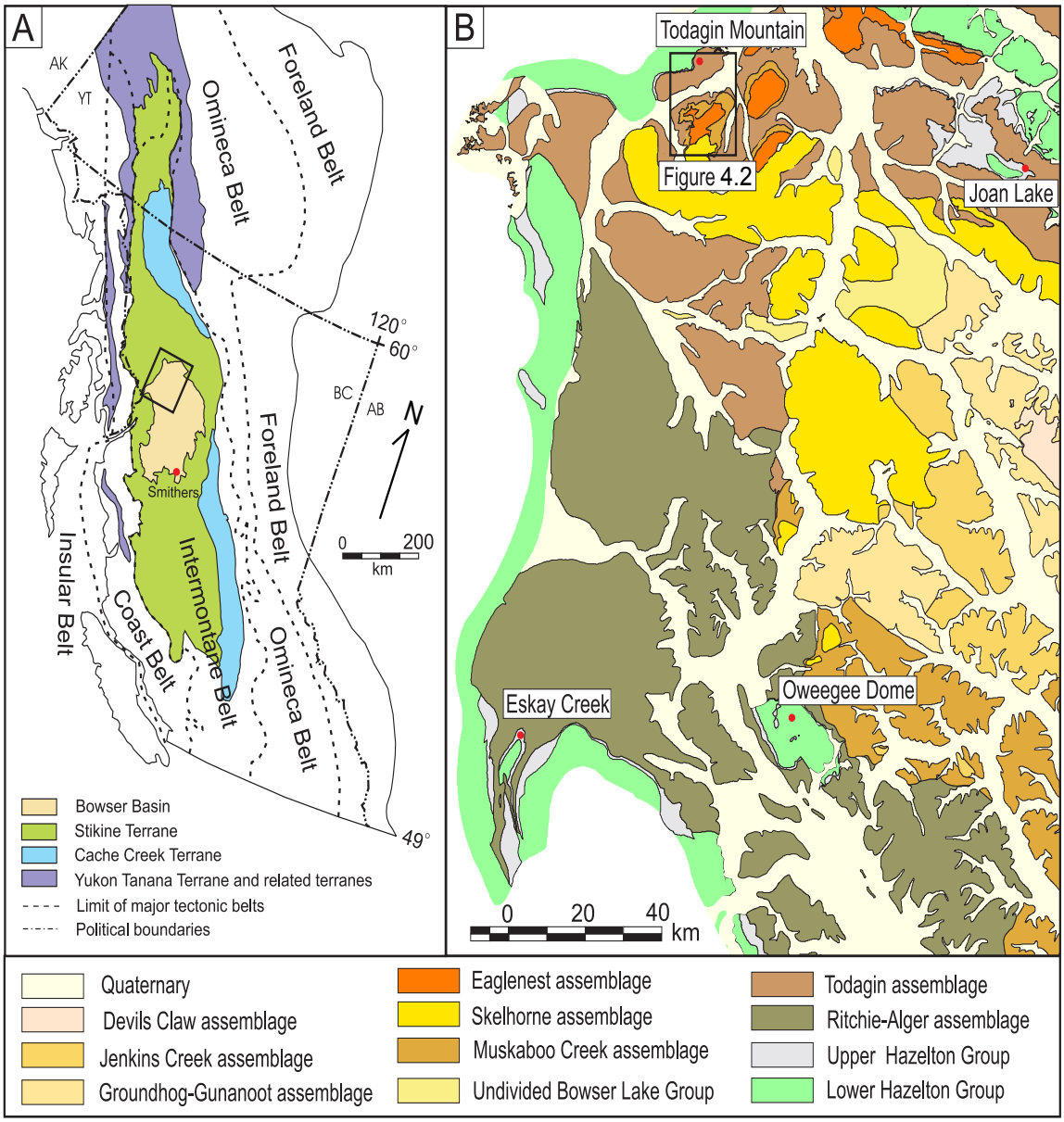

Figure 4.1: A) Location of the Bowser basin in relation to principal tectonic belts of the Canadian Cordilleran Orogen modified from Wheeler and McFeely (1991) and Colpron et al. (2006). Box encloses area shown in B. B) Simplified geology map of the Bowser basin showing the distribution of lithofacies assemblages, and the area of study in the vicinity of Todagin Mountain (box encloses area of geology map in figure 4.2). Modified from Evenchick et al. (2006).

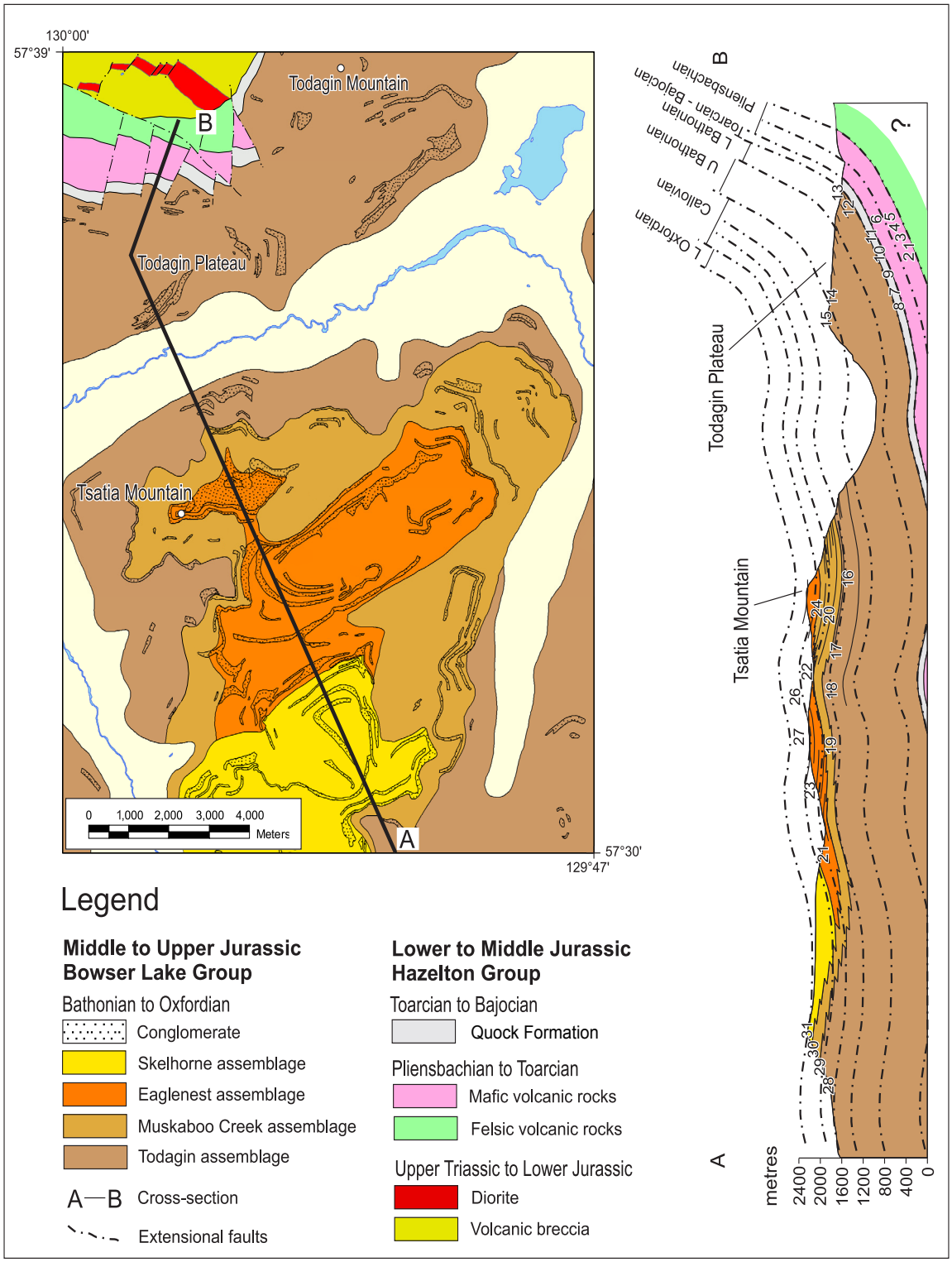

Figure 4.2: Geology map of the Todagin Mountain area showing orientation of the stratigraphic cross-section A-B. Dotted lines on the cross-section represent isochrons determined by distribution of fossil localities (numbers 1-31). No vertical exaggeration. Description of fossil localities explained in Table 4.1. Geology modified from Evenchick and Green (2004). Cross-section modified from figure 173 of Evenchick and Thorkelson (2005).

(Gabrielse et al. 1980; Samson et al. 1989; Greig and Gehrels 1995). This is consistent with SNORCLE seismic reflection profiles which indicate that for the most part, the Stikine terrane is not underlain by evolved continental crust except for a tapering wedge to the northeast (Snyder et al. 2002; Cook et al. 2004; Evenchick et al. 2005). On the other hand, the presence of an evolved Precambrian basement in the Stikinian subsurface was proposed by Thorkelson et al. (1995) based on discordant zircons. This might correspond to a minor local component in an overall juvenile crust.

The evolution of the Stikine terrane is characterized by three major episodes of volcanic activity represented by: the Lower Devonian to Upper Permian Stikine assemblage; the Middle to Upper Triassic Stuhini Group; and the widespread Lower to Middle Jurassic Hazelton Group (figure 4.3) (Alldrick 1993; Anderson 1993; Thorkelson et al. 1995). According to Tipper and Richards (1976), rocks of the Hazelton Group were deposited within the Hazelton trough, in which subsidence by graben faulting was continuous during most of the Early to Middle Jurassic. Field relationships within the northwest parts of the Hazelton trough combined with U-Pb geochronologic and biostratigraphic data have shown that calc-alkaline volcanic units of the lower Hazelton Group are unconformably overlain by Pliensbachian to Toarcian volcanic rocks and associated shallow-marine sedimentary rocks of the upper Hazelton Group (Greig and Gehrels 1995; Thorkelson et al. 1995; Chapter 2). This regional unconformity marks an important change from a volcanic-dominated depositional regime to a subsiding sedimentary basin with waning volcanic activity. Geochemical analyses of Hazelton Group volcanic rocks in the vicinity of Joan Lake (figure 4.1) show pronounced bimodality of silica concentrations and great variability of trace element compositions (Thorkelson et al. 1995), characteristics commonly observed in profiles of volcanic rocks deposited in extensional settings (Martin and Piwinski 1972; Strong 1979; Bacon et al. 1984). Other indications of extension west of the Bowser basin during deposition of the upper Hazelton Group are volcanic-hosted massive sulphide deposits (VHMS) accumulated on the sea-floor of a dissected fault-bounded basin (Anderson and Thorkelson 1990; Barrett and Sherlock 1996; McDonald et al. 1996; Roth 2002; Alldrick et al. 2005). In the area of this study, the laterally equivalent marine sedimentary succession of the upper Hazelton Group is capped by laminated radiolarian mudstone and recessive tuff bands which were originally assigned to the Quock Formation of the Spatsizi Group by Thomson et al. (1986); these units were later lowered in status to member and formation by Evenchick and Thorkelson (2005), but more recently re-elevated to the rank of formation (Chapter 2). Because the Pliensbachian to Bajocian sedimentary rocks of the upper Hazelton Group are conformably overlain by the Bowser

Lake Group with a gradational contact, we believe that they represent a continuous sedimentary succession with local disconformities associated with short periods of non-deposition.

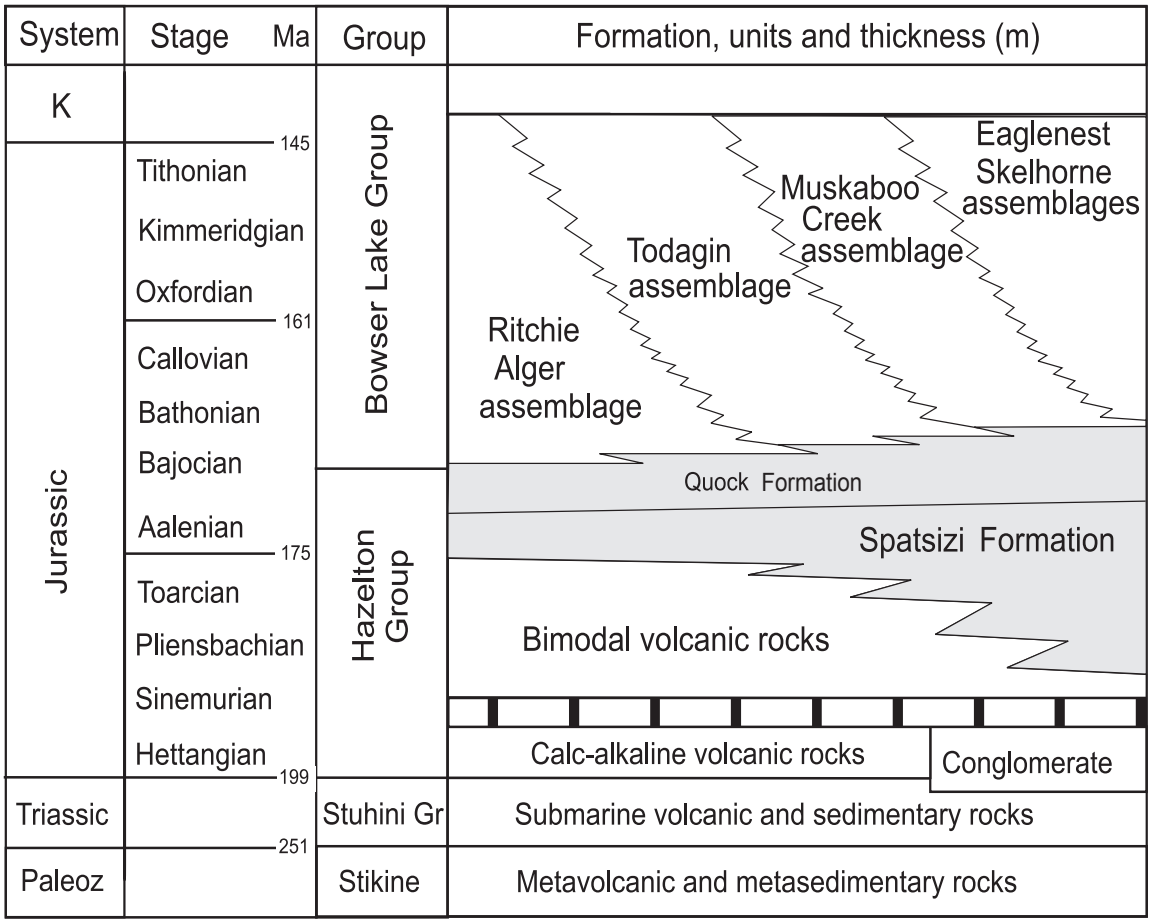

Figure 4.3: Simplified stratigraphic chart of the units found in the Spatsizi map sheet 104H. Modified from Evenchick and Thorkelson (2005).

The term Bowser group was originally assigned informally to an assemblage of mudstone, sandstone and conglomerate exposed around Bowser Lake during "Operation Stikine" conducted by the Geological Survey of Canada (1957). After Duffell and Souther (1964) proposed an Upper Jurassic to Lower Cretaceous age for those sedimentary rocks, Tipper and Richards (1976) extended the group to the area around Smithers and changed the name to Bowser Lake Group. They described it as a thick assemblage of marine and non-marine sedimentary rocks deposited in the Bowser basin. Tipper and Richards (1976) assigned a Middle to Upper Jurassic age to the group, based on an extensive fossil collection. In the north of the basin, Evenchick and Thorkelson (2005) showed that lithologically similar strata, included in the Bowser Assemblage by Eisbacher (1974),

are as young as mid-Cretaceous. The Bowser Lake Group, thus defined, consists of at least 6000 m of siliciclastic sedimentary rocks (Evenchick and Thorkelson 2005). This thick sedimentary package represents a generally shallowing-upward succession that is divided into diachronous lithofacies assemblages defined by sedimentological features (Eisbacher 1974; Evenchick et al. 2001; Evenchick and Thorkelson 2005). Submarine fan turbidites at the base pass upward and laterally into slope, shelf, deltaic and fluvial facies near the top of the succession. In the northern two-thirds of the basin these lithofacies assemblages likely prograded towards the south and southwest during Bathonian to Early Oxfordian time, as they continuously overlap in age and become progressively younger towards the south (Evenchick and Thorkelson 2005).

At the northwest edge of the basin, in the vicinity of Todagin Mountain (figure 4.2), Lower Pliensbachian to Toarcian bimodal volcanic flows interbedded with shallow marine sedimentary rocks of the upper Hazelton Group unconformably overlie subaerial welded tuffs and oxidized volcaniclastics (figure 4.4). The succession includes marine pillow basalts, hyaloclastites, and fine-grained sedimentary units with diagnostic Pliensbachian ammonoids, such as *Dubariceras freboldi* and *Oistoceras* sp., confirming the ages previously determined by Palfy et al. (2000) and Evenchick et al. (2001). Friedman and Ash (1997) also reported a radiometric age of ca. 181 Ma from a felsic layer within the bimodal succession, indicating that the top of this unit could be as young as Late Toarcian. Geological mapping suggests that the interbedded volcanic flows and sedimentary rocks are preserved preferentially in fault-bounded structures (figure 4.2), consistent with deposition in a graben system that was inverted during later deformation. A shallow discordance within the Pliensbachian interval was observed in the field. Fossils collected immediately above and below the discordance indicate no significant hiatus, which suggests that the discordance developed during syn-sedimentary faulting.

These units are overlain by 110 m of interbedded siliceous mudstone and tuffaceous siltstones of the Quock Formation (Evenchick and Green 2004; Chapter 2). Although no fossils were recovered in the Quock Formation at Todagin Mountain, well documented collections of ammonites in lithologically equivalent stratigraphic units 65 km to the east near Joan Lake yielded an Aalenian to Early Bajocian age (Thomson et al. 1986; Poulton and Tipper 1991; Chapter 2). The fine grain size, lack of bioturbation, and absence of wave-generated sedimentary structures, combined with significant organic content in the radiolarian mudstone near Joan Lake (figure 4.1) (TOC values of 1.74 to 3.45%, Ferri and Boddy 2005), suggest that the sediments accumulated mainly from suspension in a deep-marine, anoxic environment. Approximately 3 km northeast of the measured section, outside the graben structures (figure 4.2), the Quock Formation

overlies successively older rocks indicating an unconformity (Evenchick and Green 2004). On the other hand, in the Joan Lake area (figure 4.1), the formation rests without apparent discordance on the Pliensbachian to Toarcian sedimentary units of the Spatsizi River Formation (Thomson et al. 1986; Chapter 2). These relationships suggest that the base of the Quock Formation represents a regional deepening and transgression across an irregular topography of lower Hazelton Group rocks.

The Quock Formation is conformably overlain by a broad variety of lithofacies assemblages of the Bowser Lake Group. These rocks are superbly exposed in continuous sections 8 km to the south on Tsatia Mountain (figure 4.2), where they were examined in detail by Green (1991, 1992) and Evenchick and Green (2004). The lowermost units observed by Green (1991) are part of the pro-delta slope facies which includes at least 1100 m of dark grey siltstones monotonously interbedded with buff-weathered mudstones and very fine grained sandstones. Thick (30 m) conglomerate bodies are embedded in the fine-grained strata and represent a series of coalescent wedges that overlap one another (Green 1991). This unit was later assigned to the Todagin assemblage by Evenchick and Thorkelson (2005). According to Ricketts and Evenchick (1991), these sedimentary rocks were deposited on a slope where channelized conglomerates constituted infills of incised canyons and gullies. Soft-sediment deformation structures and debris flows are common in this unit, probably reflecting slope instability induced by high sedimentation rate and over-pressuring. Marine fossils found at the base of the Todagin assemblage indicate an Early Bathonian age (Green 1992) (Table 1).

Up-section, the sandstone content of the Todagin assemblage increases gradually and bioturbation becomes more common, marking a transition into a shallow marine shelf succession (Green 1992) correlated with the Muskaboo Creek assemblage (Evenchick and Thorkelson 2005). In this assemblage, trough-cross stratification and planar beds are common in medium to coarse-grained sandstone. Cyclicity in both lithology and fossil content suggests relatively shallow waters which were sensitive to base level fluctuations producing transgressive and regressive events (Green 1991). In a number of sections measured by Green (1992), the Muskaboo Creek assemblage ranges in thickness from 200 to 1050 m and is constrained to Lower Callovian–Lower Oxfordian by paleontological data (Evenchick and Thorkelson 2005) (Table 4.1). The shelf assemblage is overlain by 250 m of rusty weathered chert-pebble conglomerates of the fan-delta Eaglenest assemblage (Green 1992; Evenchick and Thorkelson 2005). Coarsening-upward cycles and diversely oriented delta fronts within sheet-like units led Ricketts and Evenchick (1991) to interpret the depositional environment as coalescent fan deltas or gravel bars on braided deltas. Rare bivalves and ammonites within the conglomerate

indicate an Oxfordian to Kimmeridgian age (Green 1992).

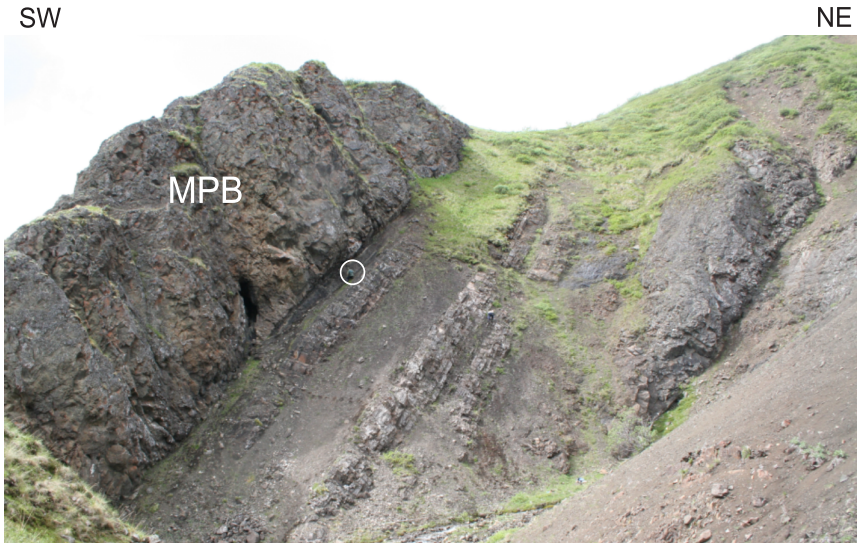

Figure 4.4: Upper Pliensbachian to Lower Toarcian? stratigraphic succession (interval 355-460 m of figure 4.5) showing laminated fine-grained sandstone and siltstone overlain by a thick unit of pillow basalt (MPB). Person in circle for scale.

4.3 Methods and data

4.3.1 Subsidence analysis

Strata of the upper Hazelton Group and Bowser Lake Group exposed near Todagin Mountain provide an excellent record of the subsidence of the northwest portion of the basin. Because much of the stratigraphic column records the transition from pro-delta slope to shallow marine shelf and coastal environments, in which water-depth can be reasonably inferred, the amount of accommodation space can be deduced from the thickness of stratigraphic units.

In subsidence analysis, isolation of the tectonic component can provide insights into the evolution of sedimentary basins (Bond and Kominz 1984; King 1994; Waldron et al. 1996; Prigmore et al. 1997; Lin et al. 2003). This enables the tectonic subsidence history of a sedimentary basin to be compared with theoretical curves associated with specific basin-forming mechanisms. Concave-upward profiles are commonly related to rifting events and subsequent cooling of the lithosphere (Steckler and Watts 1978; Keen 1979; Angevine and Turcotte 1981; Watts 1982). According to McKenzie's (1978) uniform stretching model, instantaneous extension of continental lithosphere by a factor β will produce passive upwelling of the asthenosphere in response to crustal thinning. Subsequent thermal subsidence takes place as the lithosphere cools and thickens, and the isotherms return to their pre-stretching position. On the other hand, most tectonic

foreland models predict an acceleration of subsidence with time, represented by convex-upward profiles, whether in basins developed on ancient cratonic crust (Price 1973; Beaumont 1981; Jordan 1981; Turcotte and Schubert 2002) or on more juvenile arc-dominated crust (King 1994; Trop and Ridgway 2007).

Selected stratigraphic sections of the Bowser Lake Group, previously measured and described by Green (1991, 1992) were revisited. Additional paleontological collections and observations were made on a section of upper Hazelton Group and lower Bowser Lake Group strata west of Todagin Mountain (Gagnon et al. 2007) and were added to the data set. The stratigraphic sections of Green (1991, 1992), as compiled by Evenchick and Thorkelson (2005), were extended downward with the new data to obtain a composite section with known paleontological ages at different horizons (figure 4.5).

4.3.2 Decompaction

In order to estimate the true thickness of a stratigraphic interval before burial, it is necessary to remove the effect induced by compaction. Landmark work on sediment compaction by Athy (1930) proposed an exponential decrease of porosity during burial. Following the same idea, Sclater and Christie (1980) empirically determined parameters for sediment compaction curves using an exponential porosity–depth relationship:

Porosity at depth y: $\Phi_y = \Phi_0 e^{-cy}$

where Φ_0 is the initial porosity of the sediment and c is a coefficient describing the rate at which porosity decreases with depth.

In this study, Φ_0 and c are estimated based on values empirically determined by Sclater and Christie (1980) for the observed relative abundance of sandstone, siltstone and mudstone in stratigraphic interval where there are good age constraints. These values are then entered in the general decompaction equation to obtain the original thickness of the sedimentary column before burial. The method for determining the extent of decompaction is an iterative procedure (Allen and Allen 2005). We used an equivalent formulation in a Microsoft Excel spreadsheet and applied iterative recalculations that allows the values to converge on a unique solution that satisfies the decompaction equation (Waldron and Bradley 2006).

Because the Bowser Lake Group was exhumed after its maximum burial, the observed porosity of the rocks is a function of burial under an unknown thickness of younger strata that have been removed by erosion. In order to evaluate any effect of removed overburden, helium porosity measurements were performed on samples of silty sandstones located at 2285 m on the measured section (figure 4.5). Calculated porosity measurements yielded values of 1.45% +/- 0.50%, which corresponds to a depth of

burial greater than 8 km according to the Sclater and Christie (1980) curve. However, large errors in burial depth estimation can occur when using an exponential function for low porosity values; other authors (Selley 1978; Magara 1980; Korvin 1984; Issler and

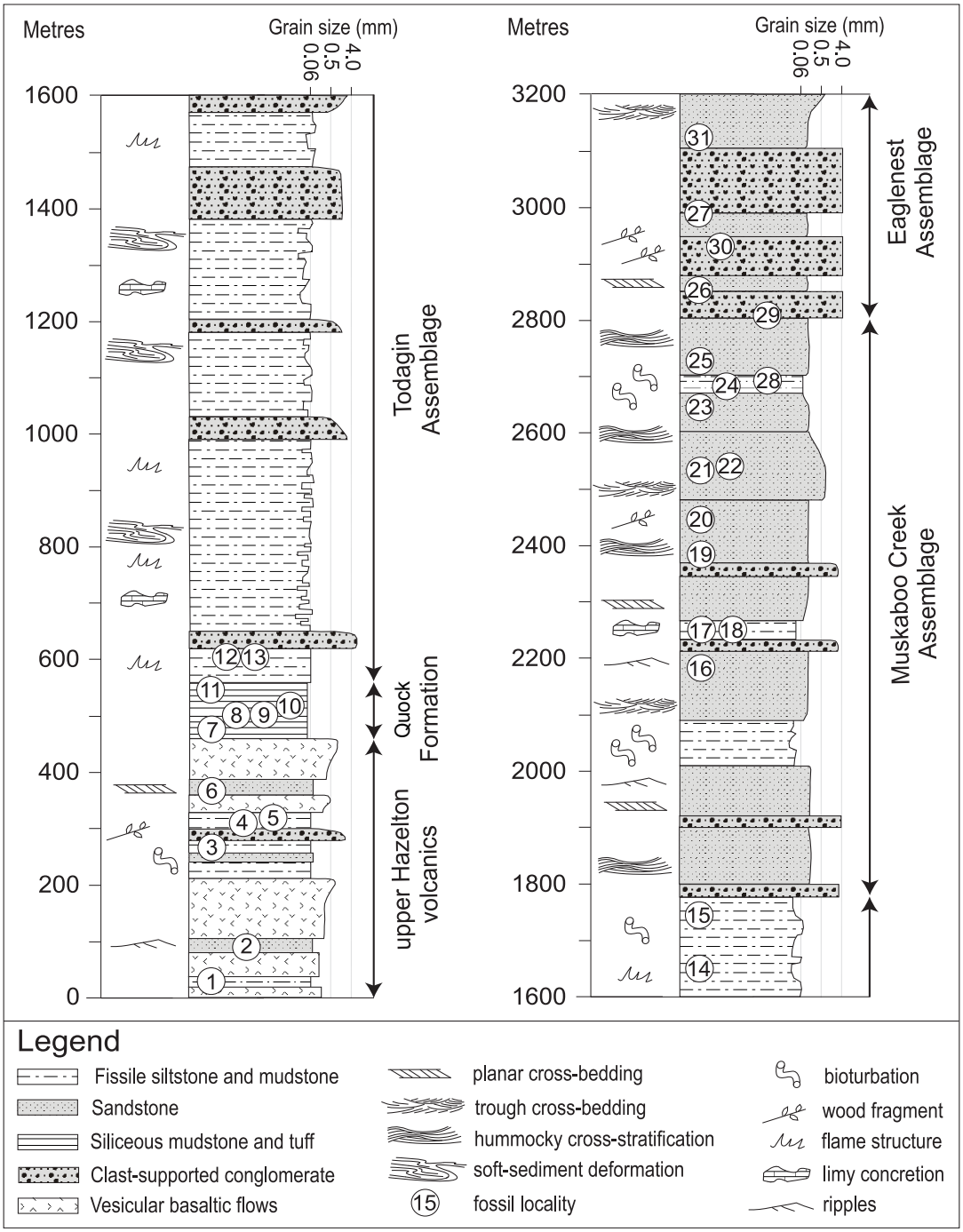

Figure 4.5: Composite stratigraphic section summarizing sedimentary facies distribution and thickness of lithostratigraphic units. Numbers 1 to 31 correspond to fossil localities used to construct the cross-section shown in figure 4.2. Stratigraphic section compiled from figure 48 of Evenchick and Thorkelson (2005).

Fossil number	Position	Identification	Age	m	Northing	Easting	Zone	Reference
C-518459	1	*Acanthopleuroceras whiteavesi*	Early Pliensbachian, Whiteavesi Zone	20	443318	6389137	09V	This study
C-518460	2	*Dubariceras freboldi*	Early Pliensbachian, Freboldi Zone	90	443220	6389026	09V	
C-518464	3	*Dubariceras freboldi* *Metaderoceras*sp. *Oistoceras* sp.	Early Pliensbachian, Freboldi Zone	268	442868	6389061	09V	This study
C-518461	4	*Dubariceras freboldi*	Early Plienbachian, Freboldi Zone	313	443019	6388787	09V	
LB012	5	*Lantus* sp. nassellarians	Early Jurassic	320	443019	6388787		This study
C-518462	6	*Amaltheus*sp.	Late Pliensbachian, Kunae Zone	372	442860	6388789	09V	
LC064B	7	*Canutus* sp. *Helvetocapsa minoensis (Matsuoka)* *Parvicingula spinifera (Takemura)*	Toarcian	~485	508348	6377149	09V	This study
LC052A	8	*Eucyrtidiellum* sp. *Praeparvicingula* sp. *Stichocapsa* sp.	Middle Jurassic	~500	503850	6381063	09V	This study
LD004A	9	*Stichocapsa* sp. *Parvicingula(?)* sp.	Middle Jurassic	~500	507059	6378342	09V	This study
C-103425	10	*Pseudolioceras* sp. *Tmetoceras* sp. *Leioceras*(?) sp. *Planammatoceras(?)* sp.	Aalenian	~525	505820	6379770	09V	Poulton and Tipper (1991)
Joan Lake Quock Member	11	*Stephanoceras* sp. *Teloceras* sp. *Chondroceras* sp. *Sonninia* sp. *Docidoceras* sp.	Lower Bajocian	~565			09V	Thomson et al. (1986)
C-107881	12	no fossil identification in file	Bathonian	600	442050	6385690	09V	Evenchick & Thorkelson (2005)
C-90728	13	no fossil identification in file	Bathonian	600	442050	6385690	09V	Evenchick & Thorkelson (2005)
C-177866	14	*Lilloettia* sp. *Xenocephalites* sp. *Astarte* sp. *Pleuromya* sp.	Late Bathonian	1650	440240	6385100	09V	Evenchick & Thorkelson (2005)
C-177864	15	*Lilloettia* sp. cf. *buckmani* (Crickmay)	Early or Middle Callovian	1750	440435	6384850	09V	Evenchick & Thorkelson (2005)
C-177871	16	*Costacadoceras* sp. *Adobofolceras* sp. *Astarte* sp. *Pleuromya* sp. bivalves	Early Callovian	2185	447070	6383050	09V	Evenchick & Thorkelson (2005)
C-177884	17	*Choffatia*sp. *Myophorella packardi* (Crickmay) *Myophorella* sp. *Pleuromya* sp.	Early Callovian	2212	442650	6380050	09V	Evenchick & Thorkelson (2005)

Table 4.1: Compiled paleontological ages with fossil description and sample localities. Numbers 1-31 correspond to position on cross-section (figure. 4.2) and composite stratigraphic section (figure. 4.5).

Fossil number	Position	Identification	Age	m	Northing	Easting	Zone	Reference
C-175604	18	*Cadoceras* sp. *Ostrea* sp. *Camptonectes* sp. *Partschiceras* sp. *Choffatia*(?) sp. *Pseudocadoceras* sp. rhynchonellid brachiopod belemnites bivalves	E Callovian	2215	443903	6379977	09V	Evenchick & Thorkelson (2005)
C-177877	19	*Myophorella* sp. aff. *Devexa* (Eichwald) *Gresslya(?)* sp. *Pleuromya* sp. *Astarte(?)* sp.	Middle Callovian to Early Oxfordian	2388	444550	6379290	09V	Evenchick & Thorkelson (2005)
C-187059	20	no fossil identification in file	Middle Callovian	2445	443200	6380620	09V	Evenchick & Thorkelson (2005)
C-181052	21	no fossil identification in file	Callovian or Oxfordian	2545	445130	6376900	09V	Evenchick & Thorkelson (2005)
C-187067	22	no fossil identification in file	Late Callovian	2560	444520	6380060	09V	Evenchick & Thorkelson (2005)
C-127488	23	*Adabofoloceras* sp. Myophorella sp. bivalves	Callovian to E Oxfordian	2650	448000	6379580	09V	Evenchick & Thorkelson (2005)
C-177886	24	*Choffatia (?)*sp. *Quenstedtoceras* sp. *Pleuromya* sp.	Late Callovian	2674	442700	6380500	09V	Evenchick & Thorkelson (2005)
C-177879	25	*Choffatia*(?) sp. *Pleuromya* sp. *Grossouvria(?)* sp. belemnites bivalves *Meleagrinella* sp.	Callovian to E Oxfordian	2720	444990	6379060	09V	Evenchick & Thorkelson (2005)
C-175606	26	*Entolium* sp. *Meleaorinella* sp *Oxytoma*(?) sp. *Partschiceras* sp. *Corbula*(?) sp.	Late Callovian to M Oxfordian	2862	445841	6380269	09V	Evenchick & Thorkelson (2005)
C-177880	27	*Adabofoloceras* sp. *Pleuromya* sp.	Callovian to Early Oxfordian	2975	445250	6379050	09V	Evenchick & Thorkelson (2005)
C-187079	28	no fossil identification in file	Callovian	2690	450200	6375340	09V	Evenchick & Thorkelson (2005)
C-187085	29	no fossil identification in file	Early Oxfordian	2808	448750	6374020	09V	Evenchick & Thorkelson (2005)
C-187077	30	no fossil identification in file	Early Oxfordian	2935	448800	6374350	09V	Evenchick & Thorkelson (2005)
C-187083	31	no fossil identification in file	Early Oxfordian	3105	447730	6373590	09V	Evenchick & Thorkelson (2005)

Table 4.1: continued

Beaumont 1988; Palciauskas and Domenico 1989; Issler 1992) have suggested that a linear reduction of porosity with depth as a result of compaction is more appropriate. In the case of a linear porosity–depth relation, sediment compaction is usually completed in the first 4 km of burial so that only a lower limit of removed overburden can be derived from low porosity values (Issler 1992). In addition, the presence of diagenetic calcareous cement filling most of the remaining primary porosity in the Bowser Lake rocks is likely to alter the compaction estimates, whether the algorithm is linear or exponential. In the case of the Todagin section, maximum paleotemperature values inferred from vitrinite reflectance Ro data on Middle Callovian Muskaboo Creek strata near Tsatia Mountain also suggest a more conservative estimate for maximum burial; Stasiuk et al. (2005) obtained Ro of 1.1 to 1.2 % which correspond to an average maximum temperature between 120–160°C. These results are consistent with apatite fission-track thermochronology analysis, which has shown average peak burial temperatures of ≥135°C for equivalent strata (O'Sullivan et al. 2005). Based on these results and available bottom-hole temperature well profiles, Majorowicz and Osadetz (2008) estimated a regional paleogeothermal gradient of 37°C / km which would correspond to a total erosional denudation of approximately 4 000 m. Consequently, this value is used as a lower estimate for overburden thickness, although the choice of a greater value would have little effect on the results of our decompaction calculations because the initial porosity of the sedimentary rocks is almost entirely eliminated at these depths (figure 4.6).

4.3.3 Age Ranges

Table 4.1 summarizes the available paleontological data used in this study. Chronostratigraphic assignments obtained from marine fossils are related to absolute time using the geological time scale of Gradstein et al. (2004), modified to take into account the recently revised Oxfordian–Kimmeridgian boundary (154.1 +/- 2.2 Ma; Selby 2007). Although uncertainties on absolute ages of stage boundaries in the Middle Jurassic are significant, the relative durations of stages are better constrained. The estimated 2-sigma error assigned to stage duration provided in Gradstein et al. (2004) is used to calculate the error for data points.

An additional uncertainty arises from positioning of fossil locations when integrating data from multiple stratigraphic sections. In order to deal with these uncertainties, additional fossil locations from this study were projected onto a cross-section on which time lines and sedimentary facies boundaries were constructed. The resulting cross-section of figure 4.2 incorporates lithostratigraphic profiles and time lines

of Ricketts and Evenchick (1991), and a structural profile with previous fossil localities after Evenchick and Thorkelson (2005). The cross-section shows how facies boundaries become progressively younger to the south, indicating a southward progradation of deltaic systems in the Middle to Late Jurassic (Evenchick and Thorkelson 2005). The thickness of each chronostratigraphic unit was then corrected for post-depositional decompaction to determine sediment accumulation with time (figure 4.6).

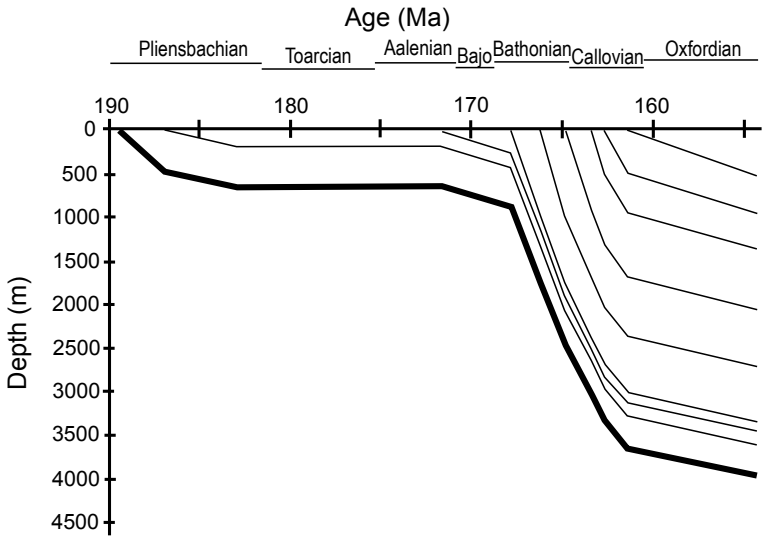

Figure 4.6: Burial history diagram corrected for sediment compaction showing the amount of sedimentation through time. Bold curve represents the position of the basement below sediment surface. Time scale from Gradstein et al. (2004).

4.3.4 Eustasy and water depth

Eustatic change and water depth can have a significant impact on subsidence curves, especially for deep marine conditions. Information on water depth is usually deduced from benthic fossil records, sedimentary facies and geochemical signatures (Allen and Allen 2005). In the absence of consistent benthic fossil information for the Bowser basin, sedimentary structures that reflect physical processes are used to estimate water depth. However, such structures are not necessarily diagnostic of specific water depth. For example, there is incomplete information on the size and the geometry of the basin and therefore the depth of storm wave base is uncertain. If the Bowser basin was open to the Panthalassan Ocean to the west, as proposed by Poulton et al. (1994), it would have had a fetch resulting in waves with great wavelength and amplitude. In this case, sedimentary structures generated by storm waves could have conceivably occurred at depths up to 100 m.

The base of the composite stratigraphic section contains interbedded bimodal subaqueous volcanic flows and marine sediments that disconformably overlie a subaerial unit of welded tuff and oxidized volcaniclastics (figure 4.4). A high proportion of terrestrial debris along with sparse bioturbation and oscillation ripple marks suggest that most of the Pliensbachian–Lower Toarcian succession was dominated by shallow water environments. Establishment of deep water conditions (> 500 m) by the Aalenian is inferred from the characteristics of the Quock Formation (Thomson et al. 1986). This condensed section consists of unburrowed finely laminated radiolarian mudstone and tuff, mainly deposited from suspension in an anoxic environment, and is completely devoid of coarse clastic input.

The prodelta slope facies of the Todagin assemblage is dominated by thinly bedded turbidites with abundant soft-sediment deformation features that attest to a deep-marine slope environment (Ricketts and Evenchick 1991; Evenchick and Thorkelson 2005). Fine parallel-laminated siltstone and mudstone are locally incised by coarse-grained meandering channel complexes. The absence of wave-generated structures suggests that the depth of water was at least 100 m at the time of deposition. Hummocky cross-stratification and planar cross-bedding occur at the base of the Muskaboo Creek assemblage and become more common up section (Green 1992). Increasing grain size along with more diversified bioturbation indicators are probably correlative with an overall shallowing on the marine shelf. Near the top of the Muskaboo Creek assemblage, repetitions of sedimentary facies reflect relatively shallow water conditions which would have been sensitive to eustasy (Green 1991). Since the fluctuations of sea-level during the Late Callovian were probably in the order of a few tens of metres (Haq et al. 1987; Sahagian et al. 1996), it is reasonable to infer that water depth must have been less than 50 m. Rusty-weathered chert-pebble conglomerate, coarsening-upward cycles and abundance of terrestrial plant fragments in the Eaglenest assemblage (Ricketts and Evenchick 1991) attest to a near-shore environment where water depths were probably in the range of 25 m or less. Even though development of local swamps on the braided delta plain led to deposition of coal, rare marine fossils throughout the succession indicate that sediments accumulated near sea-level.

Uncertainties associated with eustatic variations are minor compared to those attributed to paleo-water depth. The eustatic curve from Haq et al. (1987) suggests that sea level remained generally low throughout the early and middle Jurassic, with the exception of a minor rise in the Bajocian. After falling again in the Bathonian, the long term sea-level trend was reversed at the onset of the Callovian and continued to rise until the Kimmeridgian. Another eustatic curve proposed by Sahagian (1996) displays

similar long term trends, with more pronounced high frequency sea-level oscillations for the Middle and Late Jurassic. The quantified eustatic curve of Haq (1987) was used to calibrate the detailed subsidence curves because it provides detailed information for the entire Jurassic. Subsidence analyses for the basin examined are not sensitive to the precise curve used, as stratal thicknesses are much greater than the global range of eustatic variation.

4.4 Subsidence history

By applying decompaction calculations to detailed measured stratigraphic sections in the Todagin Mountain area, we are able to restore each sedimentary layer to its original thickness at the time of deposition to produce a burial history diagram (figure 4.6). Once all stratigraphic layers of the section have been successively decompacted, the restored sediment thickness is added to the approximate water depth at the time of deposition of each unit, to calculate the accommodation space at that specific time. The accommodation space is then adjusted for eustatic variations to determine the subsidence history of the basin. The total subsidence equation is therefore:

$$H = H_0 - \Delta SL + W_d + S$$

where H is the total subsidence, H_0 is the initial elevation of the basin floor, ΔSL is the eustasy, W_d is the water depth and S represents the sediment thickness corrected for compaction (Allen and Allen 2005).

Figure 4.7 shows the effect of corrections for decompacted sediment thickness, water depth and eustasy on the subsidence curves. In decompaction analysis, imprecise assumptions of parameters for the porosity-depth relationship can affect the predicted subsidence curve in the order of 100 m or less (Gallagher 1989). Lacking in-situ porosity measurements at depth for the Bowser basin, uncertainties related to the use of Sclater and Christie's (1980) compaction parameters are included in the errors shown in figure 4.7.

Although sea-level fluctuations are relatively well constrained for the Jurassic period (Haq et al. 1987), the errors associated with water depth estimation remain significant. For the deep-water sedimentary rocks deposited during the Aalenian and Bajocian, the uncertainty could be as much as 3000 m. In addition, the age constraint associated with this interval is relatively poor because of the scarcity of available paleontological data. Thus, many different subsidence curves would be consistent with the data. Possible subsidence histories within the range portrayed by figure 4.8 have specific implications for tectonic history and stratigraphy. To explore these in detail it is necessary to distinguish between the tectonic and isostatic contributions to subsidence.

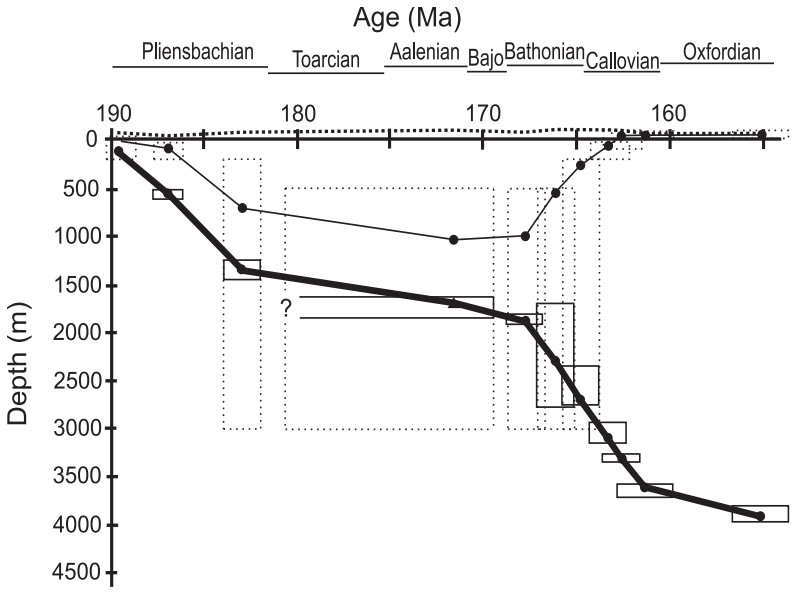

Figure 4.7: Possible subsidence curve corrected for eustasy (bold dotted line; curve from Haq (1987)) and water depth. Estimated sea-floor position is shown by continuous line below the eustatic curve. Position of the basin floor is represented by the bold curve. Uncertainties on paleobathymetry are shown in dotted rectangles (relative to the sea-floor position) whereas solid rectangles (positioned relative to subsidence curve) represent potential inaccuracies in positioning of fossil locations on the cross-section, and potential errors in the duration of chronostratigraphic units. Time scale from Gradstein et al. (2004).

4.5 Implications of subsidence history

4.5.1 Backstripping

Backstripping attempts to remove the effect of sedimentary loading to isolate the component of subsidence driven solely by tectonic processes. The significance of sedimentary loading depends in part on the flexural behaviour of the lithosphere. Deposition of the upper Hazelton Group rocks in Early to Middle Jurassic occurred over a young and hot lithosphere dominated by volcanic arc rocks. Even at the present day, thermal investigations indicate high heat flow (90 mW/m^2) in the Intermontane Belt, which can be attributed to the presence of a thin (60 km) and weak lithosphere (Lewis et al. 2003). These high heat flow values exert a primary control on the elastic effective thickness (Te), estimated at 25 km for the Bowser basin (Flueck et al. 2003). Because the tectonic setting in the Middle Jurassic was characterized by active subduction and terrane accretion, it is likely that the lithosphere was significantly warmer and weaker than it is today, as suggested by Majorowicz and Osadetz (2008). Based on this assumption, the loading effect on subsidence can be calculated using a simple Airy isostatic model in which the lithosphere is assumed to be completely weak such that any applied load

is locally compensated by depression of less dense lower crust into more dense mantle (McKenzie 1978). In reality, the lithosphere always has a flexural strength and it is likely that the sediment load will be compensated by deflection over a large distance rather than locally; this distance is likely to be greater in regions of low geothermal gradient, such as fore-arc basins. However, if the flexural thickness of the lithosphere is relatively small compared to the width of the basin the sediment load is weakly supported and the utilisation of Airy-type isostasy is appropriate (Allen and Allen 2005). For a broad basin with a young volcanic substrate, such as the Hazelton trough–Bowser basin, the assumption of Airy isostasy as a first order approximation is reasonable. For Airy isostasy, the tectonic component of subsidence (Y) involving a basement with overlying column of water filled to constant sea-level is given by:

$$Y = S\,[\,(\rho_m - \rho_s)/(\rho_m - \rho_w)\,] - \Delta SL\,[\,\rho_w/(\rho_{m\_}\rho_w)\,] + [\,W_d - \Delta SL\,]$$

where S is the thickness of the sedimentary column corrected for compaction, ΔSL is the eustatic change, W_d is the paleowater depth, ρ_m, ρ_s and ρ_w are mantle (3300 kg/m^3), mean sediment column (2720 kg/m^3) and water densities (1030 kg/m^3) respectively.

4.5.2 Subsidence history scenarios

After performing backstripping calculations on the stratigraphic sections for multiple water depth scenarios, a wide variety of subsidence profiles were generated. Figure 4.8 shows different subsidence profiles where the position of the basement has been adjusted to represent possible end-member scenarios of water depth variations and other uncertainties, within the ranges shown in figure 4.7. For shallow water, such as in the Pliensbachian and Middle Callovian and younger, the subsidence curve is well constrained and does not vary much from one case to another, whereas during intervals of deeper water (e.g. Aalenian to Bathonian), the constraints on water depth are much poorer. In scenario 1, it is assumed that deep-water sediments were deposited just below the maximum estimated storm wave base (100 m). The resulting subsidence profile (figure 4.8A) shows an exponentially declining curve from the Pliensbachian until the Bajocian, followed by acceleration in subsidence until Early Bathonian time. The tectonic curve follows a similar trend; both the initial subsidence and the acceleration of subsidence ca. 170 Ma would require a tectonic driving mechanism.

In contrast, if abyssal water depth conditions are assumed (figure 4.8B), an acceleration of subsidence in the Bathonian has to be followed by a significant uplift at a rate of about 1600 m / m.y. in order to bring the sea-floor back to shallow water conditions during the interval where constraints are good. Such rapid uplift would be expected to be associated with an unconformity somewhere in the basin, yet mapping

relationships show no interruption of sedimentation. As paleocurrent measurements are consistent throughout the Callovian interval (Green 1992; Evenchick and Thorkelson 2005), it is unlikely that the northern basin geometry was radically altered. Since the stratigraphic section appears conformable, except for shallow discordances in the Pliensbachian interval and possibly below the Quock Formation, scenario 2 does not

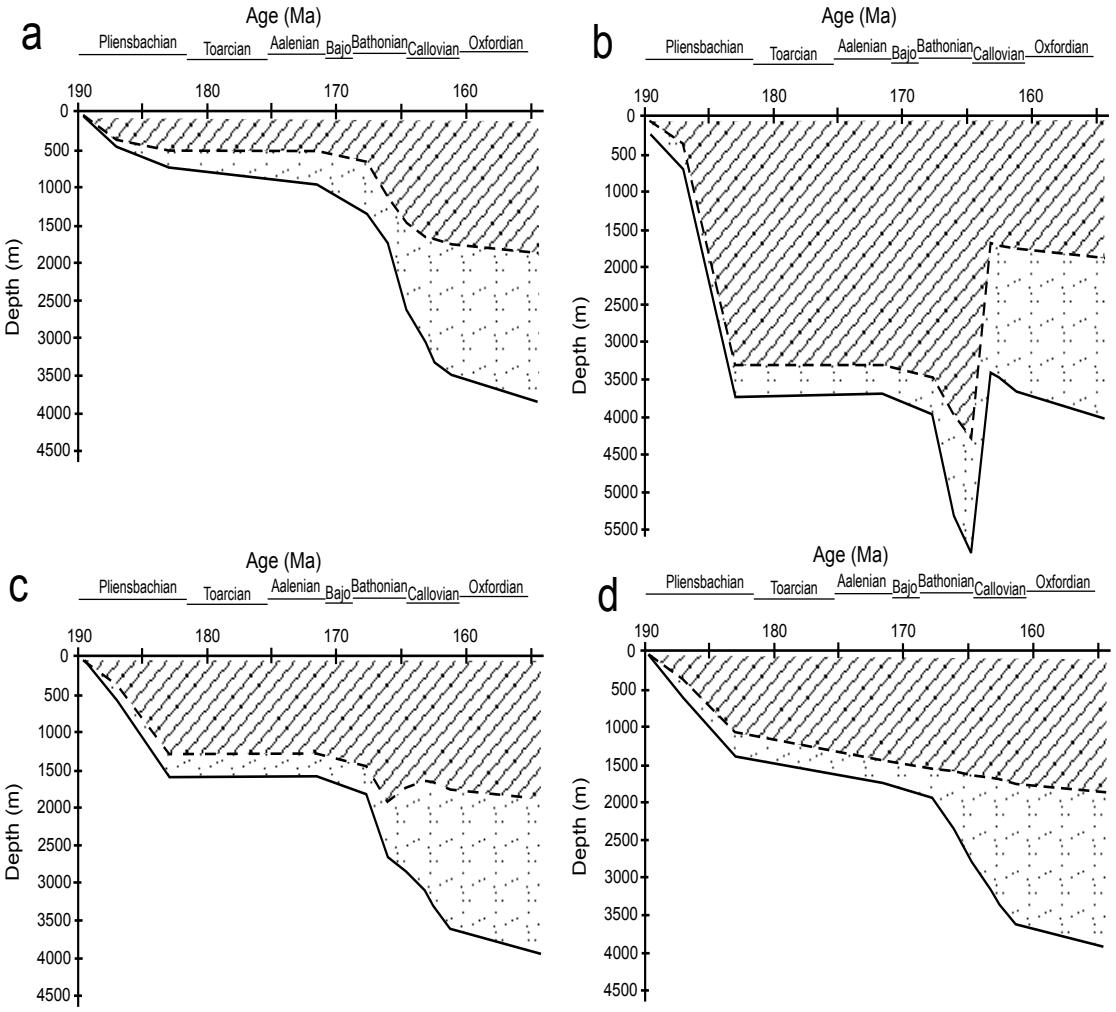

Figure 4.8: Subsidence curves showing the effect of different assumptions about water depth at time of sediment deposition. Basin floor position shown by continuous line; tectonic curve obtained from backstripping calculations represented by dashed line. In each scenario, the dotted area corresponds to the component of subsidence that can be attributed to sediment loading and the cross-hatched area indicates portion of subsidence driven by tectonic forces involving the basement. Graph A is constructed using water depth of 100 m for the deep-water facies; graph B assumes abyssal water depth conditions (3 000 m) for the deep-water facies; graph C represents an intermediate scenario arbitrarily set at 1 000 m water depth; and graph D represents a similar scenario where variable water depths were determined in order to fit a thermally subsiding tectonic model for which the acceleration of subsidence in the Bathonian is entirely related to sediment loading. Time scale from Gradstein et al. (2004).

represent a viable hypothesis.

Figure 4.8C represents an intermediate scenario where water depths in the deep-water interval were arbitrarily set at 1000 m. When the effect of sediment loading is removed, the resulting tectonic subsidence curve shows a much more subdued profile, indicating that the second (Bathonian to Callovian) pulse is largely the result of sediment loading.

Scenario 4 (figure 4.8D) tests the hypothesis that the Bathonian to Callovian pulse was entirely due to sediment loading. By selecting values of the water-depth that are entirely consistent with field observations, it is possible to produce a subsidence curve in which the second pulse of subsidence is driven entirely by sediment loading (figure 4.8D). Based on these results, this more linear interpretation is considered as the most realistic because the tectonic curve can be explained by a simple concave-up profile with rapid initial subsidence in the Pliensbachian, followed by a gently decreasing trend from the Toarcian onward (figure 4.8D). This interpretation was used as the basis for the initial curve shown in figure 4.7.

4.5.3 Stretching factor

In order to further investigate an extensional model for the basin, the backstripped tectonic curve of scenario 4 (figure 4.8D) was plotted against multiple curves of different stretching factor β following the quantitative uniform stretching model of McKenzie (1978). Assuming a pre-rift elevation of 1 000 m and instantaneous rifting at ca. 189 Ma (Early Pliensbachian), a good fit is found between the computed tectonic subsidence curve and a post-rift subsidence curve associated with a stretching factor $\beta = 2.3$ (figure 4.9).

Other, more complex stretching models may be envisaged to explain the subsidence history observed at Todagin Mountain. In order to validate the calculated post-subsidence curve shown in figure 4.9, various modifications to the uniform instantaneous stretching model were tested. First, prolonged rapid subsidence prior to the onset of thermal subsidence in the Toarcian seems to indicate that stretching was not instantaneous, but instead lasted 6 m.y., ending at ca. 183 Ma. In the case of uniform protracted rifting, heat diffuses laterally before the stretching is completed which causes additional subsidence prior to the end of rifting (Jarvis and Mackenzie 1980). However, since the period of extension in the Hazelton trough is thought to have been short, the differences between the predictions of the two models are negligible in relation to other errors in the subsidence curve.

Other authors have explored the effect on subsidence history of variations

in stretching with depth, and of deviations from the pure shear model assumed by Mackenzie (1978). Transtensional environments, such as those associated with oblique rifting, would be expected to show similar subsidence histories to orthogonal rifts, because the MacKenzie (1978) model considers only the thermal and mechanical behaviour of vertical columns of stretched lithosphere. Calculations using two distinct stretching factors were performed to test the depth-dependant stretching model of Royden and Keen (1980). Although the fit with the observed data was slightly poorer than the curves shown in figure 4.9, the differences were again small in comparison with the errors inherent in the data. The data from Todagin Mountain are therefore insufficient to discriminate between these models.

A simple shear scenario with asymmetric extension could also potentially be considered to explain the unusual rapid subsidence in the Pliensbachian. In the Basin and Range area, Wernicke (1985) proposed a simple shear model in which a gently dipping crustal-scale shear zone physically separates a zone of fault-controlled extension from a zone of asthenosphere upwelling. The latter seems unlikely for the Hazelton trough–Bowser basin because no large scale detachment surface has been reported, and no core complexes of unroofed deep metamorphic rocks have been observed.

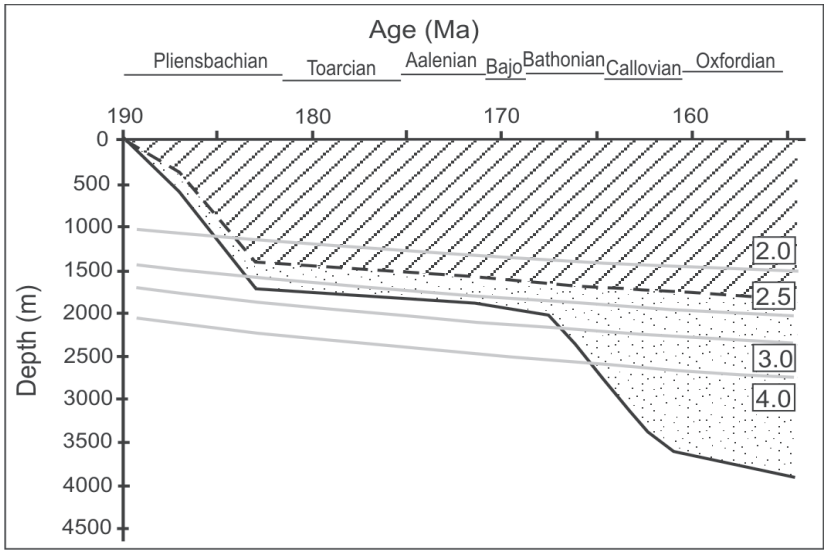

Figure 4.9: Backstripped subsidence curve (dashed line) showing tectonic component of subsidence based on Airy isostasy, and total subsidence history of the basin floor (continuous line). Dotted area corresponds to the component of subsidence attributed to sediment loading and the cross-hatched area indicates portion of subsidence driven by tectonic forces involving the basement. Grey lines show thermal subsidence paths associated with different values of extension factor β for instantaneously extended crust, following McKenzie (1978). Time scale from Gradstein et al. (2004).

4.6 *Discussion: Tectonic implications*

Subsidence profiles obtained from the backstripped stratigraphic section near Todagin Mountain indicate two major episodes of subsidence. Both show generally concave-upward geometry, which typifies basins undergoing thermal, rather than flexural subsidence. However, the second episode can be explained by loading due to the deposition of sediment that filled the accommodation space generated in the first episode. This section considers possible tectonic scenarios that may explain these two episodes.

The Pliensbachian stage corresponds to a rifting episode on Stikinia. Combined syn-depositional faulting and waning bimodal volcanism in a back-arc geodynamic setting were responsible for at least 2.6 km of subsidence in the Joan Lake area (Thorkelson et al. 1995). Deposition of mafic and intermediate lavas of the Mount Brock volcanics constitute the last pulse of volcanism in the vicinity of Todagin Mountain before the onset of marine sedimentation (Read and Psutka 1990). These events coincide approximately with the establishment of decreasing subsidence rates in the Toarcian (figures 4.8A, C and D). Pliensbachian rifting can thus explain the general form of the early part of the subsidence curve. In detail, minor fluctuations of accommodation space probably occurred, as suggested by the unconformities observed within the Pliensbachian section, but were almost certainly not detected in the subsidence curve because of the limitations of the data. Such fluctuations, attributable to short periods of uplift and subsidence, are common in extensional settings. For similar reasons, the curve would not allow discrimination between orthogonal rifting and a transtensional model such as that suggested by Greig et al. (1991).

Terrane amalgamations have been proposed as driving mechanisms for subsidence during deposition of the Bowser Lake Group (Gabrielse 1991; Ricketts et al. 1992). Gabrielse (1991) and Evenchick et al. (2005) interpreted the King Salmon Fault as a low angle thrust fault responsible for the obduction of Cache Creek onto Stikinia in the Middle Jurassic; Evenchick et al. (2007) further considered it to be at the western leading edge of a growing accretionary orogen that included Quesnellia and pericratonic terranes of the North American craton. Although the significance of the structure is debated, all authors consider the King Salmon Fault to have been a syn-collisional contractional structure (see also Mihalynuk et al. 2003; English and Johnston 2005). Timing of the initial movement along the King Salmon Fault is poorly constrained, but cross-cutting relationships demonstrate that significant thrusting occurred after the deposition of the Takwahoni Formation (Gabrielse 1998). Extensive ammonite collections from tuffaceous mudstones and muddy sandstones successions have established the age of the strata assigned to the Takwahoni Formation as ranging from Sinemurian to Lower Toarcian

(Tipper 1978). Strata of the Bowser Lake Group containing Bajocian fossils are also cut by splays of the fault, indicating that movement continued at least until the Bajocian (Gabrielse 1998). Additional evidence on the timing of this collisional event was provided by Mihalynuk et al. (2004), who proposed an Aalenian age based on a 173.7 +/- 0.8 Ma ^{40}Ar / ^{39}Ar cooling age of blueschists that were emplaced along structures that ceased to be active before ca. 172 Ma, the age of the oldest post-kinematic plutons. In southern Cache Creek, Cordey et al. (1987) presented microfossil data that support a Middle Jurassic amalgamation. Additional regional data which constrain the timing of amalgamation between Stikinia and terranes to the east are given by Evenchick et al. (2007).

Several authors have suggested that obduction of the Cache Creek terrane on Stikinia during the Middle Jurassic led to the deposition of a clastic wedge of foredeep sedimentary rocks in the northern Bowser basin (Eisbacher 1981; Gabrielse 1991), and triggered flexural loading of the lithosphere (Eisbacher 1985; Ricketts et al. 1992). If tectonic loading occurred during early Middle Jurassic, the corresponding subsidence profiles should show an acceleration of subsidence for that time interval. However, subsidence curves presented in figure 4.8 all indicate that the area was subsiding slowly at this time, and probably experienced its most rapid subsidence episodes earlier (Pliensbachian) and later than this (Bathonian–Callovian).

Other terrane amalgamations might be considered as possible driving mechanisms for the initial subsidence episode. There are multiple interpretations regarding the origin of metamorphic rocks that occur at the northwest boundary of Stikinia (figure 4.1). Some authors have interpreted these as continental margin units related to the Yukon-Tanana terrane (YTT) (e.g. Gehrels et al. 1990, 1992; Colpron et al. 2006) whereas others infer that they represent meta-igneous basement to Stikinia (e.g. Currie and Parrish 1997). Although it has been claimed that stratigraphic links between Stikinia and YTT were established by Late Triassic time (Werner 1977; Bultman 1979; Mihalynuk and Mountjoy 1990; Jackson et al. 1991), Sm-Nd isotopic data indicate that the two terranes evolved separately for the entire duration of their respective magmatic activity (Samson et al. 1989, 1991). Furthermore, upper Lower to lower Middle Jurassic sediments of the upper Hazelton Group also yield unevolved isotopic values (ε_{Nd} = +4.2) (Samson et al. 1989), which suggests that YTT did not act as a significant sediment source for the evolving Bowser basin.

Therefore, it appears that neither overthrusting of the Cache Creek terrane on Stikina, nor amalgamation with other terranes, can explain the initial subsidence episode observed in the Pliensbachian. In addition, our curve shows deceleration of subsidence

through the Late Pliensbachian, Toarcian, and Aalenian interval, in contrast to the acceleration which would be expected in the case of a simple flexural basin characterized by a migrating tectonic front (Beaumont 1981; Jordan 1981; Turcotte and Schubert 2002). Although the Toarcian to Bajocian part of the curve is only constrained by one data point, good constraints in Late Pliensbachian and Early Bathonian require an overall concave-upward profile (figure 4.7). Thus, we regard a back-arc rift mechanism as a more likely explanation for the initial subsidence episode observed in the Pliensbachian.

The second episode of rapid subsidence identified at Todagin Mountain during Bathonian and Callovian time could provide new insights on the timing of interaction between Stikinia and the Cache Creek terrane. It is generally accepted that the high proportion of radiolarian chert clasts in the conglomerate and sandstone units of the Bowser Lake Group records a provenance link between the Cache Creek terrane and Stikinia (Tipper and Richards 1976; Eisbacher 1985; Gabrielse 1991; Green 1992). We propose that much of the observed subsidence pulse in the Bathonian-Callovian interval is attributable to loading of the crust by chert-rich sediments that were shed from the uplifted Cache Creek terrane. Map relationships in the Cry Lake area (NTS 104I) (Gabrielse 1998) indicate that splays of the King Salmon fault were active until after deposition of basal sandstones of the Bowser Lake Group, and therefore that tectonic activity on this boundary continued at least until Bajocian time (ca. 168 Ma). Depending upon the precise assumptions made about water-depth (figures 4.8C, D), it is possible to envisage that sediment loading may have been combined with tectonic loading by thrust sheets to result in concave-downward subsidence profiles. In addition, a variety of models for interaction between Stikinia and Cache Creek, such as episodic or oblique convergence, would be consistent with the data. Nonetheless, the concave-upward form of the latest part of the subsidence curves, from Callovian to Oxfordian, suggests that this was not a typical foreland basin.

4.7 Conclusion

During its tectonic history, the Hazelton trough–Bowser basin area was characterized by two distinct phases of rapid subsidence. The first one occurred in Pliensbachian and Early Toarcian time. This is attributed to extensional faulting associated with waning volcanism of the Hazelton trough in a back-arc setting, which generated up to half of the accommodation space for the basin. This initial phase was followed by a period of slow sedimentation from pelagic environments in deep water setting. The early Middle Jurassic episode represents an history of thermal subsidence, and is unlikely to have been driven by collisional events along the Stikinia–Cache

Creek boundary as suggested by Ricketts et al. (1992). The basin remained underfilled throughout the Toarcian and Aalenian until the first sediments of the Bowser Lake Group were deposited in the Bowser basin in Bajocian time, shortly after exhumation of the Cache Creek terrane as recorded by ^{40}Ar / ^{39}Ar cooling ages of blueschists by Mihalynuk et al. (2004). A second pulse of rapid subsidence, observed in the Bathonian–Callovian interval, can be explained by sediment loading as denudation of the adjacent Cache Creek terrane provided clastic sediment to the already deep trough between the Stikine and Skeena arches. As the volume of water was replaced by denser sediment, the basin floor subsided, creating new accommodation space. Thus, it is possible to explain the Pliensbachian to Oxfordian subsidence history observed in the Todagin Mountain area with a simple extensional model defined by a rifting episode followed by thermal contraction of the crust, and a later episode of sediment loading associated with erosion of the Cache Creek terrane. Tectonic loading along late splays of the King Salmon fault may also have played a role, but is not required by the subsidence model. The Early Jurassic formation of the Hazelton trough created accommodation space which was amplified by sediment loading in Middle and Late Jurassic time, contributing substantially to the subsidence of the Bowser basin.

4.8 References

Alldrick, D.J. 1993. Geology and metallogeny of the Stewart mining camp, northwestern British Columbia. British Columbia Ministry of Energy, Mines and Petroleum Resources, Report 85, 105 p.

Alldrick, D.J., Nelson, J.L. and Barresi, T. 2005. Geology and mineral occurrences of the Upper Iskut River Area: tracking the Eskay rift trough northern British Columbia (Telegraph Creek NTS 104G/1, 2; Iskut River NTS 104B/9, 10, 15, 16). *In:* Geological Fieldwork 2004, British Columbia Ministry of Energy, Mines and Petroleum Resources, Paper 2005-1, pp. 1-30.

Allen, P.A. and Allen, J.R. 2005. Basin Analysis 2nd Edition. Blackwell Publishing Ltd, 549 p.

Anderson, R.G. 1993. A Mesozoic stratigraphic and plutonic framework for northwestern Stikinia (Iskut River area), northwestern British Columbia, Canada. *In:* Dunne, G., McDougall, K. (Eds.), Mesozoic Paleogeography of the Western United States II. Society of Economic Paleontologists and Mineralogists, Pacific Section, vol. 71, pp. 477-494.

Anderson, R.G. and Thorkelson, D.J. 1990. Mesozoic stratigraphy and setting for some mineral deposits in Iskut River map area, northwestern British Columbia. *In:* Current Research, Part E. Geological Survey of Canada Paper 90-1E, pp. 131-139.

Angevine, C.L. and Turcotte, D.L. 1981. Thermal subsidence and compaction in sedimentary basins; application to Baltimore Canyon Trough. AAPG Bulletin, vol. 65, pp. 219-225.

Athy, L.F. 1930. Density, porosity and compaction of sedimentary rocks. AAPG Bulletin, vol. 14, pp. 1-24.

Bacon, C.R., Kurasawa, H., Delevaux, M.H., Kistler, R.W. and Doe, B.R. 1984. Lead and strontium isotopic evidence for crustal interaction and compositional zonation in the source regions of Pleistocene basaltic and rhyolitic magmas of the Coso volcanic field, California. Contributions to Mineralogy and Petrology, vol. 85, p. 36.

Barrett, T.J. and Sherlock, R.L. 1996. Geology, Lithogeochemistry and Volcanic Setting of the Eskay Creek Au-Ag-Cu-Zn Deposit, Northwestern British Columbia. Exploration Mining Geology, vol. 5, pp. 339-368.

Beaumont, C. 1981. Foreland basins. Geophysical Journal of the Royal Astronomical Society, vol. 65, pp. 291-329.

Bond, G.C. and Kominz, M.A. 1984. Construction of tectonic subsidence curve for the early Paleozoic miogeocline, southern Canadian Rocky Mountain: Implications for subsidence mechanisms, age of breakup, and crustal thinning. Geological Society of America Bulletin, vol. 95, pp. 155-173.

Brown, D.A., Gunning, M.H., Orchard, M.J. and Bamber, W.E. 1991. Stratigraphic evolution of the Paleozoic Stikine assemblage in the Stikine and Iskut rivers area, northwestern British Columbia. Canadian Journal of Earth Sciences, vol. 28, pp. 958-972.

Bultman, T.R. 1979. Geology and Tectonic history of the Whitehorse Trough west of Atlin, British Colombia. Ph.D. thesis, Yale University, New Haven, Connecticut.

Bustin, R.M. and Moffat, I.W. 1989. Semianthracite, anthracite and meta-anthracite in the central Canadian Cordillera: their geology, characteristics and coalification history. International Journal of Coal Geology, vol. 13, pp. 303-326.

Colpron, M., Nelson, J.L. and Murphy, D.C. 2006. A tectonostratigraphic framework for the pericratonic terranes of the northern Canadian Cordillera. *In:* Colpron, M., Nelson, J.L. (Eds.), Paleozoic Evolution and Metallogeny of Pericratonic Terranes at the Ancient Pacific Margin of North America. Geological Association of Canada, Special Paper 45, pp. 1-23.

Cook, F.A., Clowes, R.M., Snyder, D.B., van der Velden, A.J., Hall, K.W., Erdmer, P. and Evenchick, C. A. 2004. Precambrian crust beneath the Mesozoic northern Canadian Cordillera discovered by Lithoprobe seismic reflection profiling. Tectonics, vol. 23, pp. 1-28.

Cordey, F., Mortimer, N., DeWever, P. and Monger, J.W.H. 1987. Significance of Jurassic radiolarians from the Cache Creek Terrane, British Columbia. Geology, vol. 15, pp. 1151-1154.

Currie, L.D. and Parrish, R.R. 1997. Paleozoic and Mesozoic rocks of Stikinia exposed in northwestern British Columbia: Implications for correlations in the northern Cordillera. Geological Society of America Bulletin, vol. 109, pp. 1402-1420.

Dickinson, W.R. 1976. Sedimentary basins developed during evolution of Mesozoic-Cenozoic arc-trench system in western North America. Canadian Journal of Earth Sciences, vol. 13, pp. 1268-1287.

Duffell, S. and Souther, J.G. 1964. Geology of Terrace Map-Area, British Columbia. Geological Survey of Canada, Memoir 329, 117 p.

Eisbacher, G.H. 1974. Deltaic sedimentation in the northeastern Bowser Basin, British Columbia. Geological Survey of Canada, Paper 73-33, 13 p.

Eisbacher, G.H. 1981. Late Mesozoic-Paleogene Bowser Basin molasse and Cordilleran tectonics, western Canada. *In:* Miall, A.D. (Ed.), Sedimentation and Tectonics in Alluvial Basins. Geological Association of Canada, vol. 23, pp. 125-151.

Eisbacher, G.H. 1985. Pericollisional strike-slip faults and synorogenic basins, Canadian Cordillera. *In:* Biddle, K.T., Christie-Blick, N. (Eds.), Strike-slip deformation, basin formation, and sedimentation. Society of Economic Paleontologists and Mineralogists, Special Publication 37, pp. 265-282.

English, J.M. and Johnston, S.T. 2005. Collisional orogenesis in the northern Canadian Cordillera: Implications for Cordilleran crustal structure, ophiolite emplacement, continental growth, and the

terrane hypothesis. Earth and Planetary Science Letters, vol. 232, pp. 333-344.

Evenchick, C.A., Ferri, F., Mustard, P.S., McMechan, M.E., Osadetz, K.G., Stasiuk, L.D., Wilson, N.S.F., Enkin, R.J., Hadlari, T. and McNicoll, V.J. 2003. Recent results and activities of the Integrated Petroleum Resource Potential and Geoscience Studies of the Bowser and Sustut Basins project. *In:* Current Research. Geological Survey of Canada, Report 2003-A13, 11 p.

Evenchick, C.A., Gabrielse, H. and Snyder, D. 2005. Crustal structure and lithology of the northern Canadian Cordillera: alternative interpretations of SNORCLE seismic reflection lines 2A and 2b. Canadian Journal of Earth Sciences, vol. 42, pp. 1149-1161.

Evenchick, C.A. and Green, G.M. 2004. Geology, Kluea Lake (104H/12), British Columbia. Geological Survey of Canada, Map 2028A.

Evenchick, C.A., Hayes, M.C., Buddell, K.A. and Osadetz, K.G. 2002. Vitrinite and bitumen reflectance data and preliminary organic maturity model for the northern two thirds of the Bowser and Sustut basins, north-central British Columbia. Geological Survey of Canada, Open File 4343 *and* British Columbia Ministry of Energy and Mines, Petroleum Geology Open File 2002-1, 26 p.

Evenchick, C.A., McMechan, M.E., McNicoll, V.J. and Carr, S.D. 2007. A synthesis of the Jurassic-Cretaceous tectonic evolution of the central and southeastern Canadian Cordillera: exploring links across the orogen. *In:* Sears, J.W., Harms, T.A., Evenchick, C.A. (Eds.), Whence the mountains? The contribution of Raymond A. Price. Geological Society of America, Special Paper 433, pp. 117-145.

Evenchick, C.A., Mustard, P.S., McMechan, M.E., Ferri, F., Ritcey, D.H. and Smith, G.T. 2006. Compilation of geology of Bowser and Sustut basins draped on shaded relief map, north-central British Columbia. Geological Survey of Canada, Open File 5313 *and* British Columbia Ministry of Energy, Mines and Petroleum Resources, Petroleum Geology Open File 2006-1.

Evenchick, C.A., Poulton, T.P., Tipper, H.W. and Braidek, I. 2001. Fossils and facies of the northern two-thirds of the Bowser Basin, British Columbia. Geological Survey of Canada, Open File 3956.

Evenchick, C.A. and Thorkelson, D.J. 2005. Geology of the Spatsizi River map area, north-central British Columbia. Geological Survey of Canada, Bulletin 577, 276 p.

Ferri, F. and Boddy, M. 2005. Geochemistry of Early to Middle Jurassic Organic-rich Shales, Intermontane Basins, British Columbia. *In:* Summary of Activities 2004. British Columbia Ministry of Energy and Mines, pp.132-151.

Ferri, F., Osadetz, K.G. and Evenchick, C.A. 2004. Petroleum source rock potential of Lower to Middle Jurassic clastics, Intermontane Basins, British Columbia. *In:* Summary of Activities 2004. British Columbia Ministry of Energy and Mines, pp. 87-97.

Flueck, P., Hyndman, R.D. and Lowe, C. 2003. Effective elastic thickness Te of the lithosphere in Western Canada. Journal of Geophysical Research, vol. 108, 13 p.

Friedman, R.M. and Ash, C.H. 1997. U-Pb Age of Intrusions related to Porphyry Cu-Au Mineralization in the Tatogga Lake Area, Northwestern British Columbia. *In:* Geological Fieldwork 1996, British Columbia Ministry of Energy, Mines and Petroleum Resources, Paper 1997-1, pp. 291-297.

Gabrielse, H. 1991. Late Paleozoic and Mesozoic terrane interactions in north-central British Columbia. Canadian Journal of Earth Sciences, vol. 28, pp. 947-957.

Gabrielse, H. 1998. Geology of the Cry Lake and Dease Lake map areas, north-central British Columbia. Geological Survey of Canada, Bulletin 504, 147 p.

Gabrielse, H., Wanless, R.K., Armstrong, R.L. and Erdman, L.R. 1980. Isotopic dating of Early Jurassic

volcanism and plutonism in north-central British Columbia. *In:* Current Research, Part A: Geological Survey of Canada Paper 80-1A, pp. 27-32.

Gagnon, J.-F., Loogman, W., Waldron, J.W.F., Cordey, F. and Evenchick, C.A. 2007. Stratigraphic Record of Initiation of Sedimentation in the Bowser Basin (NTS 104A, H), Northwestern British Columbia. *In:* Geological Fieldwork 2006, British Columbia Ministry of Energy, Mines and Petroleum Resources, Paper 2007-1, pp. 275-283.

Gallagher, K. 1989. An examination of some uncertainties associated with estimates of sedimentation rates and tectonic subsidence. Basin Research, vol. 2, pp. 97-114.

Gehrels, G.E., McClelland, W.C., Samson, S.D. and Patchett, P.J. 1992. Geology of the western flank of the Coast Mountains between Cape Fanshaw and Taku Inlet, southeastern Alaska. Tectonics, vol. 11, pp. 567-585.

Gehrels, G.E., McClelland, W.C., Samson, S.D., Patchett, P.J. and Jackson, J.L. 1990. Ancient continental margin assemblage in the northern Coast Mountains, southeast Alaska and northwest Canada. Geology, vol. 18, pp. 208-211.

Geological Survey of Canada. 1957. Stikine River area, Cassiar District, British Columbia. Geological Survey of Canada, Map 9-1957.

Gradstein, F.M., Ogg, J.G., Smith, A.G., Agterberg, F.P., Bleeker, W., Cooper, R.A., Davydov, V., Gibbard, P., Hinnov, L.A., House, M.R., Lourens, L., Luterbacher, H.P., McArthur, J., Melchin, M.J., Robb, L.J., Shergold, J., Villeneuve, M., Wardlaw, B.R., Ali, J., Brinkhuis, H., Hilgen, F. J., Hooker, J., Howarth, R.J., Knoll, A.H., Laskar, J., Monechi, S., Plumb, K.A., Powell, J., Raffi, I., Röhl, U., Sadler, P., Sanfilippo, A., Schmitz, B., Shackleton, N.J., Shields, G.A., Strauss, H., Van Dam, J., van Kolfschoten, T., Veizer, J., Wilson, D. 2004. A Geological Time Scale 2004. Cambridge University Press, 610 p.

Green, G.M. 1991. Detailed sedimentology of the Bowser Lake Group, northern Bowser Basin, British Columbia. *In:* Current Research, Part A. Geological Survey of Canada Paper 91-1A, pp. 187-195.

Green, G.M. 1992. Detailed sedimentology of the Bowser Lake Group, northern Bowser Basin, north-central British Columbia, M.Sc. thesis, Department of Earth Sciences, Carleton Universiy, Ottawa, Ont.

Greig, C.J. and Gehrels, G.E. 1995. U-Pb zircon geochronology of Lower Jurassic and Paleozoic Stikinian strata and Tertiary intrusions, northwestern British Columbia. Canadian Journal of Earth Sciences, vol. 32, pp. 1155-1171.

Greig, C.J., Gehrels, G.E., Anderson, R.G. and Evenchick, C.A. 1991. Possible transtensional origin of the Bowser Basin, British Columbia. *In:* Geological Society of America, Abstract with Programs, vol. 23, p. 30.

Gunning, M.H., Hodder, R.W. and Nelson, J.L. 2006. Contrasting volcanic styles and their tectonic implications for the Paleozoic Stikine assemblage, western Stikine Terrane, northwestern British Columbia. *In:* Colpron, M., Nelson, J.L. (Eds.), Paleozoic Evolution and Metallogeny of Pericratonic Terranes at the Ancient Pacific Margin of North America. Geological Association of Canada, Special Paper 45, pp. 201-227.

Haq, B.U., Hardenbol, J. and Vail, P.R. 1987. Chronology of Fluctuating Sea Levels Since the Triassic. Science, vol. 235, pp. 1156-1167.

Issler, D.R. and Beaumont, C. 1988. A finite element model of subsidence and thermal evolution of

extensional basins: application to the Labrador continental margin. *In:* Naeser, N.D., McCulloh, T.H. (Eds.), Thermal History of Sedimentary Basins. Springer-Verlag, pp. 239-267.

Issler, D.R. 1992. A New Approach to Shale Compaction and Stratigraphic Restoration, Beaufort-Mackenzie Basin and Mackenzie Corridor, Northern Canada. American Association of Petroleum Geologists Bulletin, vol. 76, pp. 1170-1189.

Jackson, J.L., Gehrels, G.E., Patchett, P.J. and Mihalynuk, M.G. 1991. Stratigraphic and isotopic link between the northern Stikine Terrane and an ancient continental margin assemblage, Canadian Cordillera. Geology, vol. 19, pp. 1177-1180.

Jarvis, G.T. and McKenzie, D.P. 1980. The development of sedimentary basins with finite extension rates. Earth and Planetary Science Letters, vol. 48, pp. 42-52.

Jordan, T.E. 1981. Thrust loads and foreland basins evolution, Cretaceous, western United States. American Association of Petroleum Geologists Bulletin, vol. 65, pp. 2506-2520.

Keen, C.E. 1979. Thermal history and subsidence of rifted continental margins - evidence from wells on the Nova Scotian and Labrador Shelves. Canadian Journal of Earth Sciences, vol. 16, pp. 505-522.

King, L.M. 1994. Subsidence analysis of Eastern Avalonia sequences: implications for Iapetus closure. Journal of the Geological Society of London, vol. 151, pp. 647-657.

Korvin, G. 1984. Shale compaction and statistical physics. Geophysical Journal of the Royal Astronomical Society, vol. 78, pp. 35-50.

Lewis, T.J., Hyndman, R.D. and Flueck, P. 2003. Heat flow, heat generation, and crustal temperatures in the northern Canadian Cordillera: Thermal control of tectonics. Journal of Geophysical Research, vol. 108, 18 p.

Lin, A.T., Watts, A.B. and Hesselbo, S.P. 2003. Cenozoic stratigraphy and subsidence history of the South China Sea Margin in the Taiwan region. Basin Research, vol. 15, pp. 453-478.

Magara, K. 1980. Comparison of porosity-depth relationships of shale and sandstone. Journal of Petroleum Geology, vol. 3, pp. 175-185.

Majorowicz, J. and Osadetz, K.G. 2008. Cordilleran Intermontane thermotectonic history and implications for neotectonic structure and petroleum systems, British Columbia, Canada. International Journal of Earth Sciences, vol. 97, pp. 269-287.

Martin, R.F. and Piwinski, A.J. 1972. Magmatism and tectonic settings. Journal of Geophysical Research, vol. 77, pp. 4966-4975.

McDonald, A.J., Lewis, P.D., Thomson, J.F.H., Nadaraju, G., Bartsch, R.D., Bridge, D.J., Rhys, D.A., Roth, T., Kaip, A., Godwin, C.I. and Sinclair, A.J. 1996. Metallogeny of an Early to Middle Jurassic Arc, Iskut River Area, Northwestern British Columbia. Economic Geology, vol. 91, pp. 1098-1114.

McKenzie, D. 1978. Some remarks on the development of sedimentary basins. Earth and Planetary Science Letters, vol. 40, pp. 25-32.

Mihalynuk, M.G., Erdmer, P., Ghent, E.D., Cordey, F., Archibald, D.A., Friedman, R.M., Johannson, G.G. 2004. Coherent French Range blueschist: Subduction to exhumation in <2.5 m.y.? Geological Society of America Bulletin, vol. 116, pp. 910-922.

Mihalynuk, M.G., Johnston, J.T., English, J.M., Cordey, F., Villeneuve, M.E., Rui, L. and Orchard, M.J. 2003. Atlin TGI part II: Regional Geology and Mineralization of the Nakina Area (NTS 104N/2W and 3). *In:* Geological Fieldwork 2002. British Columbia Ministry of Energy and Mines, Paper 2003-1, pp. 9-37.

Mihalynuk, M.G. and Mountjoy, K.J. 1990. Geology of the Tagish Lake area (104M/8, 9E). *In:* Geological Fieldwork, British Columbia Ministry of Energy, Mines and Petroleum Resources, Paper 1990-1, pp. 181-196.

O'Sullivan, P.B., Donelick, R.A., Osadetz, K.G., Evenchick, C.A., Ferri, F., Wilson, N.S.F. and Hayes, M. 2005. Apatite Fission-Track Data from seventy-one Bowser and Sustus Basin rock samples. Geological Survey of Canada, Open File 4840, 500 p.

Osadetz, K.G., Evenchick, C.A., Ferri, F., Stasiuk, L.D. and Wilson, N.S.F. 2003. Indications for effective Petroleum Systems in Bowser and Sustut Basins, North-Central British Columbia. *In:* Geological Fieldwork 2002. British Columbia Ministry of Mines, Energy and Petroleum Resources, Paper 2003-1, pp. 257-264.

Osadetz, K.G., Jiang, C., Evenchick, C.A., Ferri, F., Stasiuk, L.D., Wilson, N.S.F. and Hayes, M. 2007. Compositions and significance of crude oil stains in Bowser and Sustut basins (Intermontane Belt) British Columbia. Bulletin of Canadian Petroleum Geology, vol. 55, pp. 285-305.

Palciauskas, V.V. and Domineco, P.A. 1989. Fluid pressures in deforming porous rocks. Water Resources Research, vol. 25, pp. 203-213.

Palfy, J., Mortensen, J.K., Smith, P.L., Friedman, R.M, McNicoll, V.J. and Villeneuve, M. 2000. New U-Pb zircon ages integrated with ammonite biochronology from the Jurassic of the Canadian Cordillera. Canadian Journal of Earth Sciences, vol. 37, pp. 549-567.

Poulton, T.P., Hall, R. and Callomon, J.H. 1994. Ammonite and bivalve assemblages in Bathonian through Oxfordian strata of northern Bowser Basin, northwestern British Columbia, Canada. GEOBIOS, vol. 17, pp. 415-421.

Poulton, T.P. and Tipper, H.W. 1991. Aalenian ammonites and strata of western Canada, Geological Survey of Canada, Bulletin 411, 71 p.

Price, R.A. 1973. Large-scale gravitational flow of supracrustal rocks, southern Canadian Rockies. *In:* de Jong, K., Scholten, R. (Eds.), Gravity and Tectonics. Wiley, pp. 491-502.

Prigmore, J.K., Butler, A.J. and Woodcock, N.H. 1997. Rifting during separation of Eastern Avalonia from Gondwana: Evidence from subsidence analysis. Geology, vol. 25, pp. 203-206.

Read, P.B. and Psutka, J.F. 1990. Geology of Ealue Lake east-half (104 H/13) and Cullivan Creek (104 H/14) map areas, British Columbia. Geological Survey of Canada, Open File 2241.

Ricketts, B.D. and Evenchick, C.A. 1991. Analysis of the Middle to Upper Jurassic Bowser Basin, northern British Columbia. *In:* Current Research, Part A. Geological Survey of Canada, Paper 91-1A, pp. 65-73.

Ricketts, B.D., Evenchick, C.A., Anderson, R.G. and Murphy, D.C. 1992. Bowser Basin, northern British Columbia: constraints on the timing of initial subsidence and Stikinia-North America terrane interactions. Geology, vol. 20, pp. 1119-1122.

Roth, T. 2002. Physical and chemical constraints on mineralization in the Eskay Creek Deposit, northwestern British Columbia; evidence from petrography, mineral chemistry, and sulfur isotopes. Ph.D. thesis, Earth and Ocean Sciences Department, University of British Columbia, Vancouver, B.C.

Royden, L. and Keen, C.E. 1980. Rifting Process and Thermal Evolution of the Continental Margin of Eastern Canada Determined from Subsidence Curves. Earth and Planetary Science Letters, vol. 51, pp. 343-361.

Ryan, B. and Dawson, M. 1993. Coal and coalbed methane resource potential of the Bowser Basin northern

British Columbia. British Columbia Ministry of Energy, Mines and Petroleum Resources, Open File 1993-31, 33 p.

Sahagian, D., Pinous, O., Olferiev, A. and Zakharov, V. 1996. Eustatic Curve for the Middle Jurassic-Cretaceous Based on Russian Platform and Siberian Stratigraphy: Zonal Resolution. American Association of Petroleum Geologists Bulletin, vol. 80, pp. 1433-1458.

Samson, S.D., McClelland, W.C., Patchett, P.J., Gehrels, G.E. and Anderson, R.G. 1989. Evidence from neodymium isotopes for mantle contributions to Phanerozoic crustal genesis in the Canadian Cordillera. Nature, vol. 337, pp. 705-709.

Samson, S.D., Patchett, P.J., McClelland, W.C. and Gehrels, G.E. 1991. Nd isotopic characterization of metamorphic rocks in the Coast Mountains, Alaska and canadian Cordillera: ancient crust bounded by juvenile terranes. Tectonics, vol. 10, pp. 770-780.

Sclater, J.G. and Christie, P.A.F. 1980. Continental stretching: an explanation of the post-mid-Cretaceous subsidence of the central North Sea basin. Journal of Geophysical Research, vol. 85, pp. 3711-3739.

Selby, D. 2007. Direct Rhenium-Osmium age of the Oxfordian-Kimmeridgian boundary, Staffin Bay, Isle of Skye, U.K., and the Late Jurassic time scale. Norwegian Journal of of Geology, vol. 87, pp. 291-299.

Selley, R.C. 1978. Porosity gradients in the North Sea oil-bearing sandstones. Journal of Geological Society of London, vol. 135, pp. 119-132.

Snyder, D.B., Clowes, R.M., Cook, F.A., Erdmer, P., Evenchick, C.A., Van der Velden, A.J. and Hall, K.W. 2002. Proterozoic prism arrests suspect terranes; insights into the ancient Cordilleran margin from seismic reflection data. GSA Today, vol. 12, p. 4-10.

Stasiuk, L.D., Evenchick, C.A., Osadetz, K.G., Ferri, F., Ritcey, D., Mustard, P.S. and McMechan, M.E. 2005. Regional thermal maturation and petroleum stage assessment using vitrinite reflectance, Bowser and Sustut basins, north-central British Columbia. Geological Survey of Canada, Open File 4945, 13 p.

Steckler, M.S. and Watts, A.B. 1978. Subsidence of the Atlantic-type continental margin off New York. Earth and Planetary Science Letters, vol. 41, pp. 1-13.

Strong, D.F. 1979. The mount Peyton Batholith, central Newfoundland: A bimodal calc-alkaline suite. Journal of Petrology, vol. 20, pp. 119-138.

Thomson, R.C., Smith, P.L. and Tipper, H.W. 1986. Lower to Middle Jurassic (Pliensbachian to Bajocian) stratigraphy of the northern Spatsizi area, north-central British Columbia. Canadian Journal of Earth Sciences, vol. 23, pp. 1963-1973.

Thorkelson, D.J., Mortensen, J.K., Marsden, H. and Taylor, D.C. 1995. Age and tectonic setting of Early Jurassic episodic volcanism along the northeastern margin of the Hazelton Trough, northern British Columbia. *In:* Miller, D.M., Busby, C.J. (Eds.), Jurassic magmatism and tectonics of ther North American Cordillera. Geological Society of America, Special Paper 299, pp. 83-94.

Tipper, H.W. 1978. Jurassic biostratigraphy, Cry Lake map-area, British Columbia. *In:* Current Research, Part A. Geological Survey of Canada, Paper 78-1A, pp. 25-27.

Tipper, H.W. and Richards, T.A. 1976. Jurassic stratigraphy and history of north-central British Columbia. Geological Survey of Canada, Bulletin 270, 73 p.

Trop, J.M. and Ridgway, K.D. 2007. Mesozoic and Cenozoic tectonic growth of southern Alaska: A sedimentary basin perspective. *In:* Ridgway, K.D., Trop, J.M., Glen, J.M.G., O'Neil, J.M. (Eds.),

Tectonic Growth of a Continental Margin: Crustal Evolution of Alaska. K.D. Geological Society of America, Special Paper 431, pp. 55-94.

Turcotte, D.L. and Schubert, G. 2002. Geodynamics, 2nd Edition, Cambridge University Press.

Waldron, J.W.F. and Bradley, J.C. 2006. Data integration and subsurface structure modelling of coal seams from a strike-slip basin, Stellarton, Nova Scotia. *In:* Harris, J.R. (Ed.), GIS for the earth sciences. Geological Association of Canada, Special Paper 44, pp. 557-590.

Waldron, J.W.F., Murphy, J.B., Melchin, M.J. and Davis, G. 1996. Silurian Tectonics of Western Avalonia: Strain-Corrected Subsidence History of the Arisaig Group, Nova Scotia. Geology, vol. 104, pp. 677-694.

Watts, A.B. 1982. Tectonic subsidence, flexure and global changes in sea level. Nature, vol. 297, pp. 469-474.

Werner, L.J. 1977. Metamorphic terrane, northern Coast Mountains west of Atlin Lake, British Colombia. *In:* Current Research, Part A: Geological Survey of Canada, Paper 77-1A, pp. 267-269.

Wernicke, B.P. 1985. Uniform-sense normal simple shear of the continental lithosphere. Canadian Journal of Earth Sciences, vol. 22, pp. 108-125.

Wheeler, J.O. and McFeely, P. 1991. Tectonic assemblage map of the Canadian Cordillera and adjacent parts of the United States of America. Geological Survey of Canada, Map 1712A.

Chapter 5: Sedimentation styles and depositional processes in a Middle to Late Jurassic slope environment, Bowser Basin, Northwestern British Columbia, Canada[4]

5.1. Introduction

Deep-water channel complexes located in modern slope environments have received increased attention as exploration has demonstrated that coarse-grained submarine channel systems constitute important hydrocarbon reservoirs (e.g. Stelting 1985; Mayall and Stewart 2000; Kolla et al. 2001; Abreu et al. 2003; Deptuck et al. 2003). However, the spatial distribution and internal architecture of these deep-water bodies are difficult to observe in situ as bed-scale heterogeneities are beyond the resolution of most 3D seismic-reflection techniques (Mutti and Normark 1991; Slatt 2000). One approach to mitigate this problem has been to study outcrop analogues that allow characterization of individual beds and their depositional processes (e.g. Clark and Pickering 1996; Hickson and Lowe 2002; Beaubouef 2004; Schwarz and Arnott 2007; Crane and Lowe 2008; Armitage et al. 2009; Fildani et al. 2009).

The Middle to Upper Jurassic Todagin assemblage of the Bowser Lake Group exposed in the tectonically active Bowser basin of northwestern British Columbia, Canada, provides an excellent record of slope processes that characterize deep-marine siliciclastic depositional environments (Green 1992; Ricketts and Evenchick 1999; Evenchick and Thorkelson 2005). The Todagin assemblage consists mostly of a fine-grained succession with isolated channelized conglomerate units. These lenticular conglomerate bodies occur at various stratigraphic levels throughout the succession and range from a few metres to tens of metres thick.

This study documents and compares two exceptional exposures of channelized deep-water systems of the Todagin assemblage in northwestern British Columbia. Compilation of detailed measured sections and observation of field relationships between channel-fill and inter-channel lithofacies provide new insights on the mechanisms of sediment transport and deposition that affected channelized systems of the Todagin assemblage. Furthermore, this work allows a better understanding of the stratigraphic evolution of deep-water architectures associated with variations of boundary conditions (e.g. provenance, sediment supply, basin configuration) in active tectonic regimes such as the Bowser Basin.

[4] *A version of this chapter has been accepted for publication on June 3rd 2010. Gagnon, J.-F. and Waldron, J.W.F. Journal of Marine Petroleum Geology.*

5.2 *Geological setting*

The Todagin assemblage is a thick (~3 000 m) unit of deep-water siliciclastic sedimentary rocks deposited in the Bowser basin of western Canada during the Middle to Late Jurassic (figure 5.1). It constitutes one of the many diachronous lithofacies divisions recognized within the Bowser Lake Group by Evenchick and Thorkelson (2005) (figure 5.2). Middle Jurassic to Lower Cretaceous sedimentary rocks of the Bowser Lake Group were deposited over the arc-related rocks of the Lower Jurassic Hazelton Group, which constitutes the last widespread volcanic phase of the allochthonous Stikine terrane (Anderson 1993). Volcanic and associated sedimentary rocks of the Hazelton Group accumulated in an elongated, southeast-northwest oriented intra-arc basin referred to as the Hazelton trough (Tipper and Richards 1976; Marsden and Thorkelson 1992). Evidence of back-arc rifting on the northwestern edge of the basin was also recorded in the early Middle Jurassic, and is represented by the Eskay Creek volcanogenic massive sulphide deposit (Barrett and Sherlock 1996; McDonald et al. 1996; Roth et al. 1999; Sherlock et al. 1999; Alldrick et al. 2005). Subsidence analyses have shown that tectonic

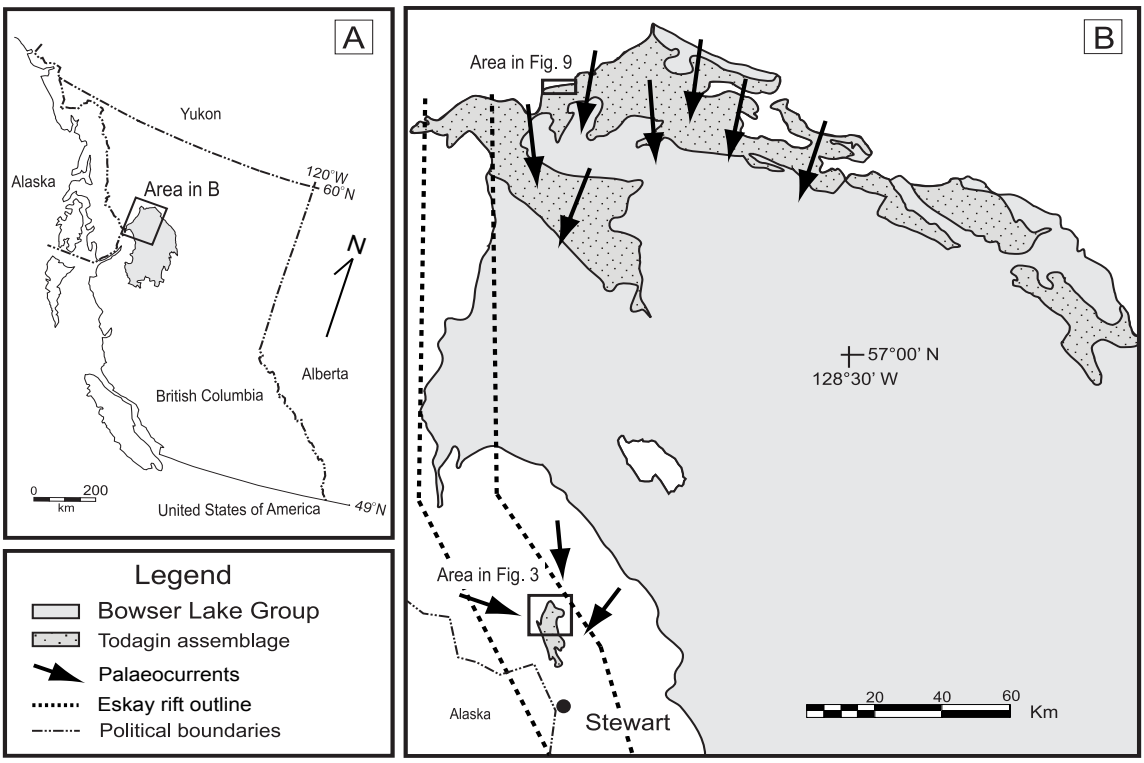

Figure 5.1: A) Regional location map of the Bowser basin in northwest British Columbia, Canada. Solid black square delineates the area shown in B. B) Geographic distribution of the Middle to Upper Jurassic Todagin assemblage within the Bowser Lake Group. Paleocurrent data for the Todagin assemblage after Evenchick and Thorkelson (2005). Solid black squares delineate the extent of the two study areas. Modified from Evenchick et al. (2009).

extension in the northern portion of the Hazelton trough during Pliensbachian time generated a significant amount of accommodation prior to initiation of coarse clastic sedimentation in the Bowser basin in the Bajocian (Thorkelson et al. 1995; Gagnon et al. 2009; Chapter 4).

Rapid progradation of fan deltas in Middle to early Late Jurassic time was responsible for the transfer of a huge volume of gravel, sand and mud to the deep portions of the Bowser basin (Ricketts and Evenchick 1991, 2007). According to Evenchick and Thorkelson (2005), the distribution of fossils in deep-marine to marginal marine lithofacies illustrates that the shelf remained relatively narrow throughout that period. This particular shelf width configuration was probably a major control for deep-water sedimentation in the early history of the Bowser Basin. Description of modern analogues situated along the tectonically active California margin by Covault et al. (2007) indicates that the narrow shelf between the canyon head and the littoral zone is the primary control on canyon-channel system activity and delivery of sediment to the deepwater.

In parts of the Bowser basin, the transition between the Todagin assemblage and the underlying Ritchie-Alger assemblage represents the progradation of the slope over more distal submarine fan facies; however, elsewhere the Todagin assemblage appears

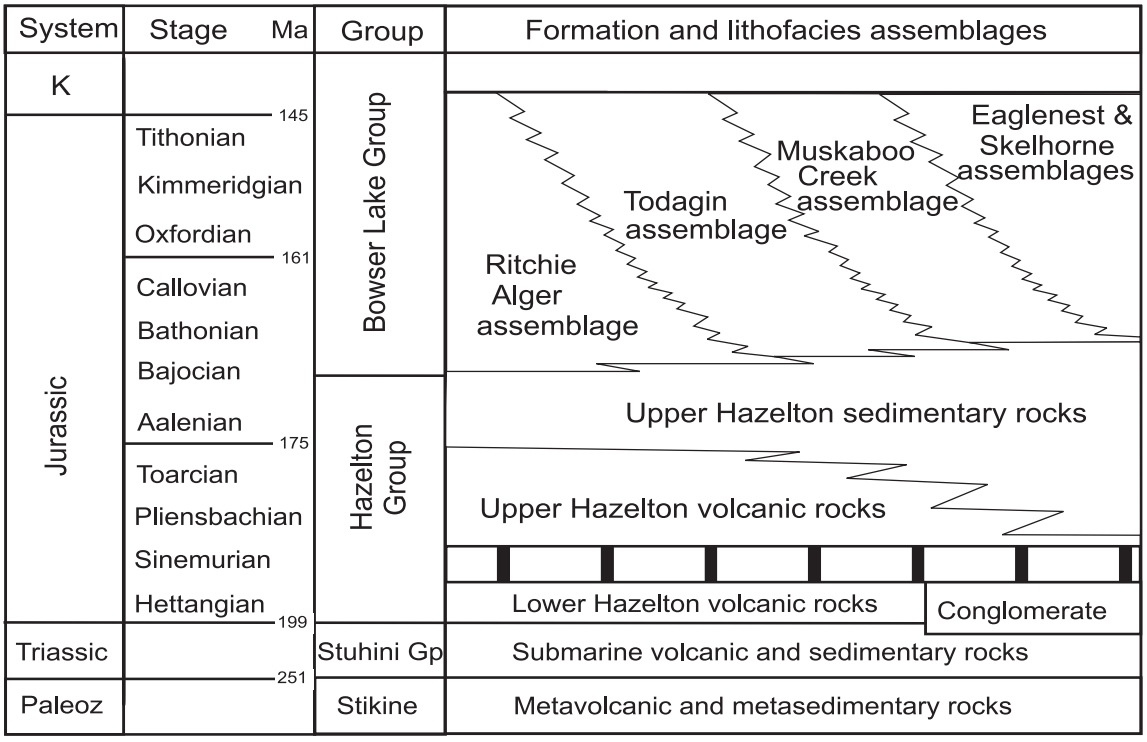

Figure 5.2: Generalized stratigraphic framework of the northern Bowser basin showing the main lithostratigraphic units and relationships of the Todagin assemblage. Modified after Evenchick and Thorkelson (2005).

to directly overlie fine-grained hemipelagic and volcanic rocks of the upper Hazelton Group (Evenchick et al. 2009). The Todagin assemblage, in turn, is gradually overlain by shelf and deltaic facies of the Muskaboo Creek, Skelhorne and Eaglenest assemblages respectively (figure 5.2). This shallowing-upward succession records the filling of the active Bowser basin as lithofacies assemblages likely prograded towards the south and southwest over a rifted basin floor during Bathonian to Early Oxfordian time (Evenchick and Thorkelson 2005). Provenance studies combined with extensive paleocurrent data suggest that sediment filling the Bowser basin was derived mostly from erosion of radiolarian chert associated with the overthrusted oceanic Cache Creek terrane to the north (Eisbacher 1985; Gabrielse 1991; Evenchick and Thorkelson 2005). However, our petrological analyses and preliminary detrital zircon work indicate that Bowser Lake Group sediments in the vicinity of one of our case studies, at Mount Dilworth (figure 5.1), contain a high proportion of volcanogenic and feldspathic grains derived from local sources, in addition to less abundant Cache Creek material.

The Bowser basin constitutes a linking assemblage that records the amalgamation of the Stikine and Cache Creek terranes in the Middle Jurassic. The two terranes are separated by the King Salmon Fault, a syn-collisional contractional structure interpreted by Gabrielse (1991) and Evenchick et al. (2005) as a shallow southwest-vergent reverse fault. Renewed regional contraction in Early Cretaceous to earliest Tertiary deformed the basin fill, producing the Skeena Fold Belt, which accommodated at least 150 km of shortening along blind thrusts and related folds (Evenchick 1991).

5.3 Methods

The present study employs the deep-water architectural-element method of Ghosh and Lowe (1993) and Hickson and Lowe (2002). This method establishes a hierarchy in which individual depositional units and their associated physical structures represent the finest scale of observation. Lithofacies constitute the next order of observation, in which sedimentation units with similar characteristics are grouped together. Because of their convenient application to large 2D outcrops, lithofacies are the basic mappable components presented in this dataset (Table 5.1). A total of nine lithofacies were identified over the two mapping areas.

In the first case study (Mount Dilworth), recurring packages of genetically related lithofacies were grouped into three lithofacies assemblages (LA), following the method outlined by Collinson (1969). Detailed geological mapping was carried out by physically walking out beds and recording lithological observations on aerial photographs at 1:5 000 scale. In the second case study (Todagin Mountain), six stratigraphic sections

Lithofacies	Grain size	Bedding character and sedimentary structures	Thickness	Depositional process
Lm: Thinly bedded mudstone and siltstone	Mud and silt with 10 to 30% very-fine to fine-grained sand	Normally graded Bouma T_{acd} and T_{bcde} divisions Strata laterally extensive for 100s of metres Flames stuctures and convolute laminations Toolmarks: flute and groove casts Orange-weathering claystone beds Locally extensive bioturbation: *Phycosiphon, Helminthopsis* and *Chondrites*	5 m to 200 m	Low-density turbidity currents
Lmf: laminated silty mudstone	Mud with 10 to 25% silt	Normally graded Bouma T_{de} divisions Horizontal laminations	30 cm to 5 m	Diluted muddy turbidity currents
Lfst: Thin to thick sand-stone and siltstone	Fine to medium-grained sand with minor mud and silt interbeds	Massive to normally graded thin to medium beds Bouma T_{abcd} and T_{abc} divisions Abundant ripple cross-laminations Laterally extensive for 10s of metres Toolmarks: flute and groove casts Sparse bioturbation: *Chondrites*/*Planolites* Rare medium to coarse-grained sand intervals	5 m to 100 m	Moderate- to low-density turbidity currents
Lst: Thickly bedded sandstone	Medium to coarse-grained sand beds separated by mud laminations	Normally graded to massive beds; well-sorted Low-angle cross-stratification Pale beige-weathering calcareous concretions Toolmarks: flute and groove casts	5 m to 25 m	Moderate- to high-density turbidity currents
Lgc: Clast-supported granule to pebble conglomerate	Granule to pebble clasts in very coarse-grained sand matrix (10 to 30%)	Inverse to normally graded beds Moderately sorted clasts; trough cross-bedding Monomictic chert clasts; no bioturbation	30 cm to 5 m	High-density turbidity currents

Table 5.1: Summary of the main lithofacies described in the Todagin assemblage at Mount Dilworth and Todagin Mountain.

Lithofacies	Grain size	Bedding character and sedimentary structures	Thickness	Depositional process
Lpc: Clast-supported conglomerate	Pebble to cobble clasts with 10 to 25% very-coarse sand to granule matrix	Mostly clast-supported with occasional matrix-supported lenses Monomictic chert clasts Thick to very thick beds Moderately to well-sorted clasts Well rounded clasts with high sphericity Pale beige-weathering calcareous concretions No bioturbation observed Erosional and irregular basal contact **Lpc1**: Massive, weakly to strongly imbricated clasts Rare coarsening-upward cycles **Lpc2**: Fining- and coarsening-upward cycles Large-scale cross-beds Internally well-stratified beds	10 m to 60 m	Combination of sediment gravity flows, including high-density turbidity currents and modified grain flows
Lmc: Sand-matrix-supported mud clast conglomerate	Pebble to boulder mud clasts in a very coarse sand to granule matrix	Angular to well rounded clasts Monomictic, poorly sorted mud clasts Inversely graded; erosive lower contact	20 cm to 150 cm	Lower portion of high-density turbidity currents
Ld: Mud-matrix-supported conglomerate	Mixture of sand, pebble, mud clasts and large boulders (>10 m) in a mud matrix (50 to 75%)	Chaotic, heterogeneous mud matrix Very poorly sorted and ungraded polymictic clasts Well-rounded to angular clasts Largest clasts up to several metres in size (rafts) Synsedimentary folds and faults	1 m to 100 m	Cohesive debris flows
Lsl: Complicated deformed mudstone and sandstone interbeds	Mud and silt with fine to medium-grained sand	Syn-sedimentary faults and folds Basal shear surface Preservation of depositional layering	1 m to 20 m	Slumps and slides

Table 5.1: continued

representing more than 900 m were recorded with a resolution of 30 cm. These sections were tied by physically walking out beds and/or correlation from the photomosaic.

5.4 Case Study 1 – Mount Dilworth

On the western margin of the Bowser basin, 25 km north of Stewart, British Columbia, Canada (figure 5.1), Upper Callovian to Lower Oxfordian sedimentary rocks of the Todagin assemblage are preserved in the core of a southeast-plunging synclinorium (figure 5.3). They unconformably overlie Lower Pliensbachian dacitic volcanic rocks of the Mount Dilworth Formation of the lower Hazelton Group (e.g. Grove 1986; Alldrick 1987, 1993; Anderson and Thorkelson 1990; Anderson 1993; Evenchick and McNicoll 2002). This boundary marks a major change in the tectonic evolution of the Stikine terrane from an active volcanic arc setting to a subsiding sedimentary basin. The slope succession investigated at Mount Dilworth crops out on the overturned western limb of a syncline (figure 5.3). The beds are very steep (60° to 90° dip) and record more than 850 m of continuous deep-water sedimentary strata (figure 5.4).

5.4.1 Stratigraphic architecture of the Mount Dilworth area

5.4.1-1 Lithofacies association 1: Thinly bedded mudstone and siltstone with thick sandstone

Lithofacies association 1 (LA-1) is mostly exposed at the base of the Mount Dilworth section on the eastern side of a steep post-depositional fault (figure 5.4). It consists predominantly of normally graded siltstone-mudstone and sandstone-mudstone couplets (Lm; Table 5.1). Some 30 to 60 cm thick, massive to normally graded fine-grained sandstone beds (Lfst; Table 5.1) are interstratified with the finer-grained intervals. The beds are laterally extensive, and can be followed up to 200 m along strike before being covered by glacial sediments. Sedimentary structures including T_{bcd} and T_{abcde} divisions, groove casts, and asymmetric ripple cross-lamination are abundant in the sandy sedimentation units (figure 5.5A). Paleocurrent measurements obtained from these sedimentary structures indicate predominant flows towards the southwest (corrected for post-depositional tilting, mean = 203°) (figure 5.4). Loading features such as flame structures and convolute laminations are common at the base of sandstone beds (figures 5.5B and C). The mud-rich T_{de} intervals occasionally show evidence of biogenic reworking. Distinctive ichnogenera include *Phycosiphon* and *Helminthopsis,* which are characterized by horizontal to gently inclined, meandering burrows filled with mud (figure 5.5D).

Interpretation: Sedimentation units of LA-1 are interpreted as low- to moderate-density turbidity current deposits, separated by thin intervals of mudstone derived from suspension fallout or more dilute turbidity currents (Bouma 1962; Lowe 1982).

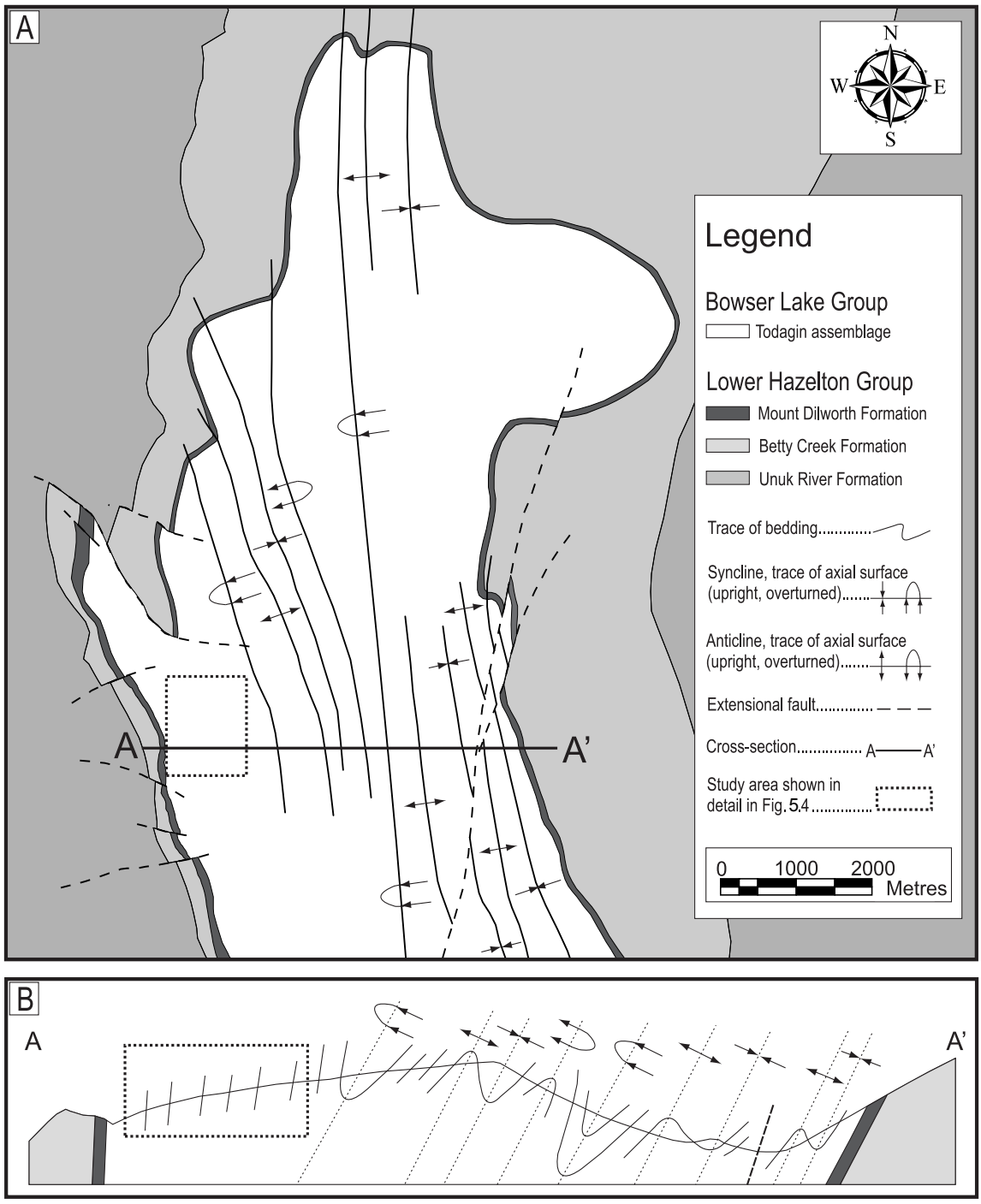

Figure 5.3: A) Geology map of the Mount Dilworth area showing the main lithostratigraphic units and structural elements. B) Cross-section showing the complicated folded structure of the area. Modified after Grove (1986), Alldrick (1987), and Evenchick and McNicoll (2002).

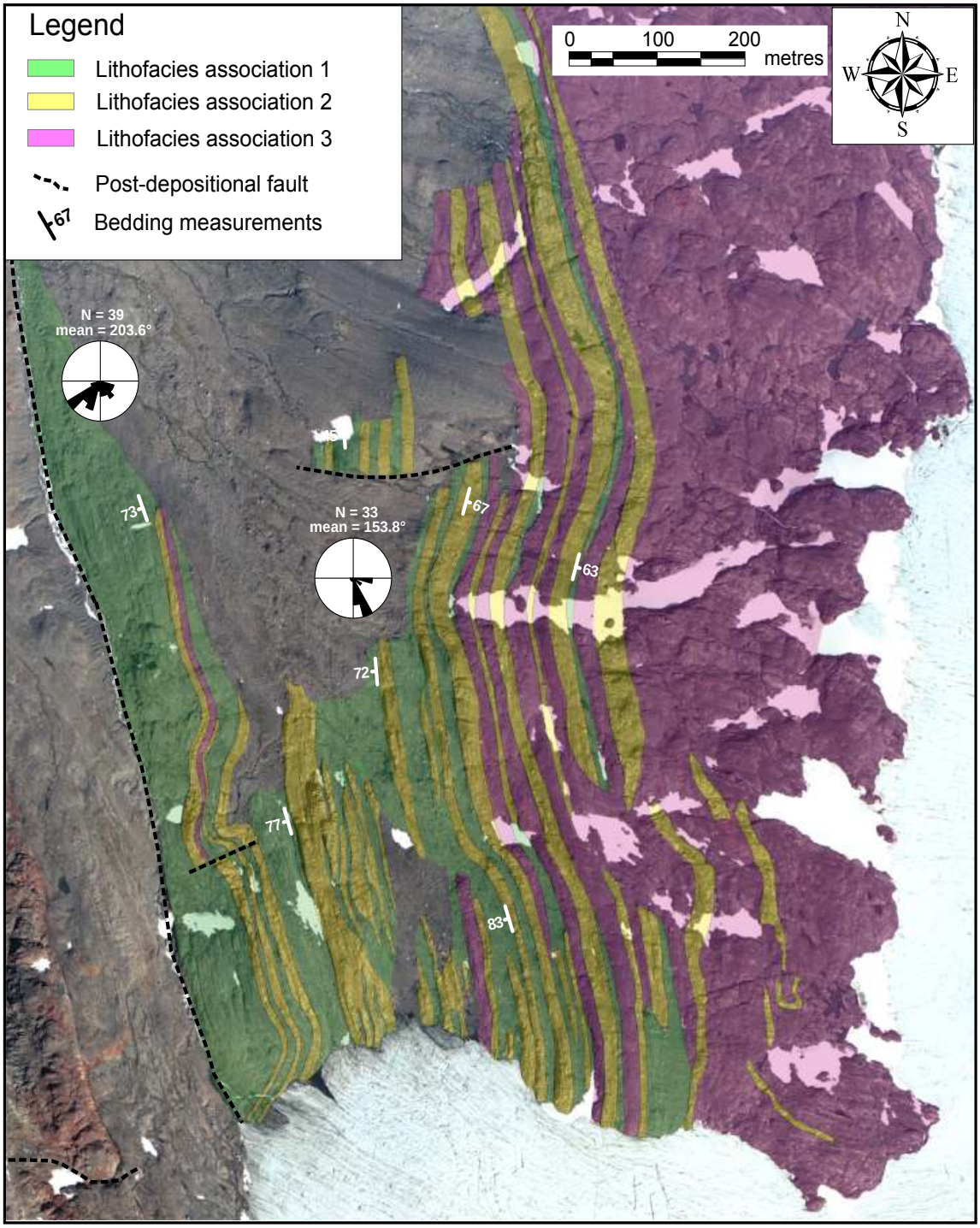

Figure 5.4: Annotated aerial photograph of the sedimentary succession exposed at Mount Dilworth showing the distribution of lithofacies associations and paleocurrent data. Stratigraphic top is to the east.

Helminthopsis and *Phycosiphon* concentrated in T_{de} are generally interpreted as grazing trails of vermiform organisms and typically occur near the sediment-water interface (figure 5.5D) (Pemberton et al. 2001). This suggests that organic matter was introduced mostly by suspension in a low-energy environment, outside the principal axis of gravity-flow activity. Loading features are attributed to discrete episodes of increased sedimentation rate, which led to a density inversion in water-saturated sediments shortly after deposition. In some cases, rapid deposition also produced pore pressure that exceeded the hydrostatic equilibrium and led to partial liquefaction of the sediments to produce convoluted beds (figure 5.5C). The lateral continuity of individual beds along strike suggests accumulation in a low-gradient, relatively unconfined environment.

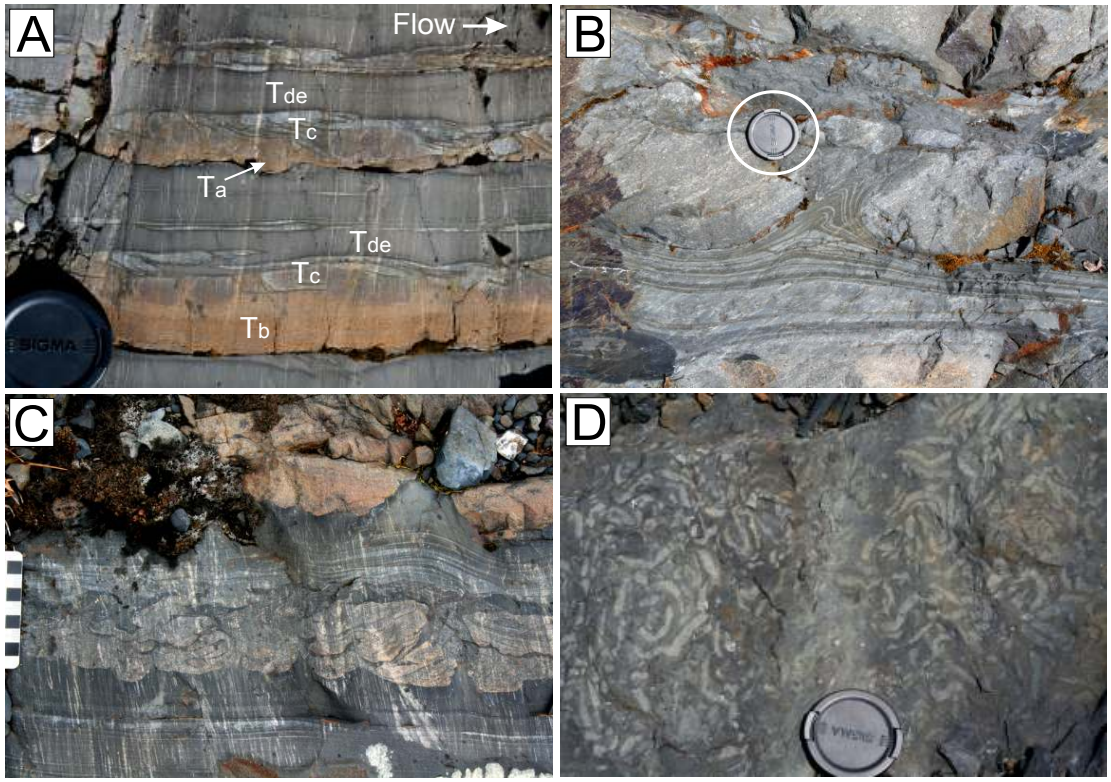

Figure 5.5: Lithofacies association 1 (LA-1). A) Normally graded fine-grained turbidites (Lm) with Tbcde and Tacde divisions. B) Flame structures attributed to relatively high sedimentation rates. C) Convolute laminations in sandier turbiditic intervals. Scale bar divisions in cm. D) Biogenic traces (*Helminthopsis*) interpreted as grazing trails of vermiform organisms on the sea-floor. Lens cap in A, B and D is 6 cm in diameter.

5.4.1-2 Lithofacies association 2: Thick channelized units of conglomerate, sandstone and mudstone

Lithofacies association 2 (LA-2) is observed above the thinly bedded fine-grained units of LA-1, and is dominated by vertically stacked, medium to thickly bedded sandstone (25 to 60 cm) separated by mudstone laminations (Lst; Table 5.1). Some individual sandstone beds become amalgamated over 100 m along strike and suggest channelized geometries. Sedimentation units are massive to normally graded, and typically consist of well sorted, medium- to coarse-grained sandstone with calcareous concretions (figure 5.6A). Traction structures such as horizontal planar lamination and low-angle cross stratification are common in this unit. Well-preserved flutes and grooves at the bases of T_{abc} divisions indicate a restored paleocurrent in the range of 150° to 180° (figure 5.4).

An isolated two metre interval of laminated mudstone and siltstone drapes (Lmf; Table 5.1) was observed in the sandstone-dominated succession of LA-2. The normally

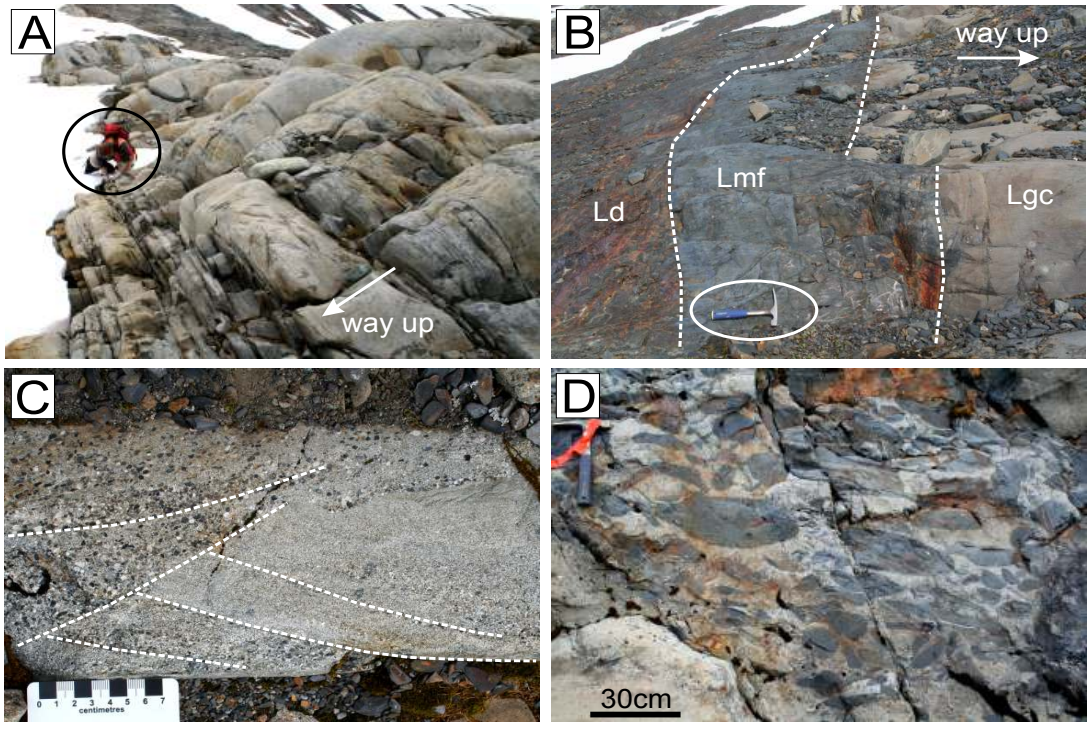

Figure 5.6: Lithofacies association 2 (LA-2). A) Thickly bedded and amalgamated sandstone beds (Lst). Note the fining- and thinning-upward character of the beds. Stratigraphic top is to the left. Person for scale. B) Mud-filled channel (Lmf) above cohesive debris flow unit (Ld). Hammer is 25 cm long. Stratigraphic top is to the right. C) Trough-cross stratification in granule to coarse-grained sandstone beds (Lgc). Scale bar divisions in cm. D) Sand-matrix-supported mud-clast conglomerate found near the base of channel complexes (Lmc). This lithofacies is indicative of local erosion and sediment bypass.

graded mudstone-siltstone couplets occur above scours of an incised, five metre thick mud-matrix conglomerate (figure 5.6B). Sedimentary structures including 1-5 cm thick T_{de} divisions and parallel laminations indicate that these are the products of dilute muddy turbidity currents. Three detailed sections were measured at 7.5 m intervals along strike to document the lateral extent of the mud-rich unit and the vertical change in grain size (figure 5.7) Units of Lmf, in turn, are overlain by granule to pebble conglomerate lenses with high-angle cross-stratification (figures 5.6C and 5.7). These coarse-grained sedimentary units (Lgc; Table 5.1) are moderately sorted, normally to inversely graded, and lack burrows. In each measured section, coarse-grained sandstone and conglomerate are interbedded with thin laminated units of siltstone (figure 5.7).

The fourth lithofacies identified in LA-2 consists of poorly sorted, sand-matrix-supported mud-clast conglomerate (Lmc; Table 5.1 and figure 5.6D). These intervals are 20 to 150 cm thick and occur at the bases of amalgamated sandstone beds where they fill prominent scours. Clasts have a wide range of shapes, from angular elongated prisms to well-rounded approximately spherical shapes. The elongated clasts display weak imbrication and the orientation of their long axes is parallel to the flow direction determined from toolmarks at the base of adjacent beds.

Interpretation: The normally graded, medium- to coarse-grained sedimentation units of LA-2 are interpreted to represent the deposits of moderate- to high-density turbidity currents (Bouma 1962; Lowe 1982). The presence of isolated conglomerate lenses with medium to large scale trough-cross stratification in large 3D dunes of facies Lgc suggests discrete episodes of increased energy but lower sedimentation rate, during which traction prevailed. Infill of deep scours by laminated mudstone and siltstone (Lmf) above the irregular upper surface of an isolated debris flow unit (Ld) is interpreted to represent deposits of a mud-filled channel (figure 5.7). The confined nature of the channel with steep margins indicates that the underlying cohesive debris flow unit was resistant to erosive bottom currents, which produced topographic relief. The lack of coarse-grained material immediately above the erosional contact suggests that significant sediment bypass occurred prior to the accumulation of the mud-filled channel.

Facies Lmc is interpreted to represent lower portions of high-concentration, coarse-grained turbidity current deposits that eroded and incorporated large rip-up clasts (Johansson and Stow 1995). The abundance of larger clasts along specific horizons within the beds could be attributed to turbulent shear stresses related to flow stratification (Postma et al. 1988) (figure 5.6D). Based on experimental observations, Postma et al. (1988) suggested that outsized clasts tend to glide along the rheological boundary between a fast-moving turbulent layer and an underlying laminar inertia-flow layer. The

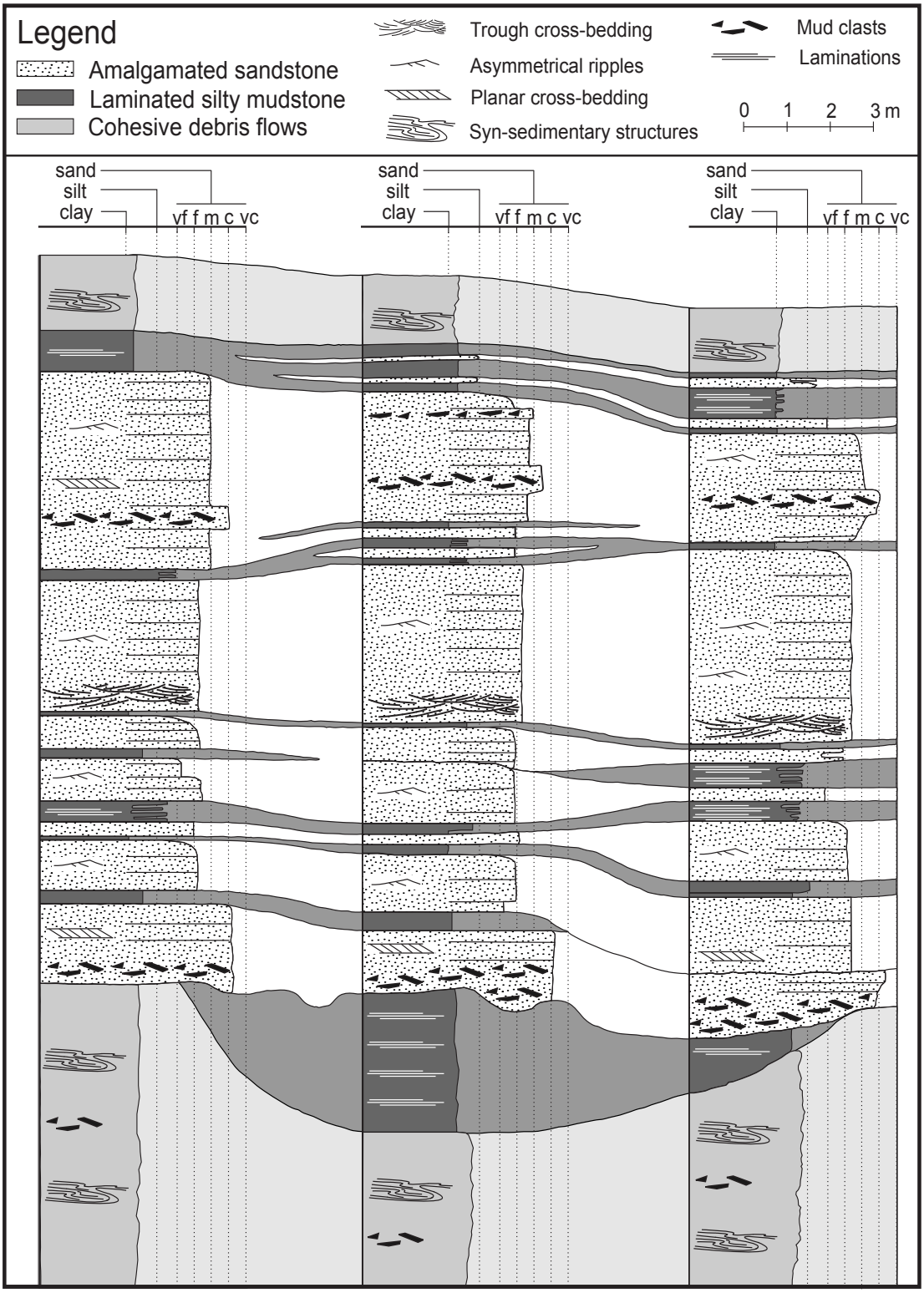

Figure 5.7: Stratigraphic cross-section of a mud-filled channel. Fine-grained turbidites (Lmf) are preserved in topographic lows above a cohesive debris flow unit (Ld). This lithofacies is interpreted to represent bypass of coarse-grained sedimentary units to more distal parts of the basin. No vertical exaggeration.

occurrence of inverse grading in 20 to 30 cm intervals near the bases of the beds, and the weak imbrication of elongated clasts parallel to the flow direction further suggest that dispersive pressure derived from grain collision might also have played a role in sediment transport (Nardin et al., 1979) (figure 5.6D). The unimodal composition of the clasts, combined with their internal T_{de} divisions, suggests that they were probably eroded from local mudstone layers situated updip or along channel margins.

5.4.1-3 Lithofacies association 3: Mud-matrix-supported conglomerate and contorted mudstone and sandstone

Mass-transport lithofacies association 3 (LA-3) is the most widespread assemblage observed at Mount Dilworth. It is especially well-exposed near the top of the succession where LA-3 is interstratified with thick sandstone beds and mud-filled channels of LA-2 (figure 5.4). LA-3 mainly consists of dark purplish-grey mudstone that supports chaotic calcareous concretionary blocks and large layered rafts of sandstone and siltstone (Ld; Table 5.1 and figures 5.4 and 5.8A). The clasts are very poorly sorted, ungraded, and show no preferred orientation. Highly contorted stratified fine-grained sedimentary rock fragments are also present in LA-3 (Lsl; Table 5.1 and figures 5.8B-D). Soft-sediment deformation features such as syndepositional recumbent folds, rotated blocks, and micro-faults are pervasive in these units.

In one particularly well-exposed example of Lsl, a transition from undisturbed thinly bedded turbidites into deformed strata occurs in a zone 3 to 4 m thick (figure 5.8D). Near the base of the deformed unit, a mudstone layer displays gentle parallel folds of constant thickness (class 1B geometry of Ramsay 1967), whereas the underlying folded sandstone layer varies in thickness from 3 to 10 cm over a wavelength of 1 m (figure 5.8D). Pull-apart boudins of mudstone in a sandy matrix and sandstone dykes filling fissures at the top of the mudstone bed are indicative of the rheology contrast between strata of different grain size (figure 5.8D). The degree of deformation increases progressively near the top of the slump where folds become tighter and more abundant. The initial sediment fabric is also destroyed and replaced by a homogeneous sand-mud mixture.

The uppermost mass-transport complex (MTC) of LA-3 is at least 300 m thick and contains many 100 m-long rafted blocks of sandstone near its base (figure 5.4). The basal contact of the MTC is sharp and shows only modest incision in the underlying sandstone to the south. Intervals of homogeneous mudstone 10 to 50 m thick with uniform parallel laminations suggest that they represent large displaced blocks within the slumps. Rafted blocks locally display intense folding and numerous small faults. At the

scale of the outcrop, the complex contains no visible internal discontinuities, but could nonetheless correspond to several amalgamated units.

Interpretation: The chaotic sedimentation units of LA-3 are interpreted as deposits of cohesive gravity flows (i.e. debris flows) and slumps (Nardin et al., 1979). In the matrix-supported debris-flow deposits (Ld), the combination of matrix strength, buoyancy and pore pressure were high enough to support and transport boulders several metres in diameter (Lowe 1979, 1982). This is principally attributed to high levels of cohesion due to elevated clay content, which is common in mass flows where plastic mechanical behaviour dominates (Dott 1963; Lowe 1979; Nardin et al. 1979). The variable distribution of some rafted blocks suggests that they experienced significant rotation during transport. The deformation features at the base of the distorted units are evidence of plastic deformation and local shearing (Tripsanas et al. 2008a). These features are usually attributed to slumped units which are the product of coherent mass movements over discrete basal shears (Nardin et al. 1979; Coleman and Prior 1988). In the example

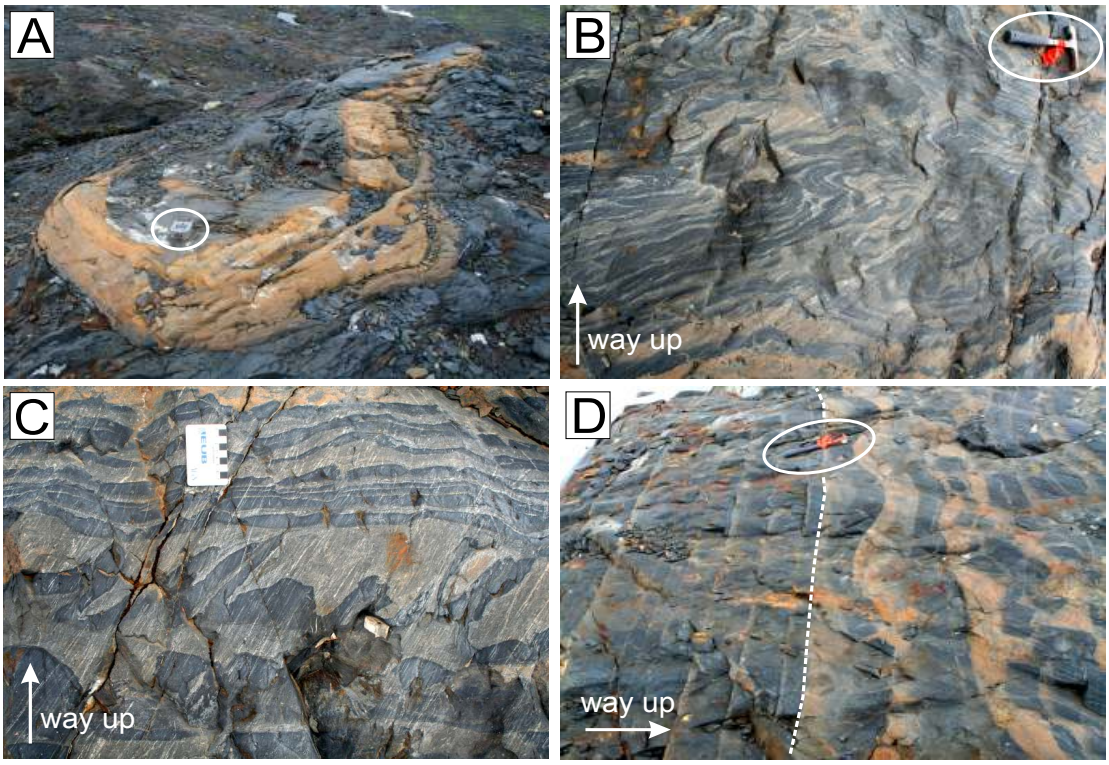

Figure 5.8: Lithofacies association 3 (LA-3). A) Folded calcareous concretionary block in a chaotic dark purplish-grey mudstone (Ld). Brunton compass for scale is 8 cm wide. B and C show intensely deformed slump units with syndepositional isoclinal folds (Lsl). Hammer in B is 25 cm long and scale bar divisions in C are in cm. D) Slump unit containing abundant syn-sedimentary deformation structures. During slope failure, the underlying thinly bedded turbidites remained undisturbed while the MTD was subject to compressional and extensional deformation. Hammer is 25 cm long.

shown in figure 5.8D, cohesive mudstone beds were folded during shearing but retained their original thickness, whereas softer sand-rich units were subject to more thorough ductile deformation. Up-section, complete liquefaction of the sediment mass, likely in response to increased pore-fluid pressure, is recorded and the slump is transformed into an incoherent debris flow (cf. Iverson et al. 1997). This upward change in character of deformation could be a function of the grain size of the pre-slide sediment pile, where liquefaction in sandier beds became an important deformation mechanism as shear was distributed throughout the sediment mass.

5.4.2. Lithofacies succession and depositional environment

The lower part of the succession exposed at Mount Dilworth consists of 150 m of laterally extensive (200 m) thinly bedded turbidites intercalated with thick sandstone bodies (LA-1). The apparent unconfined nature and sheet-like geometry of those units, combined with the high proportion of normally graded fine-grained rocks, suggest deposition from low-density turbidity currents in a low-gradient submarine fan environment (Lowe 1982). The radial distribution of paleocurrent indicators in these units might be attributed to progradation of depositional lobes to the south-west, although these morphological features are usually much larger in size than the outcrop described in this study (cf. Reading and Richards 1994) (figure 5.4). The overall coarsening-upward trend of LA-1 possibly reflects a basinward advance of proximal frontal splays over the basin floor, as inferred by Evenchick and Thorkelson (2005) in other areas of the Bowser basin.

The top of LA-1 is an erosion surface above which vertically stacked, lenticular sandstone bodies fill prominent scours. The channelized sandstone bodies range in thickness from 10 to 50 m and are laterally extensive for at least 100 m. Even though channel margins could not be observed directly in the field due to the extensive snow cover, geometries interpreted from aerial photographs taken at times of minimal snow suggest that they eventually pinch out laterally into finer-grained overbank deposits (figure 5.4). The sharp stratigraphic transition from LA-1 to LA-2 marks a sudden change from unconfined, laterally continuous strata to a more confined architecture where coarse-grained sedimentation occurred exclusively in channel thalwegs.

The proportion of mass-transport deposits (MTDs) increases gradually up-section (figure 5.4). Incoherent debris flows and slump units become interbedded with amalgamated sandy channel-fills, whereas fine-grained turbiditic intervals are generally absent. The presence of confined and deeply incised mud-filled channels above irregular scoured surfaces suggests that incision and sediment bypass were important. The impressive thickness of MTDs observed at Mount Dilworth (>300 m) suggests that this

area of the Bowser basin might have been subject to considerable tectonic instability and/or very high sedimentation rates during accumulation of the Todagin assemblage in Late Callovian to Early Oxfordian. These factors probably resulted in progressively increasing depositional slopes, which were responsible for the upward transition from unchannelized fine-grained units of LA-1 and channelized high-density turbidity current deposits of LA-2 to very thick mass-transport complexes of LA-3.

5.5. *Study Area 2 – Todagin Mountain*

At the northwest edge of the Bowser basin, in the vicinity of Todagin Mountain (figure 5.1), the Todagin assemblage is at least 1 100 m thick and consists of multiple conglomerate bodies encased in thinly bedded turbidites (Evenchick and Thorkelson 2005). It conformably overlies bimodal volcanic rocks and fine-grained sedimentary rocks of the upper Hazelton Group (Evenchick and Green 2004; Gagnon et al. 2009; Chapter 4). Geological mapping suggests that units of the upper Hazelton Group are preserved preferentially in fault-bounded structures, consistent with deposition in a graben system that was inverted during later deformation (Gagnon et al. 2009) (figure 5.9). Detailed study was focused on the stratigraphically lowermost channel complex of the Todagin assemblage (here termed the Lower Todagin channel complex; LTCC). Fossil

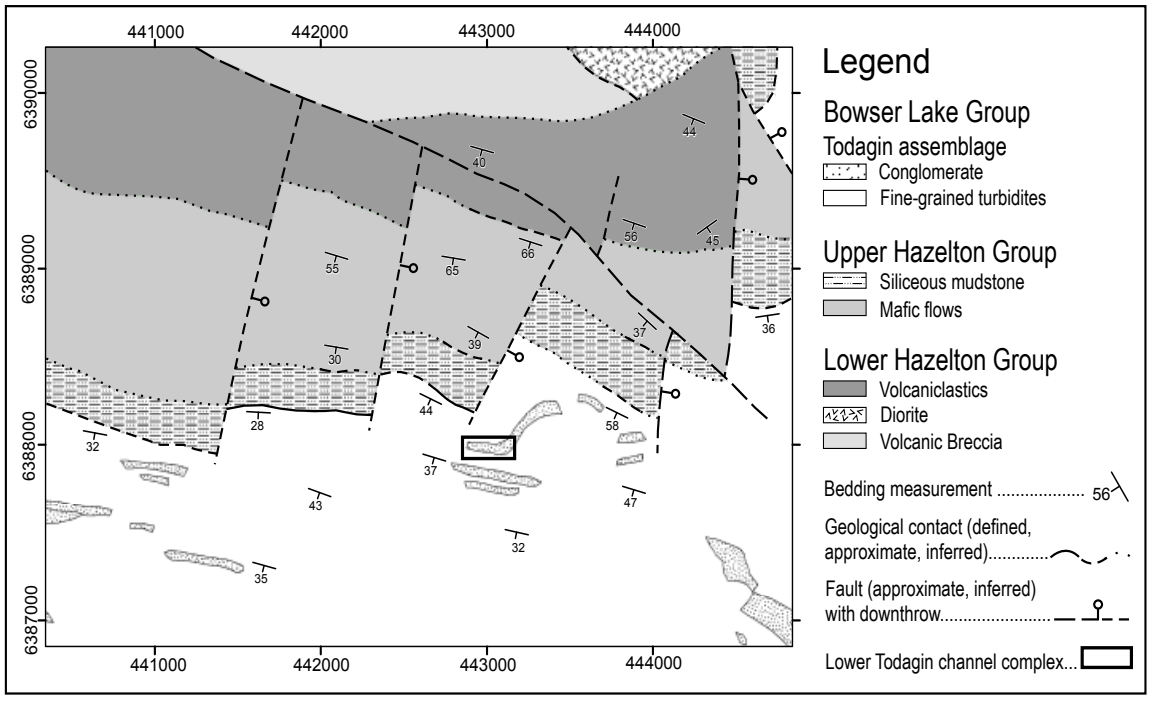

Figure 5.9: Geology map of the Todagin Mountain area showing the main lithostratigraphic units and structural features. Universal Transverse Mercator Projection in NAD 83. Modified after Evenchick and Green (2004) and Gagnon et al. (2009).

collections located above and below the LTCC indicate a Bathonian depositional age (Evenchick and Thorkelson 2005; Gagnon et al. 2009), slightly older than the Todagin assemblage in study area 1. The channelized conglomerates of the LTTC crop out on the northern flank of an E-W trending ridge where the dip of bedding averages 30° to 45° south (figure 5.10). Individual units associated with channel and/or interchannel complexes were defined based on their dominant lithological content and separated into main lithofacies and lithofacies associations following the classification used at the Mount Dilworth study area (Table 5.1).

5.5.1 Architectural elements of the Lower Todagin channel complex

5.5.1-1 Lithofacies association 1: Thinly bedded interchannel units of sandstone, siltstone and mudstone

Sedimentary rocks exposed at the base of the Lower Todagin channel complex (LTCC) consist of massive dark grey to black mudstone and laminated siltstone (Lm; Table 5.1 and figure 5.10). Beds extend laterally up to 300 m along strike until covered by scree. Rusty orange-weathering claystone beds and very fine-grained sandstone 1-10 cm thick are also present in the section (figure 5.12A). Soft-sediment deformation is pervasive in these strata and includes features such as convoluted beds, sandstone dikes and micro-faults (figure 5.12B). Curvilinear mud-filled tubes 1-5 mm in diameter, corresponding to the trace fossil *Phycosiphon*, tend to occur in the upper part of normally graded beds. Flutes and groove casts preserved at the base of the sandier layers indicate a preferential restored paleocurrent direction towards 230° (figure 5.11).

In the middle part of section 1, a 22 m interval of interbedded thin to medium sandstone and siltstone beds (Lfst; Table 5.1) onlaps conglomerate of channel-fill 1 above a sharp contact (figures 5.10, 5.11 and 5.12C). This sandstone-dominated package (Lfst) gradually fines upward into very thinly bedded turbidites characteristic of Lm (figure 5.12C). The fine to medium-grained sandstone beds are normally graded with well-developed T_{abcd} and T_{bc} divisions. Common ripple cross-stratification indicates flow approximately towards 160°-180° (figure 5.11). Lithofacies Lfst also comprises most of measured sections 4 and 6, in addition to the upper part of section 3 (figures 5.10; 5.11; 5.12D). Traction sedimentary structures including horizontal planar lamination and climbing ripple cross-lamination were observed in normally graded T_{bcd} divisions.

Interpretation: Thinly bedded mudstone, siltstone and very fine-grained sandstone of LA-1 are interpreted to represent sedimentation from low- to moderate-density turbidity currents in which fluid turbulence was the main particle-support mechanism

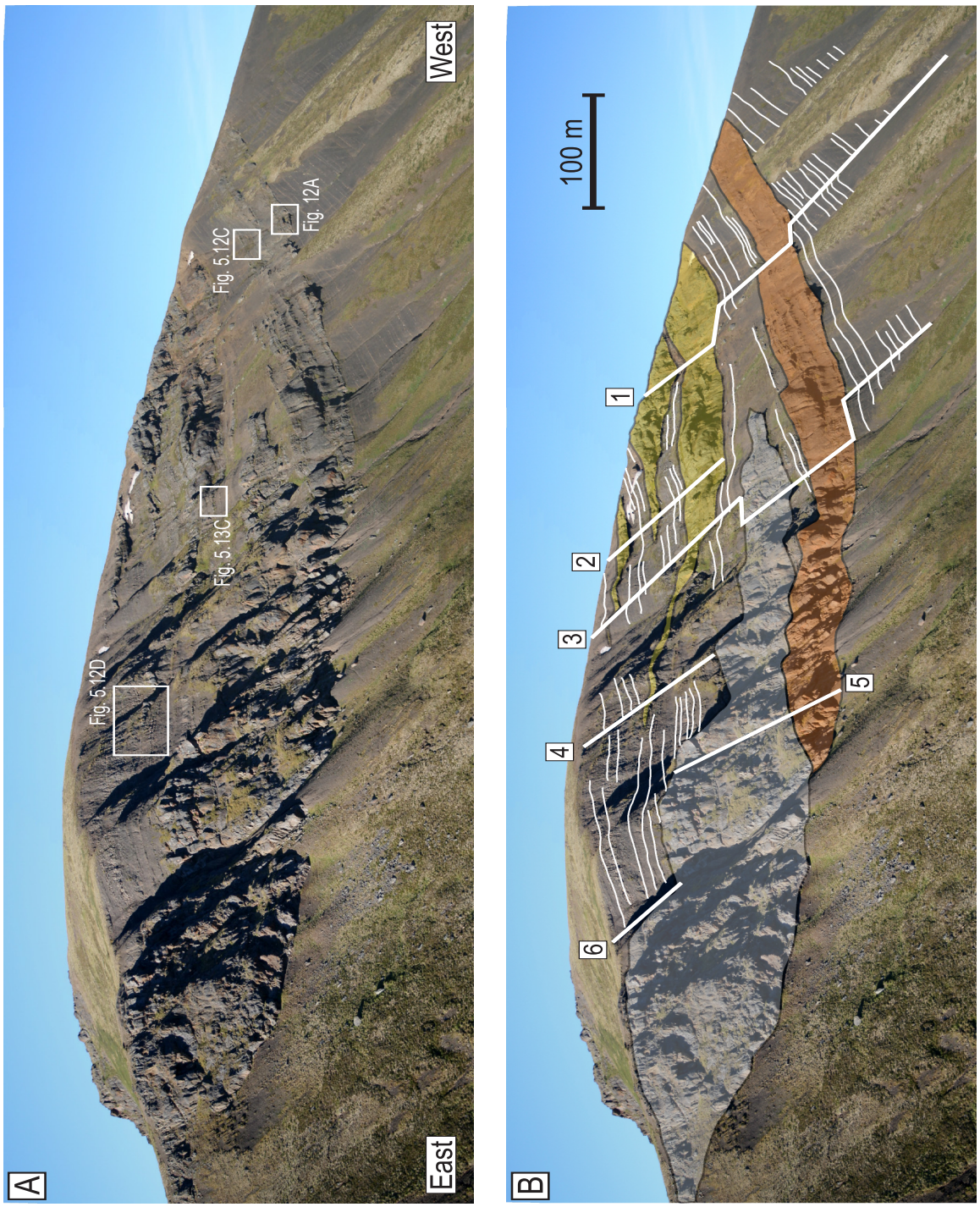

Figure 5.10: Stratigraphic architecture of the Lower Todagin channel complex. A) Photograph of the Lower Todagin channel complex showing location of close-up photographs. B) Simplified line drawing of the Lower Todagin channel complex. Conglomeratic lithofacies (Lpc) of channel fills 1 to 3 are represented in shaded areas (channel-fill 1 - orange; channel-fill 2 - light grey; channel-fill 3 - yellow). Location of stratigraphic sections 1 to 6 are represented by thick solid white lines.

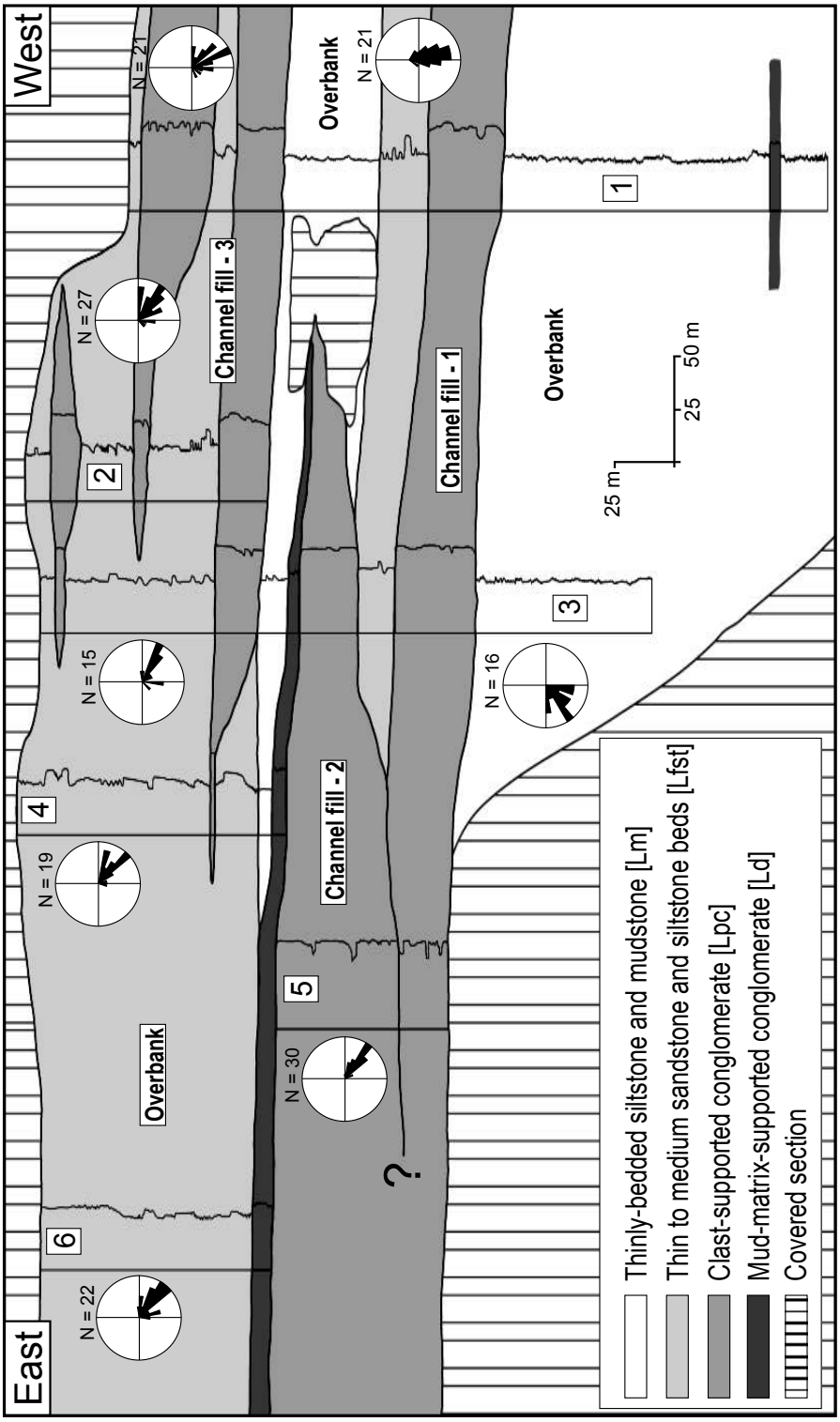

Figure 5.11: Generalized stratigraphic relationships and paleocurrent data of units present in the Lower Todagin channel complex. Stratigraphic sections are labeled 1 to 6 and their locations is shown in figure 5.10. Note: paleocurrents are plotted relative to N (up) which is towards the observer in this section.

(Bouma 1962; Lowe 1982). These sedimentation units accumulated in the overbank areas of the main channel axes. Some more restricted sandstone-dominated intervals with well-developed T_{abc} divisions and climbing ripples (Lfst) indicate occasional increased rates of sediment fallout. The limited lateral continuity of these sandy units compared with the finer-grained mudstone suggests that they represent localized small crevasse-splay deposits (cf. Beaubouef 2004). Deformation features formed by processes similar to those in the thinly bedded turbidites of LA-1 at Mount Dilworth. The overall fine-grained nature of the depositional units in LA-1, combined with their lateral continuity over several hundred metres, indicate deposition in relatively unconfined environments.

5.5.1-2 Lithofacies association 2: Thick channelized units of conglomerate and sandstone

A total of three distinct channel-fills comprising a variety of lithofacies associated with LA-2 are recognized in the LTCC (figures 5.10 and 5.11). In measured section 1, the base of channel-fill 1 is defined by an irregular erosional surface where a 30 m thick package of clast-supported conglomerate (Lpc1; Table 5.1 and figure 5.12A) overlies dark grey siltstone and mudstone of LA-1. The basal surface of channel-fill 1 gradually cuts into stratigraphically lower beds in a westward direction to produce a relief up to 20 m (figures 5.10 and 5.11). The conglomeratic beds are 40 to 80 cm thick, and vary from clast-supported to matrix-supported, with well rounded and moderately to well sorted chert pebbles mixed in a sandy matrix (Table 5.1 and figure 5.13A). No apparent grading trend was observed in the amalgamated beds of this package. The top of channel-fill 1 is onlapped by interstratified siltstone and sandstone (Lfst) of LA-1 over a sharp contact (figure 5.12C).

Channel-fill 2 consists of vertically stacked, clast-supported pebble to cobble conglomerate in a coarse-grained sandy matrix (Lpc1; Table 5.1). Bed thickness can be over 1 m in places. Most beds are normally graded but inverse grading occurs in intervals of 50 cm or less. Paleocurrent data deduced from the orientation of the long axes of imbricated pebbles indicate that mean depositional flows were oriented towards 125° (figure 5.11). The lower contact of channel-fill 2 scours into fine-grained turbidites of LA-1 (Lm) and can be traced eastward towards section 5 where it becomes amalgamated with channel-fill 1 (figure 5.11). At this location, the amalgamated channel-fills constitute the thickest vertically continuous coarse-grained package of the LTCC (~60 m). The uppermost unit associated with channel-fill 2 consists of a 4 m thick mud-matrix-supported conglomerate (Ld; Table 5.1). The clasts are poorly sorted and include moderately to well-rounded chert pebbles and laminated mudstone clasts (figure 5.13B).

Channel-fill 3 consists mostly of three offstacked conglomerate units characterized by wedge-shaped geometries and channel margins that pinch-out laterally into thin to medium sandstone beds of Lfst (figures 5.10 and 5.11). The basal contact of the lowermost conglomerate is erosive and scours into the underlying fine-grained rocks (Lm) of LA-1 (figure 5.13C). Conglomerate units are clast-supported, arranged in 25-50 cm upward-fining intervals with sharp contacts, and contain rare medium-scale cross-strata near the tops of beds (Lpc2; Table 5.1 and figure 5.13D). Pale beige-weathering calcareous concretions are common in the sandier intervals. Paleocurrent measurements from cross-laminated ripples and flute casts in medium-grained sandstone beds of channel-fill 3 indicate a radial distribution from south to east with a minor component to the southwest (figure 5.11).

Interpretation: The range of sedimentary textures and fabrics observed in LA-2 suggests that multiple mechanisms were involved during transport and accumulation of gravity flow deposits. The lack of grading, imbrication of clasts, and overall clast-

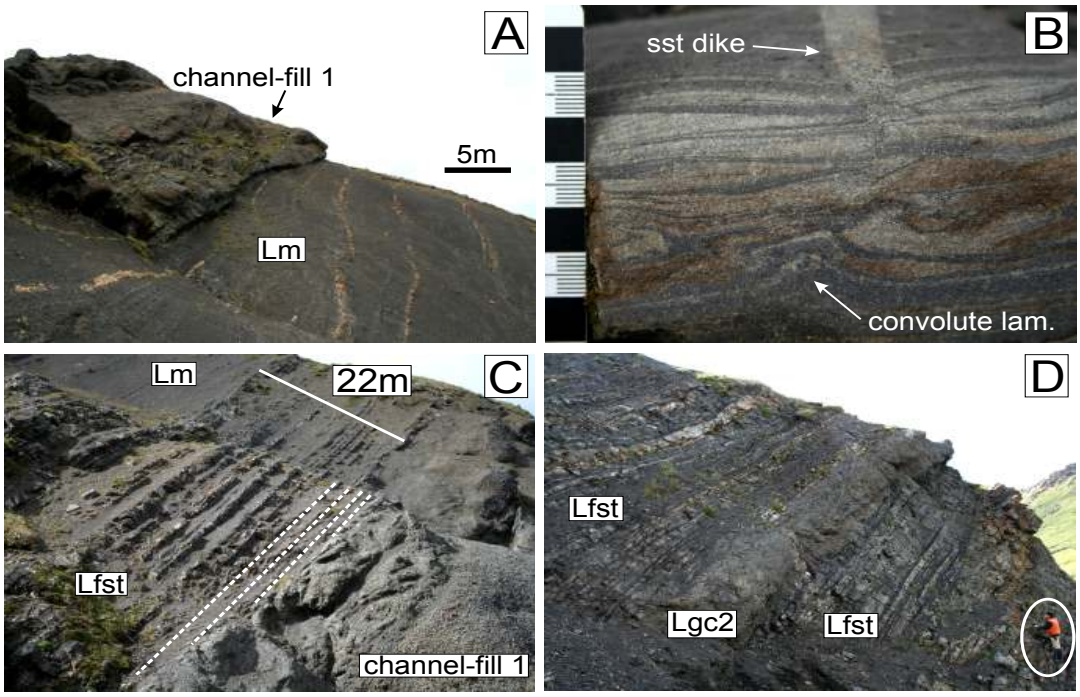

Figure 5.12: A) Erosional contact at the base of channel-fill 1 showing thinly bedded turbidites (Lm) overlain by pebble to cobble clast-supported conglomerate (Lpc1). B) Convolute laminations and syn-sedimentary sandstone dike in thinly bedded turbidites (Lm) below channel-fill 1. Scale bar divisions in cm. C) Onlap of thin to medium sandstone and siltstone beds (Lfst) above the conglomerate unit of channel-fill 1 (Lpc1). The succession eventually fines upward into thinly bedded turbidites (Lm). D) Medium to thick sandstone units interbedded with mudstone layers (Lfst). These sedimentation units are interpreted as crevasse-splay deposits in the overbank region of channel-fill 3. Person for scale. See figure 5.10 for photograph locations.

supported nature of Lgc1 indicate that dispersive pressure derived from grain interactions probably played a significant role in particle support (cf. Lowe 1976). Even though fully inertial grain flows are unlikely to result in accumulation of thick sedimentation units (Lowe 1976), other subordinate particle-support mechanisms including buoyancy, pore pressure and matrix strength could have been enough to ensure transport of these flows over long distances (Lowe 1976; Ilstad et al. 2004; Tripsanas et al. 2008b). Gravel flows characterized by a combination of similar processes were termed density-modified grain flows by Lowe (1976) and hyperconcentrated density flows by Mulder and Alexander (2001). Rare poorly sorted mud-matrix conglomerate (Ld), interpreted to represent deposition from cohesive debris flows, constitutes a minor component in the LTCC. Normally graded conglomerate beds mainly observed in channel-fill 3 are interpreted

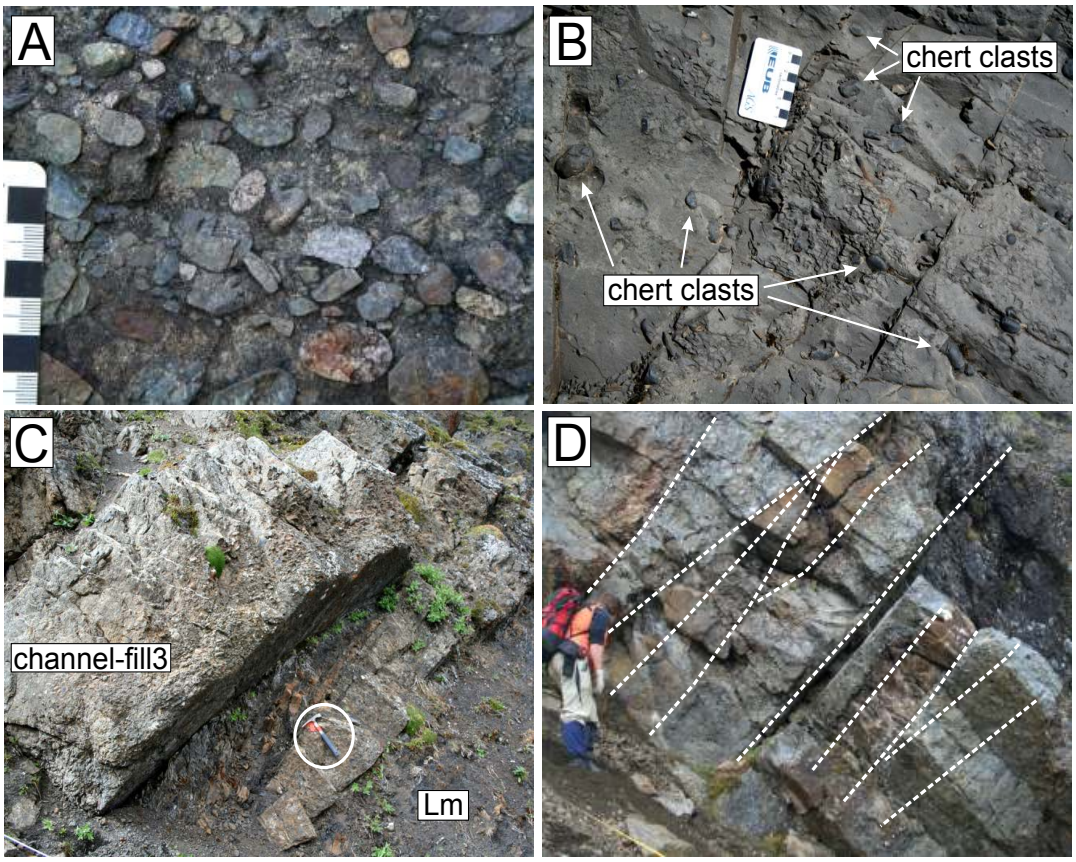

Figure 5.13: A) Ungraded clast-supported conglomerate showing well-rounded and moderately-to well-sorted chert pebbles mixed in a sandy matrix (Lpc1). Scale bar divisions in cm. B) Close-up of the cohesive debris flow unit (Ld) exposed at the top of channel-fill 2. Chert clasts are supported in a homogeneous mudstone matrix. Scale bar divisions in cm. C) Erosional contact at the base of channel-fill 3 showing a conglomerate unit (Lgc2) filling scoured surfaces above fine-grained overbank deposits (Lm). Hammer is 30 cm long. See figure 5.10 for location. D) Normally graded and internally stratified clast-supported conglomerate of channel-fill 3 showing large cross-stratification structures in some beds (Lpc2). Person for scale.

to represent deposition from high-density turbidity currents (Lgc2) (Lowe 1982). In addition to fluid turbulence, the pebble to cobble sized material probably required dispersive pressure from grain collisions to maintain grain support (Lowe 1982). The rare occurrence of medium-scale cross-stratification in units of channel-fill 3 (Lgc2) is indicative of bed load transport.

5.5.2 Depositional model of the Lower Todagin channel complex

The architectural organization of strata associated with the Lower Todagin channel complex indicates that thick sandy conglomerate bodies represent three successive phases of channel sedimentation. These coarse-grained channel-fills are separated by thinly interstratified mudstone, siltstone and very-fine sandstone corresponding to interchannel deposition. Erosive processes are dominant at the base of the channel complex. Accumulation of channel-fill 1 was preceded by a relatively modest incision phase that produced an irregular surface with up to 20 m of negative relief cut into older overbank deposits (figures 5.10 and 5.11). The occurrence of gravel lags and scours at the bases of individual beds are related to bypass processes. While sediment bypassed through the channel conduit, overbank deposits (LA-1) began to aggrade laterally to the channel axis. Transition from sediment bypass to sediment accumulation in channel-fill 1 probably reflects a general reduction in flow energy, which led to filling and deposition of pebble conglomerate and sandstone. The sharp contact at the top of channel-fill 1 is interpreted as a result of temporary deactivation of the channel, where pelagic sediments, or dilute turbidity-current deposits from channels located out of the plane of the outcrop, draped the whole system (figures 5.11 and 5.12C). There is no evidence for lateral migration of the channel (e.g. lateral accretion deposits) in conglomerate of channel-fill 1.

Reactivation of the LTCC is marked by the erosive surface found at the base of channel-fill 2 (figure 5.11). The degree of incision is high compared with the relatively flat basal contact of channel 1 (figures 5.10 and 5.11). Deposits of channel-fill 2 indicate a return to high-density gravity flows which accumulated the coarsest sediments observed within the channel complex. Tight clustering of paleoflow directions obtained from imbricated clasts and tool marks suggests that channel 2 was confined overall and probably not highly sinuous (figure 5.11). Significant thickness change along strike suggests that the channel pinches out laterally to the west but scree cover prevented direct observation of the exact channel margin (figures 5.10 and 5.11). Levees and overflow deposits associated with construction of channel-fill 2 are poorly developed relative to channel 3. This is attributed to the high degree of amalgamation between channel-fills 1

and 2, which decreased the preservation potential of interchannel deposits (cf. Eschard et al. 2003). The uppermost unit confined to channel 2 consists of a 4 m muddy matrix-supported conglomerate (Ld). The occurrence of a debris flow unit immediately above the clast-supported conglomerate could have caused rapid plugging and deactivation of the channel system (cf. Schwarz and Arnott 2007). The upper contact of channel-fill 2 is onlapped by recessive fine-grained turbidites that healed the positive topography inherited from deposition of the cohesive debris flow (figures 5.10 and 5.11).

Initiation of channel-fill 3 is interpreted as a third episode of scouring by energetic gravity flows. The degree of incision is similar to that observed at the base of channel 2, as suggested by the steep margins of individual channel forms (figures 5.10 and 5.11). However, the stacking pattern of the channelized coarse-grained beds associated with channel-fill 3 is significantly different. Channel forms are disconnected, stacked in multistorey bodies, thinner, and narrower at the base (figure 5.11). Each conglomerate body laterally pinches out into thinly bedded strata that represent intervening episodes of overbank sedimentation (figure 5.11). Overbank sedimentation units accumulated adjacent to the main channel axis, and their preservation suggests significant aggradation (cf. Eschard et al. 2003). Abundant paleocurrent data from the eastern margin of channel-fill 3 indicate deposition from flows moving generally to the northwest (figure 5.11). As the high-density gravelly currents spilled over the confining walls of the channels, the low-density portion of the flows located near the top extended above the channel banks and led to sedimentation of finer-grained units (Piper and Normark 1983). Paleocurrents in the overbank deposits of channel-fill 3 show a range of directions with a mean that is directed away from the channel axis, supporting the interpretation of flows escaping the channel confinement (Hickson and Lowe 2002).

The channel geometries observed at Todagin Mountain indicate that erosion and amalgamation were dominant processes in the lower part of the channel complex, while aggradation and construction of levees prevailed in upper part. Mass-transport complexes constitute only a minor component at of the LTCC, and where present, are confined to channel axes. Upward evolution of the LTCC is consistent with normal progradation of a slope system, in which gradual rise in sea-floor topography facilitated aggradation of channel and inter-channel deposits over time.

5.6 *Discussion*

The occurrence of one specific type of gravity flow over another in the slope environment is mainly a function of sediment delivery beyond the shelf edge (Piper and Normark 1983). In well-known examples from the Magallanes Basin, Fildani et al. (2009) argued that deep-water sedimentological changes between the conglomeratic channel-fill deposits of the Cerro Toro Formation and the mudstone-rich mass transport deposits of the Tres Pasos Formation were attributable to either variations in the source and/or staging areas, and in the general shape of the basin. Increase of sediment flux and sediment calibre to the deep sea can also be attributed to variations in sea-level and/or tectonic activity (Hunt and Tucker 1992; Posamentier and Kolla 2003; Catuneanu et al. 2009). Although generally applied to passive margin settings, models considering the effects of sea-level fluctuations on sedimentation in deep-water environments could provide insights on active tectonic basins such as the Bowser basin.

The stratigraphic successions exposed at Mount Dilworth and Todagin Mountain provide unique insights into the evolution of a progradational slope system represented by the Todagin assemblage. The nature and relative abundance of lithofacies in each area differs significantly. Thick debris flow and slump deposits associated with MTDs at Mount Dilworth are laterally extensive, and represent more than 50% of the exposed succession (figure 5.4). In contrast, MTDs of the LTCC at Todagin Mountain are minor, restricted to channel confines, and thin compared to channel and interchannel deposits (figure 5.11). These differences highlight the fact that parameters influencing slope stability in the Todagin assemblage were variable at the scale of the Bowser basin.

5.6.1 Controls at Todagin Mountain

The rare occurrence of MTDs associated with the LTCC suggests that the overall slope of the basin margin remained relatively constant through time as the system evolved. Aside from a 4 m thick cohesive debris flow unit located near the top of channel-fill 2, the LTCC is dominated by a variety of low- to high-concentration turbidity flow deposits. These observations are consistent with the aggradational stacking of multiple prograding Gilbert-type deltas proposed by Ricketts and Evenchick (2007), for Upper Callovian to Lower Oxfordian deltaic successions of the Eaglenest assemblage located 50 km east of Todagin Mountain. In the Ricketts and Evenchick (2007) model, these were interpreted to represent repeated episodes of footwall subsidence along steep reverse faults; however, our observations do not show strong evidence for local tectonic activity, and are consistent with subsidence analyses by Gagnon et al. (2009) which suggest that the vicinity of Todagin Mountain may have been tectonically relatively quiet at this time.

The channel geometries described at Todagin Mt. display a vertical increase in thalweg incision and aggradation of channel-interchannel elements from channel 1 and 2 to channel 3 (figures 5.10 and 5.11). Similar trends have been reported from seismic profiles in modern passive margin turbidite slope channels, where initially erosive channel complexes evolve towards aggradation with elevation of the equilibrium profile through time (Beaubouef and Friedman 2000; Mayall and Stewart 2000; Pirmez et al. 2000; Kolla et al. 2001; Kneller 2003). Architectures observed in the LTCC also bear resemblance with the Lower Pab turbiditic system, deposited on the Late Cretaceous Indo-Pakistani passive margin (Eschard et al. 2003). According to Eschard et al. (2003), backstepping evolution of the Lower Pab channel complexes was related to a decrease in the general sediment supply to the basin. Other evidence for backstepping slope channel systems, based on high resolution 3D seismic data of the Pliocene Nile Delta, was observed by Samuel et al. (2003) who suggested that reduced efficiency of flows will favor aggradation over erosion. At Todagin Mountain, the amalgamated and erosive nature of channels 1 and 2 indicate that most flows bypassed the upper slope area and deposited the coarsest material of the channel complex at the base of the slope where the local gradient was less (figure 5.14A). Even though no evidence of lateral accretionary deposits was observed in these units, lateral migration of channels may be expected in such setting (Abreu et al. 2003; Arnott 2007). Later in the depositional history, reduction in flow density and sustained sediment supply from the staging area produced a steeper

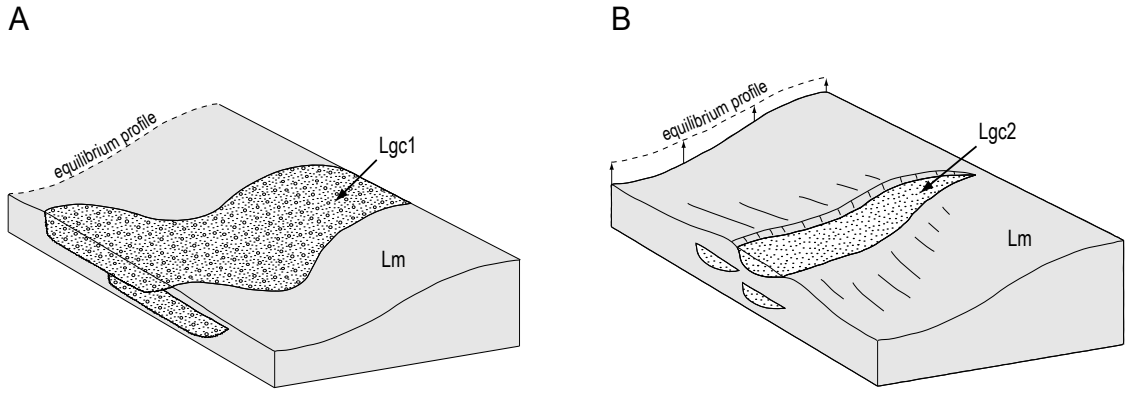

Figure 5.14: Depositional model for the Lower Todagin channel complex. A) Amalgamated channel-fills 1 and 2 were deposited in the lower part of the LTCC where the local gradient was less. B) Offstacked conglomerate bodies of channel-fill 3 in the upper part of the LTCC. High sedimentation rates and reduction in flow density resulted in elevation of the equilibrium profile, which generated more accommodation on the slope. This favored aggradation of channels, and construction and preservation of levees.

slope profile, which caused the channel/levee systems to aggrade (cf. Kneller 2003) (figure 5.14B). Following bypass of the coarsest sediment during passage of erosive turbulent flow heads, deposition in channel 3 occurred mainly from the bodies or tail-ends of less efficient turbidity flows. This would explain the overall reduction in grain-size and increase of traction structures in channel-fill 3 compared to channels 1 and 2. This evolution towards a graded depositional profile (cf. Ross et al. 1994) is consistent with normal progradation of the slope system, in which gravity flow processes are in equilibrium with sediment supply, basin subsidence, and basin physiography, and does not require the influence of tectonic input.

5.6.2 Controls at Mount Dilworth

The abundance of thick MTDs in the upper part of the Mount Dilworth section suggests an important change in boundary conditions along the western margin of the Bowser basin during Late Callovian to Early Oxfordian. Other examples of slope successions dominated by MTDs have been described by Shultz et al. (2005) and Armitage et al. (2009) for units of the Tres Pasos Formation exposed at Sierra Contreras in southern Chile. According to Armitage et al. (2009), the scale of stacking of sandstone units and MTDs is linked to an alternation of graded versus out-of grade conditions, in which mass-wasting events constitute critical phases during accretion of the slope. Additional MTDs of similar scale have also been reported from modern deep-water environments such as the Gulf of Mexico (Tripsanas et al. 2004) and the Amazon Fan (Piper et al. 1997). In these passive margin settings, the high frequency of mass-transport events is interpreted to represent repeated episodes of sea-level fall and/or salt movements. Since fluctuations of sea-level during Late Callovian to Early Oxfordian were probably in the order of a few tens of metres (Haq et al. 1987; Sahagian et al. 1996), it is unlikely that triggering of mass-transport events in the Bowser basin was related to an extended period of falling eustatic sea-level. Similarly, slope instability related to halokinetic processes can be discarded as the basement of the Bowser basin is largely dominated by magmatic arc rocks (Anderson 1993). Therefore, the main factor that contributed to upward-increasing instability at Mt. Dilworth was probably local tectonic activity, most likely due to reactivation of faults of the underlying Eskay rift system (figure 5.15). According to Ross et al. (1994), tectonic activity is one of the main mechanisms that can significantly affect the basin geometry and lead to slope overstepening, erosional mass-wasting, and sediment bypass. Spectacular architectural changes related to rapid tectonic variations have also been documented from other collisional tectonic settings such as the Eocene Talara basin (Fildani et al., 2008) and

the Cretaceous Magallanes basin (Fildani et al., 2009). In both of these analogues, modifications of provenance patterns and basin morphology controlled the type of gravity flows deposits and general layout of deep-water depositional systems. Local uplift and tilting in the vicinity of the Mount Dilworth area is consistent with our preliminary detrital zircon work which shows that the greatest population of grains was derived from local volcanic sources. The abundance of volcanic fragments in the siliciclastic sedimentary rocks at Mount Dilworth, compared with other Bowser Lake Group sandstone, suggest localized sources in the Stikine terrane. This is a strong contrast with the chert-dominated provenance typical elsewhere in the Bowser basin, where sediment was derived predominantly from the Cache Creek terrane to the northeast (Eisbacher 1985; Gabrielse 1991; Green 1992; Evenchick and Thorkelson 2005).

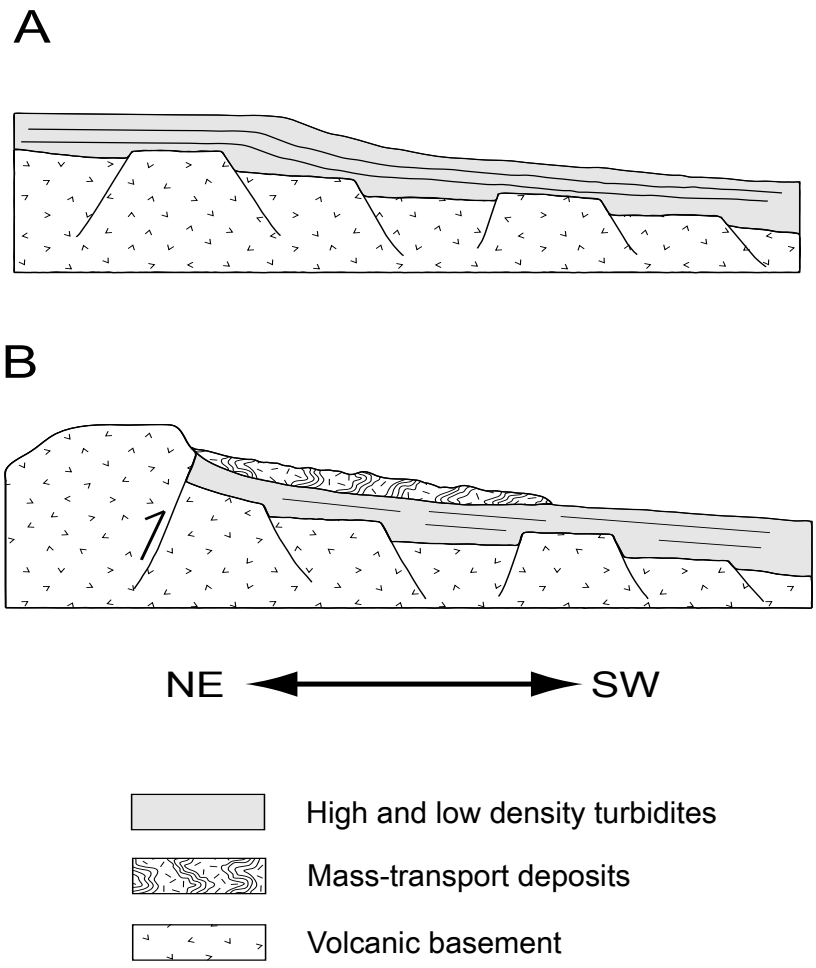

Figure 5.15: Conceptual cross-section for Mount Dilworth succession. A) Normal progradation of the Todagin assemblage over faulted basement inherited from the Eskay rift. B) Deposition of very thick MTDs derived from fault reactivation which increased sediment supply from newly uplifted souce areas and produced instability on the slope.

5.7 *Conclusions*

Detailed observation of two exceptional exposures of the Todagin assemblage provides new understanding of the depositional processes that affected channelized slope systems of the Bowser basin in Middle to Late Jurassic. The architectural organization of strata observed at Todagin Mountain indicates that emplacement of the LTCC was initially dominated by erosional processes at the base of a submarine slope which led to deposition of ungraded clast-supported conglomerate in amalgamated channels. Gradual change from erosive and amalgamated channel deposits in phases 1 and 2, to more aggradational channels in phase 3, indicates a basinward advance of graded depositional profile under sustained sediment supply. This vertical change is analogous to many turbidite slope channels reported from passive continental margins. Under increased sedimentation of low density flows, elevation of the equilibrium profile will promote aggradation and preservation of overbank deposits as the system evolves. In contrast, the great abundance of thick MTDs in the upper part of the Mount Dilworth section suggests an important change in boundary conditions along the western margin of the Bowser basin during Late Callovian to Early Oxfordian. Steepening of the depositional gradient produced instability on the slope, which interrupted the normal progradation of the deep-water system and accumulated thick MTDs. We suggest that steep normal faults associated with the development of the isolated Eskay rift along the western margin of the Bowser basin in the early Middle Jurassic were reactivated during basin inversion, and influenced the stratigraphic evolution of the deep-water architectures observed in the Todagin assemblage.

5.8 *References*

Abreu, V., Sullivan, M., Pirmez, C. and Mohrig, D. 2003. Lateral accretion packages (LAPs): an important reservoir element in deep water sinuous channels. Marine and Petroleum Geology, vol. 20, pp. 631-648.

Alldrick, D.J. 1987. Geology and mineral deposits of the Salmon River Valley, Stewart Area. British Columbia Ministry of Energy, Mines and Petroleum Resources, Open File Map 1987-22.

Alldrick, D.J. 1993. Geology and metallogeny of the Stewart mining camp, northwestern British Columbia. British Columbia Ministry of Energy, Mines and Petroleum Resources, Report 85, 105 p.

Alldrick, D.J., Nelson, J.L. and Barresi, T. 2005. Geology and mineral occurrences of the Upper Iskut River Area: tracking the Eskay rift trough northern British Columbia (Telegraph Creek NTS 104G/1,2; Iskut River NTS 104B/9, 10, 15, 16). *In:* Geological Fieldwork 2004. British Columbia Ministry of Energy, Mines and Petroleum Resources, Paper 2005-1, pp. 1-30.

Anderson, R.G. 1993. A Mesozoic stratigraphic and plutonic framework for northwestern Stikinia (Iskut River area), northwestern British Columbia, Canada, *In:* Dunne, G., McDougall, K. (Eds.), Mesozoic Paleogeography of the Western United States--II. SEPM Pacific Section, vol. 71, pp.

477-494.

Anderson, R.G. and Thorkelson, D.J. 1990. Mesozoic stratigraphy and setting for some mineral deposits in Iskut River map area, northwestern British Columbia. *In:* Current Research Part E, Geological Survey of Canada, Paper 90-1E, pp. 131-139.

Armitage, D.A., Romans, B.W., Covault, J.A. and Graham, S.A. 2009. The influence of mass-transport-deposit surface topography on the evolution of turbidite architecture: The Sierra Contreras, Tres Pasos Formation (Cretaceous), southern Chile. Journal of Sedimentary Research, vol. 79, pp. 287-301.

Arnott, R.W.C. 2007. Stratal architecture and origin of lateral accretion deposits (LADs) and conterminuous inner-bank levee deposits in a base-of-slope sinuous channel, lower Isaac Formation (Neoproterozoic), East-Central British Columbia, Canada. Marine and Petroleum Geology, vol. 24, pp. 515-528.

Barrett, T.J. and Sherlock, R.L. 1996. Geology, lithogeochemistry and volcanic setting of the Eskay Creek Au-Ag-Cu-Zn deposit, Northwestern British Columbia. Exploration Mining Geology, vol. 5, pp. 339-368.

Beaubouef, R.T. 2004. Deep-water leveed-channel complexes of the Cerro Toro Formation, Upper Cretaceous, southern Chile. AAPG Bulletin, vol. 88, pp. 1471-1500.

Beaubouef, R.T. and Friedman, J. 2000. High resolution seismic/sequence stratigraphic framework for the evolution of Pleistocene intra-slope basins, Western Gulf of Mexico: depositional models and reservoir analogs, *In:* Weimer, P., Slatt, R.M., Coleman, J.M., Rosen, N.C., Nelson, H., Bouma, A.H., Styzen, M.J., Lawrence, D.T. (Eds.), Deep-water Reservoirs of the World, 20th Annual Research Conference, Gulf Coast Section SEPM, pp. 40-60.

Bouma, A.H., 1962. Sedimentology of some Flysch Deposits: A graphic approach to facies interpretation. Elsevier, Amsterdam, 168p.

Catuneanu, O., Abreu, V., Bhattacharya, J.P., Blum, M.D., Dalrymple, R.W., Eriksson, P.G., Fielding, C.R., Fisher, W.L., Galloway, W.E., Gibling, M.R., Giles, K.A., Holbrook, J.M., Jordan, R., Kendall, C.G.S.C., Macurda, B., Martinsen, O.J., Miall, A.D., Neal, J.E., Nummeral, D., Pomar, L., Posamentier, H.W., Pratt, B.R., Sarg, J.F., Shanley, K.W., Steel, R.J., Strasser, A., Tucker, M.E. and Winker, C. 2009. Towards the standardization of sequence stratigraphy. Earth Science Reviews, vol. 92, pp. 1-33.

Clark, J.D. and Pickering, K.T. 1996. Architectural elements and growth patterns of submarine channels: application to hydrocarbon exploration. AAPG Bulletin, vol. 80, pp.194-221.

Coleman, J.M. and Prior, D.B. 1988. Mass-wasting on continental margins. Annual Review of Earth and Planetary Sciences, vol. 16, pp. 101-121.

Collinson, J.D. 1969. The sedimentology of the Grindslow Shales and the Kinderscout Grit: a deltaic complex in the Namurian of northern England. Journal of Sedimentary Petrology, vol. 39, pp. 194-221.

Covault, J.A., Normark, W.R., Romans, B.W. and Graham, S.A. 2007. Highstand fans in the California borderland: The overlooked deep-water depositional systems. Geology, vol. 35, pp. 783-786.

Crane, W.H. and Lowe, D.R. 2008. Architecture and evolution of the Paine channel complex, Cerro Toro Formation (Upper Cretaceous), Silla Syncline, Magallanes Basin, Chile. Sedimentology, vol. 55, pp. 979-1009.

Deptuck, M.E., Steffens, G.S., Barton, M. and Pirmez, C. 2003. Architecture and evolution of upper fan

channel belts on the Niger Delta slope and in the Arabian Sea. Marine and Petroleum Geology, vol. 20, pp. 649-676.

Dott, R.H.J. 1963. Dynamics of subaqueous gravity depositional processes. AAPG Bulletin, vol. 47, pp. 104-128.

Eisbacher, G.H. 1985. Pericollisional strike-slip faults and synorogenic basins, Canadian Cordillera. *In:* Biddle, K. T., Christie-Blick, N. (Eds.), Strike-slip deformation, basin formation, and sedimentation. SEPM Special Publication 37, pp. 265-282.

Eschard, R., Albouy, E., Deschamps, R., Euzen, T. and Ayub, A. 2003. Downstream evolution of turbiditic channel complexes in the Pab Range outcrops (Maastrichtian, Pakistan). Marine and Petroleum Geology, vol. 20, pp. 691-710.

Evenchick, C.A. 1991. Geometry, evolution, and tectonic framework of the Skeena Fold Belt, north-central British Columbia. Tectonics, vol. 10, pp. 527-546.

Evenchick, C.A., Gabrielse, H. and Snyder, D. 2005. Crustal structure and lithology of the northern Canadian Cordillera: alternative interpretations of SNORCLE seismic reflection lines 2A and 2b. Canadian Journal of Earth Sciences, vol. 42, pp. 1149-1161.

Evenchick, C.A. and Green, G.M. 2004. Geology, Kluea Lake, British Columbia. Geological Survey of Canada, "A" Series Map 2028A.

Evenchick, C.A. and McNicoll, V.J. 2002. Stratigraphy, structure, and geochronology of the Anyox Pendant, northwest British Columbia, and implications for mineral exploration. Canadian Journal of Earth Sciences, vol. 39, pp. 1313-1332.

Evenchick, C.A., Mustard, P.S., McMechan, M.E., Greig, C.J., Ferri, F., Ritcey, D., Smith, G., Hadlari, T. and Waldron, J.W.F. 2009. Geology, compilation geology of Bowser and Sustut basins draped on shaded relief map, north-central British Columbia. Geological Survey of Canada, Open File 5794.

Evenchick, C.A. and Thorkelson, D.J. 2005. Geology of the Spatsizi River map area, north-central British Columbia. Geological Survey of Canada, Bulletin 577, 276 p.

Fildani, A., Hessler, A.M. and Graham, S.A. 2008. Trench-forearc interactions reflected in the sedimentary fill of Talara basin, northwest Peru. Basin Research, vol. 20, pp. 305-331.

Fildani, A., Hubbard, S.M. and Romans, B.W. 2009. Stratigraphic Evolution of Deep-Water Architecture: Examples of controls and deposition styles from the Magallanes Basin, southern Chile. Outcrop Atlas and Field Guide for SEPM Research Conference, SEPM Fieldtrip Guidebook 10, 73 p.

Gagnon, J.-F., Evenchick, C.A., Waldron, J.W.F., Cordey, F. and Poulton, T.P. 2009. Jurassic subsidence history of the Hazelton Trough-Bowser Basin in the area of Todagin Mountain, north-central British Columbia. Bulletin of Canadian Petroleum Geology, vol. 57, pp. 430-448.

Ghosh, B. and Lowe, D.R. 1993. The architecture of deepwater channel complexes, Cretaceous Venado Sandstone Member, Sacramento Valley, California. *In:* Graham, S.A., Lowe, D.R. (Eds.), Advances in the Sedimentary Geology of the Great Valley Group, Sacramento Valley, California. SEPM, Pacific Section, pp. 51-65.

Gabrielse, H. 1991. Late Paleozoic and Mesozoic terrane interactions in north-central British Columbia. Canadian Journal of Earth Sciences, vol. 28, pp. 947-957.

Green, G.M. 1992. Detailed sedimentology of the Bowser Lake Group, northern Bowser Basin, north-central British Columbia. M.Sc. thesis, Department of Earth Sciences, Carleton Universiy, Ottawa, Ont.

Grove, E.W. 1986. Geology and mineral deposits of the the Unuk River - Salmon River - Anyox area.

British Columbia Ministry of Energy, Mines and Petroleum Ressources, Bulletin 63, 152 p.

Haq, B.U., Hardenbol, J. and Vail, P.R. 1987. Chronology of Fluctuating Sea Levels since the Triassic. Science, vol. 235, pp. 1156-1167.

Hickson, T. A. and Lowe, D. R. 2002. Facies architecture of a submarine fan channel-levee complex: the Juniper Ridge Conglomerate, Coalinga, California. Sedimentology, vol. 49, pp. 335-362.

Hunt, D. and Tucker, M.E. 1992. Stranded parasequences and the forced regressive wedge systems tract: deposition during base-level fall. Sedimentary Geology, vol. 81, pp. 1-9.

Ilstad, T., Elverhoi, A., Issler, D.R. and Marr, J.G. 2004. Subaqueous debris flow behaviour and its dependence on the sand/clay ratio: a laboratory study using particle tracking. Marine Geology, vol. 213, pp. 415-438.

Iverson, R.M., Reid, M.E. and LaHusen, R.G. 1997. Debris flow mobilization from landslides. Annual Review of Earth and Planetary Sciences, vol. 25, pp. 85-138.

Johansson, M. and Stow, D.A.V. 1995. A classification scheme for shale clasts in deep-water sandstones. *In:* Hartley, A.J., Prosser, D.J. (Eds.), Characterization of Deep Marine Clastic Systems. Geological Society of London, Special Publication 216, pp. 123-137.

Kneller, B. 2003. The influence of flow parameters on turbidite slope channel architecture. Marine and Petroleum Geology, vol. 20, pp. 901-910.

Kolla, V., Bourges, P., Urruty, J.M. and Safa, P. 2001. Evolution of deep-water Tertiary sinuous channel offshore Angola (west Africa) and implications for reservoir architecture. AAPG Bulletin, vol. 85, pp. 1371-1405.

Lowe, D.R. 1976. Grain flow and grain flow deposits. Journal of Sedimentary Petrology, vol. 46, pp. 188-199.

Lowe, D.R. 1979. Sediment gravity flows: their classification and some problems of application to natural flows and deposits. *In:* Doyle, L.J., Pilkey, O.H. (Eds.), Geology of continental slopes, SEPM, Special Publication 27, pp. 75-82.

Lowe, D.R. 1982. Sediment gravity flows; II. Depositional models with special references to the deposits of high-density turbidity currents. Journal of Sedimentary Petrology, vol. 52, pp. 279-297.

Marsden, H. and Thorkelson, D.J. 1992. Geology of the Hazelton volcanic belt in British Columbia: Implications for the Early to Middle Jurassic evolution of Stikinia. Tectonics, vol. 11, pp. 1266-1287.

Mayall, M. and Stewart, I. 2000. The architecture of turbidite slope channels. *In:* Weimer, P., Slatt, R.M., Coleman, J.M., Rosen, N.C., Nelson, H., Bouma, A.H., Styzen, M.J., Lawrence, D.T. (Eds.), Deep-water Reservoirs of the World. 20th Annual Research Conference, Gulf Coast Section SEPM, pp. 578-586.

McDonald, A.J., Lewis, P.D., Thomson, J.F.H., Nadaraju, G., Bartsch, R.D., Bridge, D.J., Rhys, D.A., Roth, T., Kaip, A., Godwin, C.I. and Sinclair, A.J. 1996. Metallogeny of an Early to Middle Jurassic Arc, Iskut River Area, Northwestern British Columbia. Economic Geology, vol. 91, pp. 1098-1114.

Mulder, T. and Alexander, J. 2001. The physical character of subaqueous sedimentary density flows and their deposits. Sedimentology, vol. 48, pp. 269-299.

Mutti, E and Normark, W.R. 1991. An integrated approach to the study of turbidite systems. *In:* Weimer, P., Links, M.H. (Eds.), Seismic Facies and Sedimentary Processes of Modern and Ancient Submarine Fans. Springer Verlag, New York, pp. 75-106.

Nardin, T.R., Hein, F.J., Gorsline, D.S. and Edwards, B.D. 1979. A review of mass-movement processes,

sediment accoustic characteristics, and contrasts in slope and base of slope systems versus canyon-fan-basin floor systems. *In:* Doyle, L.J., Pilkey, O.H. (Eds.), Geology of continental slopes. SEPM, Special Publication 27, pp. 61-73.

Pemberton, S.G., Spila, M., Pulham, A.J., Saunders, T., MacEachern, J.A., Robbins, D. and Sinclair, I.K. 2001. Ichnology and sedimentology of shallow to marginal marine systems: Ben Nevis and Avalon reservoirs, Jeanne d'Arc Basin. Geological Association of Canada, Special Volume 15, 343 p.

Piper, D.J.W. and Normark, W.R. 1983. Turbidite depositional patterns and flow characteristics, Navy submarine fan, California borderland. Sedimentology, vol. 30, pp. 681-694.

Piper, D.J.W., Pirmez, C., Manley, P.L., Long, D., Flood, R.D., Normark, W.R. and Showers, W. 1997. Mass-transport deposits of the Amazon Fan. *In:* Flood, R.D., Piper, D.J.W., Klaus, A., Peterson, L.C. (Eds.), Proceedings of the Ocean Drilling Program Scientific Results, vol. 155, pp. 109-146.

Pirmez, C., Beaubouef, R.T., Friedman, J. and Mohrig, D. 2000. Equilibrium profile and base-level in submarine channels: examples from Late Pleistocene systems and implications for the architecture of deep-water reservoirs. *In:* Weimer, P., Slatt, R.M., Coleman, J.M., Rosen, N.C., Nelson, H., Bouma, A.H., Styzen, M.J., Lawrence, D.T. (Eds.), Deep-water Reservoirs of the World. 20th Annual Research Conference, Gulf Coast Section SEPM, pp. 782-805.

Posamentier, H.W. and Kolla, V. 2003. Seismic geomorphology and stratigraphy of depositional elements in deep-water settings. Journal of Sedimentary Research, vol. 73, pp. 367-388.

Postma, G., Nemec, W. and Kleinspehn, K.L. 1988. Large floating clasts in turbidites: a mechanism for their emplacement. Sedimentary Geology, vol. 58, pp. 47-61.

Ramsay, J.G. 1967. Folding and Fracturing of Rocks. McGraw Hill Book Company, New York, 560p.

Reading, H.G. and Richards, M. 1994. Turbidite Systems in Deep-Water Basin Margins Classified by Grain Size and Feeder System. AAPG Bulletin, vol. 78, pp. 792-822.

Ricketts, B.D. and Evenchick, C.A. 1991. Analysis of the Middle to Upper Jurassic Bowser Basin, northern British Columbia. *In:* Current Research, Part A. Geological Survey of Canada, Paper 91-1A, pp. 65-73.

Ricketts, B.D. and Evenchick, C.A. 1999. Shelfbreak gullies; products of sea-level lowstand and sediment failure: examples from Bowser Basin, northern British Columbia. Journal of Sedimentary Research, vol. 69, pp. 1232-1240.

Ricketts, B.D., Evenchick, C.A. 2007. Evidence of different contractional styles along foredeep margins provided by Gilbert deltas: examples from Bowser Basin, British Columbia, Canada. Bulletin of Canadian Petroleum Geology, vol. 55, pp. 243-261.

Ross, W.C., Halliwell, B.A., May, J.A., Watts, D.E. and Syvitski, J.P.M. 1994. Slope readjustment: A new model for the development of submarine fans and aprons. Geology, vol. 22, pp. 511-514.

Roth, T., Thompson, J.F.H. and Barrett, T.J. 1999. The precious metal - rich Eskay Creek deposit, northwestern British Columbia. *In:* Barrie, C.T., Hannington, M.D. (Eds.), Volcanic-Associated Massive Sulfide Deposits: Processes and Examples in Modern and Ancient Settings. Reviews in Economic Geology, vol. 8, pp. 357-373.

Sahagian, D., Pinous, O., Olferiev, A. and Zakharov, V. 1996. Eustatic Curve for the Middle Jurassic-Cretaceous based on Russian Platform and Siberian Stratigraphy: Zonal Resolution. AAPG Bulletin, vol. 80, pp. 1433-1458.

Samuel, A., Kneller, B., Raslan, S., Sharp, A. and Parsons, C. 2003. Profilic deep-marine slope channels of the Nile Delta, Egypt. AAPG Bulletin, vol. 87, pp. 541-560.

Schwarz, E. and Arnott, R.W.C. 2007. Anatomy and evolution of a slope channel-complex set (Neoproterozoic Isaac Formation, Windermere Supergroup, southern Canadian Cordillera); implications for reservoir characterization. Journal of Sedimentary Research, vol. 77, pp. 89-109.

Sherlock, R.L., Roth, T., Spooner, E.T.C. and Bray, C.J. 1999. Origin of the Eskay Creek pecious metal-rich volcanogenic massive sulphide deposit: Fluid inclusion and stable isotope evidence. Economic Geology, vol. 94, pp. 803-824.

Shultz, M.R., Fildani, A., Cope, T.A. and Graham, S.A. 2005. Deposition and stratigraphic architecture of an outcropping ancient slope system: Tres Pasos Formation, Magallanes Basin, southern Chile. *In*: Hodgson, D.M., Flint, S.S. (Eds.), Submarine Slope Systems: Processes and Products. Geological Society of London Special Publication 244, pp. 27-50.

Slatt, R.M. 2000. Why outcrop characterization of turbidite systems. *In:* Bouma, A.H., Stone, C.G. (Eds.), Fine-grained Turbidite Systems. AAPG Memoir 72, pp. 181-186.

Stelting, C.E. 1985. Migratory characteristics of a mid-fan meander belt, Mississippi fan. *In:* Normark, W.R., Barnes, N.E. (Eds.), Submarine Fans and Related Turbidites Sequences. Springer, New York, pp. 283-290.

Thorkelson, D.J., Mortensen, J.K., Marsden, H. and Taylor, D.C. 1995. Age and tectonic setting of Early Jurassic episodic volcanism along the northeastern margin of the Hazelton Trough, northern British Columbia. *In:* Miller, D.M., Busby, C.J. (Eds.), Jurassic magmatism and tectonics of the North American Cordillera. Geological Society of America, Special Paper 299, pp. 83-94.

Tipper, H.W. and Richards, T.A. 1976. Jurassic stratigraphy and history of north-central British Columbia. Geological Survey of Canada, Bulletin 270, 73 p.

Tripsanas, E.K., Bryant, W.R. and Phaneuf, B.A. 2004. Slope instability interaction with halokinetic processes in a complex deep-water environment, Bryant Canyon area, northwest Gulf of Mexico. AAPG Bulletin, vol. 88, pp. 801-823.

Tripsanas, E.K., Piper, D.J.W., Jenner, K.A. and Bryant, W.R. 2008a. Submarine mass-transport facies: new perspectives on flow processes from cores on the eastern North American margin. Sedimentology, vol. 55, pp. 97-136.

Tripsanas, E.K., Piper, D.J.W. and Campbell, D.C. 2008b. Evolution and depositional structure of earthquake-induced mass-movements and gravity flows: Southwest Orphan Basin, Labrador Sea.. Marine and Petroleum Geology, vol. 25, pp. 645-662.

Chapter 6: Development of the Hazelton Trough–Bowser Basin: Implications for the Jurassic evolution of the Stikine terrane, Northern British Columbia[5]

6.1 Introduction

The Canadian Cordillera is commonly regarded as a long-lived accretionary orogen, in which successive volcanic arcs and associated subduction complexes were added to the western margin of Laurentia in late Paleozoic to Mesozoic time (e.g. Gabrielse 1991; Monger and Nokleberg 1996; Price and Monger 2000). Some of these cordilleran components, referred to as "suspect terranes" by Coney et al. (1980), possess an uncertain paleogeographic origin and are geologically different from their immediate neighbours. They include a group of pericratonic terranes generated along the North American passive margin as a series of rifted continental fragments, superimposed volcanic arcs, and marginal oceanic basins (Yukon-Tanana, Kootenay, Slide Mountain), and a second group of accreted terranes divided into an inboard Intermontane domain (Stikinia, Quesnellia, Cache Creek) and an outboard Insular domain (Alexander and Wrangellia) (Colpron et al. 2006; Colpron and Nelson 2009) (figure 6.1). Tectonic interactions between those terranes, and the precise timing of their final accretion to the passive margin of Laurentia have been subjects of much debate for some time (e.g. Monger 1977; Gabrielse 1991; Marsden and Thorkelson 1992; Nelson and Mihalynuk 1993; Mihalynuk et al. 2004; English and Johnston 2005; Colpron et al. 2006; Evenchick et al. 2007; Johnston and Borel 2007; Johnston 2001, 2008; Colpron and Nelson 2009; Hildebrand 2009). The controversy is largely based on conflicting paleontological, geochronologic, structural, paleomagnetic, stratigraphic, geochemical, and provenance studies.

In this chapter, we discuss subsidence profiles (Chapter 4) and detrital zircon data (Chapter 2) from the Hazelton trough–Bowser basin, which developed entirely on Stikinia during Jurassic time. New stratigraphic correlations and paleontological data for the Hazelton trough–Bowser basin are also considered (Chapters 2, 3 and 5). Formation of the Hazelton trough–Bowser basin in the Early to Middle Jurassic yields valuable insights on the possible interaction of Stikinia with adjacent terranes, and provides new information on the evolution of the Canadian Cordillera.

[5] *A version of this chapter will be submitted for publication under the authorship of Gagnon, J.-F., Waldron, J.W.F. and Heaman, L.M.*

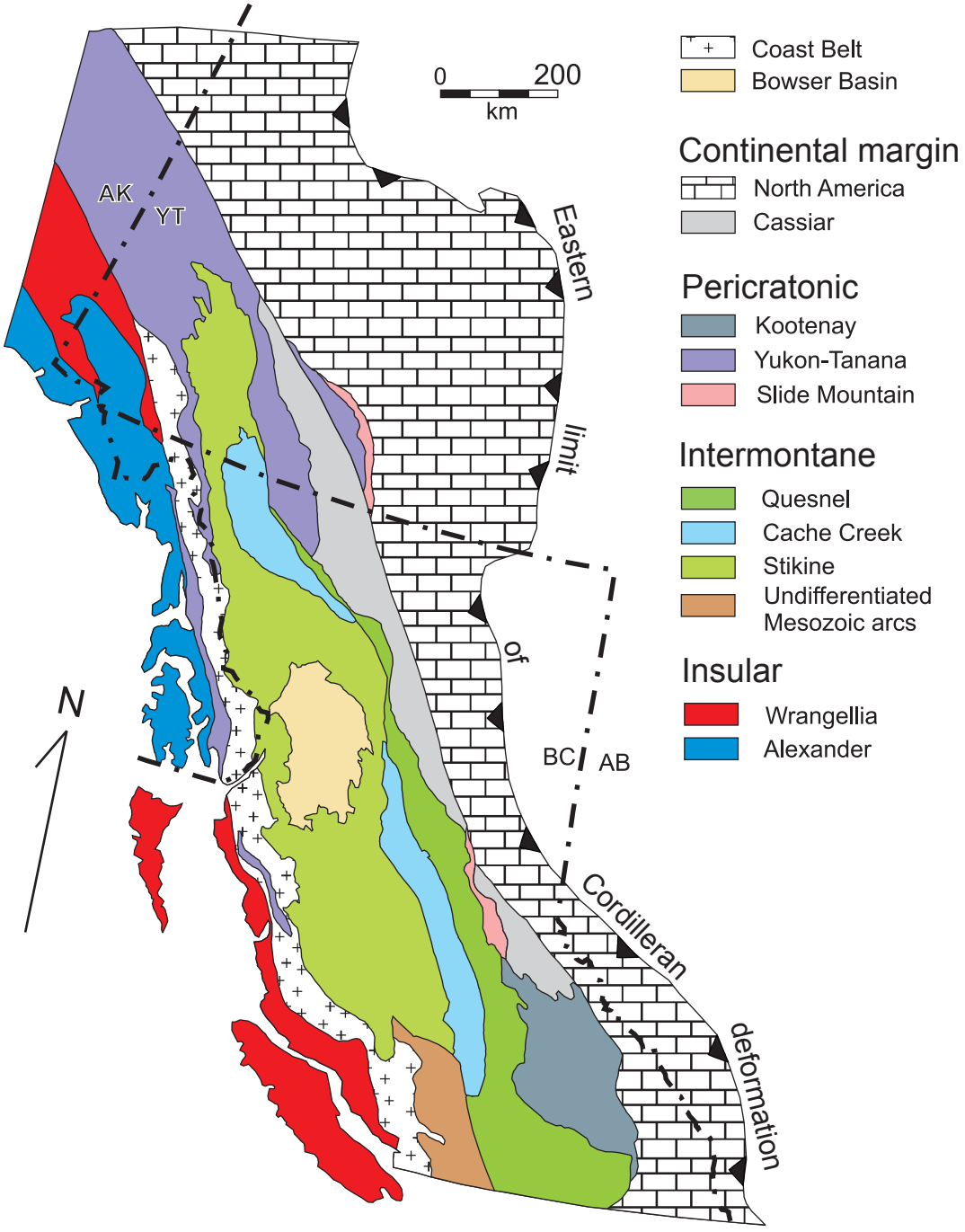

Figure 6.1: Terrane map of the Canadian Cordillera showing the location of the Bowser basin. Tectonic elements shown here are subdivided into four groups: continental margin assemblage, pericratonic terranes, accreted Intermontane domain, and accreted Insular domain. Modified after Colpron et al. (2006) and Colpron and Nelson (2009).

6.2 *Early Mesozoic terrane interaction*

The Late Triassic-Early Jurassic tectonic evolution of the Canadian Cordillera was characterized by eastward obduction of Quesnellia and the Slide Mountain terrane onto pericratonic terranes near the margin of the North American craton (Murphy et al. 1995). Further outboard, oceanic rocks of the Cache Creek terrane were probably being subducted underneath the volcanic arc rocks of Stikinia (Nelson and Mihalynuk 1993; Mihalynuk et al. 1994; English and Johnston 2005). Although Quesnellia and Stikinia contain rocks of similar age and lithology, the former has stratigraphic and structural ties with the Yukon-Tanana (YTT), Slide Mountain, and Kootenay terranes dating back to Permian time (ca. 285 Ma) (Nelson et al. 2006). Triassic clastic strata of Quesnellia and YTT also contain significant Proterozoic to Archean detrital zircon populations, which indicate that they were receiving detritus ultimately derived from the North American craton to the east (Roback and Walker 1995; Nelson and Friedman 2004; Nelson and Gehrels 2007). In contrast, the oldest detrital zircon population reported from Stikinia is Late Mississipian in age (ca. 320 Ma) (Greig and Gehrels 1995; McNicoll et al. 2005; Evenchick et al. 2007).

In the current configuration of the Intermontane Belt, Stikinia and Quesnellia are separated by the Cache Creek terrane (figure 6.1). Late Paleozoic to Early Jurassic oceanic rocks of the Cache Creek terrane contain distinctive Permian fauna of Tethyan affinity, which contrast with the McCloud fauna characteristic of adjacent terranes (Monger and Ross 1971; Orchard et al. 2001). Therefore, Cache Creek probably originated in low latitudes far from the North American margin. In order to explain the incorporation of the exotic Cache Creek terrane between less far-travelled magmatic arcs, Nelson and Mihalynuk (1993) proposed an oroclinal enclosure model involving anticlockwise rotation of Stikinia. In an alternative model, Johnston and Borel (2007) suggested that accretion of the Cache Creek terrane with Stikinia was initiated in the Middle to Late Triassic (ca. 230 Ma) at >10 000 km from the North American margin. This was followed by a late Early Jurassic (ca. 180 Ma) collision with a ribbon continent comprising pericratonic terranes and the Cassiar platform, located at > 4 000 km from the autochtonous margin (Johnston and Borel 2007).

6.3 *Tectonic model for development of the Hazelton trough*

Lower to Middle Jurassic volcanic rocks and associated sedimentary rocks of the Hazelton Group accumulated in the Hazelton trough during the last major volcanic-arc episode recorded on Stikinia (Tipper and Richards 1976). The Hazelton Group unconformably overlies augite-phyric basaltic flows and associated sedimentary rocks of the Stuhini/Takla Group (Anderson 1993; MacIntyre et al. 2001), an Upper Triassic

magmatic arc built on lower Devonian to upper Permian basement known as the Stikine assemblage (Monger 1977; Brown et al. 1991; Gunning et al. 2006). Regional lithostratigraphic correlations of depositional units within the Hazelton Group suggest that the Hazelton trough evolved as an extensional basin, during and after significant arc-related magmatic activity on Stikinia (Chapter 2). Calc-alkaline volcanogenic rocks of the lower Hazelton Group are abundant at the base of the succession, and are disconformably overlain by basinal rocks of the upper Hazelton Group over a diachronous contact (Chapter 2). An extensional origin for the Hazelton trough is consistent with rapid tectonic subsidence rates observed in the vicinity of Todagin Mountain during Pliensbachian to Early Toarcian time (ca. 190-180 Ma) (Gagnon et al. 2009; Chapter 4), and with deposition of rift-related volcanic flows of the Cold Fish Volcanics near Joan Lake (Thorkelson et al. 1995). According to Thorkelson et al. (1995), Upper Sinemurian-Lower Pliensbachian biomodal felsic-mafic volcanic rocks of the Cold Fish Volcanics accumulated in the back-arc area of a coeval magmatic arc represented by calc-alkaline volcanic rocks the Toodoggone formation to the east (Diakow et al. 1991; Duuring et al. 2009). This tectonic setting, involving an east-facing arc system with southwestward subduction of Cache Creek oceanic crust underneath Stikinia (in present coordinates), is consistent with the tectonic model proposed by English and Johnston (2005) for generation of the Whitehorse trough (figure 6.2A). In their model, English and Johnston (2005) interpreted the Whitehorse trough as an elongated arc-marginal sedimentary basin that originated as a fore-arc basin located between the arc magmatic rocks of Stikinia and the accretionary complex of the Cache Creek terrane. The infill of the Whitehorse trough consists mostly of Lower Sinemurian to Middle Bajocian clastic units of the Laberge Group that were deposited above the arc-related Kutcho assemblage of Stikinia (Gabrielse 1998; English and Johnston 2005). The Laberge Group also contains detritus from the Upper Triassic Stuhini Group and the Lower Jurassic Hazelton Group, which clearly indicates that Stikinia was the major source of sediments (Gabrielse 1998). Therefore, it appears that these tectonic elements were linked together by Late Triassic-Early Jurassic time (ca. 200 Ma) as a single arc system, and recorded the evolution of a convergent margin until closure of the Cache Creek ocean and obduction of the Cache Creek terrane above Stikinia along the southwest-verging Nahlin and King Salmon faults in the Middle Jurassic (ca. 172 Ma) (Gabrielse 1991; Mihalynuk et al. 2004; Evenchick and Thorkelson 2005).

Establishment of stratigraphic links between Stikinia and YTT as early as Late Triassic time has been postulated by several authors. In the northernmost portion of Stikinia, Werner (1977) and Bultman (1979) identified metamorphic clasts in a unit of

Triassic conglomerate which they interpreted to be derived from YTT. Further west, Aleinikoff et al. (1987) and Dusel-Bacon et al. (1995) correlated granitic plutons of Late Triassic to Early Jurassic age across the cryptic boundary of these two terranes. However, the original juxtaposition geometry was obliterated by emplacement of the Middle Cretaceous to Eocene Coast Mountain Batholith, with the result that this inferred relationship cannot be verified (figure 6.1). In addition, the evolved ε_{Nd} isotopic composition observed in calc-alkaline rocks of YTT contrasts drastically with the more juvenile, mantle-derived isotopic composition of the Stikine crust (Samson et al. 1989, 1991). This suggests that these two terranes evolved separately for the entire duration of their volcanic arc activity, which in the case of Stikinia, ended in late Early Jurassic time (ca. 180 Ma). Furthermore, upper Hazelton Group sedimentary rocks also yield unevolved isotopic values (Samson et al. 1989), suggesting that YTT did not act as a significant sediment source for the evolving Hazelton trough. This is consistent with our U-Pb detrital zircon data from basal sandstone of the Smithers Formation, which shows no input of Precambrian zircons (Chapter 2) and with the data of McNicoll et al. (2005) and Evenchick et al. (2007), who record no Precambrian zircon in the overlying Bowser Lake Group (BLG). Detrital zircon ages from sample MC022A at Quinlan Mountain show a strong population at 172.4 +/- 1.2 Ma, and minor peaks at ca. 192 Ma and ca. 202 Ma. Nevertheless, the debate regarding timing of amalgamation of Stikinia and YTT would greatly benefit from additional detrital zircon provenance studies in coarse-grained units of the upper Hazelton Group.

6.4 Waning volcanism and marine transgression of the Hazelton arc

Widespread deposition of mainly sedimentary rocks of the upper Hazelton Group (Chapter 2) records declining volcanic activity in Stikinia in Late Pliensbachian–Early Toarcian time (ca. 183 Ma). Exponentially decreasing subsidence rates observed at the Todagin Mountain section are consistent with thermal contraction of the Hazelton arc (Gagnon et al. 2009; Chapter 4). In the southern portion of the basin, lowermost coarse grained strata of the siliciclastic Smithers Formation, in parts characterized by a *Skolithos* ichnofacies assemblage, are overlain by extensively bioturbated siltstone and fine-grained sandstone representative of the *Cruziana* ichnofacies (Chapter 3), recording a transgressive trend consistent with thermal subsidence and rising sea-level relative to the basement of Stikinia on which the sediments were deposited. Transgression of the waning volcanic arc culminated in Late Toarcian-Early Aalenian with establishment of deep-water conditions and initial deposition of a condensed section comprised of thinly bedded siliceous mudstone and tuff ("pyjama beds") of the Quock Formation over a regional

flooding surface (Chapter 2).

6.5 *Late stage extensional volcanism on the western margin of the Hazelton trough: the Eskay rift*

Units of the Quock Formation are widely correlated throughout much of the Hazelton trough. However, in the Iskut River area, contemporaneous strata of the upper Hazelton Group are dominated by very thick piles of basaltic rocks, fanglomerates, and rhyolite domes, suggesting that rifting continued into the Middle Jurassic (Chapter 2). Isolated rifting on the northwestern margin of Stikinia in Late Toarcian-Middle Bajocian time (ca. 178-168 Ma) is also well documented from volcanically hosted massive sulphide mineralized units of the Iskut River Formation at the Eskay Creek mine (e.g. Ettlinger 1992; Bartsch 1993; Nadaraju 1993; Sherlock et al. 1994; McDonald et al. 1996; Roth 2002). The extreme thickness change of lithological units within the Iskut Formation is consistent with fault-controlled subsidence in an extensional setting, which compartmentalized multiple sub-basins and isolated volcanic feeders.

Inception of rift-related volcanism at Eskay Creek occurred after the significant decrease of back-arc volcanism associated with extension in the main axis of the Hazelton trough, and probably represents an independent rifting event (Chapter 2). However, the narrow age bracket of the Iskut River Formation (ca. 178-168 Ma) overlaps in time with final amalgamation of Stikinia and the Cache Creek subduction complex (figure 6.2B). This deformational event is constrained by the age of the youngest blueschists in the Cache Creek terrane (173 +/- 0.8 Ma; Mihalynuk et al. (2004), and by the age of the oldest post-kinematic intrusions that stitched the two domains together (ca. 172 Ma; Bath 2003; Mihalynuk et al. 1992). Therefore, cessation of volcanism in the Hazelton trough appears to coincide not only with decelerating subsidence rates regionally, but is also coeval with initiation of localized rifting in the Iskut River area. This could possibly reflect plate reorganization during a protracted period of terrane accretion, and/or might be related to subduction reversal under Stikinia. In early Middle Jurassic, the long-lived west-dipping subduction on the eastern margin of Stikinia could have been replaced by east-dipping subduction and associated transtension on its western margin, which could have triggered extensional volcanism at Eskay Creek (figure 6.2B). Eventual exhumation of the Cache Creek subduction complex along syn-collisional contractional structures, such as the southwest-vergent King Salmon and Nahlin faults, provided a new source of sediment which led to deposition of the BLG above the thermally subsiding Hazelton trough (Gabrielse 1991; Evenchick and Thorkelson 2005) (figure 6.2B).

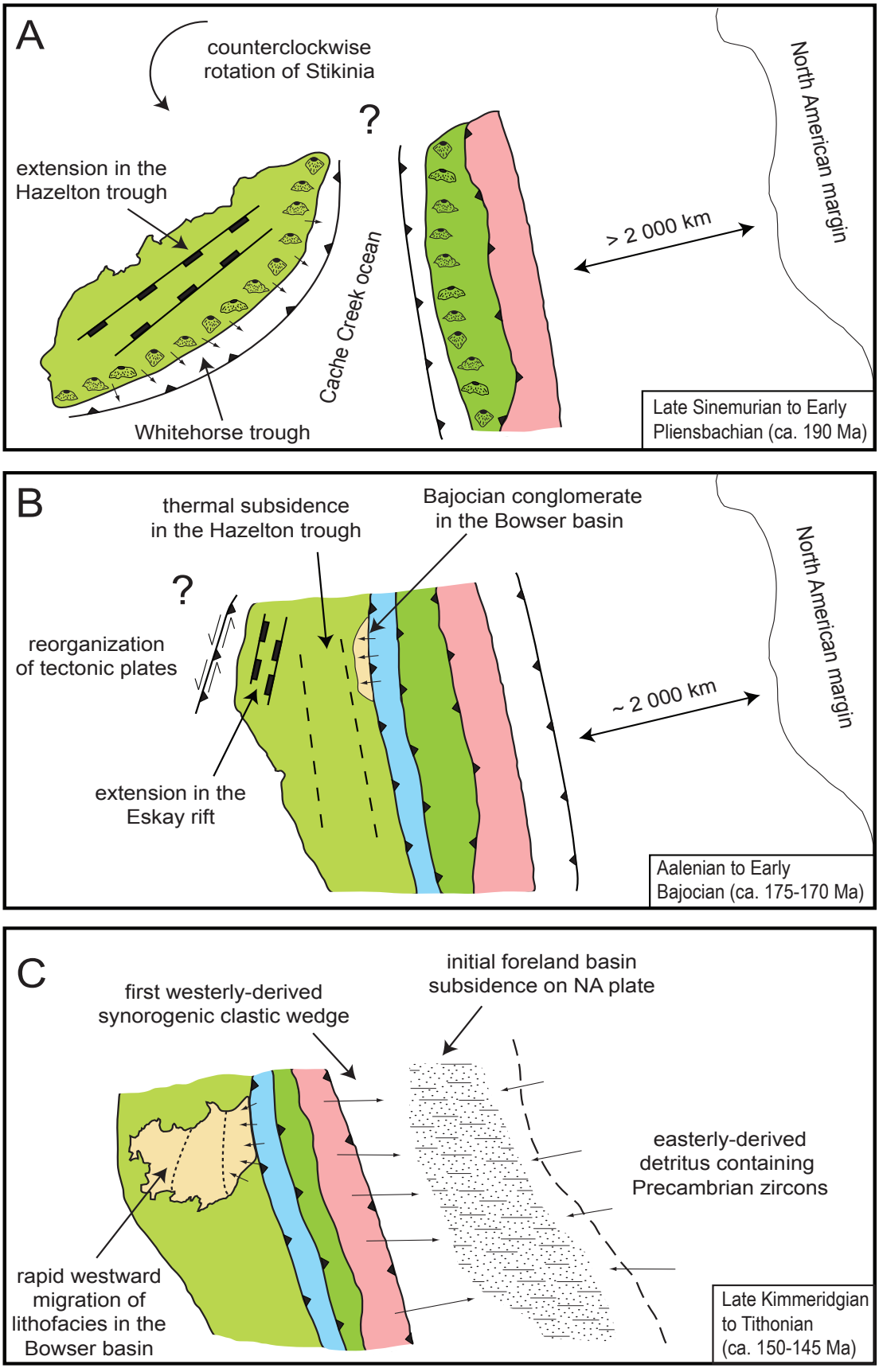
A
counterclockwise
rotation of Stikinia
?
extension in the
Hazelton trough
Cache Creek ocean
> 2 000 km
North American margin
Whitehorse trough
Late Sinemurian to Early
Pliensbachian (ca. 190 Ma)
B
thermal subsidence
in the Hazelton trough
Bajocian conglomerate
in the Bowser basin
?
reorganization
of tectonic plates
~ 2 000 km
North American margin
extension in the
Eskay rift
Aalenian to Early
Bajocian (ca. 175-170 Ma)
C
initial foreland basin
subsidence on NA plate
first westerly-derived
synorogenic clastic wedge
easterly-derived
detritus containing
Precambrian zircons
rapid westward
migration of
lithofacies in the
Bowser basin
Late Kimmeridgian
to Tithonian
(ca. 150-145 Ma)

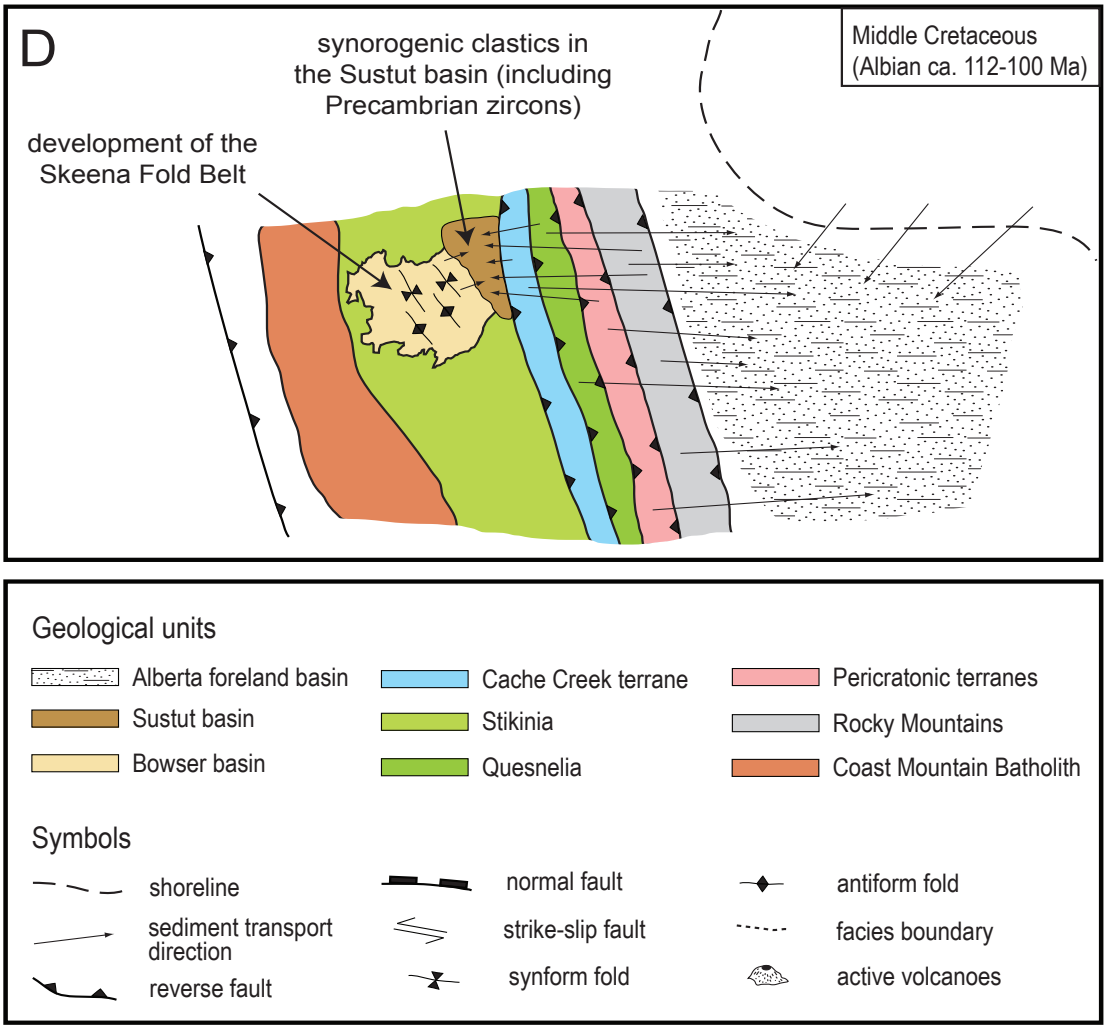

Figure 6.2: Conceptual tectonic model showing paleogeographic maps for the Early Jurassic through Middle Cretaceous. A) Westward-directed subduction underneath Stikinia during Late Sinemurian–Early Pliensbachian was responsible for volcanic arc magmatism, generation of the Hazelton trough in the back-arc area, and accumulation of arc-derived detritus in the fore-arc Whitehorse trough. Entrapment of the exotic Cache Creek terrane probably resulted from counter-clockwise rotation of the Stikine terrane. B) Closure of the Cache Creek ocean in the early Middle Jurassic resulted in the obduction of a subduction complex between Stikinia and the formally accreted Quesnel terrane and pericratonic terranes. Cessation of subduction underneath the eastern margin of Stikina was associated with a decrease in arc volcanism, and thermal subsidence in the Hazelton trough. Reorganization of tectonic plates triggered extension and rift-related volcanism on the western margin of Stikinia. Initial deposition of Cache Creek derived conglomerate in the Bowser basin began in the Bajocian. C) Collision of the formally accreted group of terranes with the autochthonous North American margin in Late Jurassic triggered flexural subsidence on the platform and accumulation of the first westerly-derived clastic wedge in the Alberta Foreland basin. D) The Middle Cretaceous was characterized by a major period of ductile deformation, metamorphism and magmatism in the Coast Belt. This was associated with development of the Skeena Fold Belt on Stikinia and northeast-directed thrust faulting and metamorphism in the Omineca Belt and Foreland Belt. First deposition of easterly-derived metamorphic clasts in the Sustut basin, including Precambrian zircon grains. Sources of information include Eisbacher (1974);

Tipper and Richards (1976); McDonough and Simony (1988); Gabrielse (1991); Nelson and Mihalynuk (1993); Poulton et al. (1994); Murphy et al. (1995); Thorkelson et al. (1995); Evenchick et al. (2001); English and Johnston (2005); Evenchick and Thorkelson (2005); Evenchick et al. (2007); Johnston and Borel (2007).

6.6 Bowser Lake Group: implications for terrane amalgamation

It is generally accepted that the high proportion of radiolarian chert clasts in coarse-grained depositional units of the BLG records a provenance link between the Cache Creek terrane and Stikinia from Bajocian time onwards (Tipper and Richards 1976; Eisbacher 1985; Gabrielse 1991; Green 1992). In addition, recent detrital zircon provenance studies in Middle Jurassic to Lower Cretaceous BLG rocks have shown that the dominant population in each sample consistently falls within the paleontologically determined depositional age of the rocks (McNicoll et al. 2005). In their interpretation, McNicoll et al. (2005) suggested that wind-blown ash from synsedimentary volcanism probably introduced contemporaneous zircons into the evolving Bowser basin. Although very few grains yielded ages as old as Late Devonian (ca. 360 Ma), no Precambrian zircon were reported; this suggests that the North American craton did not act as a source of sediment during deposition of the entire BLG (Evenchick et al. 2007).

Detrital zircon data from sample LT035A in Upper Callovian-Lower Oxfordian BLG strata near Mount Dilworth yielded two main populations of grains at 164 +/- 2 Ma and 196.4 +/- 2.0 Ma respectively (Chapter 2). Although the youngest population observed is consistent with the depositional age of the rocks, it does not constitute the most significant peak. This is slightly different from the data obtained by McNicoll et al. (2005) in coeval strata elsewhere in the basin. Instead, the greatest population of grains ranges in age from ca. 180-220 Ma, with minor inputs as old as ca. 390 Ma; no Precambrian zircons were recovered in sample LT035A at Mount Dilworth.

This anomaly in the provenance data, combined with the occurrence of very thick mass-transport deposits in deep-water strata of the Todagin assemblage, is interpreted to indicate rejuvenation of a local source area following reactivation of faults inherited from the restricted Eskay rift (Chapter 5). Reactivation of pre-existing structures during basin inversion in early Late Jurassic on the western margin of the Bowser basin is consistent with the model presented by van der Heyden (1992) for timing of initial collision between the Insular and the Intermontane terranes (figure. 6.1). According to van der Heyden (1992), intrusion of granitoids, ductile deformation, and metamorphism dated at ca. 160-155 Ma in the central Coast Mountains suggest that Stikinia and the Alexander terrane were colliding with each other at that time. Although the data presented here can not clearly discriminate between models for amalgamation of the Insular and Intermontane

domains in the Middle to Late Jurassic (McClelland et al. 1992; van der Heyden 1992) or the Middle Cretaceous (Monger et al. 1982; Monger and Nokleberg 1996), they provide evidence that Stikinia and the Alexander terrane might have been in contact as early as the Middle to Late Jurassic.

Palinspastic reconstruction of Stikinia, which accounts for ~800 km of right-lateral strike-slip displacement during Cretaceous and Eocene time, places the Bowser basin on the same latitude as the southern Alberta foreland basin in Aalenian-Bajocian time (Gabrielse et al. 2006; Evenchick et al. 2007). In a recent synthesis by Evenchick et al. (2007), both the Bowser basin and the Alberta foreland basin were interpreted to have received detritus from the rising Omineca highland, which is composed predominantly of Proterozoic to Paleozoic rocks formed on the margin of the North American craton, and previously accreted pericratonic terranes. Although the Alberta foreland basin started to receive sediments from the Columbian Orogen as early as the Bajocian (Fuentes et al. 2009), the first westerly-derived orogenic clastic wedge indicative of increased sediment supply and foreland basin subsidence only began in Kimmeridgian-Tithonian time (ca. 152 Ma) with the accumulation of the coarsening- and shallowing-upward Kootenay Group (Poulton et al. 1994) (figure 6.2C). On the other hand, the Bowser basin experienced an increase in subsidence much earlier, in Bathonian and Callovian time (ca. 167 to 161 Ma) (Gagnon et al. 2009; Chapter 4). Extensive paleontological data in Late Jurassic BLG rocks suggest that the Bowser basin was characterized by a rapid westward migration of lithofacies (Evenchick et al. 2001; 2009) (figure 6.2C). This rapid progradation of deltaic and terrestrial lithofacies over deep-marine lithofacies indicate that sediment supply progressively out-paced subsidence rates and filled the basin. Furthermore, unlike the exponentially increasing subsidence rates observed for the Alberta foreland basin from the middle Early Cretaceous (ca. 127 Ma) onwards (Fuentes et al. 2009), the concave-upward form of the tectonic subsidence curve for the Bowser basin suggests that the latter was not a typical foreland basin (Chapter 4).

The absence of Precambrian detrital zircon grains in strata of the BLG also strongly suggests that these basins were sourced from a different hinterland (McNicoll et al. 2005; Chapter 2). In their proposed tectonic model, Evenchick et al. (2007) attributed this discrepancy to the position of an hypothetic drainage divide that separated the rising Omineca highland into a western (Stikinia, Cache Creek, Quesnellia) and eastern component (pericratonic terranes, North American margin). Alternatively, amalgamation of Stikinia and the Cache Creek terrane outboard of the accreted pericratonic terranes and the North American margin could also explain the absence of recycled Precambrian zircons in BLG strata (figure 6.2). In a controversial model, Johnston (2001, 2008) and

Hildebrand (2009) suggested that collision of the intermontane and pericratonic terranes in Late Triassic-Early Jurassic occurred entirely within Panthalassa, at a location far removed from the North American platform. This orogeny resulted in the formation of a ribbon continent, termed SAYBIA or RUBIA, which was subsequently accreted to the autochthonous margin in the Late Cretaceous (Johnston 2001, 2008; Hildebrand 2009). Although our results regarding the evolution of the Hazelton trough–Bowser basin do not resolve the more highly disputed aspects of the ribbon continent model (e.g. location of a cryptic Late Cretaceous suture, exotic nature of the Cassiar carbonate platform, mid-Cretaceous westward subduction beneath the eastern margin of SAYBIA, etc.), they are consistent with the amalgamation of juvenile intermontane terranes away from the autochthonous margin during the Middle Jurassic. Assuming convergence rates at subduction zones of about 10 cm/a, amalgamation of Stikinia with the Quesnel/pericratonic terranes in the Middle Jurassic could have occurred at ~2000 km away from the North American margin (figure 6.2).

6.7 Conclusions

The Early to Middle Jurassic evolution of the Stikine terrane was characterized by intense arc-related volcanism and two independent rifting events. Establishment of a mature east-facing arc system in the Sinemurian-Pliensbachian led to extension in the back-arc region of Stikinia, which generated the Hazelton trough. Cessation of subduction on the eastern margin of the Stikine arc at the Toarcian-Aalenian boundary was coeval with closure of the Cache Creek marine basin. This protracted period of terrane accretion triggered a profound reorganization of the tectonic plates neighbouring Stikinia, which was responsible for the decrease of volcanic activity in the Hazelton trough, and inception of rift-related volcanism and sedimentation in the Iskut River area. Eventual exhumation of the Cache Creek subduction complex in the Bajocian provided a new source of sediment which led to deposition of the Bowser Lake Group on Stikinia. The absence of Precambrian zircon grains in strata of the Bowser Lake Group indicates that the autochthonous margin did not supply detritus to the Bowser basin. The latter either implies that: 1) Stikinia and the western margin of North America were kinematically connected by the Middle Jurassic but an effective drainage divide in the Omineca highland prevented fluvial transport of craton-derived material to the Bowser basin (cf. Evenchick et al. 2007); or 2) final amalgamation of Stikinia and the Cache Creek terrane occurred relatively far away from the autochthonous margin, probably a few thousand kilometres into Panthalassa (cf. Johnston 2008). The data presented in this study suggests that unconventional ideas, such as the ribbon continent model, are

compatible with the tectonic evolution of the Hazelton trough–Bowser basin and should be investigated more thoroughly.

6.8 *References*

Aleinikoff, J.N., Dusel-Bacon, C., Foster, H.L. and Nokleberg, W.J. 1987. Lead isotopic fingerprinting of tectonostratigraphic terranes, east-central Alaska. Canadian Journal of Earth Sciences, vol. 24, pp. 2089-2098.

Anderson, R.G. 1993. A Mesozoic stratigraphic and plutonic framework for northwestern Stikinia (Iskut River area), northwestern British Columbia, Canada. *In:* Dunne, G., McDougall, K. (Eds.), Mesozoic Paleogeography of the Western United States--II. Society of Economic Paleontologists and Mineralogists, Pacific Section, vol. 71, pp. 477-494.

Bartsch, R.D. 1993. A rhyolite flow dome in the upper Hazelton Group, Eskay Creek area (104B/9, 10). *In:* Geological Fieldwork 1992. British Columbia Ministry of Energy, Mines and Petroleum Resources, paper 1993-1, pp. 331-334.

Bath, A. 2003. Middle Jurassic granitic plutons within the Cache Creek terrane and their aureoles: impications for terrane emplacement and deformation. *In:* Geological Fieldwork 2002. British Columbia Ministry of Energy, Mines and Petroleum Resources, Paper 2003-1, pp. 51-55.

Brown, D.A., Gunning, M.H., Orchard, M.J. and Bamber, W.E. 1991. Stratigraphic evolution of the Paleozoic Stikine assemblage in the Stikine and Iskut rivers area, northwestern British Columbia. Canadian Journal of Earth Sciences, vol. 28, pp. 958-972.

Bultman, T.R. 1979. Geology and Tectonic history of the Whitehorse Trough west of Atlin, British Colombia. Ph.D. thesis, Yale University, New Haven, Connecticut, 284 p.

Colpron, M., Nelson, J.L. and Murphy, D.C. 2006. A tectonostratigraphic framework for the pericratonic terranes of the northern Canadian Cordillera. *In:* Colpron, M., Nelson, J.L. (Eds.), Paleozoic Evolution and Metallogeny of Pericratonic Terranes at the Ancient Pacific Margin of North America. Geological Association of Canada, Special Paper 45, pp. 1-23.

Colpron, M. and Nelson, J.L. 2009. A Palaeozoic Northwest Passage: Incursion of Caledonian, Baltican and Siberian terranes into esatern Panthalassa, and the early evolution of the North American Cordillera. *In:* Cawood, P.A., Kroner, A. (Eds.), Earth Accretionary Systems in Space and Time. The Geological Society of London, Special Publication 318, pp. 273-307.

Coney, P.J., Jones, D.L. and Monger, J.W.H. 1980. Cordilleran suspect terranes. Nature, vol. 288, pp. 329-333.

Diakow, L.J., Panteleyev, A. and Schroeter, T.G. 1991. Jurassic Epithermal Deposits in the Toodoggone River Area, Northern British Columbia: Examples of Well-Preserved, Volcanic-Hosted, Precious Metal Mineralization. Economic Geology, vol. 86, pp. 529-554.

Dusel-Bacon, C., Hansen, V.L. and Scala, J.A. 1995. High-pressure amphibolite facies dynamic metamorphism and the Mesozoic tetonic evolution of the ancient continental margin, east-central Alaska. Journal of Metamorphic Geology, vol. 15, pp. 9-24.

Duuring, P., Rowins, S.M., McKinley, B.S.M., Dickinson, J.M., Diakow, L.J., Kim, Y.-S. and Creaser, R.A. 2009. Examining potential genetic links between Jurassic porphyry Cu-Au+/-Mo and epithermal Au+/-Ag mineralization in the Toodoggone district of North-Central British Columbia, Canada. Mineralium Deposita, vol. 44, pp. 463-496.

Eisbacher, G.H. 1974. Deltaic sedimentation in the northeastern Bowser Basin, British Columbia.

Geological Survey of Canada, Paper 73-33, 13 pp.

Eisbacher, G.H. 1985. Pericollisional strike-slip faults and synorogenic basins, Canadian Cordillera. *In:* Biddle, K.T., Christie-Blick, N. (Eds.), Strike-slip deformation, basin formation, and sedimentation. Society of Economic Paleontologists and Mineralogists, Special Publication 37, pp. p. 265-282.

English, J.M. and Johnston, S.T. 2005. Collisional orogenesis in the northern Canadian Cordillera: Implications for Cordilleran crustal structure, ophiolite emplacement, continental growth, and the terrane hypothesis. Earth and Planetary Science Letters, vol. 232, pp. 333-344.

Ettlinger, A.D. 1992. Hydrothermal alteration and brecciation underlying the Eskay Creek polymetallic massive sulphide deposit (104B/9W). *In:* Geological Fieldwork 1991. British Columbia Ministry of Energy, Mines and Petroleum Resources, Paper 1992-1, pp. 535-541.

Evenchick, C.A. and Thorkelson, D.J. 2005. Geology of the Spatsizi River map area, north-central British Columbia. Geological Survey of Canada, Bulletin 577, 276 p.

Evenchick, C.A., Poulton, T.P., Tipper, H.W. and Braidek, I. 2001. Fossils and facies of the northern two-thirds of the Bowser Basin, British Columbia. Geological Survey of Canada, Open File 3956.

Evenchick, C.A., McMechan, M.E., McNicoll, V.J. and Carr, S.D. 2007. A synthesis of the Jurassic-Cretaceous tectonic evolution of the central and southeastern Canadian Cordillera: exploring links across the orogen. *In:* Sears, J.W., Harms, T.A., Evenchick, C.A. (Eds.), Whence the mountains? The contribution of Raymond A. Price. Geological Society of America, Special Publication 433, pp. 117-145.

Evenchick, C.A., Mustard, P.S., McMechan, M.E., Greig, C.J., Ferri, F., Ritcey, D., Smith, G., Hadlari, T. and Waldron, J.W.F. 2009. Geology, Compilation Geology of Bowser and Sustut Basins Draped on Shaded Relief Map, North-central British Columbia. Geological Survey of Canada, Open File 5794.

Fuentes, F., DeCelles, P.G. and Gehrels, G.E. 2009. Jurassic onset of foreland basin deposition in northwestern Montana, USA: Implications for along-strike synchroneity of Cordilleran orogenic activity. Geology, vol. 37, pp. 379-382.

Gabrielse, H. 1991. Late Paleozoic and Mesozoic terrane interactions in north-central British Columbia. Canadian Journal of Earth Sciences, vol. 28, pp. 947-957.

Gabrielse, H. 1998. Geology of the Cry Lake and Dease Lake map areas, north-central British Columbia. Geological Survey of Canada, Bulletin 504, 147 p.

Gabrielse, H., Murphy, D.C. and Mortensen, J.K. 2006. Cretaceous and Cenozoic dextral orogen-parallel displacements, magmatism, and paleogeography, north-central Canadian Cordillera. *In:* Haggart, J.W., Enkin, R.J., Monger, J.W.H. (Eds.), Paleogeography of the North American Cordillera: Evidence For and Against Large-Scale Displacements. Geological Association of Canada, Special Paper 46, pp. 255-276.

Gagnon, J.-F., Evenchick, C.A., Waldron, J.W.F., Cordey, F. and Poulton, T.P. 2009. Jurassic subsidence history of the Hazelton Trough-Bowser Basin in the area of Todagin Mountain, north-central British Columbia, Canada. Bulletin of Canadian Petroleum Geology, vol. 57, pp. 430-448.

Green, G.M. 1992. Detailed sedimentology of the Bowser Lake Group, northern Bowser Basin, north-central British Columbia. M.Sc. thesis, Department of Earth Sciences, Carleton Universiy, Ottawa, 197 p.

Greig, C.J. and Gehrels, G.E. 1995. U-Pb zircon geochronology of Lower Jurassic and Paleozoic Stikinian

strata and Tertiary intrusions, northwestern British Columbia. Canadian Journal of Earth Sciences, vol. 32, pp. 1155-1171.

Gunning, M.H., Hodder, R.W. and Nelson, J.L. 2006. Contrasting volcanic styles and their tectonic implications for the Paleozoic Stikine assemblage, western Stikine terrane, northwestern British Columbia. *In:* Colpron, M., Nelson, J.L. (Eds.), Paleozoic Evolution and Metallogeny of Pericratonic Terranes at the Ancient Pacific Margin of North America. Geological Association of Canada. Special Paper 45, pp. 201-227.

Hildebrand, R.S. 2009. Did Westward Subduction Cause Cretaceous-Tertiary Orogeny in the North American Cordillera? Geological Society of America, Special Paper 457, 71 p.

Johnston, S.T. 2001. The Great Alaskan Terrane Wreck: reconciliation of paleomagnetic and geological data in the northern Cordillera. Earth and Planetary Sciences Letters, vol. 193, pp. 259-272.

Johnston, S.T. 2008. The Cordilleran Ribbon Continent of North America. Annual Review of Earth and Planetary Science, vol. 36, pp. 495-530.

Johnston, S.T. and Borel, G.D. 2007. The odyssey of the Cache Creek terrane, Canadian Cordillera: Implications for accretionary orogens, tectonic setting of Panthalassa, the Pacific superwell, and break-up of Pangea. Earth and Planetary Science Letters, vol. 253, pp. 415-428.

MacIntyre, D.G., Villeneuve, M. and Schiarrizza, P. 2001. Timing and tectonic setting of Stikine Terrane magmatism, Babine-Takla lakes area, central British Columbia. Canadian Journal of Earth Sciences, vol. 38, pp. 579-601.

Marsden, H. and Thorkelson, D.J. 1992. Geology of the Hazelton Volcanic Belt in British Columbia: Implications for the Early to Middle Jurassic Evolution of Stikinia. Tectonics, vol. 11, pp. 1266-1287.

McClelland, W.C., Gehrels, G.E. and Saleeby, J.B. 1992. Upper Jurassic-Lower Cretaceous basinal strata along the Cordileran margin: Implications for the accretionary history of the Alexander-Wrangellia-Peninsular terrane. Tectonics, vol. 11, pp. 823-835.

McDonald, A.J., Lewis, P.D., Thomson, J.F.H., Nadaraju, G., Bartsch, R.D., Bridge, D.J., Rhys, D.A., Roth, T., Kaip, A., Godwin, C.I. and Sinclair, A.J. 1996. Metallogeny of an Early to Middle Jurassic Arc, Iskut River Area, Northwestern British Columbia. Economic Geology, vol. 91, pp. 1098-1114.

McDonough, M.R., and Simony, P.S. 1988. Structural evolution of basement gneisses and Hadrynian cover, Bulldog Creek area, Rocky Mountains, British Columbia. Canadian Journal of earth Sciences, vol. 25, pp. 1687-1702.

McNicoll, V.J., Evenchick, C.A., and Mustard, P.S. 2005. Provenance studies on the depositional histories of the Bowser and Sustut Basins and their implications for tectonic evolution of the northern canadian Cordillera. *In:* Geological Association of Canada Annual Meeting Abstracts, vol. 30, p. 133.

Mihalynuk, M.G., Smith, M.T., Gabites, J., Runkle, D. and Lefebvre, D. 1992. Age of emplacement and basement character of the Cache Creek terrane as constrained by new isotopic and geochemical data. Canadian Journal of Earth Sciences, vol. 29, pp. 2463-2477.

Mihalynuk, M.G., Nelson, J.L. and Diakow, L.J. 1994. Cache Creek Terrane entrapment: oroclinal paradox within the Canadian Cordillera. Tectonics, vol. 13, pp. 575-595.

Mihalynuk, M.G., Erdmer, P., Ghent, E.D., Cordey, F., Archibald, D.A., Friedman, R.M. and Johannson, G.G. 2004. Coherent French Range blueschist: Subduction to exhumation in <2.5 m.y.? Geological Society of America Bulletin, vol. 116, pp. 910-922.

Monger, J.W.H. 1977. Upper Paleozoic rocks of the western Canadian Cordillera and their bearing on Cordilleran evolution. Canadian Journal of Earth Sciences, vol. 14, pp. 1832-1859.

Monger, J.W.H. and Ross, C.A. 1971. Distribution of fusulinaceans in the western canadian Cordillera. Canadian Journal of Earth Sciences, vol. 8, pp. 259-278.

Monger, J.W.H. and Nokleberg, W.J. 1996. Evolution of the northern North American Cordillera: generation, fragmentation, displacement and accretion of successive North American plate-margin arcs. *In:* Coyner, A.R., Fahey, P.L. (Eds.), Geology and ore deposits of the American Cordillera. pp. 1133-1152.

Monger, J.W.H., Price, R.A. and Tempelman-Kluit, D.J. 1982. Tectonic accretion and the origin of the two major metamorphic and plutonic welts in the Canadian Cordillera. Geology, vol. 10, pp. 70-75.

Murphy, D.C., van der Heyden, P., Parrish, R.R., Klepacki, D.W., McMillan, W., Struik, L.C. and Gabites, J. 1995. New geochronological constraints on Jurassic deformation of the western edge of North America, southestern Canadian Cordillera *In:* Miller, D.M., Busby, C. J. (Eds.), Jurassic Magmatism and Tectonics of the North American Cordillera. Geological Society of America, Special Paper 299, pp. 159-171.

Nadaraju, G. 1993. Triassic-Jurassic Biochronology of the eastern Iskut River map area, northwestern British Columbia. M.Sc. thesis, Department of Earth and Ocean Sciences, University of British Columbia, Vancouver, 268 p.

Nelson, J.L. and Mihalynuk, M.G. 1993. Cache Creek ocean: Closure or enclosure? Geology, vol. 21, pp. 173-176.

Nelson, J.L. and Friedman, R. 2004. Superimposed Quesnel (late Paleozoic-Jurassic) and Yukon-Tanana (Devonian-Mississipian) arc assemblages, Cassiar Mountains, northern British Columbia: U-Pb and igneous petrochemical evidence. Canadian Journal of Earth Sciences, vol. 41, pp. 1201-1235.

Nelson, J.L. and Gehrels, G.E. 2007. Detrital zircon geochronology and provenance of southestern Yukon-Tanana terrane. Canadian Journal of Earth Sciences, vol. 44, pp. 297-316.

Nelson, J.L., Colpron, M., Piercey, S.J., Dusel-Bacon, C., Murphy, D.C. and Roots, C.F. 2006. Paleozoic tectonic and metallogenic evolution of pericratonic terranes in Yukon, northern British Columbia and eastern Alaska. *In:* Colpron, M., Nelson, J.L. (Eds.), Paleozoic Evolution and Metallogeny of Pericratonic Terranes at the Ancient Pacific Margin of North America. Geological Association of Canada, Special Paper 45, pp. 323-360.

Orchard, M.J., Cordey, F., Rui, L., Bamber, W.E., Mamet, B., Struik, L.C., Sano, H. and Taylor, H.J. 2001. Biostratigraphic and biogoegraphic constraints on the Carboniferous to Jurassic Cache Creek Terrane in central British Columbia. Canadian Journal of Earth Sciences, vol. 38, pp. 551-578.

Poulton, T.P., Christopher, J.E., Hayes, B.J.R., Losert, J., Tittemore, J. and Gilchrist, R.D. 1994. Jurassic and lowermost Cretaceous strata of the western Canada sedimentary basin. *In:* Mossop, G.D. and Shetsen, I. (Eds.), Geological Atlas of the Western Canada Sedimentary Basin, chapter 18, pp. 297-316.

Price, R.A. and Monger, J.W.H. 2000. A transect of the southern Canadian Cordillera from Vancouver to Calgary. Geological Survey of Canada, Open File Report 3902, p. 170.

Roback, R.C. and Walker, N.W. 1995. Provenance, detrital zircon U-Pb geochronometry, and tectonic significance of Permian to Lower Triassic sandstone in southeastern Quesnellia, British Columbia and Washington. Geological Society of America Bulletin, vol. 107, pp. 665-675.

Roth, T. 2002. Physical and chemical constraints on mineralization in the Eskay Creek Deposit,

northwestern British Columbia; evidence from petrography, mineral chemistry, and sulfur isotopes. Ph.D. thesis, Department of Earth and Ocean Sciences, University of British Columbia, Vancouver, 401 p.

Samson, S.D., McClelland, W.C., Patchett, P.J., Gehrels, G.E. and Anderson, R.G. 1989. Evidence from neodymium isotopes for mantle contributions to Phanerozoic crustal genesis in the Canadian Cordillera. Nature, vol. 337, pp. 705-709.

Samson, S.D., Patchett, P.J., McClelland, W.C. and Gehrels, G.E. 1991. Nd isotopic characterization of metamorphic rocks in the Coast Mountains, Alaska and Canadian Cordillera: ancient crust bounded by juvenile terranes. Tectonics, vol. 10, pp. 770-780.

Sherlock, R.L., Barrett, T.J., Roth, T., Childe, F.C., Thomson, J.F.H., Kuran, D., Marsden, H. and Allen, R. 1994. Geological investigations of the 21B deposit, Eskay Creek, northwestern British Columbia (104B/9W). *In:* Geological Fieldwork 1993. British Columbia Ministry of Energy, Mines and Petroleum Resources, Paper 1994-1, pp. 357-364.

Thorkelson, D.J., Mortensen, J.K., Marsden, H. and Taylor, D.C. 1995. Age and tectonic setting of Early Jurassic episodic volcanism along the northeastern margin of the Hazelton Trough, northern British Columbia. *In:* Miller, D.M., Busby, C.J. (Eds.), Jurassic magmatism and tectonics of the North American Cordillera. Geological Society of America, Special Paper 299, pp. 83-94.

Tipper, H.W. and Richards, T.A. 1976. Jurassic stratigraphy and history of north-central British Columbia. Geological Survey of Canada, Bulletin 270, 73p.

van der Heyden, P. 1992. A Middle Jurassic to early Tertiary Andean-Sierran arc model for the Coast Belt of British Columbia. Tectonics, vol. 11, pp. 82-97.

Werner, L.J. 1977. Metamorphic terrane, northern Coast Mountains west of Atlin Lake, British Colombia. *In:* Current Research Part A, Geological Survey of Canada, Paper 77 1-A, pp. 267-269.

Chapter 7: Conclusions

Regional correlations of stratigraphic sections in Jurassic rocks of the northern Stikine terrane indicate that the Hazelton Group can be divided into two distinct lithostratigraphic intervals separated in most places by an unconformity (figure 7.1). The lower Hazelton Group (LHG) is dominated by arc-related volcanic rocks, whereas the upper Hazelton Group (UHG) contains mainly fine-grained clastic rocks and lesser bimodal rift-related volcanic rocks (Chapter 2). Deposition of the UHG mostly occurred in the Hazelton trough, an Early Jurassic intra-arc extensional basin located on Stikinia (Tipper and Richards, 1976). An extensional origin for the Hazelton trough is consistent with rapid tectonic subsidence rates observed in the vicinity of Todagin Mountain during Pliensbachian to Early Toarcian time (figure 7.2; Chapter 4), and with deposition of rift-related volcanic flows of the Cold Fish Volcanics near Joan Lake (Thorkelson et al. 1995). This tectonic episode was followed by thermal contraction of the Stikine crust and exponentially decreasing subsidence rates (Chapter 4). Lowermost coarse-grained strata of the UHG, including the bioturbated and fossiliferous units of the Smithers Formation and the Spatisizi River Formation, record a transgressive trend consistent with a regional relative sea-level rise. In the southern portion of the basin, the Smithers Formation is characterized by a sand-rich lower assemblage, in parts characterized by a *Skolithos* ichnofacies, which is overlain by extensively bioturbated siltstone and fine-grained sandstone representative of the *Cruziana* ichnofacies (Chapter 3). However, departures from the archetypal ichnofacies are common in units of the Smithers Formation and are interpreted to represent local influence of deltaic conditions and/or subaerial volcanism (figure 7.3; Chapter 3). Transgression of the Stikine arc culminated with the establishment of deep-water conditions in the Late Toarcian-Early Aalenian, and deposition of the Quock Formation (Thomson et al. 1986; Chapter 2). Interbedded siliceous mudstone and rusty-weathered tuff of the Quock Formation are correlated throughout most of the basin, except in the Iskut River area, where contemporaneous strata of the Iskut River Formation are dominated by rift-related volcanic rocks and conglomerate (Chapter 2). Inception of rifting in the Iskut River area constitutes an independent extensional event on Stikinia, and could be related to reorganization of tectonic plates during a protracted period of terrane accretion in the Middle Jurassic (figure 7.4; Chapter 6).

Obduction of the Cache Creek terrane over Stikinia in early Middle Jurassic provided a new source of sediments, which led to accumulation of the Bowser Lake Group (Tipper and Richards, 1976; Eisbacher, 1985; Gabrielse, 1991; Evenchick and Thorkelson, 2005). The second pulse of subsidence observed at Todagin Mountain can

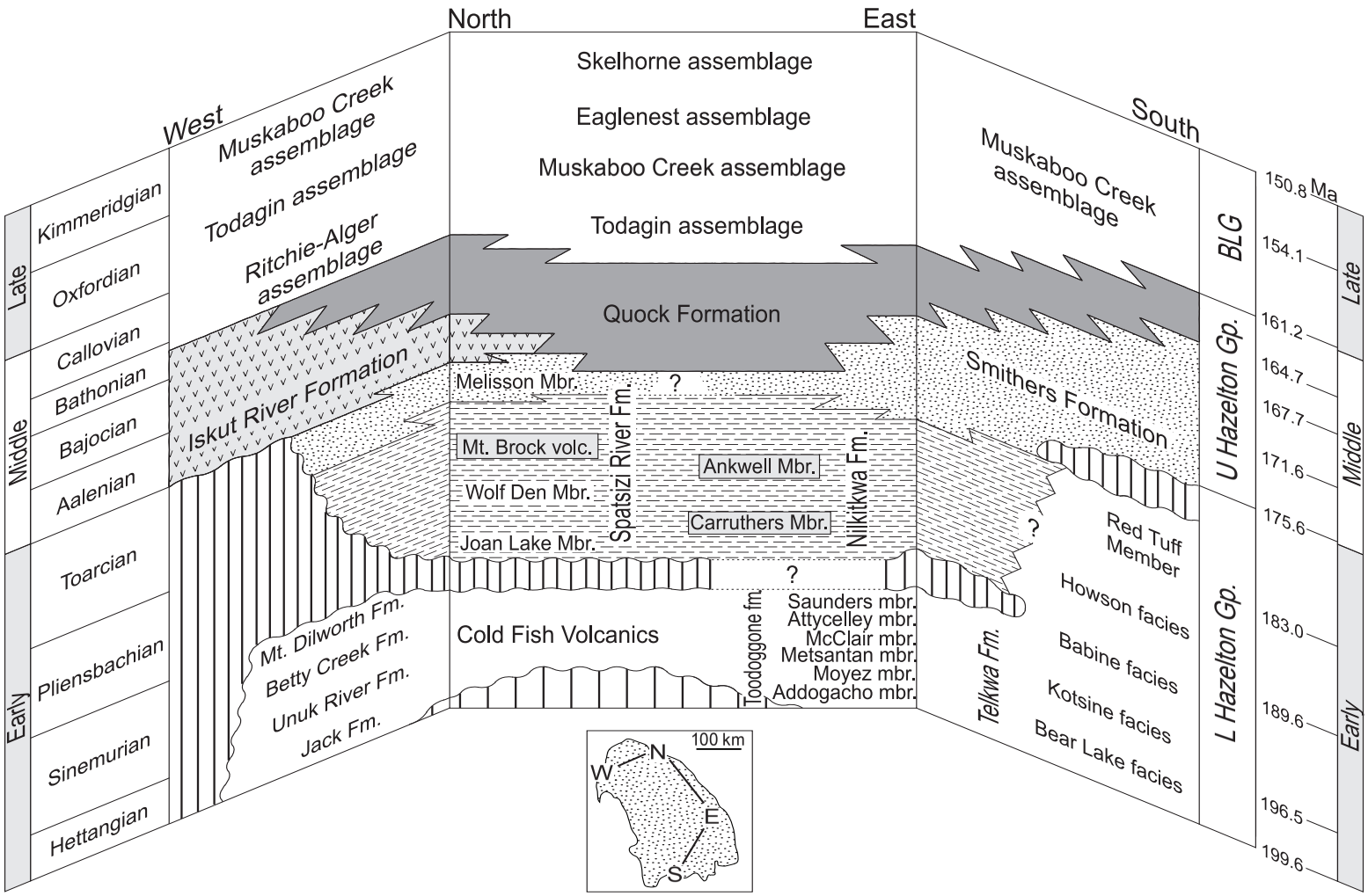

Figure 7.1: Proposed stratigraphic nomenclature for the Hazelton Group exposed in north-central British Columbia. Most significant changes include: recognition of a diachronous unconformity at the base of the upper Hazelton Group; revision of the Spatsizi River and Quock formations; introduction of a new stratigraphic unit (Iskut River Formation) for the rift-related facies in the Iskut River area.

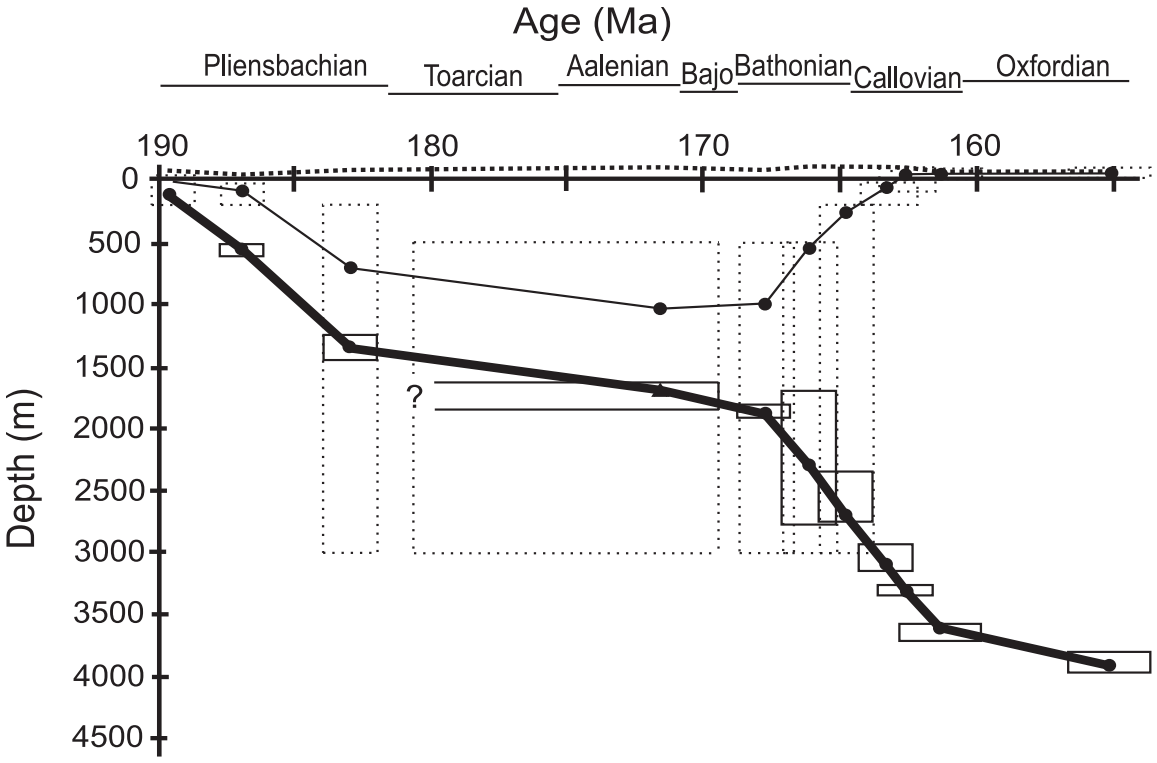

Figure 7.2: Possible subsidence curve corrected for eustatic sea-level (bold dotted line; curve from Haq (1987)) and water depth. Estimated sea-floor position is shown by continuous line below the eustatic curve. Position of the basin floor is represented by the bold curve. Uncertainties on paleobathymetry are shown in dotted rectangles (relative to the sea-floor position) whereas solid rectangles (positioned relative to subsidence curve) represent potential inaccuracies in positioning of fossil locations on the cross-section, and potential errors in the duration of chronostratigraphic units. Time scale from Gradstein et al. (2004).

be entirely explained by sediment loading of the accommodation previously generated during extension of the Hazelton trough in Early Jurassic time, and does not required the input of tectonic loading (Chapter 4). In the early stage of the Bowser basin, the bulk of siliciclastic sediment was deposited in deep-water environments, including basin slope and basin floor settings. The architectural organization of strata observed at Todagin Mountain indicates that emplacement of channelized slope systems of the Todagin assemblage were initially dominated by erosional processes at the base of a submarine slope (Ricketts and Evenchick, 1999; Chapter 5). Gradual change from erosive and amalgamated channel deposits to more aggradational channels is consistent with a basinward advance of graded depositional profile under sustained sediment supply (figure 7.5; Chapter 5). Elevation of the equilibrium profile favoured aggradation and preservation of overbank deposits as the system evolved (Chapter 5). In contrast, the great abundance of thick mass-transport deposits (MTDs) in the upper part of the Mount

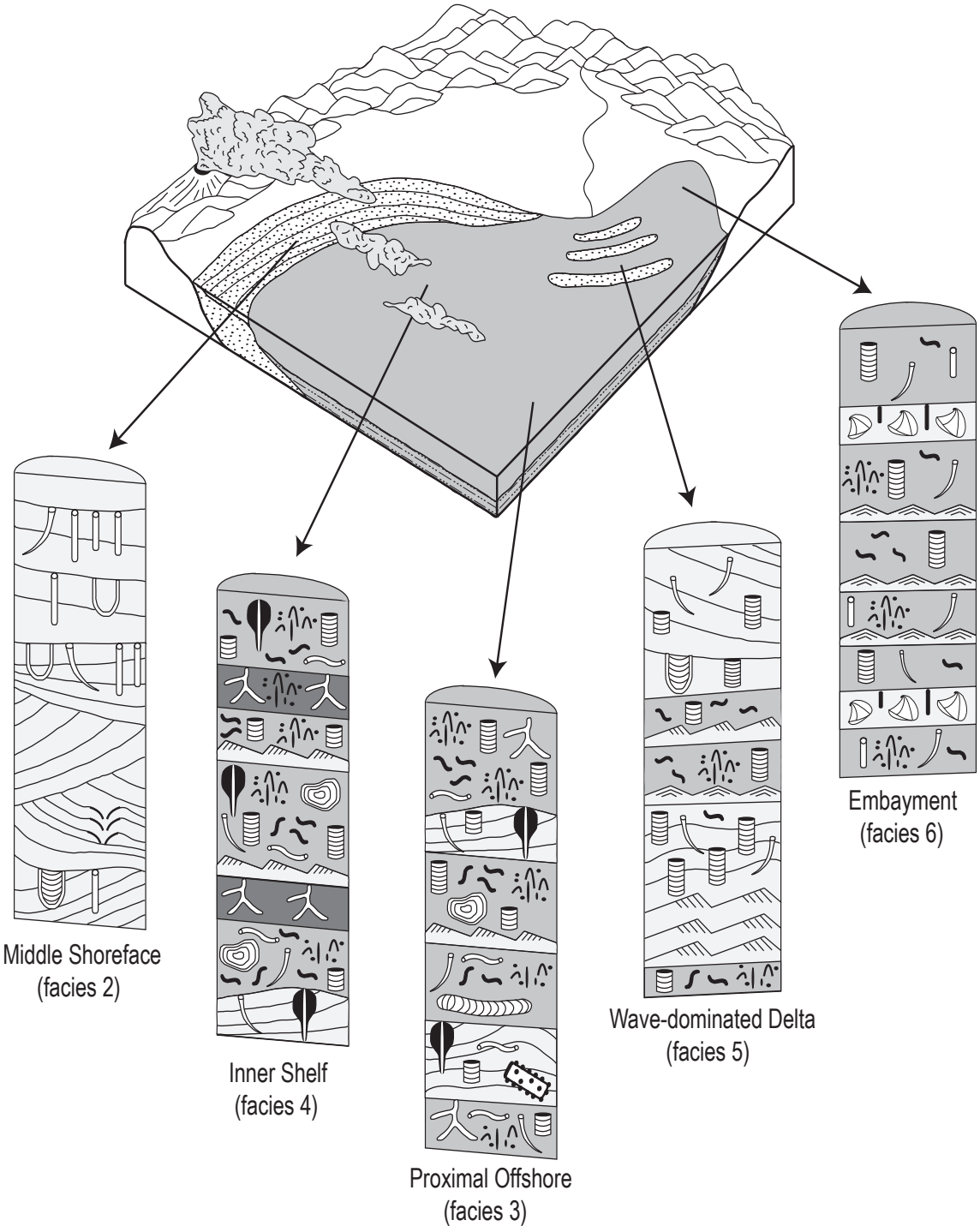

Figure 7.3: Conceptual diagram showing the interpreted depositional model of the Smithers Formation and the distribution of facies. See figure 3.3 for legend details.

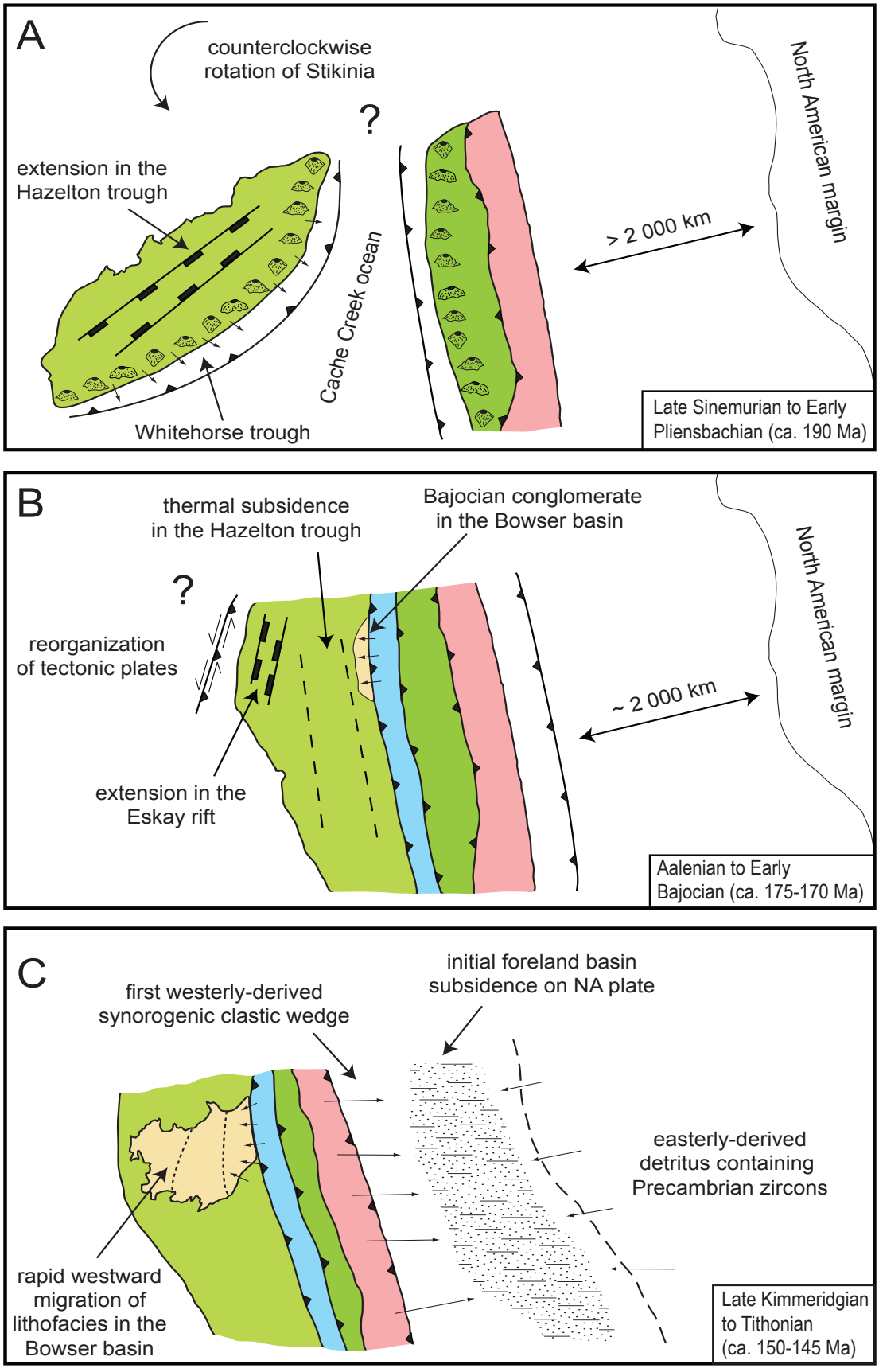
A
counterclockwise
rotation of Stikinia
?
extension in the
Hazelton trough
Cache Creek ocean
> 2 000 km
North American margin
Whitehorse trough
Late Sinemurian to Early
Pliensbachian (ca. 190 Ma)
B
thermal subsidence
in the Hazelton trough
Bajocian conglomerate
in the Bowser basin
?
reorganization
of tectonic plates
~ 2 000 km
North American margin
extension in the
Eskay rift
Aalenian to Early
Bajocian (ca. 175-170 Ma)
C
initial foreland basin
subsidence on NA plate
first westerly-derived
synorogenic clastic wedge
easterly-derived
detritus containing
Precambrian zircons
rapid westward
migration of
lithofacies in the
Bowser basin
Late Kimmeridgian
to Tithonian
(ca. 150-145 Ma)

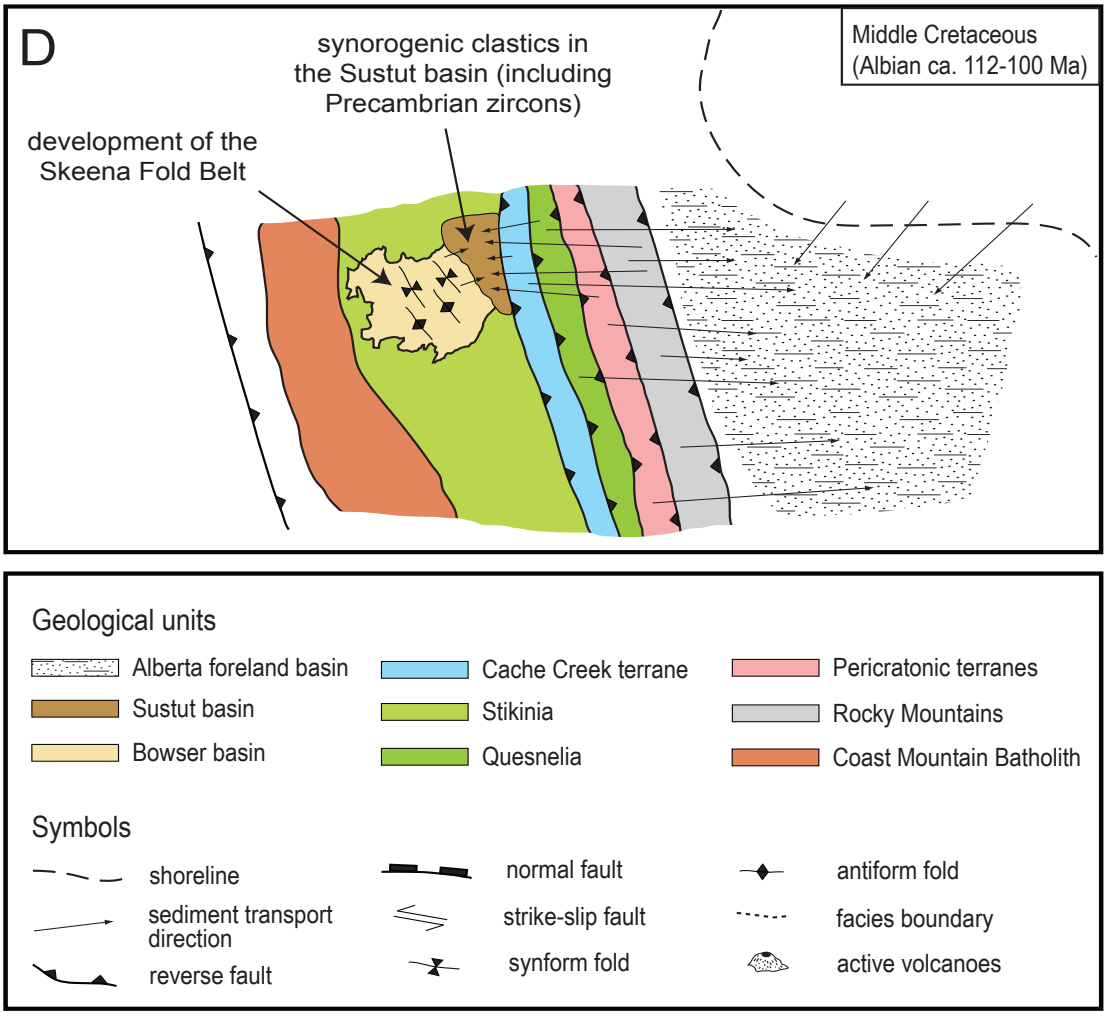

Figure 7.4: Conceptual tectonic model showing paleogeographic maps for the Early Jurassic through Middle Cretaceous. A) Westward-directed subduction underneath Stikinia during Late Sinemurian–Early Pliensbachian was responsible for volcanic arc magmatism, generation of the Hazelton trough in the back-arc area, and accumulation of arc-derived detritus in the fore-arc Whitehorse trough. Entrapment of the exotic Cache Creek terrane probably resulted from counter-clockwise rotation of the Stikine terrane. B) Closure of the Cache Creek ocean in the early Middle Jurassic resulted in the obduction of a subduction complex between Stikinia and the formally accreted Quesnel terrane and pericratonic terranes. Cessation of subduction underneath the eastern margin of Stikina was associated with a decrease in arc volcanism, and thermal subsidence in the Hazelton trough. Reorganization of tectonic plates triggered extension and rift-related volcanism on the western margin of Stikinia. Initial deposition of Cache Creek derived conglomerate in the Bowser basin began in the Bajocian. C) Collision of the formally accreted group of terranes with the autochthonous North American margin in Late Jurassic triggered flexural subsidence on the platform and accumulation of the first westerly-derived clastic wedge in the Alberta Foreland basin. D) The Middle Cretaceous was characterized by a major period of ductile deformation, metamorphism and magmatism in the Coast Belt. This was associated with development of the Skeena Fold Belt on Stikinia and northeast-directed thrust faulting and metamorphism in the Omineca Belt and Foreland Belt. First deposition of easterly-derived metamorphic clasts in the Sustut basin, including Precambrian zircon grains. Sources of information include Eisbacher (1974);

Tipper and Richards (1976); McDonough and Simony (1988); Gabrielse (1991); Nelson and Mihalynuk (1993); Poulton et al. (1994); Murphy et al. (1995); Thorkelson et al. (1995); Evenchick et al. (2001); English and Johnston (2005); Evenchick and Thorkelson (2005); Evenchick et al. (2007); Johnston and Borel (2007).

Dilworth section suggests an important change in boundary conditions along the western margin of the Bowser basin during Late Callovian to Early Oxfordian (Chapter 5). Steepening of the depositional gradient related to reactivation of faults inherited from the Eskay rift produced instability on the slope, which interrupted the normal progradation of the deep-water system and accumulated thick MTDs (Chapter 5). Local uplift and tilting in the vicinity of Mount Dilworth is consistent with detrital zircon probability density plots, which show that the greatest population of grains was derived from local volcanic sources (Chapter 2). The abundance of volcanic fragments in the siliciclastic sedimentary rocks at Mount Dilworth, compared with other Bowser Lake Group sandstone, suggest localized sources in the Stikine terrane. In addition, the absence of Precambrian zircon grains in strata of the Bowser Lake Group indicate that the autochthonous margin of North America did not supply detritus to the Bowser basin (McNicoll et al. 2005; Evenchick et al. 2007; Chapter 2). In their proposed tectonic model, Evenchick et al. (2007) attributed this discrepancy to the position of an hypothetic drainage divide that separated the rising Omineca highland into a western (Stikinia, Cache Creek, Quesnellia) and eastern component (pericratonic terranes, North American margin). Alternatively,

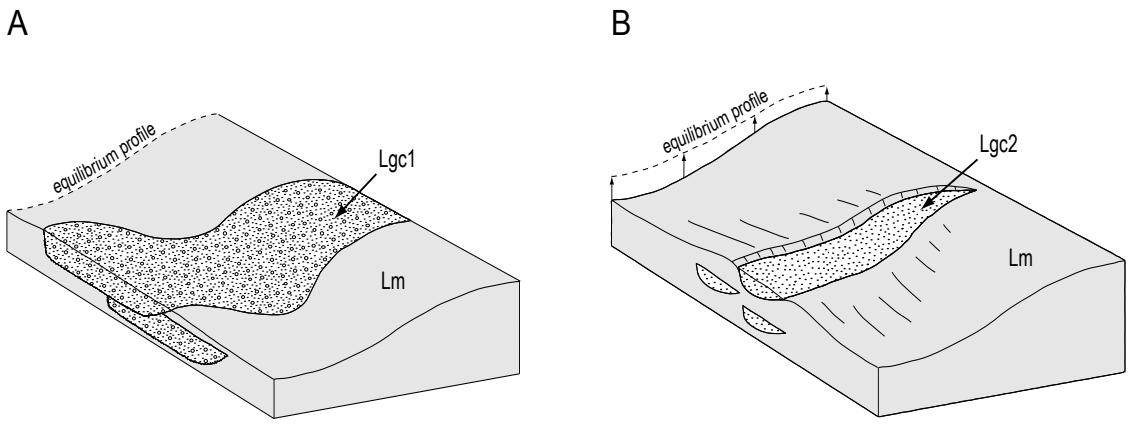

Figure 7.5: Depositional model for the Lower Todagin channel complex. A) Amalgamated channel-fills 1 and 2 were deposited in the lower part of the LTCC where the local gradient was less. B) Offstacked conglomerate bodies of channel-fill 3 in the upper part of the LTCC. High sedimentation rates and reduction in flow density resulted in elevation of the equilibrium profile, which generated more accommodation on the slope. This favored aggradation of channels, and construction and preservation of levees.

amalgamation of Stikinia and the Cache Creek terrane outboard of the accreted pericratonic terranes and the North American margin could also explain the absence of recycled Precambrian zircons in BLG strata (figure 7.4; Chapter 6). The results presented in this study suggest that the ribbon continent model (cf. Johnston 2008) is compatible with the tectonic evolution of the Hazelton trough-Bowser basin, and that the drainage divide model of Evenchick et al. (2007) remains valid but does not constitute the only possible solution to this long-lived controversy.

7.1 References

Eisbacher, G.H. 1974. Deltaic sedimentation in the northeastern Bowser Basin, British Columbia. Geological Survey of Canada, Paper 73-33, 13 pp.

Eisbacher, G.H. 1985. Pericollisional strike-slip faults and synorogenic basins, Canadian Cordillera. *In:* Biddle, K.T., Christie-Blick, N. (Eds.), Strike-slip deformation, basin formation, and sedimentation. Society of Economic Paleontologists and Mineralogists, Special Publication 37, pp. p. 265-282.

English, J.M. and Johnston, S.T. 2005. Collisional orogenesis in the northern Canadian Cordillera: Implications for Cordilleran crustal structure, ophiolite emplacement, continental growth, and the terrane hypothesis. Earth and Planetary Science Letters, vol. 232, pp. 333-344.

Evenchick, C.A. and Thorkelson, D.J. 2005. Geology of the Spatsizi River map area, north-central British Columbia. Geological Survey of Canada, Bulletin 577, 276 p.

Evenchick, C.A., Poulton, T.P., Tipper, H.W. and Braidek, I. 2001. Fossils and facies of the northern two-thirds of the Bowser Basin, British Columbia. Geological Survey of Canada, Open File 3956.

Evenchick, C.A., McMechan, M.E., McNicoll, V.J. and Carr, S.D. 2007. A synthesis of the Jurassic-Cretaceous tectonic evolution of the central and southeastern Canadian Cordillera: exploring links across the orogen. *In:* Sears, J.W., Harms, T.A., Evenchick, C.A. (Eds.), Whence the mountains? The contribution of Raymond A. Price. Geological Society of America, Special Publication 433, pp. 117-145.

Gabrielse, H. 1991. Late Paleozoic and Mesozoic terrane interactions in north-central British Columbia. Canadian Journal of Earth Sciences, vol. 28, pp. 947-957.

Gradstein, F.M., Ogg, J.G., Smith, A.G., Agterberg, F.P., Bleeker, W., Cooper, R.A., Davydov, V., Gibbard, P., Hinnov, L.A., House, M.R., Lourens, L., Luterbacher, H.P., McArthur, J., Melchin, M.J., Robb, L.J., Shergold, J., Villeneuve, M., Wardlaw, B.R., Ali, J., Brinkhuis, H., Hilgen, F. J., Hooker, J., Howarth, R.J., Knoll, A.H., Laskar, J., Monechi, S., Plumb, K.A., Powell, J., Raffi, I., Röhl, U., Sadler, P., Sanfilippo, A., Schmitz, B., Shackleton, N.J., Shields, G.A., Strauss, H., Van Dam, J., van Kolfschoten, T., Veizer, J., Wilson, D. 2004. A Geological Time Scale 2004. Cambridge University Press, 610 p.

Haq, B.U., Hardenbol, J. and Vail, P.R. 1987. Chronology of Fluctuating Sea Levels Since the Triassic. Science, vol. 235, pp. 1156-1167.

Johnston, S.T. 2008. The Cordilleran Ribbon Continent of North America. Annual Review of Earth and Planetary Science, vol. 36, pp. 495-530.

Johnston, S.T. and Borel, G.D. 2007. The odyssey of the Cache Creek terrane, Canadian Cordillera:

Implications for accretionary orogens, tectonic setting of Panthalassa, the Pacific superwell, and break-up of Pangea. Earth and Planetary Science Letters, vol. 253, pp. 415-428.

McDonough, M.R. and Simony, P.S. 1988. Structural evolution of basement gneisses and Hadrynian cover, Bulldog Creek area, Rocky Mountains, British Columbia. Canadian Journal of earth Sciences, vol. 25, pp. 1687-1702.

McNicoll, V.J., Evenchick, C.A., and Mustard, P.S. 2005. Provenance studies on the depositional histories of the Bowser and Sustut Basins and their implications for tectonic evolution of the northern canadian Cordillera. *In:* Geological Association of Canada Annual Meeting Abstracts, vol. 30, p. 133.

Murphy, D.C., van der Heyden, P., Parrish, R.R., Klepacki, D.W., McMillan, W., Struik, L.C. and Gabites, J. 1995. New geochronological constraints on Jurassic deformation of the western edge of North America, southestern Canadian Cordillera *In:* Miller, D.M., Busby, C. J. (Eds.), Jurassic Magmatism and Tectonics of the North American Cordillera. Geological Society of America, Special Paper 299, pp. 159-171.

Nelson, J.L. and Mihalynuk, M.G. 1993. Cache Creek ocean: Closure or enclosure? Geology, vol. 21, pp. 173-176.

Poulton, T.P., Christopher, J.E., Hayes, B.J.R., Losert, J., Tittemore, J. and Gilchrist, R.D. 1994. Jurassic and lowermost Cretaceous strata of the western Canada sedimentary basin. *In:* Mossop, G.D. and Shetsen, I. (Eds.), Geological Atlas of the Western Canada Sedimentary Basin, chapter 18, pp. 297-316.

Ricketts, B.D. and Evenchick, C.A. 1999. Shelfbreak gullies; products of sea-level lowstand and sediment failure: examples from Bowser Basin, northern British Columbia. Journal of Sedimentary Research, vol. 69, pp. 1232-1240.

Thomson, R.C., Smith, P.L. and Tipper, H.W. 1986. Lower to Middle Jurassic (Pliensbachian to Bajocian) stratigraphy of the northern Spatsizi area, north-central British Columbia. Canadian Journal of Earth Sciences, vol. 23, pp. 1963-1973.

Thorkelson, D.J., Mortensen, J.K., Marsden, H. and Taylor, D.C. 1995. Age and tectonic setting of Early Jurassic episodic volcanism along the northeastern margin of the Hazelton Trough, northern British Columbia. *In:* Miller, D.M., Busby, C.J. (Eds.), Jurassic magmatism and tectonics of the North American Cordillera. Geological Society of America, Special Paper 299, pp. 83-94.

Tipper, H.W. and Richards, T.A. 1976. Jurassic stratigraphy and history of north-central British Columbia. Geological Survey of Canada, Bulletin 270, 73p.

Appendix A

This appendix accompanies chapter 2 and provides a complete list of the paleontological data reported from the measured stratigraphic sections. Most fossil localities are compiled from published goverment reports, for which the appropriate reference is cited. Each fossil locality is given with its assigned Geological Survey of Canada number (GSC), except for the radiolarian microfossils identified by Dr. Fabrice Cordey at the Université de Lyon in France. In the latter case, the original field sample numbers are provided. Fossil description at the genus and species levels are given, along with the interpreted depositional age for the sub-stage level. Additional information and precision on the assigned age can be found in the respective references.

Section	GSC #	ID	Fossil Description	Age	Reference
Ashman	C-21079	AR1	*Asteroceras* cf. *saltriense(?)*; *Aegasteroceras(?)* aff. Jeletzkyi; *Asteroceras* aff. *Margarita*	L. Sinemurian	Palfy and Schmidt (1994)
Ashman	85385 C-458169	AR2	*Sonninia* sp.; *Myophorella* sp. aff. *M. montanaensis* (Meek); *Pleuromya* sp.; *Ostrea* sp.	E. Bajocian	Tipper and Richards (1976) Report J1-TPP-2008
Ashman	85427 C-458156	AR3	*Teloceras* sp.; *Stephanoceras* sp.; *Sonninia* cf. *tuxedniensis*; *Sonninia (Papilliceras)* n. sp. B; *Witchellia(?) adnata*; *Stephanoceras* sp. aff. *S. skidegatensis* (Whiteaves); *Plagiostoma hazeltonense* McLearn; *Lima tizglensis* McLearn; *Ctenostreon gikshanensis* McLearn; *Myophorella* sp. aff. *M. dawsoni* (Whiteaves); *Pinna* sp., *Gervillella* sp., *Aguilerella* sp.; *Astarte(?)* sp., *Coelastarte(?)* sp., *Meleagrinella(?)* sp.; *Brachidontes(?)* sp., *Camptonectes(?)* sp., *Pleuromya* sp.; Ostreiid bivalve(?), solitary scleractinian coral; belemnites	E. Bajocian	Tipper and Richards (1976) Johnston (2002) Report J1-TPP-2008
Ashman	85405	AR4	*Holcophylloceras costisparsum* Imlay; *Fontannesia* cf. *luculenta; Zemistephanus richardsoni* (Whiteaves); *Stephanoceras itinsae*	M. Bajocian	Tipper and Richards (1976) Johnston (2002)
Ashman	85437	AR5	*Arctocephalites (Cranocephalites) costidensus* Imlay; *Arctocephalites (Cranocephalites)* sp. aff *A. (C.) pompeckji* (Madsen); *Gryphaea* sp.	E. Bathonian	Tipper and Richards (1976)
Ashman	85413 C-458198	AR6	*Kepplerites* sp.; *Cobbanites* sp.; *Kepplerites* cf. *ingrahami; Kepplerites* cf. *costidensus; Kepplerites* cf. *chisikensis; Kepplerites* sp. aff. *K. mclearni* Imlay	E. Callovian	Tipper and Richards (1976) Johnston (2002) Report J1-TPP-2008
Ashman	?	AR7	*Pseudocadoceras* cf. *P. grewingki* (Pompeckji); belemnites; *Pseudocadoceras* cf. *P. crassicostatum* Imlay; gastropods	M. Callovian	Tipper and Richards (1976)
Ashman	85376	AR8	*Quenstedtoceras (Lamberticeras) henrici* Douville; *Quenstedtoceras (Lamberticeras) intermissum* Buckman	L. Callovian	Tipper and Richards (1976)
Ashman	85439	AR9	*Cardioceras (Scarburgiceras) martini* Reeside	E. Oxfordian	Tipper and Richards (1976)
Ashman	85442 C-458174	AR10	*Cardioceras* cf. *C. (C.) lilloetense* Reeside; *Cardioceras (Subvertebriceras)* cf. *C. (S.) Canadense* (Whiteaves); *Myophorella* sp. aff. *M. montanaensis* (Meek); *Pleuromya* sp.; *Astarte(?)* sp.; *Meleagrinella(?)* sp.	E. Oxfordian	Tipper and Richards (1976) Report J1-TPP-2008

Section	GSC #	ID	Fossil Description	Age	Reference
Quinlan	C-518674 C-532870 C-532871 C-532872 C-532873 C-532874	QM1	*Erycitoides howelli* (White); *Lissoceras* sp.; *Astarte(?)* sp.; *Pholadomya(?)* sp.; *Myophorella* spp.; *Scaphotrigonia(?)* sp.; *Scaphorella(?)* sp.; *Trigonia* sp. large; *Pronoella(?)* sp.; *Lopha* sp.; *Myopholas(?)* sp.; *Coelastarte(?)* sp.; *Grammatodon* sp.; *Entolium* sp.; *Chlamys* sp.; *Homomya(?)* sp.; *Ostrea* sp.; *Astrocoenia* sp.; *Lima(?)* sp.; *Pleuromya(?)* sp.; *Plagiostoma* sp.; gastropods; scleratinian colonial corals	Aalenian	Report J2-2007-TPP Report 1-TPP-2009
Quinlan	C-532887	QM2	*Plagiostoma hazeltonense* McLearn	E. Bajocian	Report 1-TPP-2009
Quinlan	C-518668	QM3	*Stephanoceras* sp. aff. *skidegatensis* (Whiteaves); gastropods; *Plagiostoma hazeltonense* McLearn; *Coelastarte(?)* sp.;	E. Bajocian	Report J2-2007-TPP
Quinlan	C-532877 C-532879	QM4	*Lissoceras(?)* sp.; *Plagiostoma* sp.; Scleractinian coral; solitary rugose coral	E. Bajocian	Report 1-TPP-2009
Quinlan	C-518675 C-532880 C-532882 C-532883 C-532884 C-532885 C-532886	QM5	*Witchellia(?)* sp.; *Sonninia(?)* sp.; *Lopha* sp.; *Ctenostreon* sp.; *Lima* sp.; *Zemistephanus richardsoni* (Whiteaves)	E. Bajocian	Report 1-TPP-2009 Report J2-2007-TPP
Quinlan	C-532888 C-532889	QM6	*Plagiostoma hazeltonense* McLearn *Lima tizglensis* McLearn	E. Bajocian	Report 1-TPP-2009
Quinlan	C-518673	QM7	*Kepplerites* sp.	E. Callovian	Report J2-2007-TPP
Quinlan	C-518669	QM8	*Pleuromya* sp.; *Astarte* sp.; *Pronoella(?)* sp.; *Entolium* sp.	E. Oxfordian	Report J2-2007-TPP
Tenas	88566 85408 15-1-1	TC1	*Epizigzagiceras crassicostatum* Frebold; *Chinitnites(?)* sp.; *Megasphaeroceras(?)* sp.; *Zemistephanus* sp.; *Cobbanites* cf. *talkeetnanus*	L. Bajocian	Tipper and Richards (1976) Johnston (2002)
Tenas	88570 85444 85380 15-1-6	TC2	*Epizigzagiceras evolutum; Cobbanites* cf. *talkeetnanus; Arctocephalites (Cranocephalites) costidensus; Oppelia* sp.; *Parareineckia* cf. *P. shelikofana* (Imlay); *Chinitnites(?)* sp.; *Morrisiceras(?) dubium* Frebold; *Lilloettia (Imlayoceras) milleri; Tuxednites alticostatus*	E. Bathonian	Tipper and Richards (1976) Johnston (2002)

Section	GSC #	ID	Fossil Description	Age	Reference
Tenas	85390 85413 85410 85396 15-1-8 C-532909 C-532910 C-532908	TC3	*Kepplerites* cf. *costidensus; Choffatia(?)* sp.; *Kheraiceras* sp.; *Kepplerites* cf. *chisikensis; Lilloettia(?)* sp.; *Gowericeras* sp.; *Tuxednites alticostatus*; *Cobbannites* sp.; *Parareineckia* sp.; *Iniskinites tenasensis* Frebold; *Chinitnites(?)* sp.; *Pleuromya* sp.; *Oppelia (Oxycerites)?* sp.;	L. Bathonian	Tipper and Richards (1976) Johnston (2002) Report 1-TPP-2009
Tenas	C-532913 C-532914	TC4	*Iniskinites robustus(?)* Frebold; *Iniskinites* sp.	L. Bathonian	Report 1-TPP-2009
Tenas	C-532918 C-532916 C-532917 C-532907 C-532906 C-532907	TC5	*Iniskinites tenasensis* Frebold; *Choffatia* sp.; *Retroceramus* sp.	L. Bathonian to E. Callovian	Report 1-TPP-2009
Tenas	85397 85458 85460	TC6	*Kheraiceras* spp.; *Cosmoceras* sp.; *Kepplerites* sp.; *Xenocephalites(?)* sp.; *Cobbanites* sp.; *Lilloettia* spp.	E. Callovian	Tipper and Richards (1976)
Tenas	85454 85455	TC7	*Lilloettia* spp.; *Kepplerites* sp.; *Rhynchonella* sp.	E. Callovian	Tipper and Richards (1976)
Tenas	85456 85461 85453 15-1-10 15-1-11	TC8	*Kepplerites* cf. *ingrahami; Kepplerites* cf. *costidensus;* *Kepplerites* cf. *chiskensis; Kepplerites alticostatus;* *Kepplerites (Toricellites)* sp. indet. A; *Lilloettia* cf. *lilloetensis;* *Lilloettia* cf. *mertonyarwoodi; Cobbanites* cf. *talkeetnanus;* *Xenocephalite* sp.; *Parareineckia* sp.; *Lytoceras* sp.; *Cadoceras(?)* sp.	E. Callovian to M. Callovian	Tipper and Richards (1976) Johnston (2002)
Netalzul	91098	NM1	*Tmetoceras* sp.	Aalenian	Tipper and Richards (1976)
Netalzul	91082	NM2	*Sonninia* sp.	E. Bajocian	Tipper and Richards (1976)
Netalzul	91076	NM3	*Zemistephanus* cf. *Z. richardsoni* (Whiteaves); *Stemmatoceras* sp.	E. Bajocian	Tipper and Richards (1976)
Netalzul	C-532857	NM4	*Stephanoceras* sp.	E. Bajocian	Report 1-TPP-2009
Netalzul	C-532858 C-532859	NM5	*Chondroceras* sp. *Zemistephanus richardsoni* (Whiteaves)	E. Bajocian	Report 1-TPP-2009
Netalzul	91123	NM6	*Chondroceras* sp.	E. Bajocian	Tipper and Richards (1976)

Section	GSC #	ID	Fossil Description	Age	Reference
Netalzul	C-532865 C-532864 C-532863 C-532862	NM7	*Stephanoceras* cf. *S. skidegatense* (Whiteaves); *Pinna* sp.; *Pleuromya(?)* sp.; *Pseudomytiloides(?)* sp.; *Retroceramus* sp.; *Ostrea* sp.; *Idonearca* sp.	E Bajocian	Report 1-TPP-2009
Netalzul	C-532867	NM8	*Zemistephanus richardsoni* (Whiteaves) gastropods indet., *Rhynchonellid brachiopods*	E. Bajocian	Report 1-TPP-2009
Joan L.	C-532899 C-532900 C-532891 C-532893 C-532897 C-532896 C-532898	JL1	*Dubariceras freboldi* (Dommergues, Mouterde and Rivas); *Vaugonia* cf. V. *jeletzky*i Poulton; *Retroceramus(?)* sp.; *Dubariceras* sp. cf. D. *silviesi*; *Entolium* sp.; *Miltoceras* sp.; *Weyla bodenbenderi* (Behrendsen); *Pleuromya* sp.; *Acanthopleuroceras* sp.; *Reynesocoeloceras* sp.; *Uptonia(?)* sp.; *Metaderoceras talkeetnaense*; *Tropidoceras(?)* sp.; *Metaderoceras* sp.	E. Pliensbachi.	Thomson et al. (1986) Thomson and Smith (1992) Report 1-TPP-2009
Joan L.	C-103328 C-103332 C-103325 C-103203	JL2	*Leptaleoceras* sp. aff. L. *accuratum; Arieticeras* sp. aff. A. *algovianum;* *Arieticeras* sp. cf. A. *ruthenense; Fanninoceras* sp.; *Tiltoniceras propinquum; Protogrammoceras* spp.; *Fanninoceras latum; Fanninoceras fannini*	L. Pliensbachi.	Thomson et al. (1986) Thomson and Smith (1992) Jakobs (1997)
Joan L.	C-90826	JL3	*Hildaites murleyi* (Moxon); *Cleviceras* sp.	E. Toarcian	Jakobs (1997)
Joan L.	C-90741 C-90742 C-90743 C-90744 C-90805	JL4	*Dactylioceras* sp.; *Dactylioceras* cf. D. *athleticum; Cleviceras* sp.; *Hildoceratoides* sp.; *Peronoceras pacificum* Hillebrandt; *Peronoceras verticosum* (Buckman)*; Pseudolioceras* sp.; *Peronoceras* aff. P. *desplacei; Peronoceras spinatum*; *Leukadiella* aff. L. *ionica*	M. Toarcian	Thomson et al. (1986) Jakobs (1997)
Joan L.	C-90512 C-90814	JL5	*Peronoceras* aff. P. *moerickei; Denckmannia* cf. D. *tumefacta;* *Polyplectus* sp.; *Podagrosites* sp.; *Phymatoceras hillebrandti*	M. to Late Toarcian	Jakobs (1997)
Joan L.	C-103425	JL6	*Pseudolioceras* sp.; *Erycitoides* sp.; *Tmetoceras* sp.	Aalenian	Poulton and Tipper (1991)
Joan L.	?	JL7	*Sonninia* sp.; *Docidoceras* sp.	E. Bajocian	Thomson et al. (1986)
Joan L.	?	JL8	*Stephanoceras* sp.; *Teloceras* sp.; *Chondroceras* sp.	E. Bajocian	Thomson et al. (1986)
Joan L.	?	JL9	*Iniskinites* sp.	L. Bathonian	Thomson et al. (1986) Evenchick & Thorkelson (2005)
Will 1	C-458113 C-458111 C-458214 C-458219	W1(1)	*Weyla bodenbenderi* (Behrendsen); *Agerchlamys(?)* sp.; *Fanninoceras(?)* sp.; *Lima(?)* sp.; *Pleuromya* sp.; *Trigonia* sp.	L. Pliensbachi. to E. Toarcian	Report J1-TPP-2008
Will 1	C-458112	W1(2)	*Tiltoniceras* sp.; *Harpoceratid(?)*	L. Pliensbachi. to E. Toarcian	Report J1-TPP-2008

Section	GSC #	ID	Fossil Description	Age	Reference
Will 1	LC064B	W1(3)	*Helvetocapsa minoensis* (Matsuoka); *Canutus* sp.; *Parvicingula spinifera* (Takemura)	Toarcian	F. Cordey (this study)
Will 1	C-458141 C-458142 C-458143 C-458144 C-458145 C-458146 C-458147 C-458148	W1(4)	*Harpoceras* sp. cf. H. *subplanatum* (Oppel); *Dactylioceras(?)* sp.; *Hildaites murleyi* (Moxon); *Pleuromya(?)* sp.	E. Toarcian	Report J1-TPP-2008
Will 1	C-458139 C-458119 C-458120 C-458121 C-458122	W1(5)	*Peronoceras* sp. aff. P. *verticosum* (Buckman); *Camponectes(?)* sp.; *Denckmannia* sp. cf. D. *tumefacta* (Buckman); *Polyplectus(?)* sp.; *Rarenodia(?)* sp.; *Lima(?)* sp.	M. Toarcian	Report J1-TPP-2008
Will 1	C-458123 C-458124 C-458125 C-458114 C-458115 C-458116 C-458117 C-458118	W1(6)	*Peronoceras* sp. cf. P *verticosum* (Beckman); *Rarenodia(?)* sp.; *Pleuromya* sp.; *Polyplectus* sp.; *Dactylioceras(?)* sp.; *Peronoceras(?)* sp.	M. Toarcian	Report J1-TPP-2008
Will 1	LD004A	W1(7)	*Stichocapsa* sp.; *Parvicingula(?)* sp.	M. Jurassic	F Cordey (this study)
Will 1	C-90665	W1(8)	*Iniskinites* sp.	L. Bathonian	Evenchick & Thorkelson (2005)
Will 2	C-103223 C-103224 C-103226	W2(1)	*Tiltoniceras propinquum; Leptaleoceras* sp. aff. L. *accuratum; Arieticeras* sp. aff. A. *algovianum; Canavaria(?)* sp.; *Arieticeras* sp. cf. A. *ruthenense; Protogrammoceras* spp.	L. Pliensbachi.	Evenchick & Thorkelson (2005)
Will 2	C-458083 C-458084 C-458097 C-458098 C-458099 C-458102 C-458103	W2(2)	*Dactylioceras(?)* sp.; *Peronoceras(?)* sp.; *Pleuromya* sp.; *Hildaites(?)* sp.; *Gresslya(?)* sp.	E. Toarcian	Report J1-TPP-2008

Section	GSC #	ID	Fossil Description	Age	Reference
Will 2	C-458093 C-458085 C-458086 C-458082 C-458104	W2(3)	*Rarenodia planulata* Venturi; *Phymatoceras(?)* aff. P. *crassicosta;* *Peronoceras* sp. aff. P. *verticosum* (Buckman)	M. Toarcian - Planulata regional zone	Report J1-TPP-2008
Will 2	C-458077 C-458078 C-458079 C-458080 C-458081 C-458096	W2(4)	*Myophorella* sp.; *Merlaites(?)* sp.; *Collina(?)* sp.	M. Toarcian	Report J1-TPP-2008
Will 2	C-458076 C-458094 C-458095	W2(5)	*Peronoceras(?)* sp.; *Pseudolioceras(?)* sp.; *Pleuromya* sp.; *Entolium(?)* sp.; *Cylindroteuthis(?)* sp.; *Myophorella* sp.	M. Toarcian	Report J1-TPP-2008
Will 2	C-103425 C-90719 C-90961 C-90963	W2(6)	*Pseudolioceras* (Tugurites) sp. cf. P. *whiteavesi* (White); *Pseudolioceras* sp.; *Tmetoceras* sp.; *Leioceras(?)* sp.; *Planammatoceras(?)* sp.; *Erycitooides howelli* (White); *Erycitoides* sp.; *Zurcheria(?)* sp.; *Inoceramus* sp.	Aalenian	Evenchick & Thorkelson (2005)
Will 2	C-90678	W2(7)	*Pseudolioceras(?)* sp.; *Inoceramus* sp.;	Aalenian	Evenchick & Thorkelson (2005)
Will 2	LC052A	W2(8)	*Praeparvicingula* sp.; *Stichocapsa* sp. *Eucyrtidiellum* sp.	M. Jurassic	F. Cordey (this study)
Will 2	?	W2(9)	*Iniskinites* sp.	Bathonian	Evenchick & Thorkelson (2005)
Owee. W.	125 (90-42) 170 116	OW(1)	*Weyla* sp.; bivalves; belemnites; gastropods; corals	Toarcian	Greig and Evenchick (1993) Evenchick et al. 2001
Owee. W.	C-177761 (90-EPC-48C)	OW(2)	*Parvicingula(?) burnsensis* Pessagno & Whalen; *Triversus(?)* sp.; *Parvicingula preaculeata* Carter; *Parvicingula profunda* Pessagno & Whalen; *Ristola* sp. aff. *Decora* Pessagno & Whalen; *Emiluvia* sp. A	E. Bajocian to L. Bathonian	Cordey et al. (1992) Evenchick et al. (2001)
Owee. W.	?	OW(3)	*Aulacostephanus*; *Buchia* sp. aff. *concentrica* (Sowerby)	E. Kimmeridg.	Evenchick et al. (2001)
Owee. W.	?	OW(4)	*Buchia* aff. *concentrica*; bivalves	L. Oxfordian to E. Kimmeridg.	Evenchick et al. (2001)
Owee. E.	LB045A	OE(1)	*Praeparvicingula* sp. C (Pessagno & Whalen); *Zhamoidellum(?)* sp.; *Religa(?)* sp.	Bajocian	F. Cordey (this study)
Owee. E.	KA032B	OE(2)	*Parvicingula* sp. D Carter; *Paronaella* sp.; *Orbiculiforma* sp.; *Podobursa(?)* sp.	Bajocian	Gagnon et al. 2007

Section	GSC #	ID	Fossil Description	Age	Reference
Owee. E.	KA031A	OE(3)	*Emiluvia chica* s.l. *Foreman*; *Higumastra* sp.; *Orbiculiforma* sp.; *Parvicingula* sp. cf. *dhimenaensis* s.l. *Baumgartner*; *Hsuum* sp.; *Parvicingula* sp. cf. *schoolhousensis* gr. Pessagno & Whalen; *Perispyridium* sp.; *Tetratrabs izeensis* Yeh; *Napora* sp.	E. Bajocian to L. Bathonian	Cordey et al. (1992) Evenchick et al. (2001) Gagnon et al. 2007
Owee. E.	?	OE(4)	*Vaugonia*	E. to Middle Oxfordian	Greig and Evenchick (1993) Evenchick et al. (2001)
Owee. E.	?	OE(5)	*Cardioceras* aff. *stantoni* Reeside	E. to Middle Oxfordian	Greig and Evenchick (1993) Evenchick et al. (2001)
Dilworth	C-458074	MD(1)	*ostreacean(?)* bivalves; *Cylindroteuthis(?)* sp.; *rhynchonellid* brachiopod	M. Toarcian to Callovian	Report J2-2006-TPP
Dilworth	C-458153	MD(2)	*Cardioceras* cf. *C. cordatum* (Sowerby) *Adabofoloceras(?)* aff. *A. pacificum* (Frebold and Tipper)	E. Oxfordian - Cordatum zone	Report J1-TPP-2008
Table M.	C-306903	TB(1)	*Scaphotrigonia(?)* sp.; *Gresslya(?)* sp.; bivalves; *pseudodicoelitids(?)* belemnites	M. Toarcian or M. Jurassic	Report J5-2004-TPP
Table M.	C-306904	TB(2)	*Ludwigia(?)* sp.; *Trigonia* sp. aff. *americana* Meek; *Trigonia* sp. aff.. *elegantissima* Meek; *Myophorella montanaensis(?)* Meek; *Plagiostoma hazeltonense(?)* McLearn; *Lima* sp.; *Chlamys(?)* sp.; terebratulid brachiopods	E. Bajocian	Report J5-2004-TPP
Table M.	37109	TB(3)	?	Bajocian	Souther (1972)
Table M.	85117	TB(4)	?	Bajocian	Souther (1972)
Eskay C.	C-201415	EC1	*Paracaloceras* cf. *multicostatum* Frebold; *Weyla* sp.; *Paracaloceras* sp.; gastropods	L. Hettang. to E. Sinemurian	Nadaraju (1993)
Eskay C.	C-201436 C-201437 C-201438 C-201604 C-201620	EC2	*Tiltoniceras* cf. *propinquum* (Whiteaves); *Weyla* sp.; bivalves; *Protogrammoceras* cf. *kurrianum* (Buckman); *Lioceratoides(?)* sp.; *Hildoceratacea* indet.	L. Pliensbachi. to E. Toarcian	Nadaraju (1993)
Eskay C.	C-159453 C-159464	EC3	*Acaeniotyle(?)* sp.; *Archaeocenosphaera* sp.; *Crucella* sp.; *Napora* sp. *Parvicingula* sp. indet. A; *Praeconocaryomma* sp.; *Stichocapsa* cf. *convexa; Stichocapsa* sp.; *Spumellaria* indet. E.; *Nasselarian* indet. A; *Pseudocrucella* sp. Cf. P. *sanfilippoae*	Aalenian to E. Bajocian	Nadaraju (1993)

Section	GSC #	ID	Fossil Description	Age	Reference
Eskay C.	C-159484 C-201628 C-201428	EC4	*Emiluvia* sp. B; *Hsuum; Parvicingula* sp. B.; *Nassellarian* indet. B; *Archaeohagiastrum longpipes Baumgartner; Emiluvia(?)* aff. *moresbyensis* Carter; *Paronaella variabilis* Carter;. *Perispyridium* sp. cf. *P. gouldi* MacLeod; *Spongostaurus* sp. A; *Spummellaria* indet.; *Stichacopsa* cf. *convexa*	Aalenian to E. Bajocian	Nadaraju (1993)
Eskay C.	?	EC5	bivalves	E. Bajocian	Roth (2002)
Eskay C.	C-201434	EC6	*Iniskinites* spp.; *Lilloettia* spp.; *Cobbanites* spp.	L. Bathonian	Nadaraju (1993)

Appendix B

This appendix accompanies chapter 2 and more fully describes the U-Pb geochronology methods and the specific analyses undertaken in this study. A full data set of samples from which probability density plots have been derived is also provided.

Methodology

Zircons from each sample were extrated using standard separation techniques (e.g. jaw crusher, disc mill, Wilfley table, Frantz magnetic separator, methylene iodine), and mounted on an epoxy mount. Individual grains were then analyzed for their U and Pb isotopic composition using a Nu Plasma MC-ICP-MS coupled to a New Wave Research UP213 laser ablation system following the methods of Simonetti et al. (2005). Since most samples yielded very low Pb concentrations due to their young age, the calculated error for the 206Pb/207Pb ages at a 2 sigma level was discarded. Instead, age uncertainties were entirely calculated at a 2 sigma level for 206Pb/238U ages. Probability distribution plots for ages of all results with <50% discordancy are given in figure 2.15.

Supplementary Data

The data presented below are for samples MC022A of the Smithers Formation (UHG) and LT035A of the Todagin assemblage (BLG). Plots have been generated using ISOPLOT 03.09 (Ludwig 2003).

.

U-Pb Laser Ablation MC-ICPMS U-Pb Results for Sample MC022A - January 15, 2009

#	Grain ID	spot size	^{206}Pb cps	^{204}Pb cps	$^{206}Pb/^{238}U$	2σ error	$^{207}Pb/^{235}U$	2σ error	$^{207}Pb/^{206}Pb$	2σ error	rho	206Pb/238U AGE (Ma)	2σ error	207Pb/235U AGE (Ma)	2σ error	207Pb/206Pb AGE (Ma)	2σ error	% Disc
1	MC022A-1	(40um)	39756	0	0.0281	0.0017	0.196	0.037	0.05051	0.00902	0.319	179	11	181	31	218	413	18.5
2	MC022A-2	(40um)	97313	0	0.0289	0.0017	0.221	0.143	0.05536	0.03562	0.091	184	11	202	112	427	1435	57.8
3	MC022A-3	(40um)	126073	0	0.0276	0.0017	0.194	0.013	0.05085	0.00112	0.941	176	11	180	11	234	51	25.3
4	MC022A-4	(40um)	77935	0	0.0274	0.0017	0.195	0.037	0.05143	0.00920	0.325	175	11	181	31	260	411	33.4
5	MC022A-5	(40um)	74447	0	0.0272	0.0017	0.189	0.013	0.05042	0.00126	0.927	173	11	176	11	214	58	19.6
6	MC022A-6	(40um)	10499	0	0.0261	0.0017	0.181	0.515	0.05040	0.14343	0.022	166	10	169	368	213	6593	22.6
7	MC022A-7	(40um)	15482	0	0.0268	0.0017	0.178	0.021	0.04813	0.00480	0.530	171	10	166	18	106	235	-62.3
8	MC022A-8	(40um)	31327	0	0.0264	0.0017	0.192	0.256	0.05276	0.07041	0.047	168	10	178	198	319	3033	47.9
9	MC022A-9	(40um)	92459	0	0.0318	0.0018	0.222	0.021	0.05070	0.00403	0.569	202	11	204	18	227	184	11.4
10	MC022A-10	(40um)	43651	0	0.0280	0.0017	0.289	0.692	0.07509	0.17944	0.025	178	11	258	436	1071	4801	84.5
11	MC022A-11	(40um)	76967	0	0.0270	0.0017	0.188	0.017	0.05056	0.00326	0.694	172	11	175	14	221	149	22.5
12	MC022A-12	(40um)	46311	0	0.0268	0.0017	0.222	0.015	0.05997	0.00177	0.903	171	10	203	13	602	64	72.6
13	MC022A-13	(40um)	24967	0	0.0268	0.0017	0.185	0.081	0.05008	0.02176	0.142	171	10	172	67	199	1009	14.4
14	MC022A-14	(40um)	52197	0	0.0269	0.0017	0.189	0.085	0.05080	0.02262	0.138	171	11	176	70	232	1028	26.4
15	MC022A-15	(40um)	99004	0	0.0267	0.0017	0.190	0.016	0.05154	0.00275	0.762	170	10	176	13	265	122	36.4
16	MC022A-16	(40um)	61002	0	0.0297	0.0017	0.216	0.307	0.05277	0.07479	0.041	189	11	199	228	319	3221	41.4
17	MC022A-17	(40um)	325234	0	0.0262	0.0017	0.181	0.012	0.05001	0.00058	0.984	167	10	169	10	196	27	15.0
18	MC022A-18	(40um)	67920	0	0.0276	0.0017	0.189	0.148	0.04982	0.03894	0.078	175	11	176	119	187	1820	6.2
19	MC022A-19	(40um)	125487	0	0.0268	0.0017	0.187	0.051	0.05052	0.01335	0.229	171	10	174	43	219	612	22.3
20	MC022A-20	(40um)	27104	0	0.0291	0.0017	0.438	0.419	0.10917	0.10413	0.062	185	11	369	260	1786	1738	90.9
21	MC022A-21	(40um)	128324	0	0.0269	0.0017	0.186	0.012	0.05013	0.00084	0.966	171	11	173	10	201	39	15.2
22	MC022A-22	(40um)	97835	0	0.0267	0.0017	0.185	0.013	0.05021	0.00149	0.903	170	10	172	11	205	69	17.4
23	MC022A-23	(40um)	125668	0	0.0279	0.0017	0.309	0.359	0.08022	0.09299	0.052	178	11	273	246	1202	2284	86.4
24	MC022A-24	(40um)	87386	0	0.0321	0.0018	0.222	0.077	0.05012	0.01713	0.158	204	11	204	62	201	794	-1.6
25	MC022A-25	(40um)	62563	0	0.0272	0.0017	0.193	0.037	0.05132	0.00937	0.320	173	11	179	31	255	420	32.6
26	MC022A-26	(40um)	69072	0	0.0272	0.0017	0.193	0.027	0.05155	0.00648	0.441	173	11	179	23	266	288	35.3
27	MC022A-27	(40um)	32601	0	0.0269	0.0017	0.191	0.039	0.05161	0.01010	0.303	171	10	178	33	268	449	36.7
28	MC022A-28	(40um)	32199	0	0.0260	0.0017	0.175	0.014	0.04874	0.00241	0.791	166	10	164	12	135	116	-22.7
29	MC022A-29	(40um)	35978	0	0.0268	0.0017	0.185	0.043	0.04996	0.01125	0.267	171	10	172	36	193	523	11.9
30	MC022A-30	(40um)	34725	0	0.0261	0.0017	0.177	0.040	0.04917	0.01077	0.279	166	10	165	34	156	513	-6.4
31	MC022A-31	(40um)	25273	0	0.0259	0.0017	0.176	0.024	0.04924	0.00599	0.466	165	10	164	21	159	284	-3.4
32	MC022A-32	(40um)	23009	0	0.0259	0.0017	0.217	0.017	0.06064	0.00267	0.824	165	10	199	14	626	95	74.6
33	MC022A-33	(40um)	32168	0	0.0265	0.0017	0.203	0.132	0.05566	0.03601	0.097	168	10	188	106	439	1440	62.4
34	MC022A-34	(40um)	52273	0	0.0262	0.0017	0.184	0.065	0.05092	0.01762	0.181	167	10	171	54	237	798	30.2
35	MC022A-35	(40um)	22871	0	0.0263	0.0017	0.180	0.158	0.04977	0.04361	0.072	167	10	168	128	184	2041	9.5
36	MC022A-36	(40um)	31502	0	0.0262	0.0017	0.179	0.020	0.04958	0.00455	0.569	167	10	167	17	175	214	5.0
37	MC022A-37	(40um)	86978	0	0.0260	0.0017	0.179	0.012	0.04985	0.00086	0.965	165	10	167	10	188	40	12.2

#	Grain ID	spot size	^{206}Pb cps	^{204}Pb cps	$^{206}Pb/^{238}U$	2σ error	$^{207}Pb/^{235}U$	2σ error	$^{207}Pb/^{206}Pb$	2σ error	rho	206Pb/238U AGE (Ma)	2σ error	207Pb/235U AGE (Ma)	2σ error	207Pb/206Pb AGE (Ma)	2σ error	% Disc
38	MC022A-38	(40um)	51519	0	0.0272	0.0017	0.192	0.043	0.05132	0.01092	0.279	173	11	179	36	255	489	32.7
39	MC022A-39	(40um)	44366	0	0.0266	0.0017	0.181	0.014	0.04947	0.00204	0.836	169	10	169	12	170	96	0.4
40	MC022A-40	(40um)	36440	0	0.0278	0.0017	0.243	0.454	0.06345	0.11838	0.033	177	11	221	316	723	3958	76.6
41	MC022A-41	(40um)	50844	0	0.0265	0.0017	0.194	0.118	0.05308	0.03203	0.104	169	10	180	95	332	1368	49.9
42	MC022A-42	(40um)	68975	0	0.0277	0.0017	0.191	0.012	0.05005	0.00071	0.974	176	11	178	10	198	33	10.9
43	MC022A-43	(40um)	72102	0	0.0259	0.0017	0.178	0.012	0.04973	0.00063	0.981	165	10	166	10	183	30	9.7
44	MC022A-44	(40um)	94243	0	0.0259	0.0017	0.177	0.017	0.04963	0.00368	0.654	165	10	165	15	178	173	7.5
45	MC022A-45	(40um)	23053	0	0.0273	0.0017	0.284	1.065	0.07559	0.28334	0.016	173	11	254	613	1084	7517	85.1
46	MC022A-46	(40um)	154769	0	0.0259	0.0017	0.180	0.012	0.05034	0.00058	0.984	165	10	168	10	211	27	22.0
47	MC022A-47	(40um)	97133	0	0.0301	0.0017	0.227	0.107	0.05457	0.02555	0.121	191	11	207	85	395	1050	52.3
48	MC022A-48	(40um)	27307	0	0.0321	0.0018	0.216	0.094	0.04885	0.02099	0.126	204	11	199	75	141	1009	-45.7
49	MC022A-49	(40um)	34584	0	0.0276	0.0017	0.182	0.031	0.04799	0.00757	0.361	175	11	170	26	99	373	-78.9
50	MC022A-50	(40um)	31372	0	0.0275	0.0017	0.183	0.047	0.04827	0.01195	0.240	175	11	170	39	112	584	-56.0
51	MC022A-51	(40um)	145341	0	0.0274	0.0017	0.189	0.012	0.04999	0.00068	0.976	174	11	175	10	194	32	10.6
52	MC022A-52	(40um)	50038	0	0.0274	0.0017	0.184	0.014	0.04863	0.00225	0.799	174	11	171	12	130	109	-34.6
53	MC022A-53	(40um)	86461	0	0.0274	0.0017	0.191	0.046	0.05064	0.01187	0.253	174	11	178	39	225	542	22.8
54	MC022A-54	(40um)	95674	0	0.0280	0.0017	0.197	0.041	0.05111	0.01006	0.293	178	11	183	34	246	453	27.9
55	MC022A-55	(40um)	160302	0	0.0280	0.0017	0.193	0.012	0.05018	0.00083	0.965	178	11	180	10	203	38	12.7
56	MC022A-56	(40um)	215610	0	0.0269	0.0017	0.192	0.073	0.05184	0.01940	0.164	171	10	178	60	278	857	39.2
57	MC022A-57	(40um)	123810	0	0.0280	0.0017	0.193	0.013	0.05003	0.00120	0.930	178	11	179	11	196	56	9.4
58	MC022A-58	(40um)	51992	0	0.0273	0.0017	0.185	0.026	0.04908	0.00621	0.437	174	11	172	22	151	296	-15.0
59	MC022A-59	(40um)	72257	0	0.0278	0.0017	0.207	0.118	0.05400	0.03061	0.107	176	11	191	95	371	1277	53.1
60	MC022A-60	(40um)	43680	0	0.0275	0.0017	0.227	0.227	0.06006	0.05978	0.061	175	11	208	172	606	2153	72.1
61	MC022A-61	(40um)	19862	0	0.0321	0.0018	0.468	2.231	0.10572	0.50407	0.011	204	11	390	938	1727	8753	89.5
62	MC022A-62	(40um)	80380	0	0.0278	0.0017	0.192	0.028	0.05001	0.00670	0.412	177	11	178	24	195	311	9.4
63	MC022A-63	(40um)	168758	0	0.0279	0.0017	0.195	0.017	0.05071	0.00310	0.704	177	11	181	14	228	141	22.4
64	MC022A-64	(40um)	21163	0	0.0286	0.0017	0.190	0.024	0.04826	0.00538	0.470	182	11	177	20	112	263	-62.9
65	MC022A-65	(40um)	43621	0	0.0276	0.0017	0.207	0.020	0.05455	0.00399	0.641	175	11	191	16	394	164	56.3
66	MC022A-66	(40um)	217774	0	0.0277	0.0017	0.203	0.060	0.05306	0.01546	0.204	176	11	187	50	331	661	47.5
67	MC022A-67	(40um)	52390	0	0.0284	0.0017	0.195	0.148	0.04994	0.03762	0.079	180	11	181	118	192	1752	6.4
68	MC022A-68	(40um)	18514	0	0.0295	0.0017	0.239	1.528	0.05867	0.37543	0.009	188	11	217	816	555	13960	67.2
69	MC022A-69	(40um)	21907	0	0.0274	0.0017	0.183	0.071	0.04834	0.01840	0.159	175	11	171	59	116	898	-51.5
70	MC022A-70	(40um)	126238	0	0.0314	0.0017	0.222	0.013	0.05111	0.00062	0.977	200	11	203	10	246	28	19.0
71	MC022A-71	(40um)	125728	0	0.0300	0.0017	0.208	0.015	0.05044	0.00222	0.794	190	11	192	13	216	102	11.9
72	MC022A-72	(40um)	42872	0	0.0285	0.0017	0.195	0.014	0.04973	0.00197	0.833	181	11	181	12	183	92	0.7
73	MC022A-73	(40um)	85584	0	0.0268	0.0017	0.184	0.012	0.04992	0.00093	0.958	170	10	172	10	191	43	10.9
74	MC022A-74	(40um)	237298	0	0.0280	0.0017	0.194	0.013	0.05020	0.00116	0.934	178	11	180	11	204	54	13.1
75	MC022A-75	(40um)	60313	0	0.0297	0.0017	0.204	0.013	0.04984	0.00128	0.914	189	11	189	11	187	60	-0.9
76	MC022A-76	(40um)	25057	0	0.0270	0.0017	0.184	0.030	0.04950	0.00747	0.380	172	11	172	25	172	352	-0.1
77	MC022A-77	(40um)	28760	0	0.0285	0.0017	0.241	0.074	0.06146	0.01851	0.194	181	11	220	59	655	646	73.4

#	Grain ID	spot size	^{206}Pb cps	^{204}Pb cps	$^{206}Pb/^{238}U$	2σ error	$^{207}Pb/^{235}U$	2σ error	$^{207}Pb/^{206}Pb$	2σ error	rho	206Pb/238U AGE (Ma)	2σ error	207Pb/235U AGE (Ma)	2σ error	207Pb/206Pb AGE (Ma)	2σ error	% Disc
78	MC022A-78	(40um)	65207	0	0.0273	0.0017	0.188	0.015	0.04979	0.00247	0.779	174	11	175	13	185	115	6.1
79	MC022A-79	(40um)	90939	0	0.0274	0.0017	0.189	0.017	0.05004	0.00326	0.686	174	11	176	14	197	151	11.7
80	MC022A-80	(40um)	66491	0	0.0270	0.0017	0.184	0.015	0.04943	0.00246	0.780	172	11	172	12	168	116	-2.0
81	MC022A-81	(40um)	57022	0	0.0271	0.0017	0.185	0.034	0.04948	0.00850	0.340	172	11	172	29	171	401	-1.0
82	MC022A-82	(40um)	43209	0	0.0265	0.0017	0.184	0.013	0.05050	0.00138	0.917	168	10	172	11	218	63	23.1
83	MC022A-83	(40um)	62735	0	0.0278	0.0017	0.215	0.026	0.05592	0.00576	0.507	177	11	197	21	449	229	61.4
84	MC022A-84	(40um)	56127	0	0.0269	0.0017	0.185	0.027	0.04982	0.00666	0.422	171	10	172	23	187	311	8.5
85	MC022A-85	(40um)	52437	0	0.0270	0.0017	0.185	0.021	0.04959	0.00480	0.540	172	11	172	18	176	226	2.2
86	MC022A-86	(40um)	140081	0	0.0265	0.0017	0.195	0.021	0.05343	0.00452	0.597	169	10	181	17	347	191	52.0
87	MC022A-87	(40um)	59018	0	0.0264	0.0017	0.179	0.034	0.04926	0.00880	0.333	168	10	168	29	160	418	-4.9
88	MC022A-88	(40um)	15251	0	0.0295	0.0017	0.229	0.843	0.05646	0.20756	0.016	187	11	210	530	470	8137	61.1
89	MC022A-89	(40um)	62052	0	0.0268	0.0017	0.183	0.012	0.04956	0.00088	0.961	171	10	171	10	174	42	2.1
90	MC022A-90	(40um)	49350	0	0.0269	0.0017	0.180	0.134	0.04866	0.03594	0.084	171	10	168	109	131	1737	-30.5
97	MC022A-91	(40um)	22497	0	0.0271	0.0017	0.186	0.167	0.04994	0.04457	0.069	172	11	174	134	192	2075	10.6
98	MC022A-92	(40um)	39390	0	0.0269	0.0017	0.184	0.015	0.04979	0.00249	0.780	171	10	172	13	185	116	7.8
99	MC022A-93	(40um)	66014	0	0.0263	0.0017	0.183	0.018	0.05054	0.00397	0.628	167	10	171	16	220	182	24.3
100	MC022A-94	(40um)	36452	0	0.0305	0.0017	0.208	0.050	0.04951	0.01148	0.237	194	11	192	41	172	541	-12.7
101	MC022A-95	(40um)	55326	0	0.0268	0.0017	0.184	0.032	0.04980	0.00803	0.360	171	10	172	27	186	376	8.2
102	MC022A-96	(40um)	46149	0	0.0261	0.0017	0.181	0.012	0.05031	0.00098	0.956	166	10	169	10	209	45	21.0
103	MC022A-97	(40um)	197329	0	0.0315	0.0017	0.222	0.013	0.05121	0.00088	0.955	200	11	204	11	250	40	20.6
104	MC022A-98	(40um)	70749	0	0.0273	0.0017	0.188	0.021	0.04996	0.00480	0.539	174	11	175	18	193	223	10.1
105	MC022A-99	(40um)	87296	0	0.0274	0.0017	0.189	0.015	0.05005	0.00255	0.769	174	11	176	13	197	118	11.9
106	MC022A-100	(40um)	220786	0	0.0261	0.0017	0.185	0.029	0.05140	0.00734	0.408	166	10	172	24	259	328	36.4
107	MC022A-101	(40um)	63400	0	0.0273	0.0017	0.187	0.013	0.04980	0.00166	0.879	173	11	174	11	186	78	6.7
108	MC022A-102	(40um)	60716	0	0.0268	0.0017	0.183	0.025	0.04955	0.00589	0.464	171	10	171	21	174	277	1.9
109	MC022A-103	(40um)	71267	0	0.0266	0.0017	0.182	0.013	0.04962	0.00189	0.855	169	10	170	11	177	89	4.3
110	MC022A-104	(40um)	58043	0	0.0269	0.0017	0.187	0.037	0.05049	0.00949	0.314	171	10	174	31	218	435	21.6
111	MC022A-105	(40um)	85665	0	0.0271	0.0017	0.185	0.017	0.04969	0.00334	0.677	172	11	173	14	180	157	4.7
112	MC022A-106	(40um)	65405	0	0.0271	0.0017	0.188	0.012	0.05023	0.00073	0.973	172	11	175	10	206	34	16.4
113	MC022A-107	(40um)	27748	0	0.0289	0.0017	0.494	0.100	0.12392	0.02398	0.291	184	11	408	66	2013	343	92.1
114	MC022A-108	(40um)	56926	0	0.0256	0.0017	0.176	0.012	0.04989	0.00098	0.957	163	10	165	10	190	46	14.3
115	MC022A-109	(40um)	82311	0	0.0264	0.0017	0.181	0.013	0.04968	0.00151	0.901	168	10	168	11	180	71	7.0
116	MC022A-110	(40um)	40024	0	0.0259	0.0017	0.181	0.029	0.05054	0.00750	0.396	165	10	169	25	220	343	25.3
117	MC022A-111	(40um)	25354	0	0.0266	0.0017	0.180	0.020	0.04903	0.00439	0.573	169	10	168	17	149	210	-13.8
118	MC022A-112	(40um)	66103	0	0.0262	0.0017	0.182	0.012	0.05048	0.00089	0.963	166	10	170	10	217	41	23.6
119	MC022A-113	(40um)	22749	0	0.0268	0.0017	0.205	0.477	0.05529	0.12892	0.027	171	10	189	339	424	5202	60.5
120	MC022A-114	(40um)	45635	0	0.0264	0.0017	0.183	0.014	0.05046	0.00191	0.858	168	10	171	12	216	88	22.7

#	Grain ID	spot size	^{206}Pb cps	^{204}Pb cps	$^{206}Pb/^{238}U$	2σ error	$^{207}Pb/^{235}U$	2σ error	$^{207}Pb/^{206}Pb$	2σ error	rho	206Pb/238U AGE (Ma)	2σ error	207Pb/235U AGE (Ma)	2σ error	207Pb/206Pb AGE (Ma)	2σ error	% Disc
121	MC022A-115	(40um)	77812	0	0.0270	0.0017	0.204	0.044	0.05483	0.01129	0.289	171	11	188	36	405	461	58.4
122	MC022A-116	(40um)	77679	0	0.0326	0.0018	0.322	0.485	0.07174	0.10783	0.036	207	11	284	317	979	3062	80.1
123	MC022A-117	(40um)	60986	0	0.0263	0.0017	0.181	0.012	0.05005	0.00084	0.967	167	10	169	10	197	39	15.5
124	MC022A-118	(40um)	34432	0	0.0270	0.0017	0.194	0.030	0.05214	0.00749	0.397	171	11	180	25	292	328	41.7
125	MC022A-119	(40um)	54335	0	0.0305	0.0017	0.212	0.016	0.05051	0.00259	0.742	194	11	195	14	219	119	11.6
126	MC022A-120	(40um)	65538	0	0.0279	0.0017	0.192	0.025	0.04988	0.00573	0.466	177	11	178	21	190	267	6.6
127	MC022A-121	(40um)	32730	0	0.0261	0.0017	0.186	0.054	0.05160	0.01456	0.220	166	10	173	45	268	647	38.4
128	MC022A-122	(40um)	72712	0	0.0258	0.0017	0.179	0.017	0.05021	0.00357	0.670	164	10	167	15	205	165	20.0
129	MC022A-123	(40um)	79476	0	0.0258	0.0017	0.181	0.046	0.05103	0.01259	0.252	164	10	169	39	242	569	32.6
130	MC022A-124	(40um)	56936	0	0.0261	0.0017	0.197	0.076	0.05455	0.02072	0.165	166	10	182	62	394	852	58.5
133	MC022A-125	(30um)	13387	0	0.0325	0.0018	0.209	0.027	0.04659	0.00539	0.424	206	11	193	22	28	277	-639.9
134	MC022A-126	(30um)	17209	0	0.0268	0.0017	0.177	0.015	0.04782	0.00293	0.714	170	10	165	13	90	145	-89.8
135	MC022A-127	(30um)	25934	0	0.0274	0.0017	0.178	0.014	0.04711	0.00222	0.793	174	11	166	12	55	112	-222.5
136	MC022A-128	(30um)	26722	0	0.0271	0.0017	0.181	0.020	0.04850	0.00459	0.548	172	11	169	17	124	223	-39.6
137	MC022A-129	(30um)	132896	0	0.0291	0.0017	0.210	0.147	0.05243	0.03666	0.084	185	11	194	117	304	1593	39.9
138	MC022A-130	(30um)	8708	0	0.0273	0.0017	0.167	0.424	0.04436	0.11255	0.024	174	11	157	315	-91	6223	295.3
139	MC022A-131	(30um)	17468	0	0.0276	0.0017	0.215	0.110	0.05658	0.02880	0.119	175	11	198	88	475	1126	63.9
140	MC022A-132	(30um)	10758	0	0.0278	0.0017	0.184	0.669	0.04790	0.17457	0.017	177	11	171	455	94	8631	-89.0
141	MC022A-133	(30um)	19875	0	0.0273	0.0017	0.180	0.011	0.04765	0.00073	0.971	174	11	168	10	82	36	-113.6
142	MC022A-134	(30um)	32662	0	0.0271	0.0017	0.190	0.040	0.05082	0.01025	0.293	172	11	177	34	232	466	26.2
143	MC022A-135	(30um)	25876	0	0.0279	0.0017	0.188	0.016	0.04889	0.00309	0.692	177	11	175	14	143	148	-24.5
144	MC022A-136	(30um)	44191	0	0.0277	0.0017	0.187	0.012	0.04889	0.00090	0.957	176	11	174	10	143	43	-23.7
145	MC022A-137	(30um)	18991	0	0.0274	0.0017	0.179	0.057	0.04742	0.01479	0.193	174	11	167	48	70	742	-150.0
146	MC022A-138	(30um)	16545	0	0.0286	0.0017	0.198	0.180	0.05010	0.04555	0.065	182	11	183	142	200	2111	9.0
147	MC022A-139	(30um)	17541	0	0.0273	0.0017	0.173	0.305	0.04609	0.08094	0.035	174	11	162	234	2	4232	-7901.0
148	MC022A-140	(30um)	12501	0	0.0279	0.0017	0.255	0.283	0.06645	0.07350	0.055	177	11	231	206	821	2310	79.5
149	MC022A-141	(30um)	20412	0	0.0271	0.0017	0.182	0.121	0.04853	0.03208	0.093	173	11	169	99	125	1556	-38.1
150	MC022A-142	(30um)	28232	0	0.0272	0.0017	0.183	0.015	0.04883	0.00264	0.753	173	11	171	13	140	127	-24.1
151	MC022A-143	(30um)	55888	0	0.0284	0.0017	0.196	0.022	0.05001	0.00490	0.520	181	11	182	19	196	228	7.8
152	MC022A-144	(30um)	14124	0	0.0275	0.0017	0.184	0.123	0.04858	0.03229	0.092	175	11	171	100	128	1564	-37.2
153	MC022A-145	(30um)	9095	0	0.0271	0.0017	0.176	0.198	0.04717	0.05291	0.055	172	11	165	158	58	2674	-200.5
154	MC022A-147	(30um)	40760	0	0.0265	0.0017	0.199	0.181	0.05460	0.04951	0.069	168	10	185	143	396	2033	58.2
155	MC022A-148	(30um)	16857	0	0.0268	0.0017	0.172	0.032	0.04656	0.00814	0.337	171	11	161	27	27	419	-547.4
156	MC022A-149	(30um)	11284	0	0.0263	0.0017	0.171	0.065	0.04737	0.01764	0.168	167	10	161	55	68	886	-147.9
157	MC022A-150	(30um)	11496	0	0.0275	0.0017	0.188	0.096	0.04969	0.02524	0.120	175	11	175	79	181	1183	3.4

U-Pb Laser Ablation MC-ICPMS U-Pb Results for Sample LT035A - January 14, 2009

#	Grain ID	spot size	^{206}Pb cps	^{204}Pb cps	^{206}Pb/^{238}U	2σ error	^{207}Pb/^{235}U	2σ error	^{207}Pb/^{206}Pb	2σ error	rho	206Pb/238U AGE (Ma)	2σ error	207Pb/235U AGE (Ma)	2σ error	207Pb/206Pb AGE (Ma)	2σ error	% Disc
1	LT035A-1	(40um)	49126	0	0.0327	0.0014	0.237	0.111	0.05246	0.02462	0.090	207	9	216	88	306	1069	32.6
2	LT035A-2	(40um)	65573	0	0.0302	0.0013	0.218	0.033	0.05243	0.00756	0.293	192	8	200	27	304	328	37.5
3	LT035A-3	(40um)	109849	0	0.0267	0.0013	0.188	0.022	0.05096	0.00553	0.399	170	8	175	19	239	250	29.2
4	LT035A-4	(40um)	60146	0	0.0327	0.0014	0.231	0.012	0.05132	0.00150	0.824	207	9	211	10	255	67	19.1
5	LT035A-5	(40um)	44027	0	0.0287	0.0013	0.214	0.043	0.05416	0.01066	0.225	182	8	197	36	378	443	52.4
6	LT035A-6	(40um)	122601	0	0.0305	0.0013	0.216	0.019	0.05148	0.00399	0.494	193	8	199	16	262	178	26.6
7	LT035A-7	(40um)	40336	0	0.0555	0.0019	0.416	0.022	0.05435	0.00217	0.659	348	12	353	16	386	90	9.9
8	LT035A-8	(40um)	95806	0	0.0316	0.0014	0.227	0.011	0.05213	0.00103	0.909	201	9	208	9	291	45	31.6
9	LT035A-9	(40um)	39127	0	0.0281	0.0013	0.195	0.032	0.05023	0.00787	0.281	179	8	181	27	206	363	13.4
10	LT035A-10	(40um)	26861	0	0.0326	0.0014	0.227	0.017	0.05052	0.00315	0.563	207	9	208	14	219	144	5.9
11	LT035A-11	(40um)	72245	0	0.0300	0.0013	0.212	0.020	0.05129	0.00423	0.473	190	8	195	16	254	190	25.4
12	LT035A-12	(40um)	117898	0	0.0265	0.0013	0.189	0.010	0.05171	0.00096	0.932	168	8	175	8	273	42	38.8
13	LT035A-13	(40um)	102710	0	0.0305	0.0013	0.216	0.010	0.05137	0.00080	0.942	194	8	199	8	257	36	25.0
14	LT035A-14	(40um)	78591	0	0.0330	0.0014	0.237	0.029	0.05214	0.00587	0.350	210	9	216	23	292	257	28.6
15	LT035A-15	(40um)	126492	0	0.0270	0.0013	0.189	0.011	0.05083	0.00160	0.831	171	8	176	9	233	73	26.7
16	LT035A-16	(40um)	143665	0	0.0321	0.0014	0.241	0.022	0.05436	0.00435	0.487	204	9	219	18	386	180	48.0
17	LT035A-17	(40um)	59163	0	0.0300	0.0013	0.215	0.024	0.05195	0.00536	0.396	191	8	198	20	283	236	33.1
18	LT035A-18	(40um)	60411	0	0.0455	0.0017	0.330	0.057	0.05255	0.00888	0.213	287	10	290	43	309	385	7.3
19	LT035A-19	(40um)	232610	0	0.0620	0.0021	0.477	0.017	0.05576	0.00066	0.946	388	13	396	12	443	26	12.8
20	LT035A-20	(40um)	100992	0	0.0295	0.0013	0.206	0.010	0.05055	0.00067	0.958	188	8	190	8	220	31	15.1
21	LT035A-21	(40um)	43061	0	0.0252	0.0012	0.173	0.009	0.04989	0.00078	0.953	160	8	162	8	190	36	15.8
22	LT035A-22	(40um)	136594	0	0.0292	0.0013	0.204	0.020	0.05078	0.00451	0.452	185	8	189	17	231	205	19.9
23	LT035A-23	(40um)	88835	0	0.0319	0.0014	0.223	0.011	0.05086	0.00099	0.910	202	9	205	9	234	45	13.9
24	LT035A-24	(40um)	60858	0	0.0297	0.0013	0.210	0.011	0.05119	0.00158	0.823	189	8	193	9	250	71	24.8
25	LT035A-25	(40um)	60838	0	0.0322	0.0014	0.231	0.020	0.05208	0.00397	0.489	204	9	211	17	289	174	29.8
26	LT035A-26	(40um)	94989	0	0.0293	0.0013	0.220	0.067	0.05438	0.01634	0.148	186	8	202	54	387	675	52.7
27	LT035A-27	(40um)	92374	0	0.0249	0.0012	0.173	0.013	0.05049	0.00269	0.681	159	8	162	11	218	123	27.5
28	LT035A-28	(40um)	133694	0	0.0317	0.0014	0.238	0.050	0.05436	0.01115	0.207	201	9	216	40	386	461	48.6
29	LT035A-29	(40um)	53036	0	0.0297	0.0013	0.209	0.011	0.05099	0.00133	0.863	189	8	192	9	240	60	21.8
30	LT035A-30	(40um)	27222	0	0.0264	0.0013	0.180	0.011	0.04949	0.00171	0.811	168	8	168	9	171	80	2.0
31	LT035A-31	(40um)	54816	0	0.0317	0.0014	0.226	0.012	0.05175	0.00159	0.815	201	9	207	10	274	70	27.2
32	LT035A-32	(40um)	63882	0	0.0285	0.0013	0.233	0.068	0.05926	0.01698	0.157	181	8	213	54	577	623	69.5
33	LT035A-33	(40um)	18621	0	0.0272	0.0013	0.180	0.014	0.04818	0.00288	0.616	173	8	168	12	108	141	-60.9

#	Grain ID	spot size	^{206}Pb cps	^{204}Pb cps	$^{206}Pb/^{238}U$	2σ error	$^{207}Pb/^{235}U$	2σ error	$^{207}Pb/^{206}Pb$	2σ error	rho	206Pb/238U AGE (Ma)	2σ error	207Pb/235U AGE (Ma)	2σ error	207Pb/206Pb AGE (Ma)	2σ error	% Disc
34	LT035A-34	(40um)	148230	0	0.0302	0.0013	0.212	0.014	0.05096	0.00237	0.689	192	8	196	11	239	107	19.9
35	LT035A-35	(40um)	38250	0	0.0249	0.0012	0.165	0.020	0.04813	0.00542	0.402	158	8	155	18	106	266	-50.2
36	LT035A-36	(40um)	114730	0	0.0338	0.0014	0.240	0.026	0.05157	0.00505	0.392	214	9	219	21	266	225	19.9
37	LT035A-37	(40um)	84509	0	0.0285	0.0013	0.199	0.010	0.05069	0.00100	0.918	181	8	185	8	227	46	20.4
38	LT035A-38	(40um)	73736	0	0.0285	0.0013	0.201	0.043	0.05124	0.01070	0.213	181	8	186	36	251	481	28.3
39	LT035A-39	(40um)	31412	0	0.0331	0.0014	0.230	0.314	0.05032	0.06872	0.031	210	9	210	231	210	3166	0.0
40	LT035A-40	(40um)	46133	0	0.0314	0.0014	0.218	0.052	0.05030	0.01180	0.181	199	8	200	42	209	544	4.8
41	LT035A-41	(40um)	62176	0	0.0520	0.0018	0.404	0.128	0.05631	0.01777	0.112	327	11	344	89	465	699	30.4
42	LT035A-42	(40um)	85216	0	0.0314	0.0014	0.223	0.031	0.05152	0.00680	0.311	199	8	205	25	264	303	24.9
43	LT035A-43	(40um)	168667	0	0.0256	0.0012	0.193	0.223	0.05470	0.06309	0.042	163	8	179	174	400	2585	60.0
44	LT035A-44	(40um)	54623	0	0.0285	0.0013	0.196	0.014	0.04982	0.00269	0.644	181	8	181	12	187	126	3.1
45	LT035A-45	(40um)	67129	0	0.0311	0.0014	0.216	0.027	0.05042	0.00591	0.348	197	8	199	22	215	271	8.1
46	LT035A-46	(40um)	132329	0	0.0329	0.0014	0.234	0.016	0.05149	0.00277	0.619	209	9	213	13	263	123	20.9
47	LT035A-47	(40um)	122598	0	0.0303	0.0013	0.214	0.017	0.05134	0.00324	0.572	192	8	197	14	256	145	25.3
48	LT035A-48	(40um)	56110	0	0.0319	0.0014	0.220	0.029	0.04999	0.00632	0.322	203	9	202	24	195	294	-4.0
49	LT035A-49	(40um)	131147	0	0.0554	0.0019	0.416	0.016	0.05447	0.00080	0.923	347	12	353	11	390	33	11.3
50	LT035A-50	(40um)	36494	0	0.0521	0.0019	0.391	0.194	0.05437	0.02697	0.072	328	11	335	133	387	1114	15.7
51	LT035A-51	(40um)	31693	0	0.0318	0.0014	0.213	0.038	0.04864	0.00836	0.243	202	9	196	31	131	404	-55.3
52	LT035A-52	(40um)	27416	0	0.0279	0.0013	0.179	0.201	0.04673	0.05224	0.041	177	8	168	160	35	2677	-408.2
53	LT035A-53	(40um)	83237	0	0.0261	0.0013	0.183	0.016	0.05093	0.00364	0.558	166	8	171	13	237	165	30.4
54	LT035A-54	(40um)	84375	0	0.0283	0.0013	0.209	0.020	0.05372	0.00459	0.472	180	8	193	17	359	193	50.7
55	LT035A-55	(40um)	71690	0	0.0334	0.0015	0.252	0.044	0.05480	0.00928	0.252	212	9	228	35	404	379	48.4
56	LT035A-56	(40um)	71243	0	0.0291	0.0013	0.203	0.022	0.05060	0.00505	0.411	185	8	188	19	223	231	17.1
57	LT035A-57	(40um)	69004	0	0.0308	0.0013	0.215	0.016	0.05070	0.00298	0.596	195	8	198	13	227	136	14.1
58	LT035A-58	(40um)	66358	0	0.0289	0.0013	0.213	0.023	0.05355	0.00526	0.418	183	8	196	19	352	222	48.6
59	LT035A-59	(40um)	92720	0	0.0306	0.0013	0.214	0.029	0.05071	0.00649	0.324	194	8	197	24	228	296	14.9
60	LT035A-60	(40um)	93389	0	0.0307	0.0013	0.218	0.021	0.05141	0.00444	0.452	195	8	200	17	259	198	25.1
61	LT035A-61	(40um)	42500	0	0.0322	0.0014	0.232	0.011	0.05230	0.00104	0.906	204	9	212	9	299	45	32.1
62	LT035A-62	(40um)	119967	0	0.0290	0.0013	0.217	0.772	0.05424	0.19316	0.013	184	8	199	499	381	8007	52.3
63	LT035A-63	(40um)	103750	0	0.0323	0.0014	0.259	0.096	0.05815	0.02140	0.115	205	9	234	75	536	805	62.7
64	LT035A-64	(40um)	89365	0	0.0256	0.0012	0.190	0.012	0.05367	0.00205	0.786	163	8	176	10	357	86	55.0
65	LT035A-65	(40um)	100033	0	0.0319	0.0014	0.227	0.010	0.05170	0.00080	0.941	203	9	208	9	272	35	26.0
66	LT035A-66	(40um)	30842	0	0.0319	0.0014	0.246	0.107	0.05601	0.02429	0.099	202	9	224	84	453	963	56.2
67	LT035A-67	(40um)	262360	0	0.0338	0.0014	0.249	0.388	0.05347	0.08309	0.027	214	9	226	274	349	3513	39.2
68	LT035A-68	(40um)	85944	0	0.0505	0.0018	0.421	0.143	0.06042	0.02038	0.107	317	11	356	97	619	728	49.9
69	LT035A-69	(40um)	104809	0	0.0297	0.0013	0.216	0.029	0.05277	0.00680	0.327	189	8	199	24	319	293	41.5

#	Grain ID	spot size	^{206}Pb cps	^{204}Pb cps	$^{206}Pb/^{238}U$	2σ error	$^{207}Pb/^{235}U$	2σ error	$^{207}Pb/^{206}Pb$	2σ error	rho	206Pb/238U AGE (Ma)	2σ error	207Pb/235U AGE (Ma)	2σ error	207Pb/206Pb AGE (Ma)	2σ error	% Disc
70	LT035A-70	(40um)	120082	0	0.0297	0.0013	0.210	0.016	0.05141	0.00327	0.574	188	8	194	14	259	146	27.7
71	LT035A-71	(40um)	200214	0	0.0325	0.0014	0.232	0.010	0.05174	0.00067	0.957	206	9	212	9	274	30	25.0
72	LT035A-72	(40um)	118480	0	0.0310	0.0014	0.224	0.015	0.05250	0.00252	0.672	197	8	206	12	307	109	36.5
73	LT035A-73	(40um)	112271	0	0.0311	0.0014	0.221	0.010	0.05145	0.00077	0.945	198	8	203	8	261	35	24.7
74	LT035A-74	(40um)	45590	0	0.0315	0.0014	0.235	0.043	0.05410	0.00972	0.234	200	8	214	35	375	404	47.4
75	LT035A-75	(40um)	146870	0	0.0510	0.0019	0.403	0.023	0.05726	0.00254	0.643	321	12	344	17	501	98	36.9
76	LT035A-76	(40um)	164103	0	0.0371	0.0016	0.293	0.108	0.05729	0.02107	0.114	235	10	261	82	503	809	54.3
77	LT035A-77	(40um)	155038	0	0.0322	0.0014	0.242	0.081	0.05467	0.01821	0.129	204	9	220	64	399	747	49.6
78	LT035A-78	(40um)	62689	0	0.0316	0.0014	0.227	0.017	0.05207	0.00319	0.577	200	9	207	14	289	140	31.0
79	LT035A-79	(40um)	83266	0	0.0342	0.0014	0.252	0.011	0.05353	0.00094	0.921	217	9	229	9	352	39	39.0
80	LT035A-80	(40um)	45125	0	0.0302	0.0013	0.212	0.040	0.05096	0.00945	0.232	192	8	195	33	239	428	20.0
81	LT035A-81	(40um)	59687	0	0.0333	0.0014	0.257	0.030	0.05602	0.00617	0.362	211	9	232	24	453	244	54.3
82	LT035A-82	(40um)	68169	0	0.0316	0.0014	0.329	0.149	0.07550	0.03406	0.095	200	8	289	108	1082	905	82.7
83	LT035A-83	(40um)	83260	0	0.0318	0.0014	0.229	0.011	0.05220	0.00124	0.875	202	9	209	9	294	54	31.9
84	LT035A-84	(40um)	42876	0	0.0279	0.0013	0.197	0.011	0.05122	0.00156	0.836	177	8	183	9	251	70	29.6
85	LT035A-85	(40um)	67181	0	0.0324	0.0014	0.259	0.122	0.05799	0.02727	0.091	205	9	234	94	529	1030	62.2
86	LT035A-86	(40um)	43090	0	0.0333	0.0014	0.270	0.204	0.05870	0.04425	0.056	211	9	243	151	556	1644	63.0
87	LT035A-87	(40um)	146957	0	0.0294	0.0013	0.231	0.049	0.05696	0.01184	0.211	187	8	211	40	490	459	62.8
88	LT035A-88	(40um)	62195	0	0.0329	0.0014	0.242	0.042	0.05325	0.00907	0.241	209	9	220	34	339	386	39.1
89	LT035A-89	(40um)	135859	0	0.0385	0.0018	0.288	0.015	0.05413	0.00147	0.862	244	11	257	12	377	61	35.9
90	LT035A-90	(40um)	77039	0	0.0310	0.0013	0.234	0.092	0.05468	0.02144	0.111	197	8	213	73	399	879	51.5
91	LT035A-91	(40um)	72982	0	0.0319	0.0014	0.282	0.076	0.06422	0.01717	0.158	202	9	252	59	749	565	74.1
92	LT035A-92	(40um)	62314	0	0.0292	0.0013	0.211	0.018	0.05231	0.00389	0.518	186	8	194	15	299	169	38.4
93	LT035A-93	(40um)	131070	3896	0.0532	0.0050	1.493	0.416	0.20352	0.05342	0.338	334	31	927	157	2855	427	90.5
94	LT035A-94	(40um)	109263	0	0.0297	0.0013	0.212	0.011	0.05185	0.00143	0.851	188	8	195	9	279	63	32.9
95	LT035A-95	(40um)	73226	0	0.0341	0.0014	0.250	0.018	0.05316	0.00301	0.599	216	9	227	14	336	128	36.1
96	LT035A-96	(40um)	100374	0	0.0309	0.0013	0.222	0.017	0.05205	0.00327	0.571	196	8	203	14	288	144	32.3
97	LT035A-97	(40um)	143974	0	0.0309	0.0014	0.231	0.227	0.05426	0.05319	0.045	196	9	211	172	382	2204	49.3
98	LT035A-98	(40um)	37598	0	0.0277	0.0013	0.203	0.526	0.05306	0.13760	0.018	176	8	187	368	331	5881	47.5
99	LT035A-99	(40um)	60755	0	0.0281	0.0013	0.205	0.012	0.05294	0.00174	0.813	178	8	189	10	326	75	45.9
100	LT035A-100	(40um)	94864	0	0.0460	0.0017	0.358	0.068	0.05633	0.01047	0.199	290	11	310	49	466	412	38.5
101	LT035A-101	(40um)	71085	0	0.0311	0.0014	0.225	0.010	0.05244	0.00075	0.950	198	8	206	8	305	33	35.7
102	LT035A-102	(40um)	97388	0	0.0278	0.0013	0.229	0.115	0.05981	0.02991	0.092	177	8	210	91	597	1083	71.3
103	LT035A-103	(40um)	77675	0	0.0433	0.0017	0.324	0.041	0.05423	0.00655	0.306	273	10	285	31	381	272	28.9
104	LT035A-104	(40um)	90743	0	0.0415	0.0017	0.323	0.021	0.05642	0.00278	0.650	262	11	284	16	469	109	45.0
105	LT035A-105	(40um)	55319	0	0.0317	0.0014	0.260	0.284	0.05960	0.06499	0.039	201	9	235	206	589	2365	66.9

#	Grain ID	spot size	^{206}Pb cps	^{204}Pb cps	$^{206}Pb/^{238}U$	2σ error	$^{207}Pb/^{235}U$	2σ error	$^{207}Pb/^{206}Pb$	2σ error	rho	206Pb/238U AGE (Ma)	2σ error	207Pb/235U AGE (Ma)	2σ error	207Pb/206Pb AGE (Ma)	2σ error	% Disc
106	LT035A-106	(40um)	54558	0	0.0292	0.0013	0.219	0.029	0.05436	0.00668	0.344	185	8	201	24	386	276	52.8
107	LT035A-107	(40um)	79865	0	0.0311	0.0014	0.224	0.010	0.05224	0.00067	0.960	197	8	205	8	296	29	33.9
108	LT035A-108	(40um)	55479	0	0.0370	0.0015	0.512	0.184	0.10030	0.03584	0.112	234	9	420	117	1630	664	87.1
109	LT035A-109	(40um)	87176	0	0.0316	0.0014	0.252	0.090	0.05779	0.02053	0.120	201	9	228	71	522	780	62.5
110	LT035A-110	(40um)	85345	0	0.0304	0.0013	0.223	0.011	0.05325	0.00127	0.879	193	8	204	9	339	54	43.8
111	LT035A-111	(40um)	61053	0	0.0291	0.0013	0.208	0.016	0.05190	0.00336	0.573	185	8	192	14	281	148	34.6
112	LT035A-112	(40um)	71590	0	0.0301	0.0013	0.272	0.293	0.06550	0.07057	0.041	191	8	244	210	791	2261	77.0
113	LT035A-113	(40um)	154367	0	0.0317	0.0014	0.227	0.010	0.05193	0.00062	0.964	201	9	208	8	281	27	29.2
114	LT035A-114	(40um)	88835	0	0.0297	0.0013	0.304	0.030	0.07412	0.00645	0.455	189	8	269	23	1045	176	83.1
115	LT035A-115	(40um)	114474	0	0.0297	0.0013	0.212	0.010	0.05185	0.00065	0.963	189	8	196	8	279	29	32.8
116	LT035A-116	(40um)	42434	0	0.0324	0.0014	0.240	0.023	0.05361	0.00448	0.454	206	9	218	18	355	189	42.6
117	LT035A-117	(40um)	48913	0	0.0326	0.0014	0.232	0.010	0.05164	0.00071	0.951	207	9	212	8	270	32	23.6
118	LT035A-118	(40um)	134306	0	0.0584	0.0020	0.460	0.048	0.05708	0.00559	0.332	366	12	384	33	495	216	26.8
119	LT035A-119	(40um)	97670	0	0.0292	0.0013	0.208	0.017	0.05172	0.00355	0.548	185	8	192	14	273	157	32.6
120	LT035A-120	(40um)	184982	0	0.0311	0.0014	0.222	0.011	0.05190	0.00131	0.865	197	8	204	9	281	58	30.3
121	LT035A-121	(40um)	134023	0	0.0308	0.0013	0.221	0.011	0.05206	0.00128	0.871	195	8	203	9	288	56	32.6
122	LT035A-122	(40um)	172969	0	0.0472	0.0018	0.375	0.044	0.05767	0.00648	0.317	297	11	324	32	517	247	43.5
123	LT035A-123	(40um)	73822	0	0.0325	0.0014	0.233	0.010	0.05194	0.00068	0.956	206	9	213	8	283	30	27.4
124	LT035A-124	(40um)	54982	0	0.0302	0.0013	0.233	0.118	0.05593	0.02837	0.087	192	8	212	93	449	1127	58.2
125	LT035A-125	(40um)	58480	0	0.0251	0.0012	0.176	0.011	0.05090	0.00189	0.798	160	8	164	9	236	86	32.9
126	LT035A-126	(40um)	123027	0	0.0254	0.0012	0.181	0.010	0.05182	0.00100	0.930	161	8	169	8	277	44	42.3
127	LT035A-127	(40um)	151084	0	0.0302	0.0013	0.219	0.011	0.05248	0.00130	0.871	192	8	201	9	306	57	38.0
128	LT035A-128	(40um)	69161	0	0.0319	0.0014	0.249	0.140	0.05647	0.03169	0.076	203	9	225	108	471	1242	57.9
129	LT035A-129	(40um)	77703	0	0.0308	0.0013	0.234	0.055	0.05509	0.01285	0.184	195	8	213	45	416	521	53.8
130	LT035A-130	(40um)	72313	0	0.0301	0.0013	0.213	0.011	0.05144	0.00128	0.871	191	8	196	9	261	57	27.1
131	LT035A-131	(40um)	75864	0	0.0295	0.0013	0.212	0.013	0.05197	0.00236	0.701	188	8	195	11	284	104	34.5
132	LT035A-132	(40um)	124981	0	0.0310	0.0014	0.226	0.025	0.05282	0.00536	0.395	197	8	207	20	321	230	39.2
133	LT035A-133	(40um)	64498	0	0.0294	0.0013	0.211	0.012	0.05215	0.00179	0.793	187	8	195	10	292	78	36.6
134	LT035A-134	(40um)	112270	0	0.0298	0.0013	0.218	0.010	0.05296	0.00075	0.953	189	8	200	8	327	32	42.7
135	LT035A-135	(40um)	206664	0	0.0315	0.0014	0.223	0.011	0.05150	0.00112	0.895	200	9	205	9	263	50	24.5
136	LT035A-136	(40um)	284156	0	0.0553	0.0019	0.445	0.028	0.05836	0.00305	0.556	347	12	374	19	543	114	37.1
137	LT035A-137	(40um)	114689	0	0.0300	0.0013	0.217	0.011	0.05245	0.00149	0.842	191	8	199	9	305	65	38.1
138	LT035A-138	(40um)	57552	0	0.0303	0.0013	0.224	0.012	0.05355	0.00164	0.821	193	8	205	10	352	69	46.0
139	LT035A-139	(40um)	41262	0	0.0305	0.0013	0.265	0.378	0.06304	0.08982	0.031	194	8	239	266	709	3030	73.7
140	LT035A-140	(40um)	383253	486	0.0449	0.0017	0.295	0.040	0.04765	0.00613	0.280	283	10	263	31	82	305	-251.1
141	LT035A-141	(40um)	105436	0	0.0295	0.0013	0.211	0.010	0.05191	0.00094	0.927	187	8	194	9	281	41	33.9

#	Grain ID	spot size	^{206}Pb cps	^{204}Pb cps	$^{206}Pb/^{238}U$	2σ error	$^{207}Pb/^{235}U$	2σ error	$^{207}Pb/^{206}Pb$	2σ error	rho	206Pb/238U AGE (Ma)	2σ error	207Pb/235U AGE (Ma)	2σ error	207Pb/206Pb AGE (Ma)	2σ error	% Disc
142	LT035A-142	(40um)	102315	0	0.0254	0.0012	0.181	0.009	0.05165	0.00073	0.960	162	8	169	8	270	33	40.6
143	LT035A-143	(40um)	67313	0	0.0301	0.0013	0.227	0.014	0.05460	0.00250	0.695	191	8	207	12	396	103	52.5
144	LT035A-144	(40um)	40696	0	0.0320	0.0014	0.231	0.025	0.05242	0.00510	0.403	203	9	211	20	304	222	33.6
145	LT035A-145	(40um)	121258	0	0.0319	0.0014	0.231	0.013	0.05245	0.00206	0.737	203	9	211	11	305	90	34.1
146	LT035A-146	(40um)	96973	0	0.0259	0.0012	0.183	0.010	0.05122	0.00128	0.887	165	8	170	8	251	58	34.8
147	LT035A-147	(40um)	78442	0	0.0306	0.0013	0.231	0.038	0.05485	0.00857	0.270	194	8	211	31	406	350	52.9
148	LT035A-148	(40um)	91241	0	0.0330	0.0014	0.239	0.013	0.05257	0.00176	0.783	209	9	218	11	310	76	33.0
149	LT035A-149	(40um)	81616	0	0.0483	0.0023	0.378	0.039	0.05675	0.00519	0.465	304	14	325	28	482	202	37.8
150	LT035A-150	(40um)	68606	0	0.0393	0.0015	0.290	0.013	0.05359	0.00120	0.869	248	10	259	10	354	51	30.4
151	LT035A-151	(40um)	25953	0	0.0349	0.0014	0.259	0.017	0.05388	0.00280	0.620	221	9	234	14	366	117	40.2
152	LT035A-152	(40um)	39231	0	0.0258	0.0012	0.186	0.010	0.05226	0.00095	0.936	164	8	173	8	297	42	45.3
153	LT035A-153	(40um)	87668	0	0.0328	0.0014	0.254	2.710	0.05627	0.59927	0.004	208	9	230	1168	463	23604	55.9
154	LT035A-154	(40um)	58071	0	0.0315	0.0014	0.229	0.011	0.05275	0.00082	0.941	200	8	209	9	318	35	37.7
155	LT035A-155	(40um)	52199	0	0.0281	0.0013	0.208	0.011	0.05367	0.00132	0.881	179	8	192	9	357	56	50.7
156	LT035A-156	(40um)	117263	0	0.0300	0.0013	0.216	0.013	0.05204	0.00200	0.755	191	8	198	11	287	88	34.1
157	LT035A-157	(40um)	449323	0	0.0339	0.0014	0.243	0.020	0.05197	0.00357	0.521	215	9	221	16	284	157	24.8
158	LT035A-158	(40um)	33155	0	0.0353	0.0014	0.372	0.297	0.07637	0.06098	0.051	224	9	321	199	1105	1596	81.1
159	LT035A-159	(40um)	48289	0	0.0340	0.0014	0.319	0.087	0.06786	0.01835	0.152	216	9	281	65	864	561	76.3
160	LT035A-160	(40um)	67018	0	0.0310	0.0014	0.222	0.013	0.05199	0.00209	0.734	197	8	204	11	285	92	31.5
161	LT035A-161	(40um)	42452	0	0.0327	0.0014	0.245	0.035	0.05430	0.00741	0.297	208	9	223	28	383	307	46.6
162	LT035A-162	(40um)	83085	0	0.0296	0.0013	0.217	0.010	0.05316	0.00074	0.955	188	8	199	8	335	31	44.6
163	LT035A-163	(40um)	47902	0	0.0301	0.0013	0.218	0.035	0.05264	0.00821	0.273	191	8	201	29	313	355	39.6
164	LT035A-164	(40um)	67275	0	0.0303	0.0013	0.220	0.011	0.05269	0.00103	0.914	193	8	202	9	315	45	39.5
165	LT035A-165	(40um)	151114	0	0.0300	0.0014	0.233	0.136	0.05627	0.03281	0.077	191	8	213	106	463	1292	59.7
166	LT035A-166	(40um)	79234	0	0.0339	0.0014	0.252	0.051	0.05402	0.01062	0.207	215	9	228	40	372	443	42.9
167	LT035A-167	(40um)	102040	0	0.0335	0.0014	0.243	0.012	0.05258	0.00126	0.867	212	9	221	10	311	55	32.2
168	LT035A-168	(40um)	92400	0	0.0255	0.0012	0.180	0.011	0.05134	0.00177	0.816	162	8	168	9	256	79	37.2
169	LT035A-169	(40um)	144287	0	0.0300	0.0013	0.213	0.011	0.05165	0.00133	0.864	190	8	196	9	270	59	29.9
170	LT035A-170	(40um)	96985	0	0.0319	0.0014	0.229	0.013	0.05220	0.00196	0.753	202	9	210	11	294	86	31.7
171	LT035A-171	(40um)	75444	0	0.0324	0.0014	0.233	0.018	0.05222	0.00330	0.560	206	9	213	15	295	144	30.8
172	LT035A-172	(40um)	84663	0	0.0315	0.0014	0.273	0.270	0.06282	0.06215	0.044	200	8	245	195	702	2106	72.6
173	LT035A-173	(40um)	79438	0	0.0252	0.0012	0.180	0.014	0.05187	0.00326	0.615	161	8	168	12	280	144	43.1